Novel Integrated Paired Emitter-Detector Diode Flow Analysis System

by

Martina O'Toole B.Sc.

Thesis submitted for the Degree of Doctor of Philosophy

Supervisor: Prof. Dermot Diamond

School of Chemical Sciences

Dublin City University **August 2007**

Declaration

I hereby certify that this material, which I now submit for assessment on the programme of study leading to the award of Doctor of Philosophy is entirely my own work and has not been taken from the work of others save and to the extent that such work has been cited and acknowledged within the text of my work.

Signed: Martina O'Toole.

Martina O'Toole

ID No.: 98377221

Date: 24/9/07.

For My Wonderful Mother and Father

Anne and Larry

"The only victories worth anything are those achieved through hard work and dedication."

Henry Ward Beecher

Acknowledgements

My sincerest thanks to Dermot, who was always supportive of me throughout the four years it took to complete my work. His advice, patience and encouragement from day one were invaluable. He has given me so many opportunities not only to travel to conferences both near and far to present my work but also to complete an internship at MERL, Boston, where I gained essential techniques and research skills.

I would like to thank all the past and present members of the DD research group, who made this a most enjoyable experience, especially in times of stress. Thanks to Kim and Rod who were always on hand to answer my questions. A special thanks to Sonia, Ben and Rob who throughout the past 4 years have been fantastic friends, always quick to try and help in any way, it was very much appreciated.

The sense of community spirit in The School of Chemical Sciences and the NCSR is a tribute to the wonderful staff and postgraduate students it comprises. The school were always quick to donate money in aid of social events and as a result there is a wonderful social atmosphere, which not only encourages collaboration but makes the day a little easier knowing you're working in a friendly atmosphere. I have made some wonderful friends in DCU and would like to thank you all.

Thank you to all the NCSR and School of Chemistry technical staff, who were always obliging and willing to help. Thanks also to Dr. William Yerazunis for the supervision he gave me while completing my internship at MERL.

I would like to extend my thanks to Science Foundation Ireland for funding my postgraduate study.

On a more personal note, I would like to sincerely thank my parents, family and Eoin, who helped me not only during this stressful time of completing my thesis, but who have been my constant encouragement in anything I have ever done. For all those times you cheered me up when it all got too much, for all the times you ran around after me so I could write up and most importantly for all those times when you were all so worried about Dad and still found time to check up on me I will be forever and always grateful. Mam, Dad, Laurence, Gavin, Annette, Alan and Eoin, I love you all. x

List of Publications

Paper:

1. Martina O' Toole, King Tong Lau, Dermot Diamond, Photometric detection in flow analysis systems using integrated PEDDs, *Talanta,* **66** (2005) 1340 -1344.

2. King Tong Lau, Susan Baldwin, Martina O' Toole, Roderick Shepherd, William J. Yerazunis, Shinichi Izuo, Satoshi Ueyama and Dermot Diamond, A Low-Cost Optical Sensing Device based on Paired Emitter-Detector LEDs, *Analytica Chimica Acta,* **557** (2006) 111 -116.

3. Martina O' Toole, King Tong Lau, Benjamin Shazmann, Roderick Shepherd, Pavel N. Nesterenko, Brett Paull and Dermot Diamond, Novel Integrated Paired Emitter Detector Diode as a Miniaturized Photometric Detector in HPLC, *The Analyst*, **131** (2006) 938 – 943.

4. Leon Barron, Pavel N Nesterenko, Dermot Diamond, Martina O'Toole, King Tong Lau and Brett Paull, Low Pressure Ion Chromatography with a Low Cost Paired Emitter-Detector Diode Based Detector For The Determination of Alkaline Earth Metals in Water Samples, *Analytica Chimica Acta*, **577** (2006) 32-37.

5. Martina O' Toole, King Tong Lau, Roderick Shepherd, Conor Slater and Dermot Diamond, Determination of Phosphate using a Highly Sensitive Paired Emitter-Detector Diode Photometric Detector, *Analytica Chimica Acta,* accepted.

6. Martina O'Toole, Roderick Shepherd, King-Tong Lau and Dermot Diamond, Detection of nitrite by flow injection analysis using a novel paired emitter-detector diode (PEDD) as a photometric detector, SPIE, Advanced Environmental, Chemical, and Biological Sensing Technologies V Conference Proceedings, Submitted.

7. Martina O' Toole and Dermot Diamond, Chemical Sensors Based on Light Emitting Diodes, *Sensors*, Submitted.

8. Martina O' Toole, Leon Barron, Roderick Shepherd, King-Tong Lau, Brett Paull and Dermot Diamond*, Paired emitter-detector diode (PEDD) dual wavelength monitoring procedure for sensitivity improvements in ion chromatography determinations employing a post-column spectrophotometric reaction, *Journal of Chromatography A*, In preparation (Ready to submitt October 2007)

Poster:

1. Martina O' Toole, King Tong Lau and Dermot Diamond, (Chemical Sensing using Paired Emitter-Detector Diode Devices in Transmission Mode), Irish Universities Chemistry Research Colloquium (UCRC), Limerick, Ireland, June 2004

2. Martina O' Toole, King Tong Lau and Dermot Diamond, (Paired Emitter Detector Diode (PEDD) Based Platform for Colorimetric Detection in Flow Analysis), Analytical Research Forum, University of Central Lancashire, Preston, England, July 2004

3. Martina O' Toole, King Tong Lau, Roderick Shepherd, William Yerazunis and Dermot Diamond, (A reversible fuel cell actuator micropump), Adaptive Information Cluster Annual Conference, Crowne Plaza, Santry, Ireland, November 2005

4. Leon Barron, Martina O'Toole, King Tong Lau, Dermot Diamond, Pavel Nesterenko and Brett Paull (Low pressure ion chromatography of inorganic anions and cations in environmental water samples), HPLC 2006, San Francisco, USA, June 2006.

5. Martina O' Toole, Brett Paull, Leon Barron, Edel Sugrue, King Tong Lau and Dermot Diamond, Rapid ion Chromatography of Transition Metals on a Short Polymeric Grafted Polyiminodiacetic Acid Column with Post-column Reaction Detection with a Paired Emitter-Detector Diode (PEDD) Detector, 19th Annual International Ion Chromatography Symposium, Pittsburgh, Pennsylvania, USA, September 2006 (**Nominated for Best poster**)

6. Martina O' Toole, King-Tong Lau, Roderick Shepherd and Dermot Diamond, Detection of Nitrite by Flow Injection Analysis Using a Novel Paired Emitter-Detector Diode (PEDD) as a Photometric Detector, Pittcon 2007, Chicago, USA, February 2007

Awards for Best Poster:

1. Martina O' Toole, King Tong Lau and Dermot Diamond, (Paired Emitter Detector Diode (PEDD) Based Platform for Colorimetric Detection in Flow Analysis), 3rd Biennial Conference on Analytical Sciences in Ireland, Cork University, Cork, Ireland, September 2004.

2. Leon Barron, Martina O'Toole, King Tong Lau, Dermot Diamond, Pavel Nesterenko and Brett Paull (Development of a low pressure ion chromatography for the determination of alkaline earth metals in

environmental samples), 4th Biennial Conference on Analytical Sciences in Ireland, D.I.T., Ireland, April 2006.

Oral Presentation:

1. Martina O' Toole, King-Tong Lau, Benjamin Shazmann, Roderick Shepherd, Pavel N. Nesterenko, Brett Paull and Dermot Diamond, Paired Emitter Detector Diode (PEDD) as a Miniaturized Photometric Detector in LC systems, 58th Irish Universities Chemistry Research Colloquium, NUI, Galway, June 2006

2. Martina O' Toole, King-Tong Lau, Benjamin Shazmann, Roderick Shepherd, Pavel N. Nesterenko, Brett Paull and Dermot Diamond, Novel Integrated PEDD as a Miniaturized Photometric Detector in HPLC, Analytical Research Forum 06, Cork University, July 2006

3. Martina O' Toole, King-Tong Lau, Roderick Shepherd and Dermot Diamond, Novel Integrated PEDD as a Photometric Detector in Flow Analysis Systems, X international conference of flow analysis, Porto, Portugal, September 2006

4. Martina O' Toole, Leon Barron, Roderick Shepherd, King-Tong Lau, Pavel N. Nesterenko, Brett Paull and Dermot Diamond, Paired emitter-detector diode (PEDD) dual wavelength monitoring procedure for sensitivity improvements in ion chromatography determinations employing a post-column spectrophotometric reaction, 19th Annual International Ion Chromatography Symposium, Pittsburgh, Pennsylvania, USA, September 2006

5. Martina O' Toole, King-Tong Lau, Roderick Shepherd and Dermot Diamond, Detection of Nitrite by Flow Injection Analysis Using a Novel Paired Emitter-Detector Diode (PEDD) as a Photometric Detector, SPIE Optics East 2007, Boston, USA, September 2007

6. Sonia Ramírez-García, María del Mar Baeza, Martina O'Toole, Yanzhe Wu, James Lalor, Gordon G. Wallace and Dermot Diamond, Fully integrated polymeric microfluidic platform for environmental analysis, ICFIA 2007, Berlin, Germany, September 2007

Novel Integrated Paired Emitter-Detector Diode Flow Analysis System

Abstract

My PhD programme of research at the National Centre of Sensor Research has focussed on the development of a miniaturized detection system based on the concept of a Paired Emitter-Detector Diode (PEDD) LED optical sensor as a generic optical sensor platform for colorimetric analysis as developed within the research group. This research was funded by Science Foundation Ireland (SFI). This novel optical sensor employs two LEDs, operating one as a light source and the other as a light detector. The emitter LED is forward biased and the detector reverse biased. A simple timer circuit measures the time taken for the photocurrent generated by the emitter LED to discharge the detector LED from 5 V (logic 1) to 1.7 V (logic 0).

PEDDs of various wavelengths and designs were investigated and initially calibrated using pH indicator dyes.

The PEDD has been applied as an inexpensive detector in a flow-injection system for determining low concentration levels of phosphate employing the malachite green spectrophotometric method. The novel flow detector employed within this manifold is a highly sensitive, low cost, miniaturized light emitting diode (LED) based flow detector, which achieved an improved LOD in comparison to a LED-photdiode sensor.

The PEDD has also been applied as a photometric detector in HPLC. Separation of transition metal ions, manganese (II) and cobalt (II) were carried out using a Nucleosil 100-7 (functionalised with IDA groups) column. The PEDD was calibrated using Mn (II) and Co (II) PAR complexes providing a linear response. Higher sensitivity and improved precision were obtained from the PEDD compared to the commercially available UV-vis variable wavelength detector.

TABLE OF CONTENTS

A APPENDIX 155

CHAPTER 1

INTRODUCTION

1. Introduction

1.1 Electromagnetic Radiation

Electromagnetic radiation is the phenomenon of electromagnetic waves produced by the motion of electrically charged particles [1]. The frequency of radiation is directly proportional to the energy of a photon. The amount of energy transferred per photon is given by the Einstein-Planck relation [2]:

$$E = h\nu = hc/\lambda \qquad \textbf{Equation 1.1}$$

where E = energy in joules

h = Planck's constant (6.62×10^{-34} J.s)

ν = frequency of radiation in hertz (Hz, or s^{-1})

c = speed of light (3.00×10^{8} ms^{-1})

λ = wavelength (m)

The intensity of a beam of radiation depends on the quantity of photons per unit time per unit area, but the quantum energy (E) per photon is always the same for a given frequency of the radiation. The absorption of radiation at various wavelengths is summarised in Table 1.1 [2].

Table 1.1 Interaction of radiation with matter [2].

Radiation Absorbed	*Energy Changes Involved*
Visible, ultraviolet, or X-ray	Electronic transitions, vibrational or rotational transitions
Infrared	Molecular vibrational changes with superimposed rotational changes
Far-infrared or microwave	Rotational changes
Radio-frequency	Too weak to be observed except under an intense magnetic field

Photons of the highest energy correspond to shorter wavelengths. The electromagnetic spectrum consists of a wide range of wavelengths (and photon energies) as shown in Figure 1.1. The UV – vis region extends from 190 – 400 nm (UV) and from 400-800 nm (vis) [3].

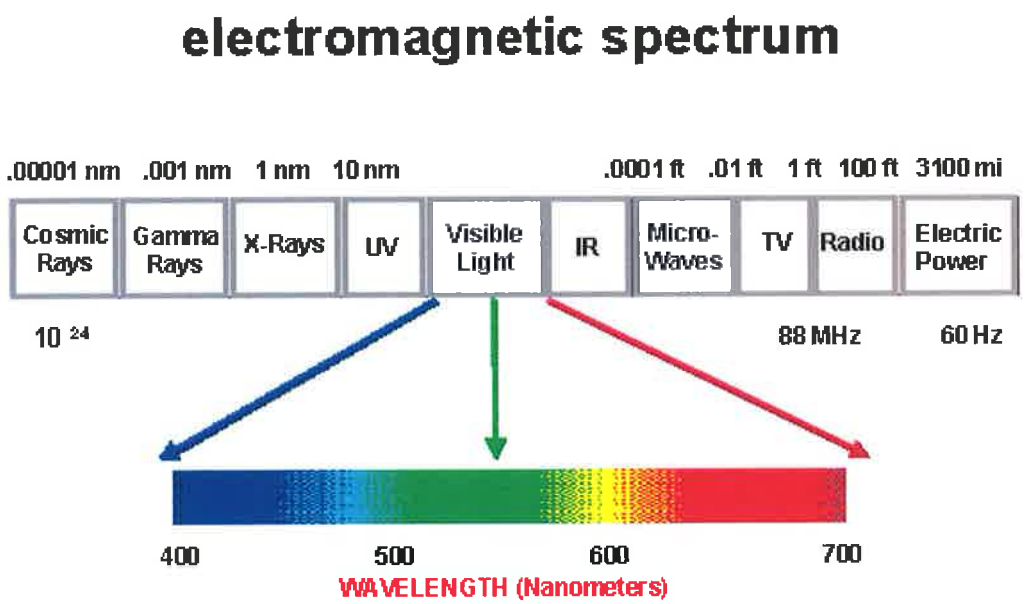

Figure 1.1 The Electromagnetic Spectrum [4].

1.2 Molecular Absorption

Absorption in the UV and visible region causes excitation of electrons to higher energy levels. In general, tightly held electrons will require energetic photons (of short wavelength) to accomplish absorption, whereas more loosely held (delocalised) electrons can be excited with longer wavelength radiation [5].

The absorption of UV or visible radiation corresponds to the excitation of outer electrons. The main types of electronic transitions can be categorised as shown in Figure 1.2 [6];

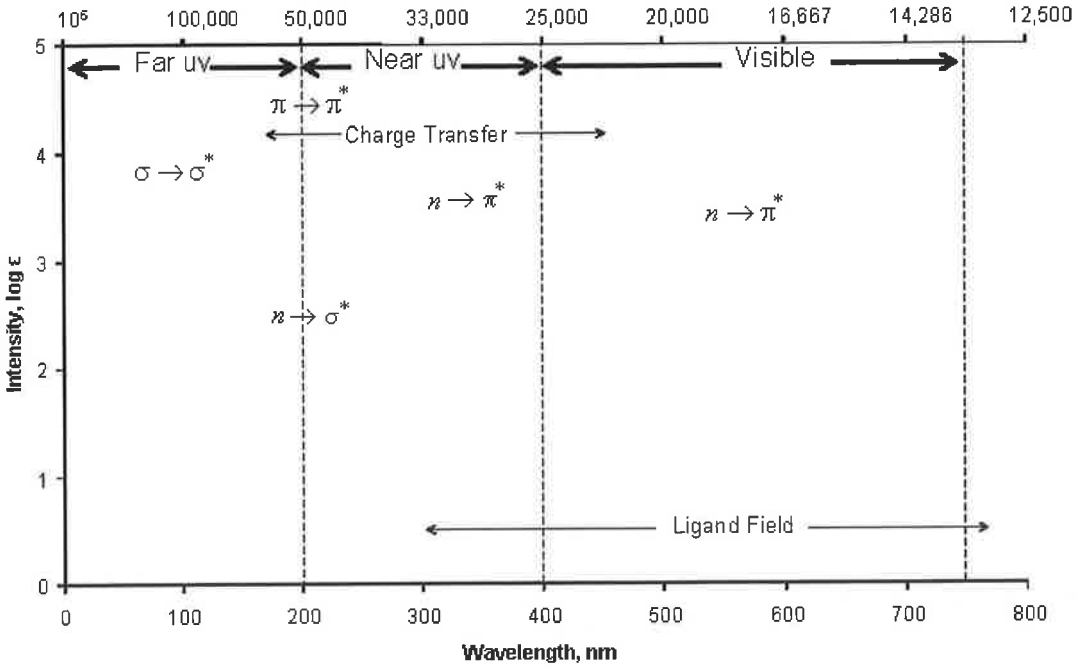

Figure 1.2 Ultraviolet and visible regions of the spectrum and the types of absorption bands that most often occur [5]

Electrons are promoted from their ground state to an excited state, when an atom or molecule absorbs energy. An atom can rotate and vibrate within a molecule resulting in discrete energy levels, which can be considered as being packed on top of each electronic level (Figure 1.3).

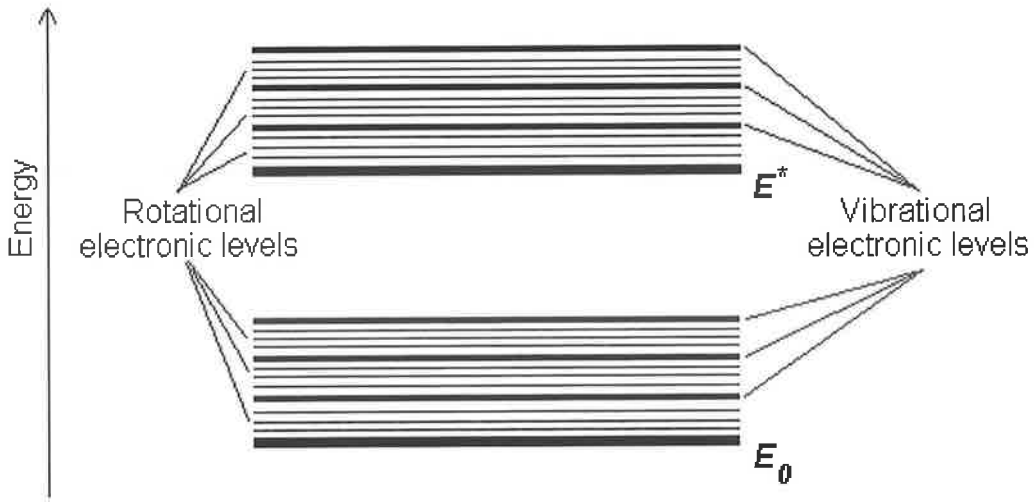

Figure 1.3 Schematic of absorbing species containing π, σ and η electrons [6]

$n \rightarrow \sigma^*$ Transitions

Saturated compounds containing atoms with lone pairs (non-bonding electrons) are capable of $n \rightarrow \sigma^*$ transitions. These transitions usually need less energy than $\sigma \rightarrow \sigma^*$ transitions. They can be initiated by light whose wavelength is in the range 150 - 250 nm. The number of organic functional groups with $n \rightarrow \sigma^*$ peaks in the UV region is small.

$n \rightarrow \pi^*$ and $\pi \rightarrow \pi^*$ Transitions

Most absorption spectroscopy of organic compounds is based on transitions of n or π electrons to the π^* excited state. This is because the absorption peaks for these transitions fall in the spectral region of 190 - 800 nm or higher. These transitions need an unsaturated group in the molecule to provide the π electrons.

The type of transition can be identified by the spectral regions in which they are generally found, their relative absorption intensities, and in some cases by spectral shifts when the solvent is varied. An example of some functional groups and their transitions are shown in Table 1.2.

Table 1.2 Absorption maxima of nonconjugated chromophores [3]

Chromophore	*Transition*	Λ_{max}
-C-C-	$\sigma \rightarrow \sigma^*$	150
-O-	$n \rightarrow \sigma^*$	185
-N<	$n \rightarrow \sigma^*$	195
-S-	$n \rightarrow \sigma^*$	195
>C=O	$\pi \rightarrow \pi^*$	190
	$n \rightarrow \pi^*$	300 (weak)
>C=C<	$\pi \rightarrow \pi^*$	190

As a rule, energetically favored electron promotion will be from the highest occupied molecular orbital (HOMO) to the lowest unoccupied molecular orbital (LUMO), and the resulting species is called an excited state[6].

1.3 The Beer-Lambert Law

The Beer-Lambert law forms the basis of light absorbance measurements on gases and solutions in the UV-Visible and IR-region [7]. A light beam of intensity I_0 strikes a sample solution within a quartz or glass cell. On passing through the cell, the light beam has a reduced intensity, I due to reflection losses at the cell, absorbance in the sample and by scattering at dispersed particles as shown in Figure 1.5.

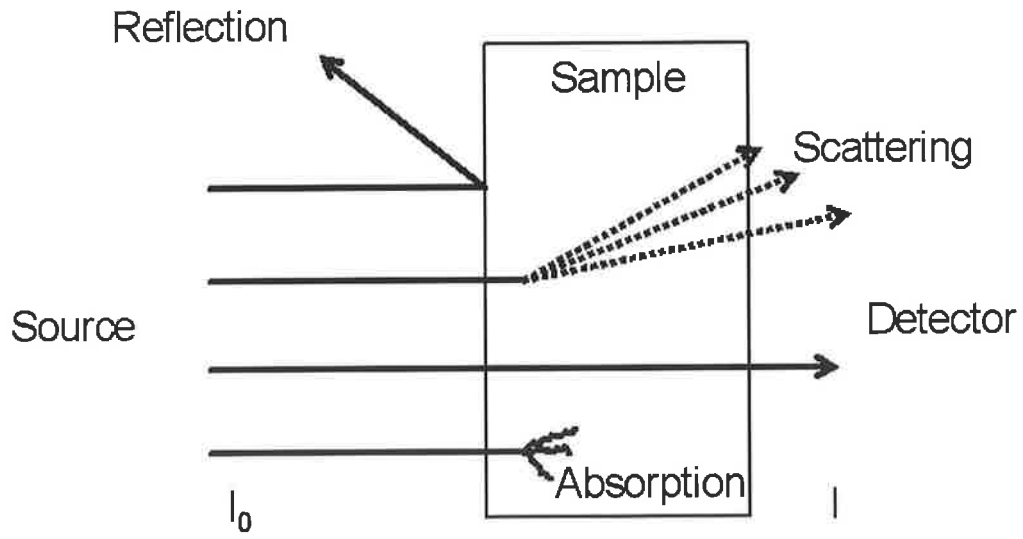

Figure 1.5 Intensity loss of a light beam of intensity I_0 by reflection, scattering and absorption [3].

For the Beer-Lambert law to hold, any absorbance losses which occur MUST be due to dissolved sample only. To compensate for any losses due to reflection and scattering a second spectrum is taken of the solvent and sample matrix only and the transmittance T is calculated as follows:

$$T = I / I_0 \approx I_{solution} / I_{solvent}$$ **Equation 1.2**

Absorbance is proportional to the number of absorbing species in the illuminated part of the cell. Absorbance, A, is defined by the equation

$$A = -\log T = \log\left(I_0 / I\right)$$ **Equation 1.3**

Absorbance is proportional to the cell path length l, cm, the concentration of the solution C, $molL^{-1}$, and a substance specific proportionality constant ε called the molar absorptivity or molar extinction coefficient, $Lmol^{-1}cm^{-1}$. The magnitude of the molar absorptivity is governed by the size of the absorbing species and by the probability of the transition.

$$A = \varepsilon C l$$ **Equation 1.4**

Hence, for an absorbing species in solution, if the Beer-Lambert law is obeyed, the absorbance at a particular wavelength is directly proportional to the concentration. It follows that provided other mechanisms for reduction in transmitted intensity can be compensated for through reference measurements (e.g. solvent effects, scattering, co-absorbing species etc.) then the measured absorbance can be easily converted into an estimation of concentration [8].

Despite the use of blanks or reference measurements to account for losses due to reflection or scattering (Figure 1.5), deviations from Beer-Lambert law can occur due to the following:

1. The bandwidth (Δλ) of the incident beam should be very narrow, ideally approximating monochromatic radiation. Deviations from the Beer-Lambert behaviour increase as Δλ increases, particularly when the Δλ is greater than the spectral width of the absorption band of the absorbing species.

2. Deviations also occur in highly absorbing or highly scattering media. Both of these effects yield a very limited linear range for the absorbance-concentration relationship.
3. Stray Light

Stray Light

As illustrated in Figure 1.6 [9]:

I_0 = intensity of incident light (I_0 is constant)

I = intensity of transmitted light (I decreases with increasing analyte concentration)

I_S = intensity of stray light (Assume I_S is constant)

Typically $I_0 >>> I_S$

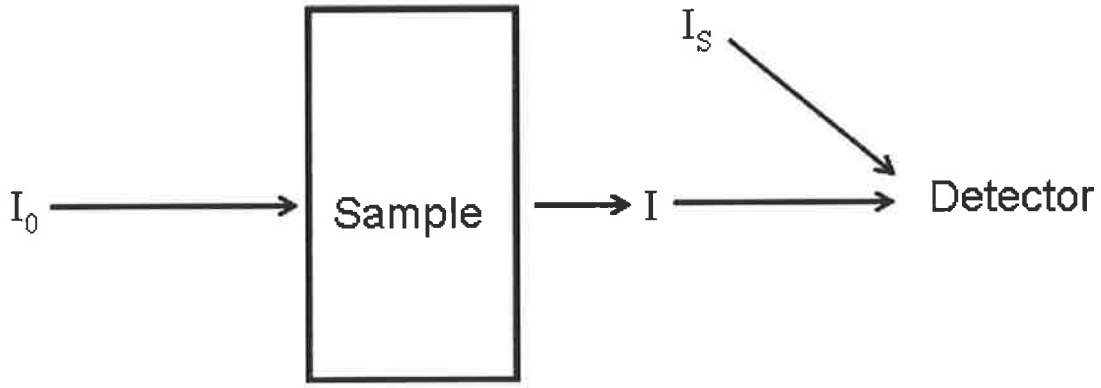

Figure 1.6 Schematic of the effect of stray light on the Beer-Lambert law.

Absence of sample = $I_0 + I_S$

Presence of sample = $I + I_S$

Therefore $A = \log\left(\left(I_0 + I_S\right)/\left(I + I_S\right)\right)$

At **low concentrations** $A = \log\left(I_0/\left(I + I_S\right)\right)$

as $I_0 >> I_S$ and $I_{observed} = I + I_S$, $I >> I_S$ therefore $I_{observed} \approx I$

Hence at low concentrations Beer-Lambert law holds as $A = \log\left(I_0/I\right)$

At **high concentrations** $I_S >>> I$ and I approaches $I_{limited}$ as most of the light is absorbed by the sample

$A = \log \left(I_0 / I_S \right)$ where I_0 and I_S are constants therefore A no longer changes. This results in a nonlinear plot as shown in Figure 1.7.

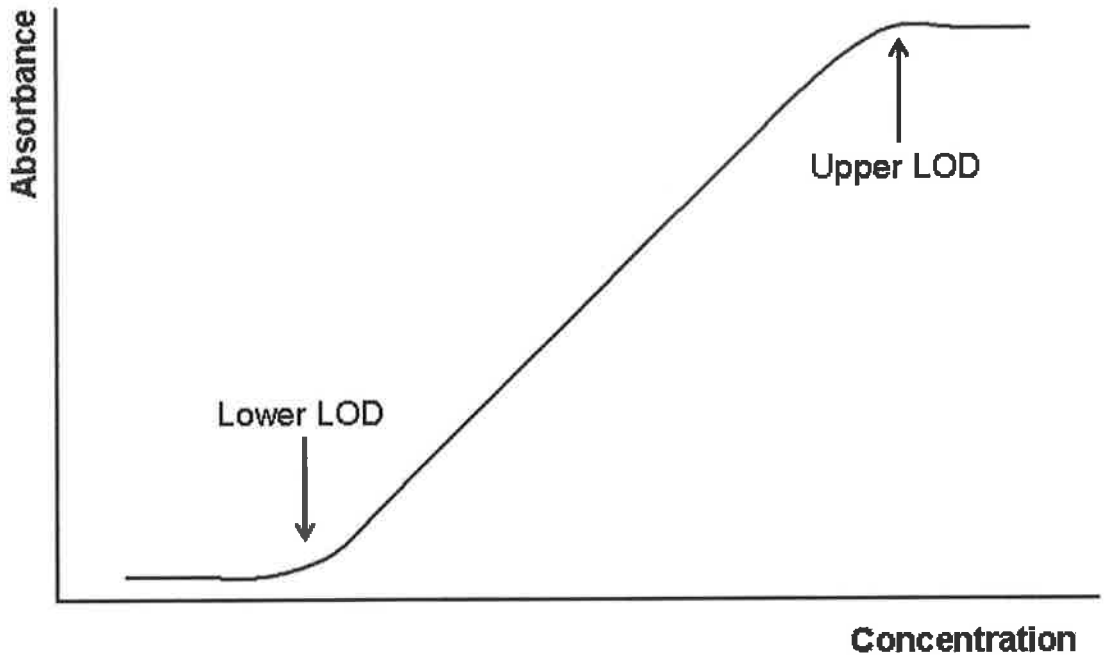

Figure 1.7 Deviation from Beer-Lambert law showing onset of nonlinearity at higher concentrations

As shown in Figure 1.7 when $I \approx I_0$ little or no absorbance is taking place therefore $\left(I_0 / I \right) = 1$ and consequently $\log \left(I_0 / I \right) = 0$.

1.4 Ultraviolet-Visible (UV-vis) Instrumentation

1.4.1 Spectrophotometers

Spectrophotometers measure the ratio of incident energy to transmitted energy. In its simplest form a spectrophotometer comprises of a polychromatic broad spectrum source, a monochromator, sample cell(s), detector and a computer for data acquisition and storage. The function of a UV-visible spectrophotometric system is to record how much light is absorbed by an analytical sample. The measurement is made at a specific wavelength (λ), selected within the ultraviolet and visible range – approximately 190 to 800 nm. All spectrophotometers pass the light energy from the source through an entrance slit of fairly narrow dimensions. The light passing through the entrance slit then proceeds to a collimating element which collects parallel light rays and directs them through the rest of the instrument. Spectrophotometers can be categorized into two types: dispersive spectrophotometers and diode array spectrophotometers.

1.4.1.1 Dispersive Spectrophotometer

In dispersive spectrophotometers, the grating is moved either by a stepping motor or by a mechanical arm which directs light of discrete wavelengths through an exit slit and onto the sample. Common detectors used in this configuration are typically either silicon photodiodes or photomultiplier tubes in the UV-vis region and lead sulfide (PbS) detectors for the NIR region.

Basic (Single-Beam) System

The basic layout of a single-beam UV-visible system is given in Figure 1.8. The light source is commonly a combined deuterium lamp (for UV light) and tungsten-filament lamp (for visible light). The source can be selected by a switchable mirror as required. The instrument automatically switches between the two sources during a scan to

TABLE OF CONTENTS

A APPENDIX 155

1. Introduction

1.1 Electromagnetic Radiation

Electromagnetic radiation is the phenomenon of electromagnetic waves produced by the motion of electrically charged particles [1]. The frequency of radiation is directly proportional to the energy of a photon. The amount of energy transferred per photon is given by the Einstein-Planck relation [2]:

$$E = h\nu = hc/\lambda \qquad \textbf{Equation 1.1}$$

where E = energy in joules

h = Planck's constant (6.62×10^{-34} J.s)

ν = frequency of radiation in hertz (Hz, or s^{-1})

c = speed of light (3.00×10^{8} ms^{-1})

λ = wavelength (m)

The intensity of a beam of radiation depends on the quantity of photons per unit time per unit area, but the quantum energy (E) per photon is always the same for a given frequency of the radiation. The absorption of radiation at various wavelengths is summarised in Table 1.1 [2].

Table 1.1 Interaction of radiation with matter [2].

Radiation Absorbed	*Energy Changes Involved*
Visible, ultraviolet, or X-ray	Electronic transitions, vibrational or rotational transitions
Infrared	Molecular vibrational changes with superimposed rotational changes
Far-infrared or microwave	Rotational changes
Radio-frequency	Too weak to be observed except under an intense magnetic field

Photons of the highest energy correspond to shorter wavelengths. The electromagnetic spectrum consists of a wide range of wavelengths (and photon energies) as shown in Figure 1.1. The UV – vis region extends from 190 – 400 nm (UV) and from 400-800 nm (vis) [3].

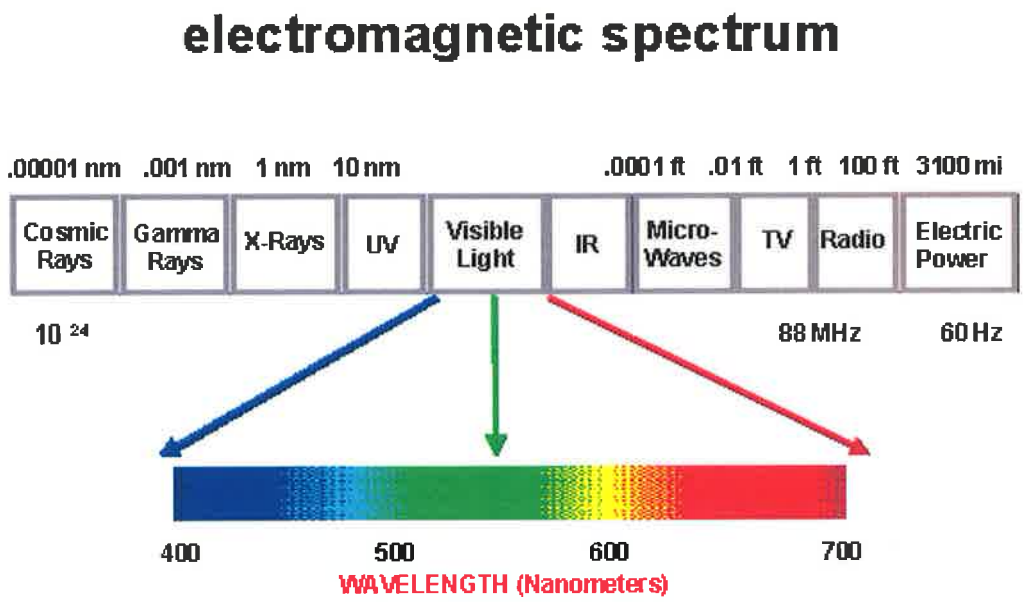

Figure 1.1 The Electromagnetic Spectrum [4].

1.2 Molecular Absorption

Absorption in the UV and visible region causes excitation of electrons to higher energy levels. In general, tightly held electrons will require energetic photons (of short wavelength) to accomplish absorption, whereas more loosely held (delocalised) electrons can be excited with longer wavelength radiation [5].

The absorption of UV or visible radiation corresponds to the excitation of outer electrons. The main types of electronic transitions can be categorised as shown in Figure 1.2 [6];

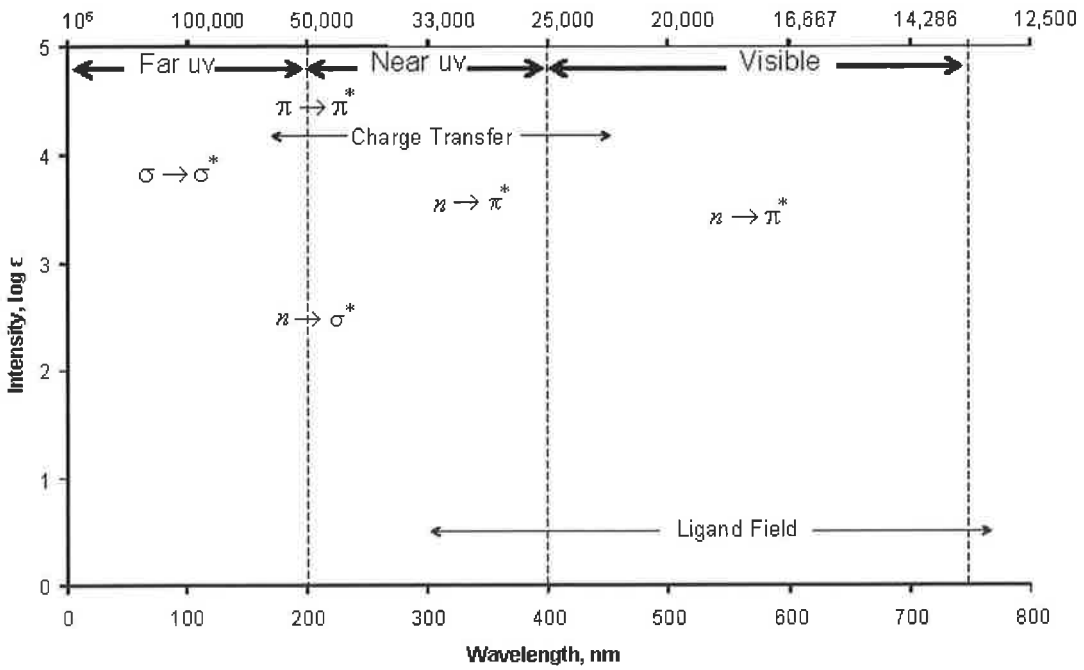

Figure 1.2 Ultraviolet and visible regions of the spectrum and the types of absorption bands that most often occur [5]

Electrons are promoted from their ground state to an excited state, when an atom or molecule absorbs energy. An atom can rotate and vibrate within a molecule resulting in discrete energy levels, which can be considered as being packed on top of each electronic level (Figure 1.3).

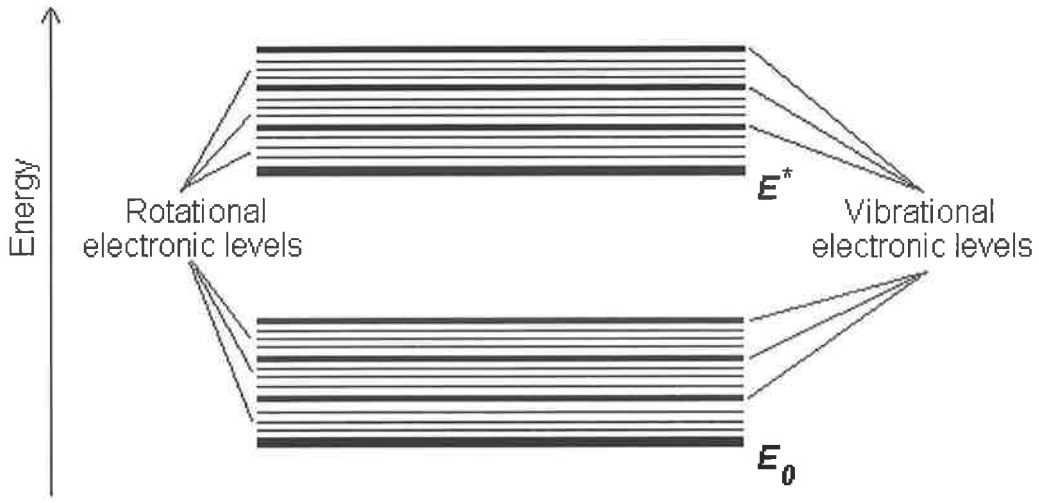

Figure 1.3 Schematic of absorbing species containing π, σ and η electrons [6]

Absorbing species containing π, σ, and *n* electrons

Absorption of ultraviolet and visible radiation in organic molecules is restricted to certain functional groups (*chromophores*) that contain valence electrons of low excitation energy. Chromophores absorb and transmit light energy. The spectrum of a molecule containing chromophores is complex due to the superposition of rotational and vibrational transitions on the electronic transitions resulting in overlapping lines. In general this appears as a continuous absorption band. Possible electronic transitions of π, σ, and *n* electrons are shown in Figure 1.4.

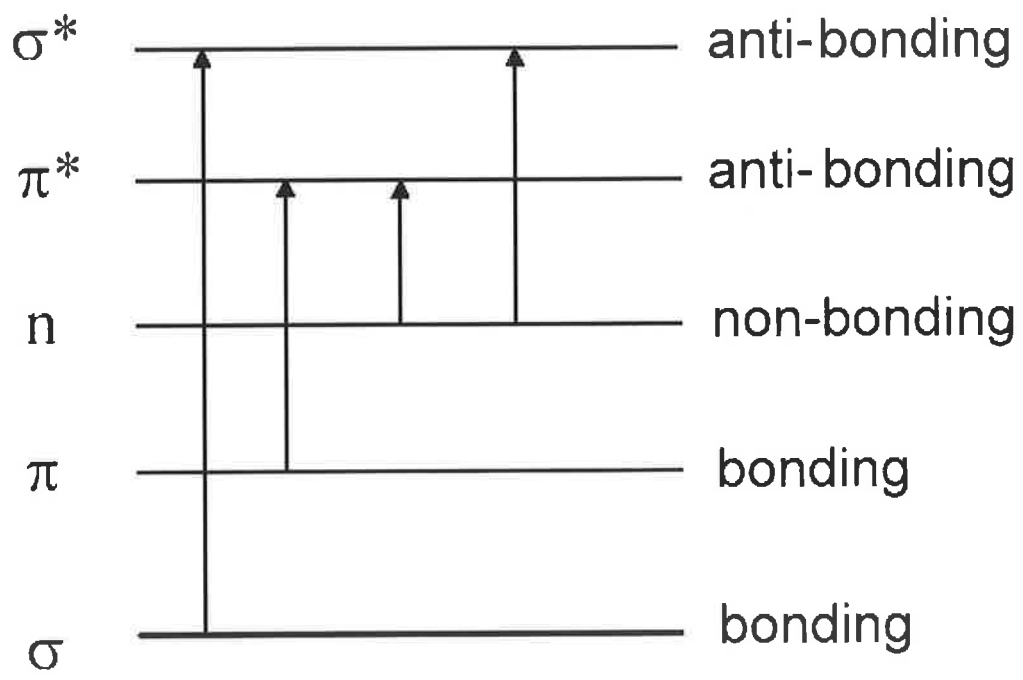

Figure 1.4 Schematic of molecular orbital energy levels [3]

$\sigma \rightarrow \sigma^*$ Transitions

The energy required to excite an electron in a bonding σ orbital to the corresponding antibonding orbital is large. Methane, for example (which has only C-H bonds, and can only undergo $\sigma \rightarrow \sigma^*$ transitions) shows an absorbance λ_{max} at 125 nm. A UV-vis spectrum is commonly regarded as ranging from 200 - 800 nm, therefore absorption maxima due to $\sigma \rightarrow \sigma^*$ transitions are not seen in the UV-vis region.

$n \rightarrow \sigma^*$ Transitions

Saturated compounds containing atoms with lone pairs (non-bonding electrons) are capable of $n \rightarrow \sigma^*$ transitions. These transitions usually need less energy than $\sigma \rightarrow \sigma^*$ transitions. They can be initiated by light whose wavelength is in the range 150 - 250 nm. The number of organic functional groups with $n \rightarrow \sigma^*$ peaks in the UV region is small.

$n \rightarrow \pi^*$ and $\pi \rightarrow \pi^*$ Transitions

Most absorption spectroscopy of organic compounds is based on transitions of n or π electrons to the π^* excited state. This is because the absorption peaks for these transitions fall in the spectral region of 190 - 800 nm or higher. These transitions need an unsaturated group in the molecule to provide the π electrons.

The type of transition can be identified by the spectral regions in which they are generally found, their relative absorption intensities, and in some cases by spectral shifts when the solvent is varied. An example of some functional groups and their transitions are shown in Table 1.2.

Table 1.2 Absorption maxima of nonconjugated chromophores [3]

Chromophore	*Transition*	λ_{max}
-C-C-	$\sigma \rightarrow \sigma^*$	150
-O-	$n \rightarrow \sigma^*$	185
-N<	$n \rightarrow \sigma^*$	195
-S-	$n \rightarrow \sigma^*$	195
>C=O	$\pi \rightarrow \pi^*$	190
	$n \rightarrow \pi^*$	300 (weak)
>C=C<	$\pi \rightarrow \pi^*$	190

As a rule, energetically favored electron promotion will be from the highest occupied molecular orbital (HOMO) to the lowest unoccupied molecular orbital (LUMO), and the resulting species is called an excited state[6].

1.3 The Beer-Lambert Law

The Beer-Lambert law forms the basis of light absorbance measurements on gases and solutions in the UV-Visible and IR-region [7]. A light beam of intensity I_0 strikes a sample solution within a quartz or glass cell. On passing through the cell, the light beam has a reduced intensity, I due to reflection losses at the cell, absorbance in the sample and by scattering at dispersed particles as shown in Figure 1.5.

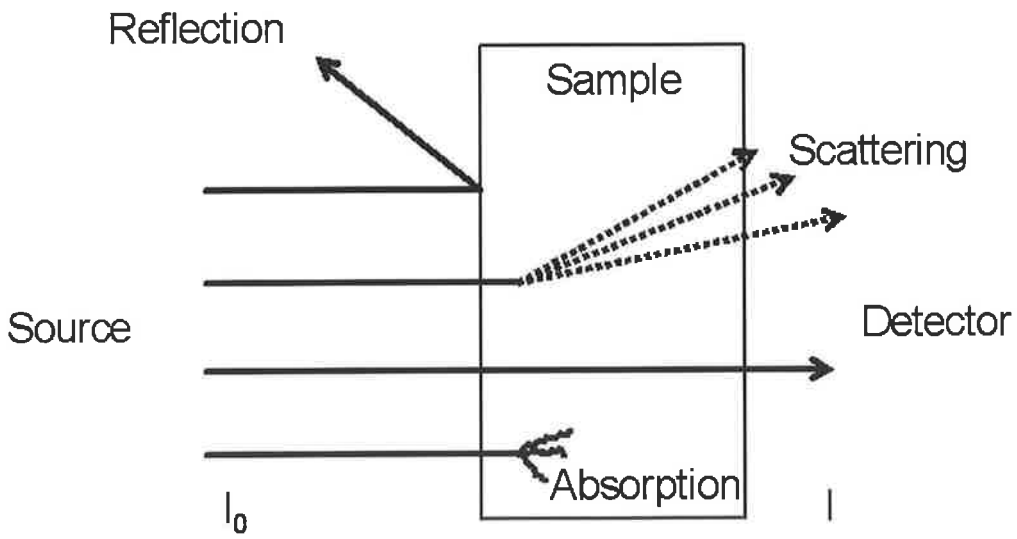

Figure 1.5 Intensity loss of a light beam of intensity I_0 by reflection, scattering and absorption [3].

For the Beer-Lambert law to hold, any absorbance losses which occur MUST be due to dissolved sample only. To compensate for any losses due to reflection and scattering a second spectrum is taken of the solvent and sample matrix only and the transmittance T is calculated as follows:

$$T = I / I_0 \approx {I_{solution}}/{I_{solvent}}$$ **Equation 1.2**

Absorbance is proportional to the number of absorbing species in the illuminated part of the cell. Absorbance, A, is defined by the equation

$$A = -\log T = \log\left({I_0}/{I}\right)$$ **Equation 1.3**

Absorbance is proportional to the cell path length l, cm, the concentration of the solution C, $molL^{-1}$, and a substance specific proportionality constant ε called the molar absorptivity or molar extinction coefficient, $Lmol^{-1}cm^{-1}$. The magnitude of the molar absorptivity is governed by the size of the absorbing species and by the probability of the transition.

$$A = \varepsilon C l$$ **Equation 1.4**

Hence, for an absorbing species in solution, if the Beer-Lambert law is obeyed, the absorbance at a particular wavelength is directly proportional to the concentration. It follows that provided other mechanisms for reduction in transmitted intensity can be compensated for through reference measurements (e.g. solvent effects, scattering, co-absorbing species etc.) then the measured absorbance can be easily converted into an estimation of concentration [8].

Despite the use of blanks or reference measurements to account for losses due to reflection or scattering (Figure 1.5), deviations from Beer-Lambert law can occur due to the following:

1. The bandwidth ($\Delta\lambda$) of the incident beam should be very narrow, ideally approximating monochromatic radiation. Deviations from the Beer-Lambert behaviour increase as $\Delta\lambda$ increases, particularly when the $\Delta\lambda$ is greater than the spectral width of the absorption band of the absorbing species.

2. Deviations also occur in highly absorbing or highly scattering media. Both of these effects yield a very limited linear range for the absorbance-concentration relationship.
3. Stray Light

Stray Light

As illustrated in Figure 1.6 [9]:

I_0 = intensity of incident light (I_0 is constant)

I = intensity of transmitted light (I decreases with increasing analyte concentration)

I_S = intensity of stray light (Assume I_S is constant)

Typically $I_0 >>> I_S$

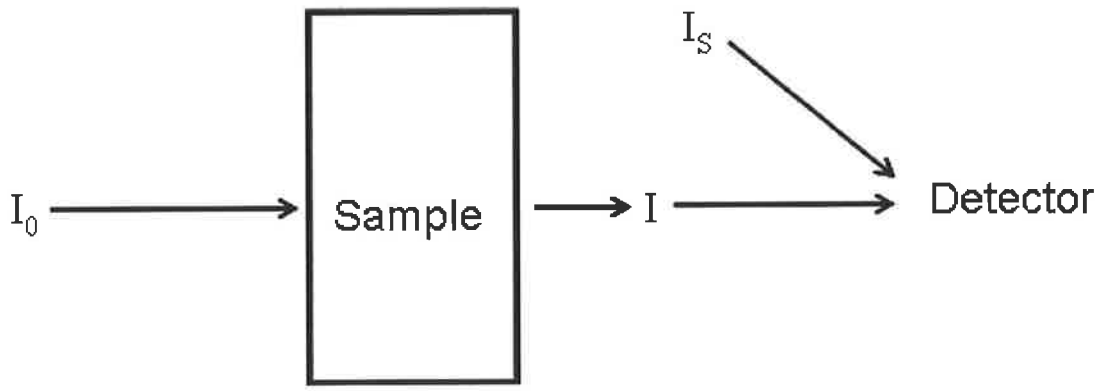

Figure 1.6 Schematic of the effect of stray light on the Beer-Lambert law.

Absence of sample = $I_0 + I_S$

Presence of sample = $I + I_S$

Therefore $A = \log\left(\left(I_0 + I_S\right)/\left(I + I_S\right)\right)$

At **low concentrations** $A = \log\left(I_0/\left(I + I_S\right)\right)$

as $I_0 >> I_S$ and $I_{observed} = I + I_S$, $I >> I_S$ therefore $I_{observed} \approx I$

Hence at low concentrations Beer-Lambert law holds as $A = \log\left(I_0/I\right)$

At **high concentrations** $I_S >>> I$ and I approaches $I_{limited}$ as most of the light is absorbed by the sample

$A = \log \left(I_0/I_S\right)$ where I_0 and I_S are constants therefore A no longer changes. This results in a nonlinear plot as shown in Figure 1.7.

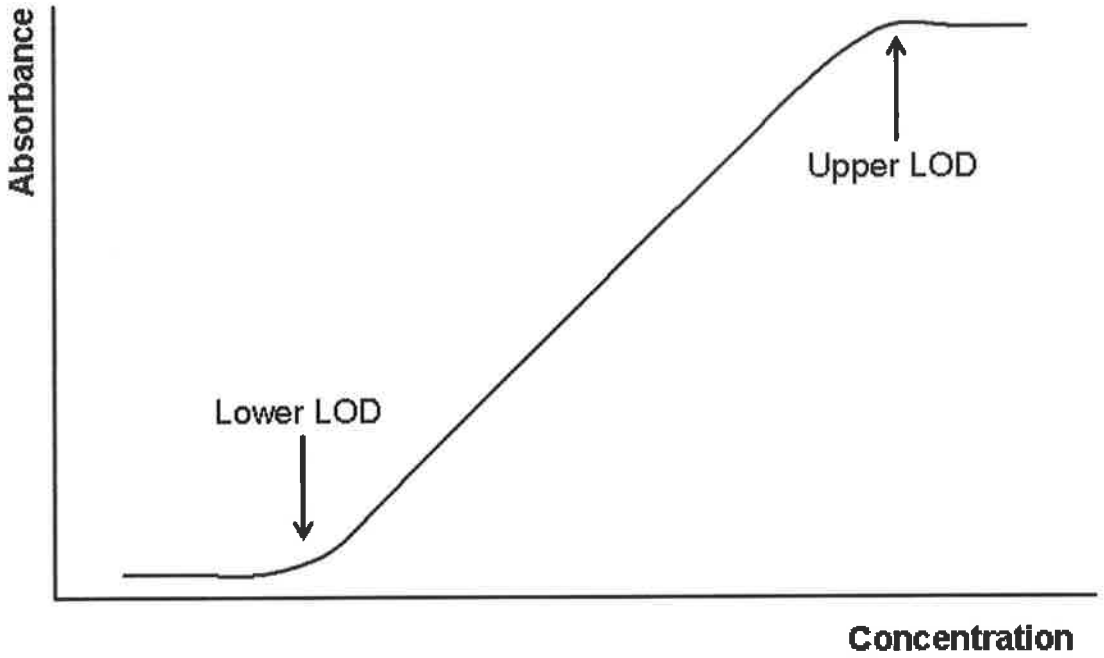

Figure 1.7 Deviation from Beer-Lambert law showing onset of nonlinearity at higher concentrations

As shown in Figure 1.7 when $I \approx I_0$ little or no absorbance is taking place therefore $\left(I_0/I\right) = 1$ and consequently $\log \left(I_0/I\right) = 0$.

1.4 Ultraviolet-Visible (UV-vis) Instrumentation

1.4.1 Spectrophotometers

Spectrophotometers measure the ratio of incident energy to transmitted energy. In its simplest form a spectrophotometer comprises of a polychromatic broad spectrum source, a monochromator, sample cell(s), detector and a computer for data acquisition and storage. The function of a UV-visible spectrophotometric system is to record how much light is absorbed by an analytical sample. The measurement is made at a specific wavelength (λ), selected within the ultraviolet and visible range – approximately 190 to 800 nm. All spectrophotometers pass the light energy from the source through an entrance slit of fairly narrow dimensions. The light passing through the entrance slit then proceeds to a collimating element which collects parallel light rays and directs them through the rest of the instrument. Spectrophotometers can be categorized into two types: dispersive spectrophotometers and diode array spectrophotometers.

1.4.1.1 Dispersive Spectrophotometer

In dispersive spectrophotometers, the grating is moved either by a stepping motor or by a mechanical arm which directs light of discrete wavelengths through an exit slit and onto the sample. Common detectors used in this configuration are typically either silicon photodiodes or photomultiplier tubes in the UV-vis region and lead sulfide (PbS) detectors for the NIR region.

Basic (Single-Beam) System

The basic layout of a single-beam UV-visible system is given in Figure 1.8. The light source is commonly a combined deuterium lamp (for UV light) and tungsten-filament lamp (for visible light). The source can be selected by a switchable mirror as required. The instrument automatically switches between the two sources during a scan to

ensure that the optimum light energy throughput is achieved across the entire spectral range.

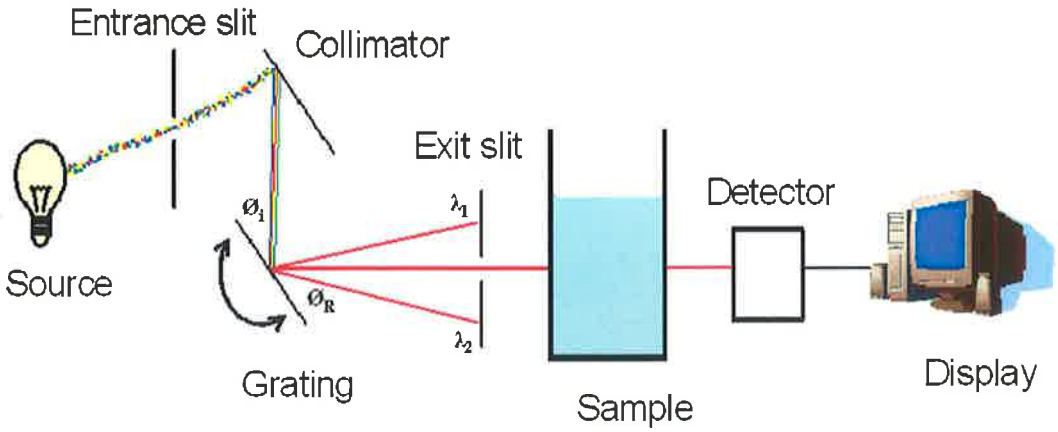

Figure 1.8 Schematic of a single beam dispersive spectrophotometer [10]

The monochromator selects the wavelength, λ, at which the measurement takes place. However, it is not possible to select only one wavelength, and a narrow band of wavelengths on either side of λ will also be transmitted. The width of this band is called the Spectral Bandwidth, Δλ. The (nearly) monochromatic radiation then passes through the sample where some absorption may take place. The intensity of the transmitted radiation, $I_T(\lambda)$, is recorded at the detector.

The detector produces an electronic signal (normally proportional to the radiation intensity) which is then amplified and made available for direct display and/or transfer to a microprocessor. A typical spectrophotometric measurement measures the absorbance of the specific analyte dissolved in a solvent. A sample containing everything except the analyte is used as the reference sample. The advantages of the single beam spectrophotometer are low cost, high throughput of light and hence high sensitivity. The disadvantage is the time lapse between taking the reference (I) and sample (I_0) measurement which can have associated problems such as baseline drift.

1.4.1.2 Double-Beam Systems

The basic layout is similar to that of the single-beam instrument except that, in the sample compartment area, the single-beam is divided into two beams as shown in Figure 1.9.

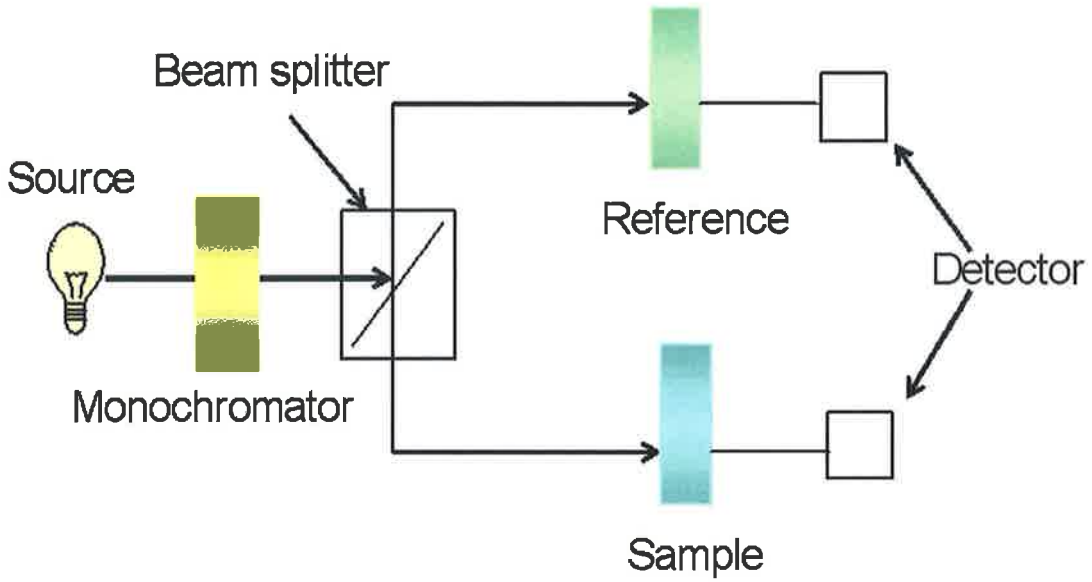

Figure 1.9 Schematic of a dual beam spectrophotometric detector.

As shown in Figure 1.9 the reference sample, R, and the test sample, T, are positioned separately, one in each of the two beams of light. The two beams are generated alternatively from the same incoming radiation by using the rotating 'chopper' mirror. The main advantage of the double-beam spectrophotometer is the removal of the time lag between measurements of I_R (λ) to I_T (λ). This reduces any drift in source output, or detector sensitivity. The disadvantages are higher cost and lower sensitivity as the throughput of light has been reduced.

1.4.1.3 Diode array spectrophotometers

One of the most widely employed detectors for HPLC is the diode array detector [11]. Significant advantages offered by diode array spectrophotometers over dispersive spectrophotometers are fast spectral acquisition times and increased wavelength precision.

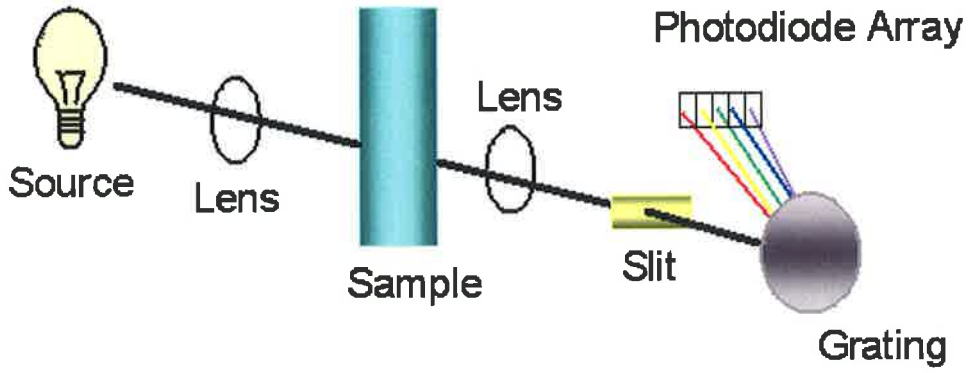

Figure 1.10 Schematic of diode array spectrophotometer.

In diode array spectrophotometers, the light from the source is collimated and passed through the sample. On passing through the sample, the beam is projected using a grating onto an array of ca. 200-500 equidistant light-sensitive diodes, each corresponding to a specific wavelength (range). Therefore all wavelengths are essentially measured simultaneously as shown in Figure 1.10.

A disadvantage of diode array spectrophotometers is the lower signal to noise ratio achieved in comparison to a single wavelength detector. This can be related to the smaller size photodiodes employed in a diode array spectrophotometer [12].

1.5 Light Emitting Diodes

1.5.1 Semiconductors

In materials science, solids are grouped according to their electrical properties into three categories: metals, insulators and semiconductors [13]. Metals conduct electric current at both high and low temperatures. Insulators do not conduct electric current, neither in high or low temperatures. At very low temperatures semiconductors act as insulators, when illuminated they act as conductors. Mobile electrons must be available for a substance to conduct an electric current.

If a material contains such "free" electrons in great numbers, the material is a conductor. The crucial aspect of a good conductor is that the highest energy band containing electrons is only partially filled [13].

In a material that is a good insulator, the highest band containing electrons called the valence band is completely filled. The next higher energy band, called the conduction band is separated from the valence band by a "forbidden" energy gap (band gap), E_g, of typically 5 to 10eV (Figure 1.11).

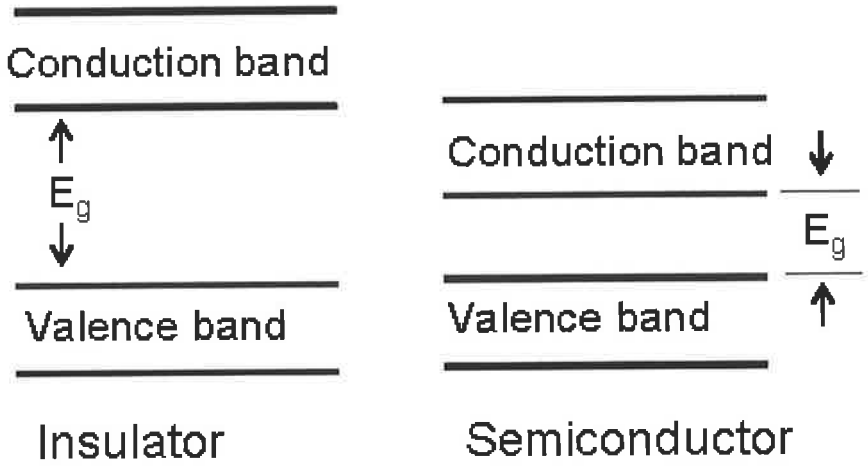

Figure 1.11 Energy bands for an insulator and a semiconductor.

The bands for a pure (or intrinsic) semiconductor such as silicon or germanium, are like that of an insulator except that the unfilled conduction band is separated from the valence band by a much smaller energy gap, E_g, typically of the order of 1eV as shown in Figure 1.11. At room temperature, a few electrons can acquire enough thermal energy to reach the conduction band and so a very small current may flow when a voltage is applied.

1.5.2 Doping

The most commonly used conductors in modern electronics are silicon (Si) and germanium (Ge). An atom of Si or Ge has four outer electrons that hold the atoms in the regular lattice crystal structure shown in Figure 1.12.

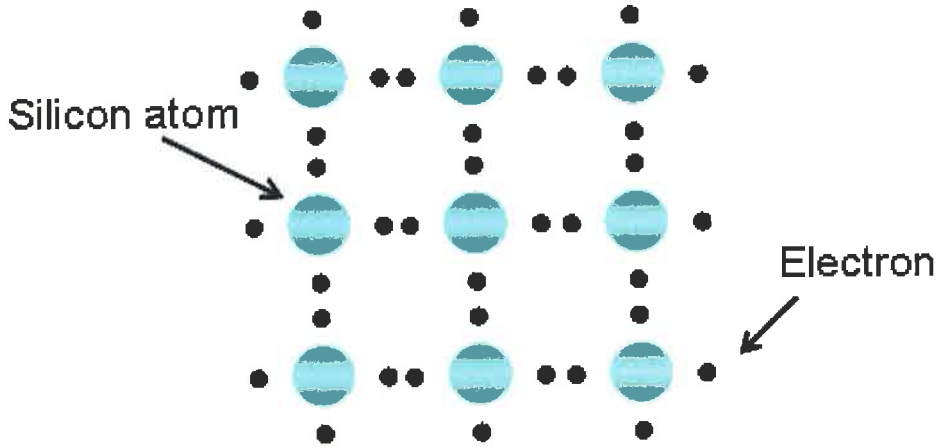

Figure 1.12 Schematic of a silicon crystal. Each silicon atom is surrounded by 4 outer electrons [13].

n-type doping

Introducing tiny amounts of impurities into the crystal structure known as doping the semiconductor can acquire useful properties. If the impurity has 5 outer electrons such as arsenic, there is an extra electron, which can move more freely, like the electrons in a conductor as shown in Figure 1.13. The extra electron doesn't fit into the crystal structure and so is therefore free to move about. This is called an *n*-type semiconductor because the negative charges (electrons) carry the electric current [13].

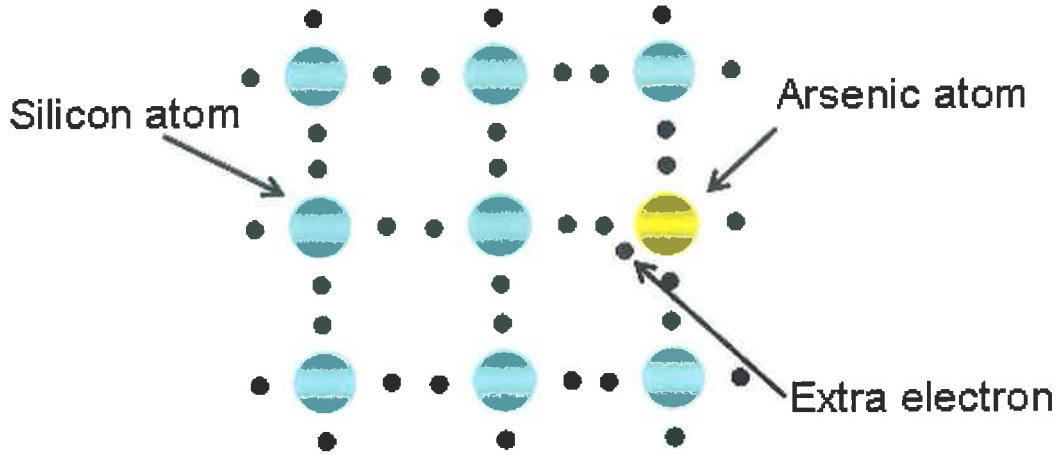

Figure 1.13 Schematic of silicon crystal doped with a few arsenic atoms.

There is only a small amount of energy required to produce a free electron and an arsenic ion. The free electron is donated to the crystal lattice and the arsenic ion is known as a donor [14].

p-type doping

Doping the semiconductor with an element with three outer electrons such as gallium is called a *p*-type semiconductor, as it is the positive holes that carry the electric current.

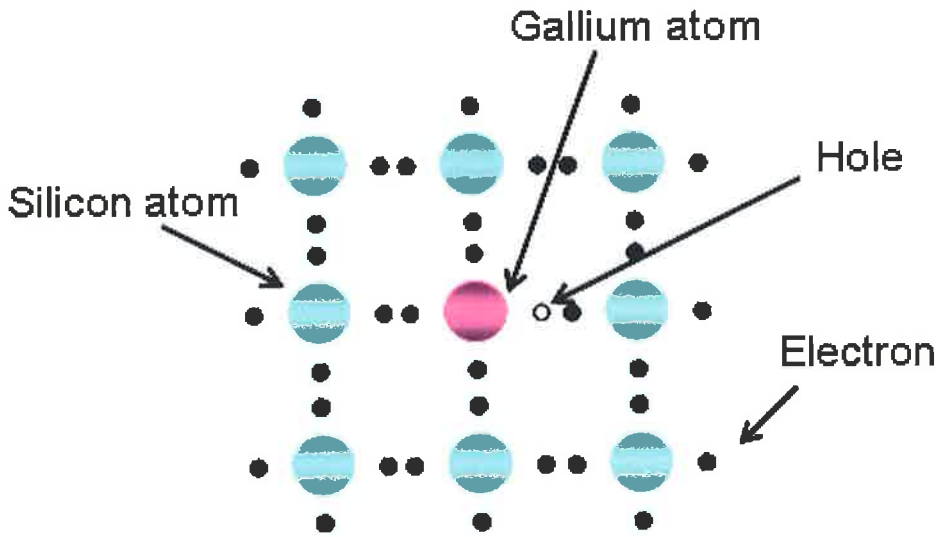

Figure 1.14 A schematic of a p-type gallium doped silicon semiconductor.

As shown in the Figure 1.14 there is a "hole" in the lattice structure near a gallium atom since it only has three outer electrons. Electrons from nearby Si atoms can move into this hole and fill it, leaving a hole where that electron had previously been. Similarly to the arsenic ion a gallium ion in silicon is known as an acceptor.

1.5.3 *p-n* junction

Separately the two semiconductors are electrically neutral. When joined, electrons in the region adjacent to the junction diffuse from the *n*-type into the *p*-type semiconductor, where they populate the holes. The *n*-type is therefore left with a positive charge, and the *p*-type acquires a net negative charge.

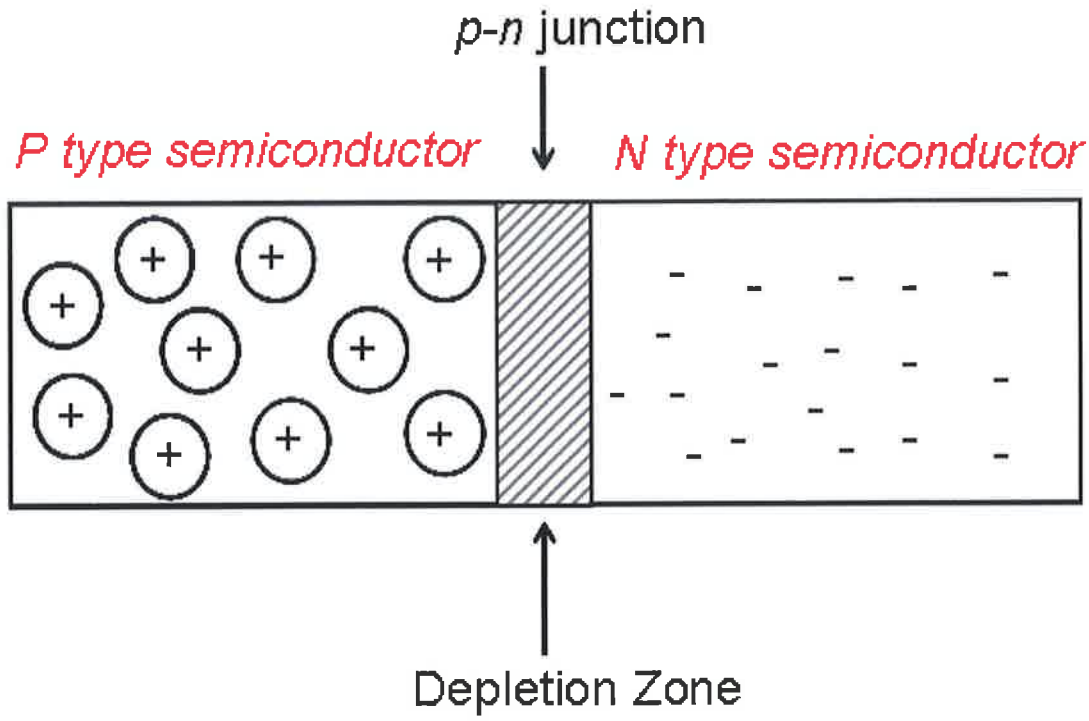

Figure 1.15 Schematic of a *p-n* junction

Equilibrium is achieved when the no further net carrier movement across the junction occurs. A region of space charge is now formed in the junction region, which is depleted of free carriers [13-15].

1.5.4 LEDs – Forward Biased p-n junction diode

If a battery is connected to a *p-n* junction diode with the positive terminal to the *p* side and the negative terminal to the *n* side the external voltage applied opposes the internal potential difference and the diode is said to be forward biased. If the voltage is large enough, (examples include 0.3 V for Ge, 0.6 V for Si) at room temp a current will flow.

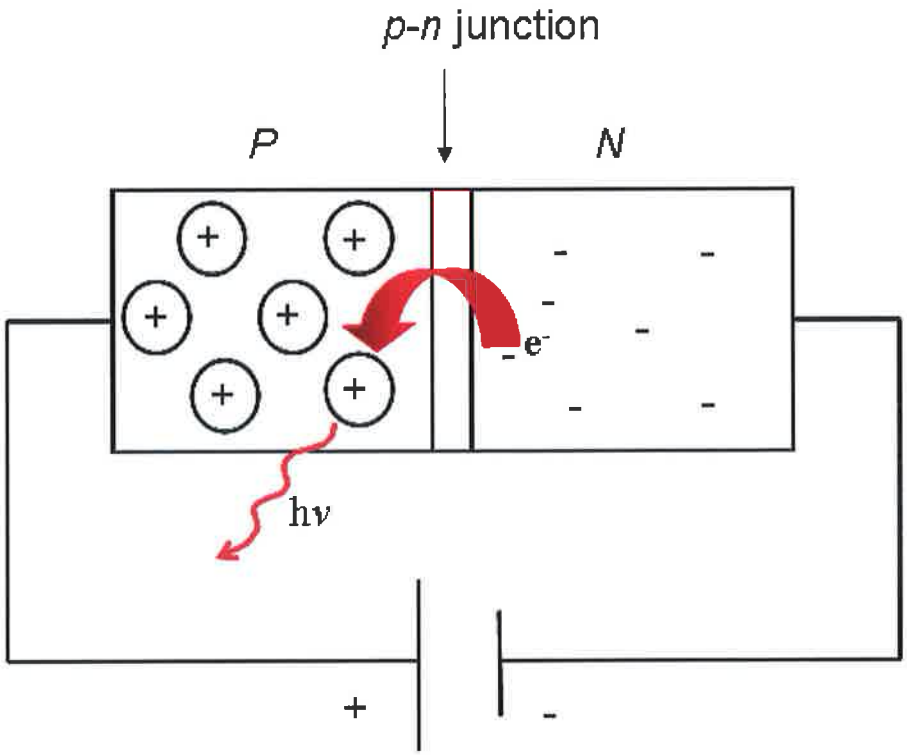

Figure 1.16 Schematic of a forward biased p-n junction.

The positive holes in the *p*-type semiconductor are repelled by the positive terminal of the battery and the electrons in the *n*-type are repelled by the negative terminal of the battery. The excess electron concentration on the *n* side enables the electrons to diffuse from *n* to *p*, and similarly holes can diffuse more easily from *p* to *n*. The holes and electrons meet at the junction, and the electrons cross over and fill the holes which emit a photon as shown in Figure 1.16. The positive terminal of the battery is pulling electrons off the *p* end forming new holes and the electrons are being supplied by the negative terminal at the *n* end. Consequently a large current flows through the diode [16]. Some common materials used to produce LEDs are listed in Table 1.3.

Table 1.3 Common III-V materials used to produce LEDs and their emission wavelengths [14]

Material	*Wavelength (nm)*
GaAs:Si	940
GaP	690
GaN	340, 430, 590
SiC	400-460

1.5.5 Photodiodes and LEDs – reverse biased *p-n* junction diode

When the diode is reverse biased as in Figure 1.17 the holes in the *p* end are attracted to the battery's negative terminal and the electrons in the *n* end are attracted to the positive terminal. The current carriers do not meet near the junction and ideally, no current flows.

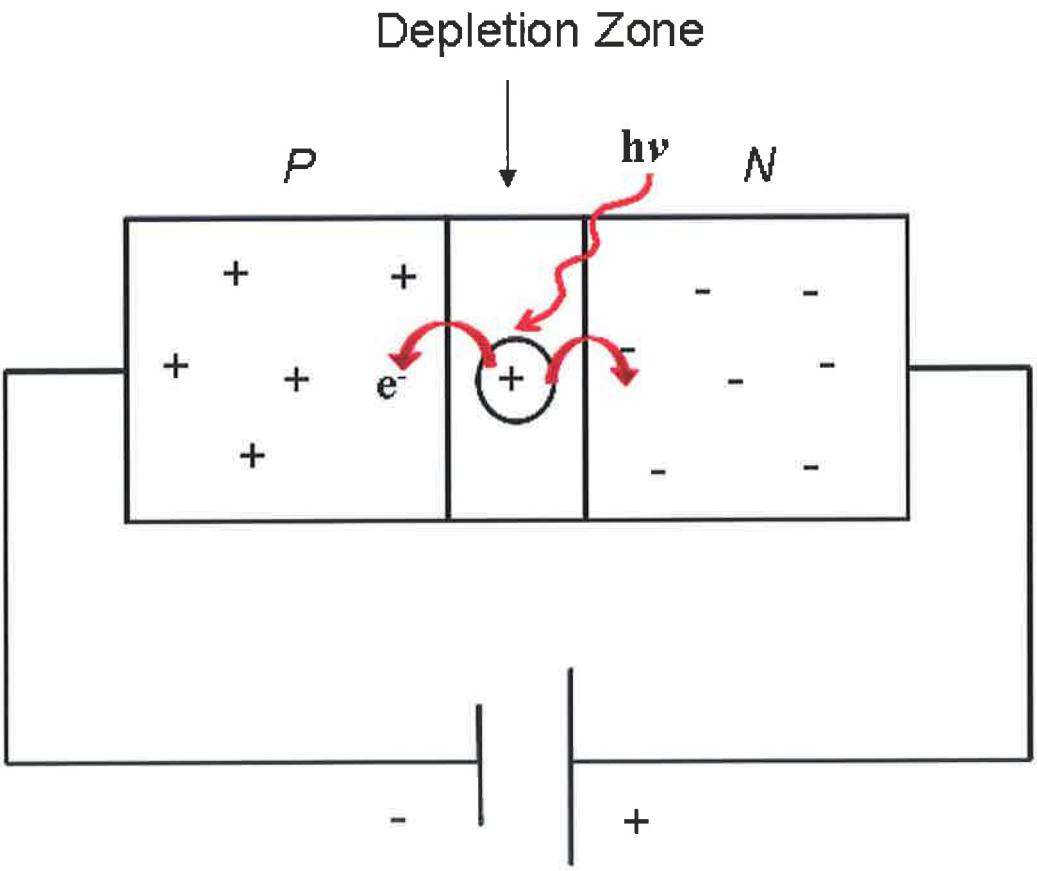

Figure 1.17 Schematic of a p-n junction in reverse biased mode.

An exposure to light can create electron-hole pairs if the photon energy is greater than the band gap energy, E_g producing a photocurrent as in a photodiode.

1.6 LEDs in Optical Sensing Devices

The communications revolution is now focusing on wireless communications between networked systems. In order to bring analytical measurements into this emerging 'networked world', appropriate analytical devices are required possessing the characteristics of reliability, low power consumption, low cost, autonomous operation capability and compatibility with wireless communications systems. The miniaturisation of analytical instruments using microfluidics is one strategy to move this concept forward. The advancement in LED sources and photodetector technologies provides compact, low power and low cost detectors for incorporating colorimetric analytical methods into remotely deployable devices [17,18].

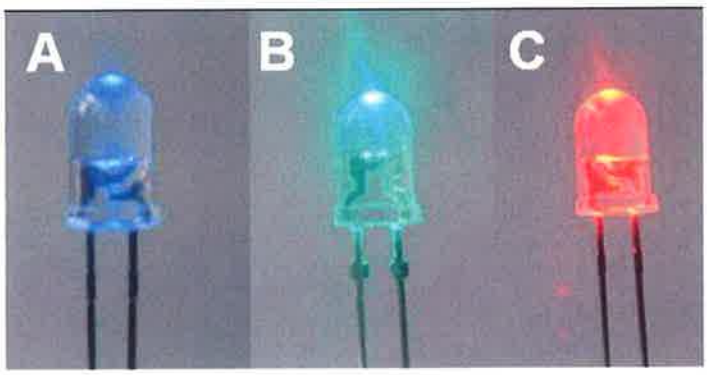

Figure 1.18 A variety of commercially available LEDs: (A) Blue LED (λ_{max} 430 nm), (B) Green LED (λ_{max} 525 nm) and (C) Red LED (λ_{max} 660 nm).

1.6.1 Introduction of LEDs in Optical Sensors

When Monsanto introduced the first commercial visible Light Emitting Diode (LED) in 1968 they produced only red light. Today LEDs in the region of 210-950 nm have been developed [15,19]. LEDs were first used for chemical analysis three decades ago [20]. LEDs offer a number of advantages compared to existing light sources in optoelectronic applications. These include increased lifetime, low cost, reduced power consumption, higher brightness, rugged construction, efficiency, flexibility, better spectral purity and suitable driving force [21]. The development of light-emitting

diodes (LED) resulted in the appearance of new optical radiation instrumentation such as that presented by Flaschka *et al.* (1973) [22], Anfält *et al.* (1978) [23] and Betteridge *et al.* (1978) [24].

LEDs have the ability to be coupled (for example, with waveguides or optical fibres) to a wide variety of detectors such as, photodiode-arrays (PDA) [25,26], photomultiplier tubes (PMT) [27,28], Ocean Optics spectrometer [29-31], light dependent resistor (LDR) [32-34], phototransistor (PT) [22,24,35], photodiodes [36-57] and LEDs [58-61].

1.6.2 LEDs coupled with Phototransistors as a detector

LED based photometers were first proposed by Barnes in 1970 (as stated by Flaschka *et al.* [22]) and the concept of an LED-phototransistor (PT) photometer with a 30 cm path length flow through cell was realised in 1973 [49].

The first practical LED based flow through photodetector of this type was described by Betteridge *et al.* [24]. A simple photometric detector consisting of a gallium phosphide light-emitting diode as the light source and a silicon phototransistor as the sensor, as shown in Figure 1.19 was developed. Determinations of metal ions at the parts per billion (ppb) level were achieved using PAR reagent. RSD of 1.5% was obtained which was further reduced to less than 1% with lower flow rates.

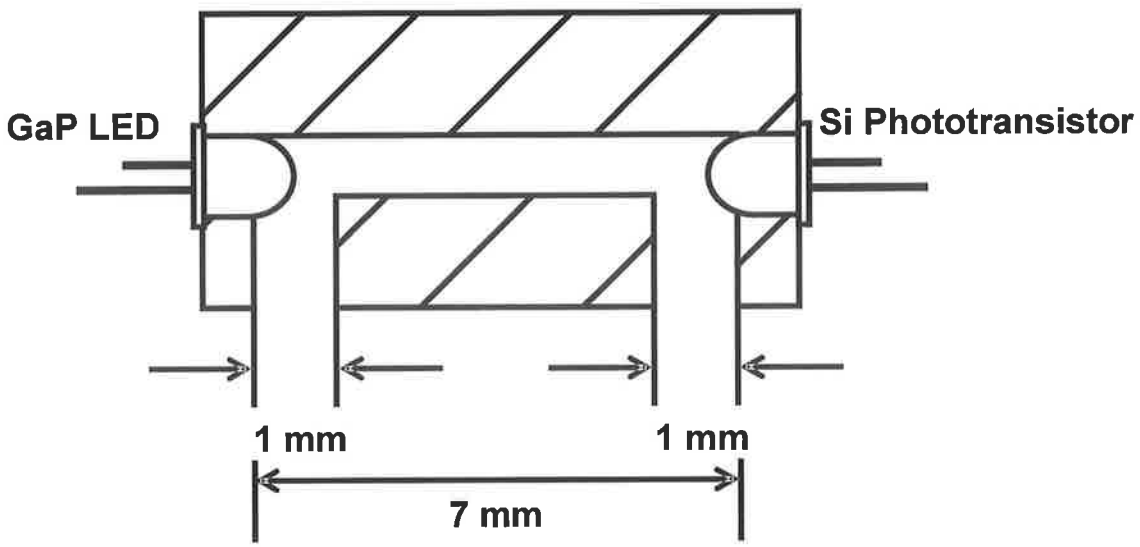

Figure 1.19 Sectional view of the transducer cell [24]

The development of this detector was of particular relevance to flow injection analysis (FIA) [62]. Phototransistors and photodiodes can both be used as detectors with phototransistors typically providing 1.5-2 orders of magnitude greater current output albeit the response is slower [49]. This does not necessarily mean that the use of phototransistors results in better S/N however, as Dasgupta *et al.* observed that phototransistors are typically more noisy than photodiodes.

1.6.3 LEDs coupled with Photodiodes as a detector

Anfält *et al.* reported the first LED coupled with a photodiode in 1976 [23]. They constructed a photometric probe instrument to determine the total alkalinity of seawater. The results obtained were found to be in good agreement with the reported potentiometric method with the added advantage of faster measurements.

To date one of the most commonly used detectors in photometry is the photodiode [43-45]. Dasgupta *et al.* have published several papers on the variations and applications of this system [46-49,51,52].

Hauser *et al.* [38-40,55] have contributed significantly to the advancement of LED as a light source and were the first to report the use of a blue LED as a spectroscopic source [39]. Hauser *et al.* describe the development of a transducer using a blue LED and a photodiode as a detector. The performance of the device was tested for commonly used spectrophotometric procedures for Cr, Mn, Zn, Fe and Cl and compared with conventional molecular absorption spectroscopy. The transducer was also investigated as a detector in flow-injection analysis. Light was passed through by the use of 1 mm plastic optical cable, allowing the location of the opto-electronic components removed from the wet chemical part as shown in Figure 1.20 [39].

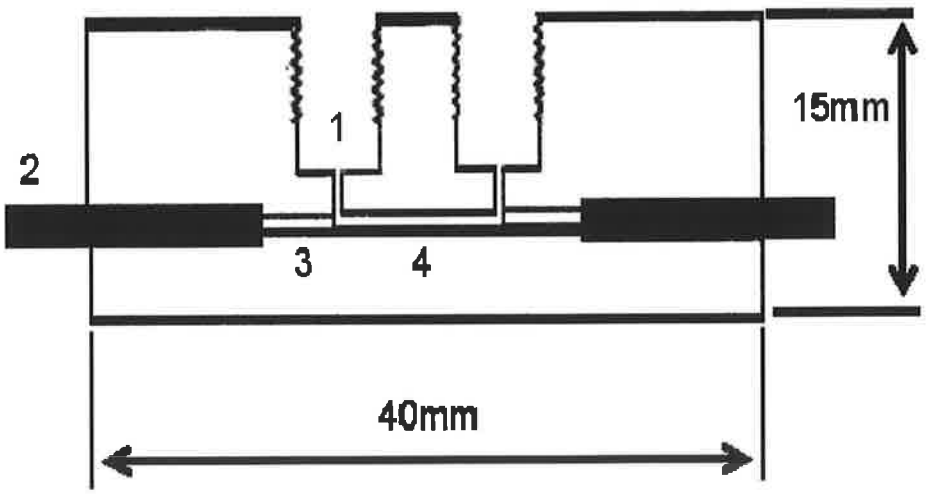

Figure 1.20 Cross-sectional view of the transducer cell: (1) inlet/outlet, (2) fibre optic cable, (3) stripped section of the fibre optic cable, (4) optical path [39].

Photodiodes are extremely versatile and have been employed in various configurations, such as flow through detectors in flow injection analysis (FIA) [37,40,62], separation systems [27,36,63-65] and probe photometers [23,66].
Photodiodes are favoured for their rapid response and wide linear range of transmitted light, which are typically three and four orders of magnitude better, respectively, than those of phototransistors [67].

1.6.4 LEDs coupled with LDRs as a detector

When used as a light source, the LED is usually configured in transmittance mode, however, Matias *et al.* [32] developed a simple low cost reflectometer for colorimetric diffuse reflectance measurements using a green LED as the light source and an LDR as a detector (Figure 1.21). The quantitative analysis of nickel, in a catalyst, using dimethylghyoxime as a colorimetric reagent, was used to test the device. An RSD% of ~ 6% was achieved.

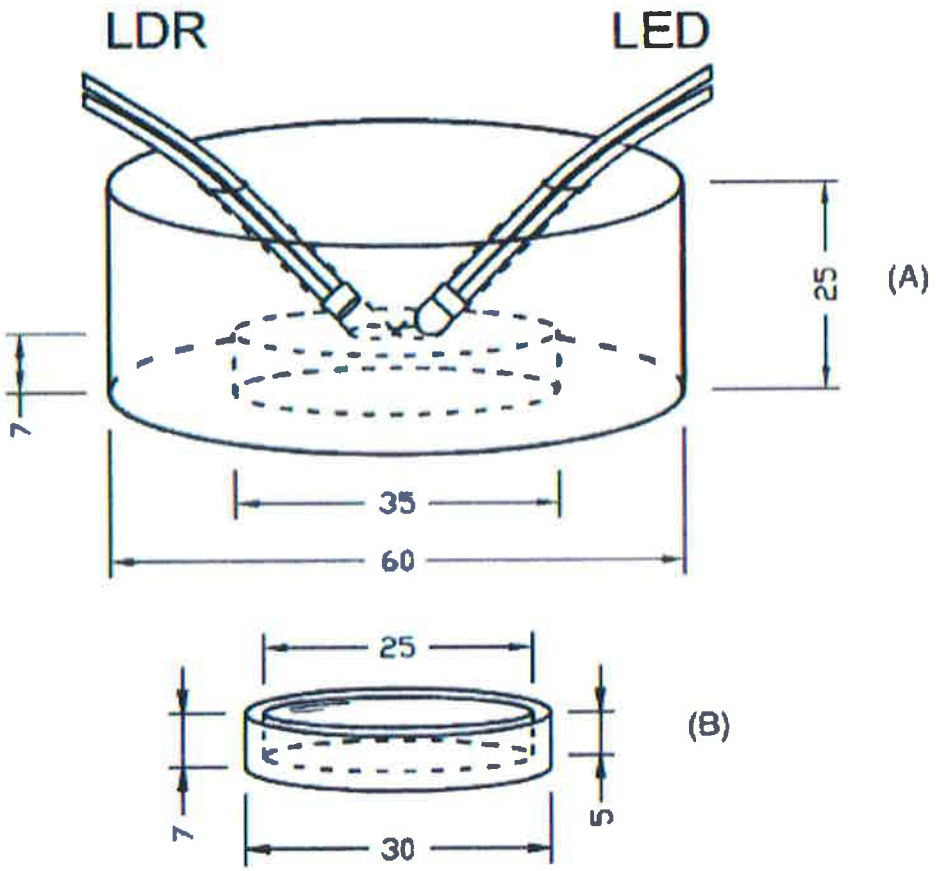

Figure 1.21 Scheme of the proposed reflectance device. (A) is the part made in black PTFE, where the LED and the LDR are placed, in the same plane, at an 45^0 angle with respect to the reflecting surface and at an angle of 90^0 with respect to each other. (B) is the reaction and reflection cell made in white PTFE. The indicated dimensions are in millimetres [32]

The LED and LDR were positioned in the same plane at 45^0 with respect to the reflecting surface at an angel of 90^0 between them. The reflectance was measured for $Ni(DMG)_2$ precipitate obtained from the nickel solution. A linear range from 0-1.25 x 10^{-3} mol L^{-1} was achieved.

1.6.5 Dual LEDs as a light source

A significant number of LED-photometers describe a fixed wavelength for a predetermined purpose. A change of wavelength had to be effected by physically changing the light source. This limitation has been caused by the difficulty in coupling light from more than one source into a single detector cell [55].

The use of two LEDs allows for the correction of colour change, RI [51] or turbidity [51,52], which was first introduced by Worsfold *et al.* [50]. A flow injection manifold based on reagent injection into the sample stream was described for the determination of phosphate in natural waters. A double beam photometric detector incorporating two LEDs at 660 nm and photodiodes enclosed in a $20cm^3$ box was employed as shown in Figure 1.22. The response is linear over the range 0-2000 μgl^{-1} phosphate-phosphorus ($R^2 = 0.9992$) and limit of detection (σ) is 12 μgl^{-1} phosphorus.

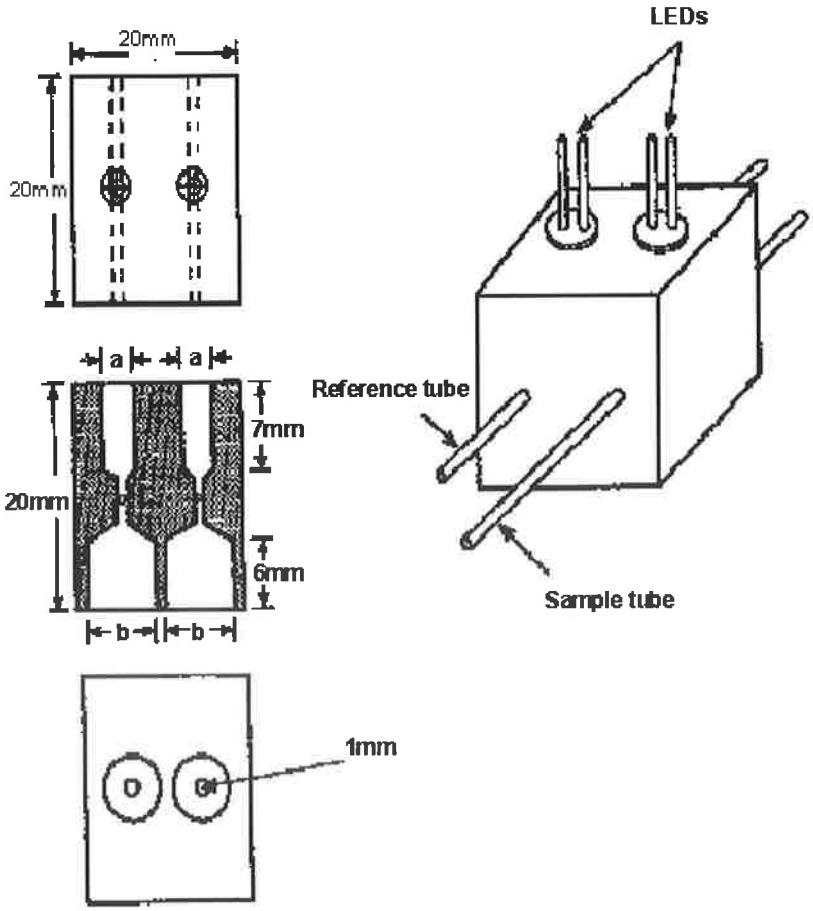

Figure 1.22 Flow cell housing made of aluminium. Bores: (a) 5mm nominal, to fit the LEDs; (b) 8.5mm nominal to fit the photodiodes [50].

The sample was pumped through the reference channel prior to the injection of reagent in order to compensate for physical changes in the sample stream (e.g. colour or turbidity).

1.6.6 Bi- / Tri- colour LEDs as a light source

The most popular type of tri-colour LED has a red and a green LED combined in one package with three leads. They are called tri-colour because mixed red and green light appears to be yellow and this is produced when both the red and green LEDs are on.

Figure 1.23 Schematic of Tri-colour LED [68].

Figure 1.23 shows the construction of a tri-colour LED. The centre lead (k) is the common cathode for both LEDs, the outer leads (a1 and a2) are the anodes to the LEDs allowing each one to be lit separately, or both together to give the third colour. The use of bi- / tri- colour LEDs allows for a compact rugged multi-wavelength spectrophotometer which allows the analysis of multicomponent samples simultaneously or for the correction of turbidity [52-54].

Huang *et al.* [52] investigated the use of a bi-colour LED as a light source coupled with a photodiode as a detector and calibrated the system using a series of bromothymol blue solutions. A red / green dual wavelength LED with emission maxima at 630 and 565 nm were used. The R^2 values of 0.9994 and 0.9999 were achieved respectively with overall RSD values of 0.25% and 0.24% for red and green colours. Such a detector with a red / yellow LED coupled with the FIA technique for the determination of 10^{-6} M levels of Co was also carried out.

1.6.7 Multi - LEDs as a light source

The use of a multi-LED photometer [55-57,61] allows a wide range of the electromagnetic spectrum to be covered simultaneously or individually without manually changing the LEDs.

Hauser *et al.* [55] employed a fibre optic coupler to guide the light from up to 7 LEDs into a single measuring cell. This single photometer allowed the detection of Al, Cu, NH_3, Cu, Ca, chromium, phosphate and nitrite using colorimetric methods. The coupler is used to merge the light from one of the 7 input channels into 2 output fibres. One is brought to the measuring and the other is brought to the reference photodiode as shown in Figure 1.24.

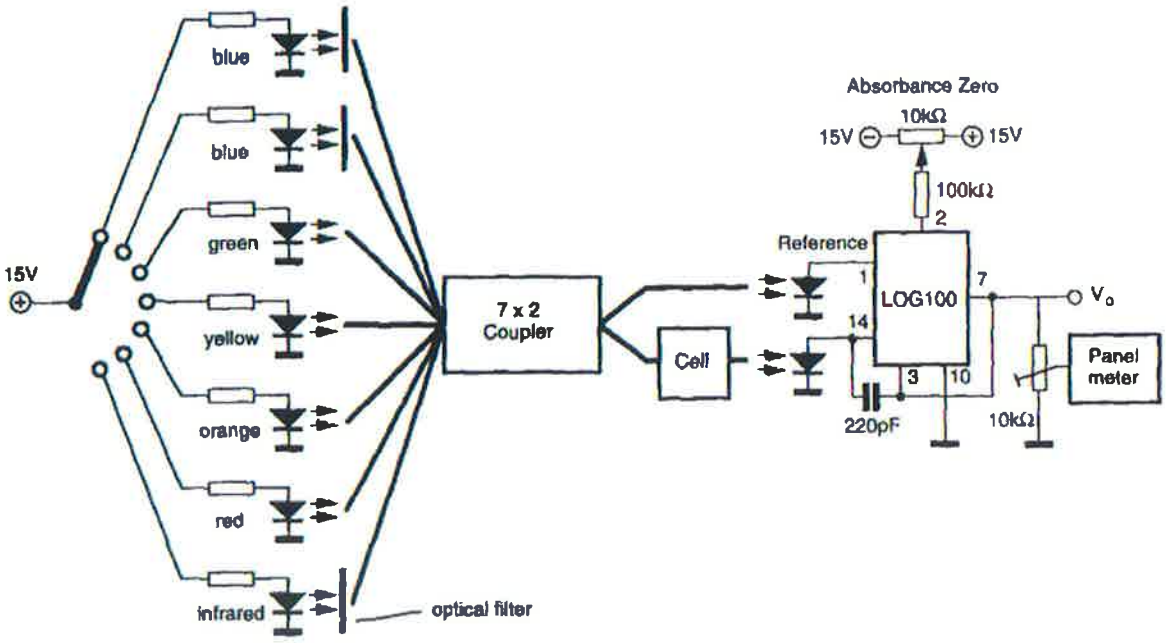

Figure 1.24 The circuit diagram for the multi-LED photometer [55]

1.7 LEDs as Light Detectors

The concept of employing an LED as a light detector was first proposed by Mims [69,70]. Using a simple circuit that contained an operational amplifier to measure the photocurrent obtained by a reversed biased LED, the LED sensor was applied to the detection of sunlight.

The novel use of an LED as both light source and detector for chemical analysis was developed by Lau *et al.* [58-61]. The emitter LED is forward biased while the detector LED is reverse biased. Instead of measuring the photocurrent directly, a simple timer circuit is used to measure the time taken for the photocurrent generated by the emitter LED to discharge the detector LED from 5 V (logic 1) to 1.7 V (logic 0) to give digital output directly without using an A/D converter. The paired emitter detector-diode (PEDD) sensor is very versatile and can be configured in a variety of ways to measure absorbance or reflectance as shown in Figure 1.25.

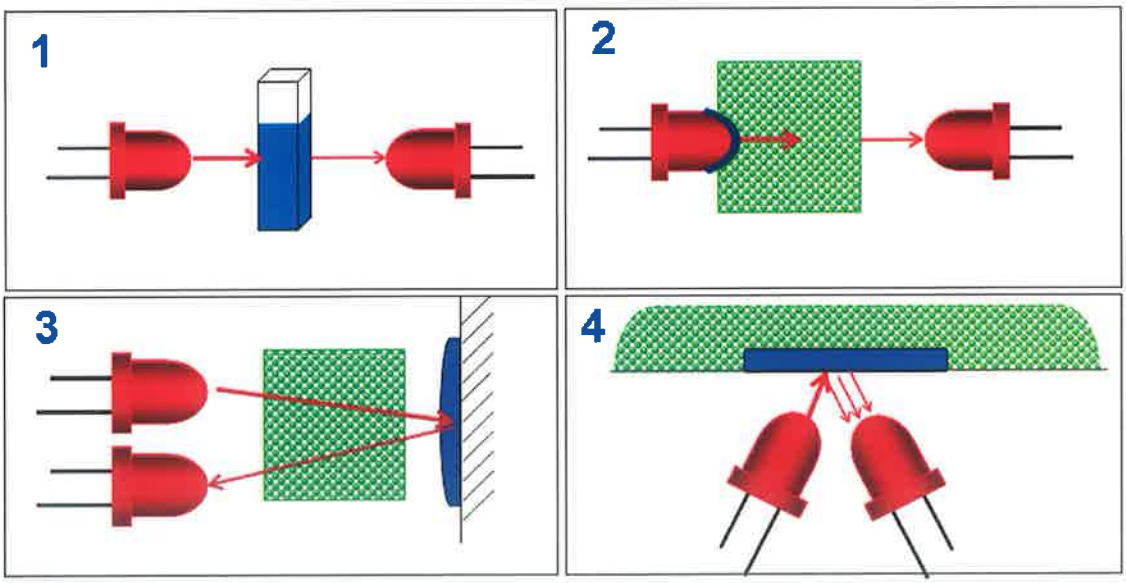

Figure 1.25 Schematic of various PEDD configurations; (1) Sample picks up reagent – direct transmission, (2) Immobilize reagent onto surface of LED source/detector, (3) Immobilize dye directly onto fabric and (4) Back-end reflectance or evanescent wave sensing of immobilised dye

Lau *et al.* constructed a pair of fused LEDs at a 90^0 angle with respect to each other to form an optical probe used for colour and colour based pH measurements as shown in Figure 1.26. The PEDD device was used in reflectance mode and placed directly into the sample of interest. Sensor function is based on the level of light received by the detector diode, which varies with the reflectance of the interface between the device and its environment, or the chemochromic membrane that covers the LEDs [58,61]. The sensor was successfully applied for colour based pH measurements and also colour detection of dyes.

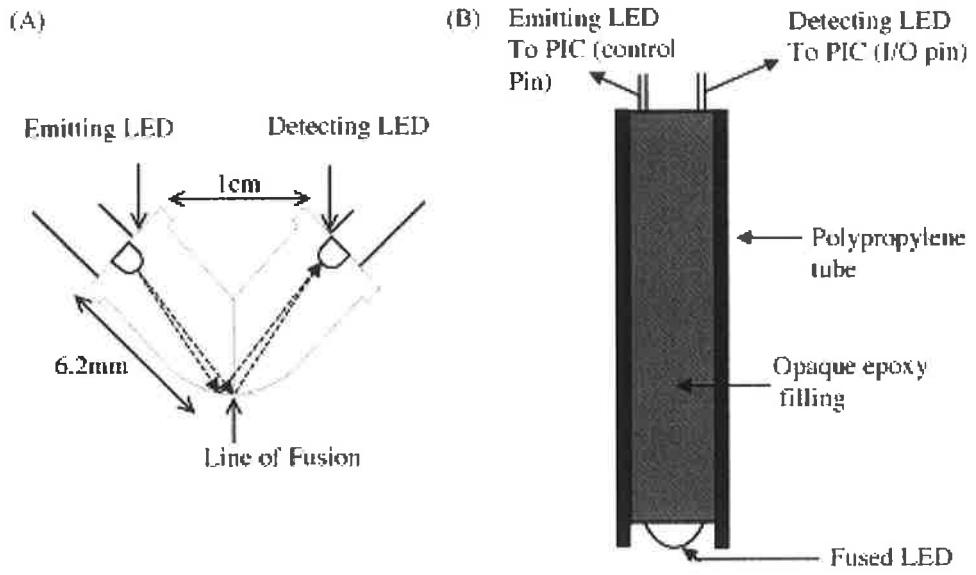

Figure 1.26 Schematic of (A) fused-LEDs and (B) cross-section of the optical probe [58].

The 'disco photometer' has been developed by Lau *et al.* as an alternative reflectance based optical sensor configuration [61]. The sensor employs an array of LEDs as the light sources, which surround the centre detector LED as shown in Figure 1.27. This approach allowed the analysis of multiple dyes separately and as dye mixtures.

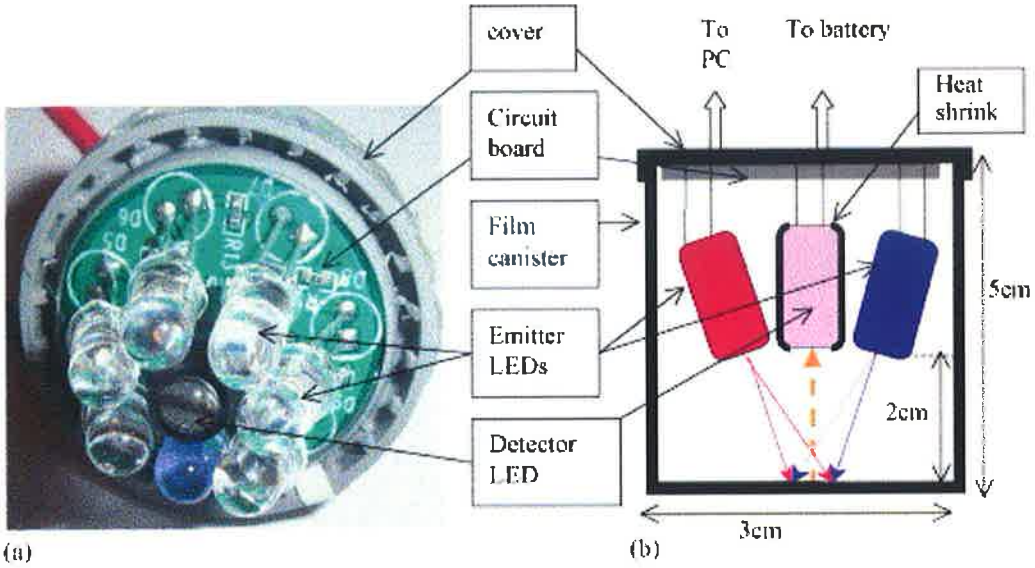

Figure 1.27 A picture of the 'disco photometer' (a) and a sketch of the disco photometer to illustrate the light detection pathway (b)[61].

A distinct advantage of using the paired emitter detector-diode optical sensor in comparison with widely used LED-photodiode system is that the LED–LED combination is a less expensive in both the cost of components (35 US cents per sensor) and the cost of the signal transduction circuitry [58]. The measuring technique employed by the PEDD device does not require a relatively expensive A/D converter as the output seen by the microprocessor is a direct pulse-duration-modulated signal. Additional advantages to the PEDD device is the size, low power consumption (can operate in microwatts range), can detect low absolute light levels (ca. 0.0001 lx), responds to a broad spectral range (280 to >900 nm) and can achieve good S/N ratio.

CHAPTER 2

PHOTOMETRIC DETECTION IN FLOW ANALYSIS USING INTEGRATED PAIRED EMITTER-DETECTOR DIODES

2. Photometric Detection in Flow Analysis using Integrated PEDDs

2.1 Introduction

Optical sensing is one of the most active areas of research in analytical chemistry. This is largely due to the availability of inexpensive, compact, low power consuming components such as LEDs. LEDs are the most efficient sources of coloured light in almost the entire visible range [18]. Presently LEDs covering a broad spectral range of 280-950 nm are commercially available [15]. Figure 2.1 illustrates some common LED wavelengths employed in optical sensors. The emission spectrum for each LED is normalised to a 0-1 range by dividing the emission values obtained by the maximum value. Typically a narrow emission bandwidth at half maximum (BWHM) of 10-30 nm is achieved.

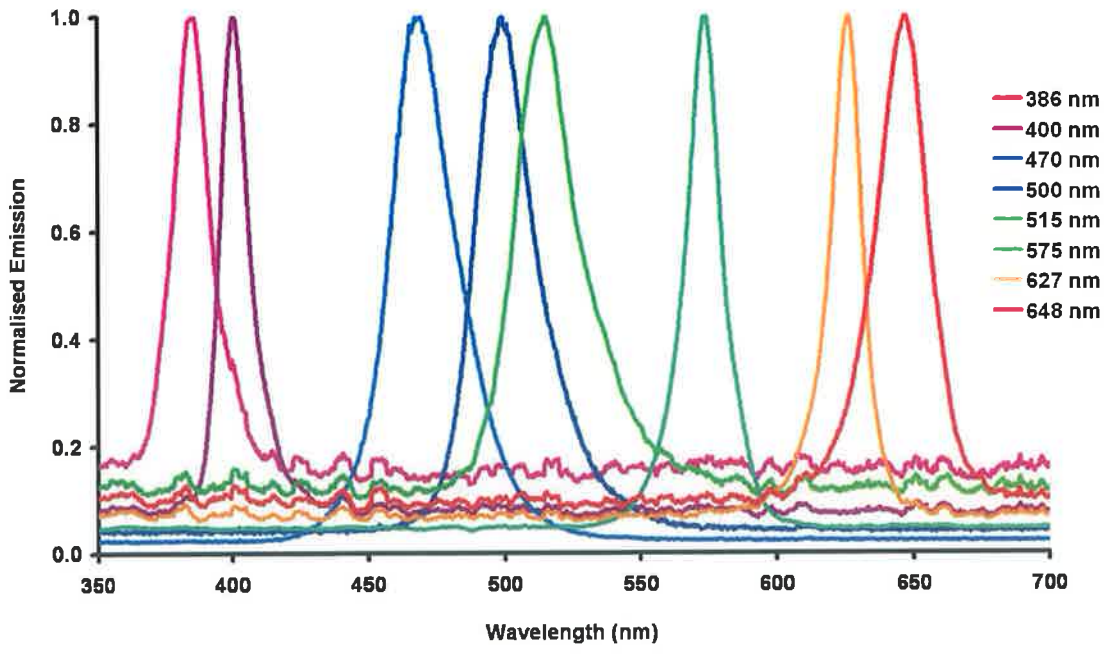

Figure 2.1 UV-vis spectral range covered by a variety of commercially available LEDs

In general optical sensors are configured using an LED as the light source coupled with a photodiode as the detector [36-39]. Typical optical sensors often comprise of expensive, cumbersome, high power components [71]. This chapter describes a novel inexpensive optical sensing device for flow analysis based on the use of two LEDs, whereby one is employed as the light source and the other as the light detector.

2.2 *Paired Emitter-Detector Diode (PEDD)*

2.2.1 Analytical Model

In this study the measurement is based on the following theoretical model, which has been derived by Lau *et al.* [58,59]. A mathematical model has been developed to relate this sensing strategy to conventional analytical measurements based on the Beer-Lambert Law.

The detector LED is reversed biased to 5V and is discharged by the photocurrent i_{light} generated by the emitter LED. Another discharging process also occurs naturally in parallel in which the circuit discharges itself in complete darkness via a small (dark) current i_{dis}, which is normally insignificant compared to i_{light}. Typically, under strong illumination, we have found the discharge time to be in the region of microseconds, whereas in complete darkness, it discharges in ca. 300 milliseconds.
In general, the total discharge time, t for the LED equivalent circuit can be described as

$$t = Q \Big/ \left(i_{dis} + i_{light}\right) \qquad \textbf{Equation 2.1}$$

where Q is accumulated charge (a constant)

When $i_{light} >> i_{dis}$

$$t = Q/(i_{light})$$ **Equation 2.2**

i.e. the time taken to discharge the capacitor is inversely proportional to the intensity of the incident light, as the quantity of electric charge (Q) is a constant.

When light passes through a coloured sample solution, the transmitted light intensity (I) is reduced relative to the incident light intensity (I_0) due to absorbance of the light energy by the analyte at a specific wavelength. The sample absorbance (A) is related to these intensities and the sample concentration in accordance to the Beer-Lambert Law;

$$\boldsymbol{A = \log\left(I_0/I\right) = \log\left(t/t_0\right) = \varepsilon Cl}$$ **Equation 2.3**

where t_o is the time to discharge to a preset voltage in the absence of the coloured species in solution (a constant), l is the optical path length through the solution (cm), ε is the molar extinction coefficient ($Lmol^{-1}cm^{-1}$) at a particular wavelength and C is the concentration of the absorbing species ($molL^{-1}$), therefore we can say;

Equation 2.3 predicts that if the Beer-Lambert law holds and the dark current from the capacitor is negligible compared to the photo-discharge current, then the concentration of the absorbing analyte is proportional to the log of the discharge time, with the intercept being log (t_o).

2.2.2 The Circuitry

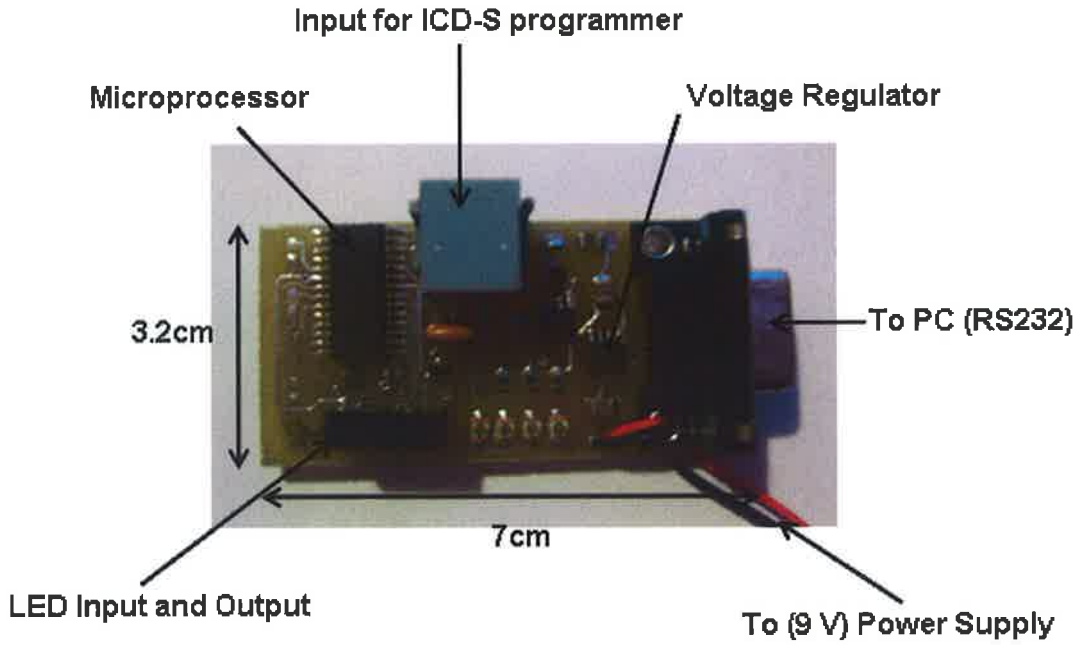

Figure 2.2 Photograph outlining the layout of the programmable interface controller (PIC) board.

Microcontroller

A microcontroller is a computer-on-a-chip used to control and monitor electronic devices [72]. Typically a microcontroller has a number of general purpose input/output (I/O) pins, internal timers, an analog-to-digital converter (ADC) and support for standard communication protocols such as RS-232. The features provided by a microcontroller are controlled by a piece of software running on the chip, and this code can be easily updated by simply reprogramming the device. Therefore microcontrollers offer a very flexible platform for developing devices that incorporate sensing, external control and communications. A microcontroller also offers the advantages of being small in size (Figure 2.2), inexpensive and low power. Within this project the PIC is used to drive an emitter LED, drive and monitor a detector LED, average the sensor readings and send these over a serial connection (RS-232) to a PC. The sample rate, average rate and data output rate are all controlled in software running on the PIC, and therefore can easily be modified. Support for this is provided

by an In Circuit Debugger for serial ports (ICD-S), which allows for easy downloading and debugging of programs for PIC microcontrollers [73].

Voltage Regulator

A voltage regulator is a small device or circuit that regulates the voltage fed to the microprocessor, providing a stable, constant voltage from a power supply operating at a higher voltage. In this case a 9 V battery was used in combination with a 5 V regulator to provide a stable 5 V source to the PIC and associated components on the board.

LED Control

The emitter LED was driven by an I/O pin on the PIC via a current limiting resistor. Output intensity of the emitter LED was controlled by the value of the resistor. The LED light detector in output mode was charged to 5 V for 100 μs and then switched to input mode. The photon flux from the emitter LED strikes the detector LED, generating a small photocurrent that discharges the capacitor voltage. The total amount of photocurrent produced is in the order of nanoamperes. The photocurrent produced is not measured directly as this would require an expensive nanoamperometer to measure it accurately. The measurement taken is the decay time (μs) taken for the discharge process to go from an initial value of 5 V (logic 1) to a preset value of 1.7 V (logic 0) [58-60]. A typical discharge profile of an LED with an emission λ_{max} of 610 nm was obtained employing a Fluke Scopemeter® (Fluke Corporation, WA, USA) by Lau *et al.* [59]. As shown in Figure 2.3 the LED was charged up to 5 V for 500 μs before being discharged under fluorescent lighting.

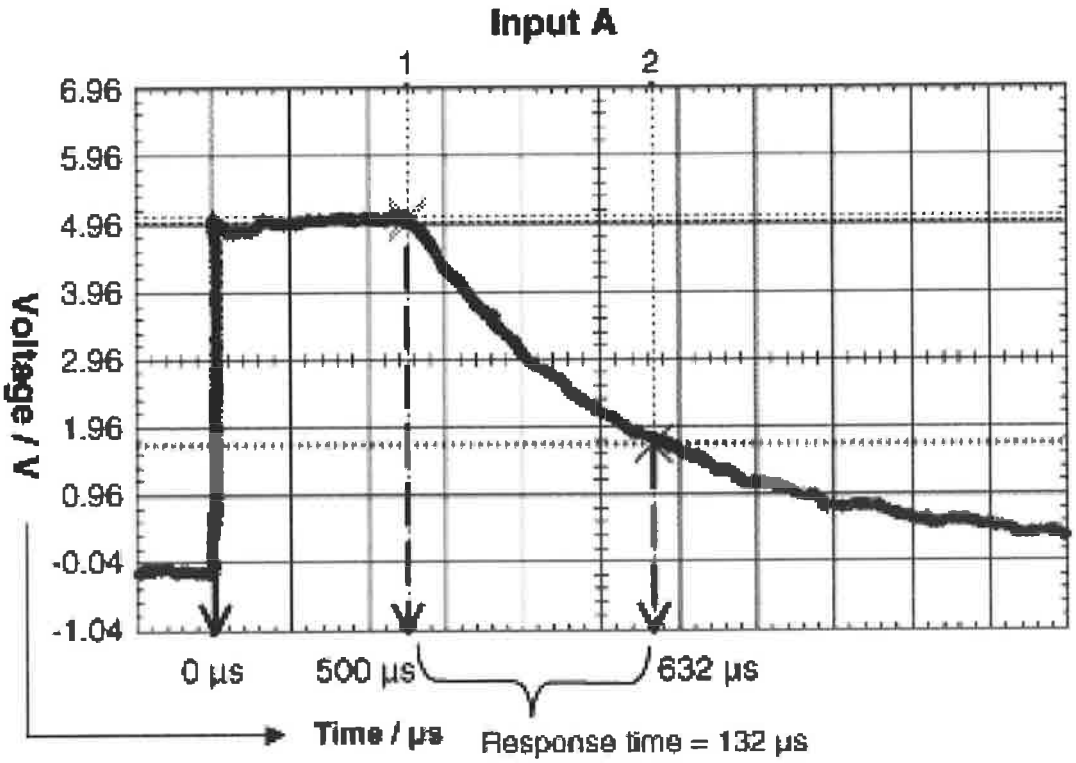

Figure 2.3 Typical discharge curve for an LED charged up to 5 V and then discharged to a threshold of 1.7 V under artificial lighting (fluorescent tube) [59].

The time taken to discharge the capacitor voltage from 5 V (logic 1) to a preset voltage of 1.7 V (logic 0) was ca. 132 µs. The measurement is subject to interference from ambient light, therefore in order to minimise this effect the measurement is performed with the emitter LED sequentially pulsed on and off as outlined in Equation 2.4.

Actual output = Decay time (LED on) – Decay time (LED off) **Equation 2.4**

2.2.3 Data Capture

For this work the PIC was programmed to measure a range between 0 – 65504 µs. Each data point reported is an average of 16 data points. The averaged discharge time was reported at a rate of 1 data point/second. Data is transferred to a PC via a RS232 port (Figure 2.2), and captured with the HyperTerminal software, and then saved as a text file for further analysis using Excel™ (Microsoft, Inc., USA) [60].

2.2.4 Project Aim

In most microanalytical systems neither the light source nor the photodetector is integrated into the same substrate as the fluidic channel network. This is because the integration of all components necessary for performing a total chemical analysis is very complex [74]. The work presented herein focuses on a novel integrated optical sensor, the PEDD.

The aim of this work is to design and develop an optical sensing device for colorimetric flow analysis that employs an LED as a light source and light detector. This work is based on the measuring technique developed by Mitsubishi Electronic Research Laboratory (MERL) in collaboration with DCU [58].

The LEDs are configured in transmittance mode at 180^0 with respect to each other. An optical flow cell was constructed using the two LEDs, which allowed sample to flow through the co-joined LEDs. This work will demonstrate the integrated PEDD flow analysis system is useful for colorimetric analysis. The PEDD has the advantages of being small, inexpensive, highly sensitive, low power and requires small sample volumes. These are desirable characteristics for miniaturized field-deployable devices used in autonomous monitoring systems [15].

Calibration of the integrated optical flow cell was carried out using pH indicator dyes. The flow rate, dynamic range, sensitivity and limits of detection were investigated. The PEDD flow cell was used for pH determination in the range of pH 2.26 – 8.10 using the indicator dye bromocresol green (BCG). The pK_a of the BCG was also examined using this technique.

2.2.5 PEDD for Colorimetric Flow Analysis

The following section outlines the design and fabrication of the PEDD flow cell (A) single inlet and (B) dual inlet.

Single Inlet PEDD Flow Cell

The optical device was fabricated using two identical (5 mm) LEDs (λ_{max} at 621 nm) (Kingbright, France), with the emission shown in Figure 2.4. To facilitate comparison the emission and absorbance are normalised to a 0-1 range by dividing values by the maximum emission and absorbance achieved.

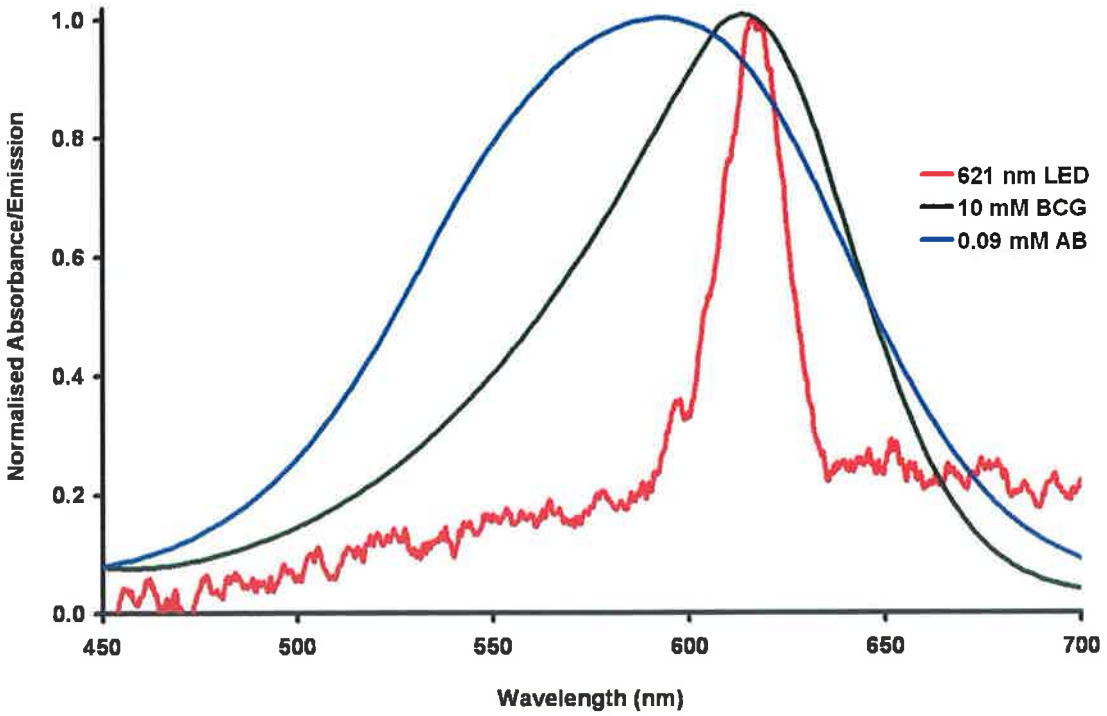

Figure 2.4 Emission spectrum (λ_{max} 621 nm) of the LED used in the integrated PEDD flow analysis device (red line), the absorption spectra (λ_{max} 616 nm) of 10 mM bromocresol green at pH 7 (green line) and 0.09 mM aniline blue in 0.1 M HCl (λ_{max} 600 nm) (blue line).

The original length of each LED was 10 mm. The PEDD sensor was prepared by first cutting 0.25 mm from the tips of each LED to give a flat top, rather than the usual

curved surface. The surface of the LEDs was then sanded down using general purpose, fine-grade paper (Homebase, Dublin) to make them smooth and flat before bonding. Using a drill bit of size 1.3 mm, a channel was machined into each LED to a depth of 1.8 mm, resulting in a path length of 3.6 mm as shown in Figure 2.5.

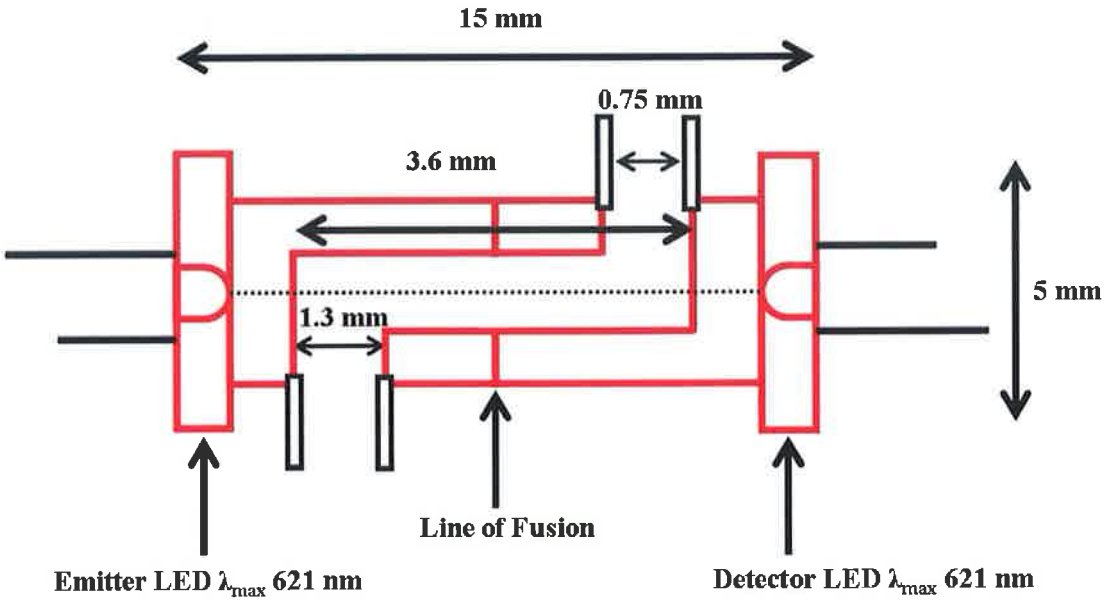

Figure 2.5 A schematic of the integrated PEDD flow analysis device used for colorimetric detection.

An inlet and outlet were also machined using the same method. Prior to bonding, the two LEDs were accurately aligned to ensure the line of fusion was perfectly round. The LEDs were then fused together using UV curable epoxy glue (Edmund Scientific: Orland 81 extra fast curing, USA), and placed under UV light (380 nm) for 30 min. Green peek tubing (i.d. 0.75 mm) was placed at either end of the channel and sealed into place using araldite epoxy glue (Homebase, Dublin). The PEDD flow cell was left to dry at room temperature for a further 30 min. The optical cell was then painted black to reduce stray light effects. The total length of the PEDD was now 15 mm.

Dual Inlet PEDD Flow Cell

The dual inlet flow cell was fabricated in a manner similar to that of the single inlet PEDD flow cell. Two (5 mm) red LEDs (λ_{max} at 621 nm) (Kingbright, France), with emission properties as shown in Figure 2.6, were employed. The LEDs were prepared as outlined in the above section (Single Inlet Flow Cell) however the inlet and outlet were machined in an alternative configuration. A longer path length of 4 mm was employed to increase sensitivity.

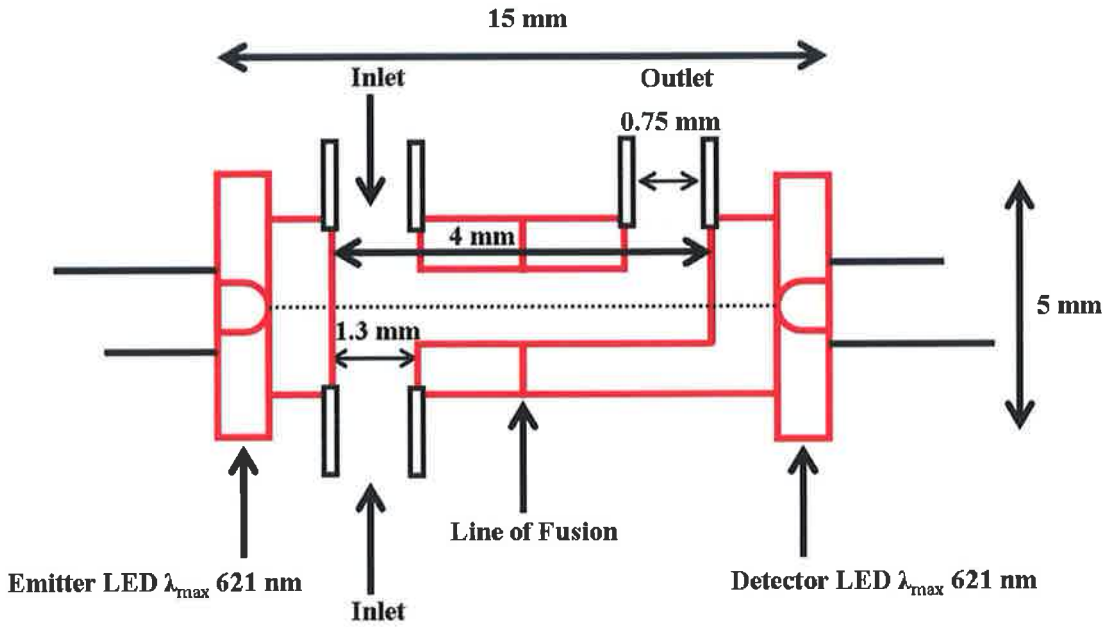

Figure 2.6 Schematic of a dual inlet PEDD flow cell.

Using a drill bit of size 1.3 mm, a channel was machined into each LED to a depth of 2 mm, resulting in a path length of 4 mm as shown in Figure 2.6. Two inlets and an outlet were also machined using the same method. Orange peek tubing (i.d. 0.5 mm) was placed at each inlet and outlet channel and sealed into place using araldite epoxy glue (Homebase, Dublin) as shown in Figure 2.7. The bonding process was repeated as described in the previous section.

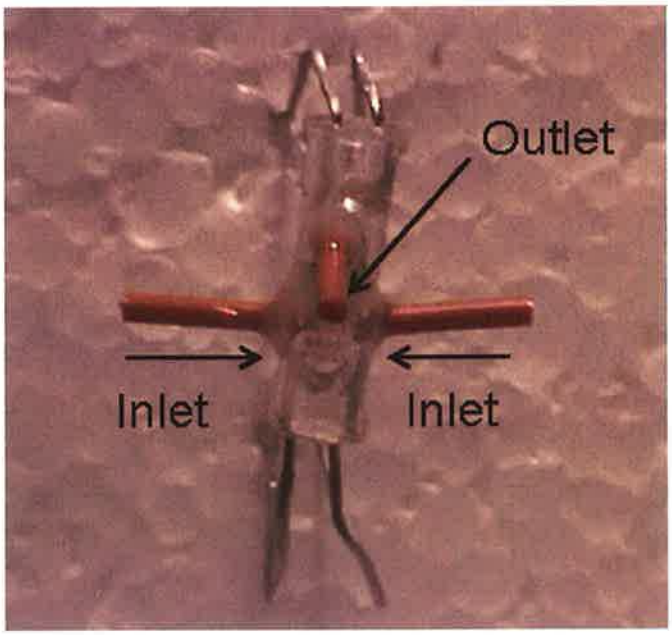

Figure 2.7 Photograph of the dual inlet PEDD flow cell using two red LEDs (λ_{max} 621 nm).

2.3 Experimental Procedure

The following section discusses the experimental procedures needed to evaluate and validate the PEDD flow cell.

2.3.1 Chemicals

All reagents used were of analytical grade.

- pH 7 buffer tablets (Lennox, Dublin)
- Bromocresol green sodium salt (Sigma Aldrich, Dublin)
- Aniline Blue diammonium salt (Sigma Aldrich, Dublin)
- Ultrapure Water (Millipore Ireland B.V., Cork, Ireland)
- Hydrochloric acid 32% (Fisher Scientific UK Ltd., Leicestershire)
- Sodium Hydroxide pellets (Sigma Aldrich, Dublin)

2.3.2 Reagents and Solutions

pH 7 buffer solution

A 100 mL pH 7 buffer solution was prepared from Milli-Q ultrapure water and pH 7 buffer tablets. Following protocol 1 buffer tablet was dissolved in 100 mL of deionised water and sonicated for approximately 20 minutes [75].

0.1 M Hydrochloric Acid

A 500 mL 0.1 M HCl solution was prepared by drop wise adding 5.70 mL of conc. HCl to ca. 200 mL of ultrapure water in a volumetric flask and then diluting to the mark.

Bromocresol Green stock

A stock solution of 10 mM BCG was prepared by dissolving 0.72 g of dye in a 100 mL pH 7 buffer solution from which dilutions were prepared.

A series of dye solutions each containing 40 μM BCG at various pHs (2.26-8.10) were also prepared.

Aniline Blue stock

A stock solution of 10 mM aniline blue was prepared by dissolving 1.97 g of dye in a 250 mL 0.1 M HCl solution from which dilutions were prepared.

2.3.3 Validation of the PEDD flow system

An experiment was carried out to investigate if the LED detector of the PEDD device demonstrated a similar response as that of a well established light dependent resistor (LDR) to an LED light source [59]. The LDR measures the photocurrent generated by the LED light source (kΩ), while the PEDD response is expressed as discharge time (μs) i.e. time taken to discharge detector diode junction capacitance from 5 V to 1.7 V due to the incident photocurrent.

The following procedure was used to determine if the optical response from the PEDD was both linear and indirectly proportional to the light intensity of the emitter LED.

Procedure

A simple measuring system was constructed using a hollow black cylindrical tube (5 mm).

LED-LED sensor

Two LEDs (λ_{max} 621 nm) were placed at either end of the cylinder, 1 cm apart as shown in Figure 2.8. The data obtained from the PEDD device was captured as outlined in section 2.2.3.

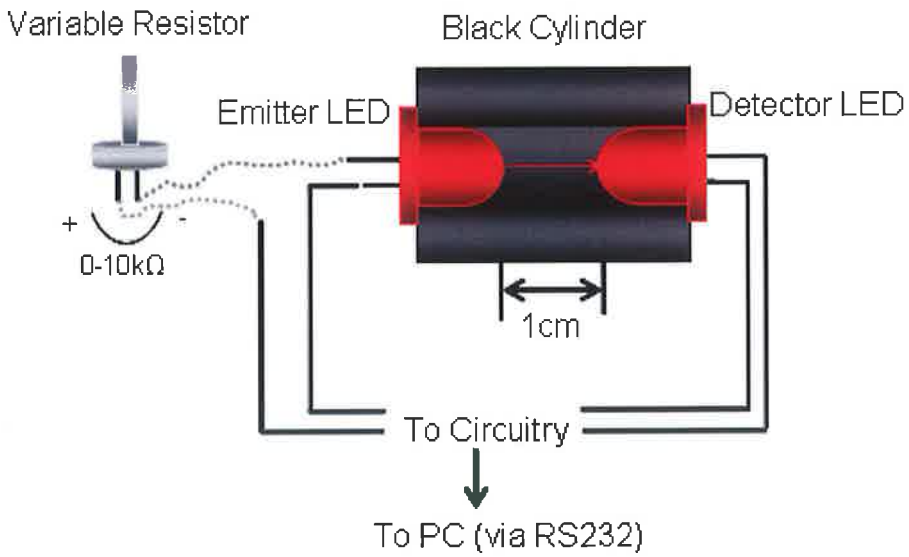

Figure 2.8 Schematic of the LED-LED device test setup.

LED-LDR sensor

The second cell was similar to that of the LED-LED configuration. An LDR was placed at the detector end of the cylinder (Figure 2.9) 1 cm from the emitter LED. The data obtained from the LDR was captured by employing a multimeter (Agilent

34401A) to measure the photocurrent of the detector. The multimeter provided a digital output of the signal which was transferred to a PC for display and post-run processing.

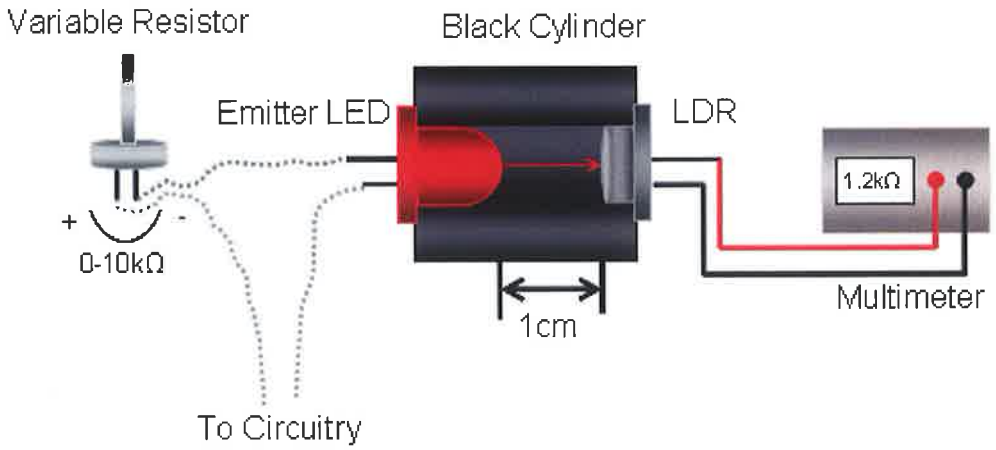

Figure 2.9 Schematic of LED-LDR device test setup.

A variable resistor (0-10 kΩ) (Radionics, Ireland) was attached directly to the emitter LED to investigate the effects of varying the light intensity of the emitter LED by controlling the amount of electrical current passing to the emitter LED.
All experiments were carried out in triplicate. Both sets of data acquired were plotted using Microsoft ™ Excel software.

2.3.4 Optimisation of the PEDD light intensity

A study has been carried out to investigate the effect of varying illumination intensity on the sensitivity of the detector [60]. The emitter intensity was controlled by using a variable resistor connected directly to the emitter LED as the amount of electrical current passing to the emitter LED is directly proportional to emission intensity. Therefore an increase in the resistance results in a decrease in the light intensity of the emitter LED, which in turn results in an increase in the time taken to discharge the detector LED. A 20 μM BCG ($\varepsilon = 1.2 \times 10^4$ $Lmol^{-1}cm^{-1}$) at pH 7 solution was selected

as it gave a significant change in discharge time, (Δt) of ca. 100 μs compared to the pH 7 background at 0.5 kΩ.

Procedure

- A pH 7 buffer solution was passed through the flow cell for ca. 4 minutes at a flow rate of 0.6 mL/min.
- This was then followed by 20 μM BCG at pH 7 for ca. 4 minutes at a flow rate of 0.6 mL/min.
- Various light intensities brought about by varying the resistance on the emitter LED as in section 2.3.3 were examined and the results obtained were shown in Figure 2.14.
- The data was captured as described in section 2.2.3.
- All experiments were carried out in triplicate.

2.3.5 Investigation of flow effect on the PEDD response

In this study the PEDD device was incorporated into a Flow Injection Analysis (FIA) system to determine the effect of flow on the response. A concentration of 20 μM BCG at pH 7 was selected as the sample of choice as it had good colour density, therefore allowing it to be easily detected. The emission spectrum of the flow cell (λ_{max} 621 nm) efficiently overlaps with the absorption spectrum of bromocresol green (λ_{max} 616 nm) as shown in Figure 2.4.

Procedure

- A 5020 Rheodyne low pressure injector valve (Sigma Aldrich, Dublin) was employed.
- The carrier solution was pH 7 buffer solution.
- A sample loop of 100 μL was used.

- 20 μM bromocresol green at pH 7 was passed through the PEDD flow cell at various peristaltic pump flow settings (mL/min).
- Data was captured as outlined in section 2.2.3.
- The experiment was carried out in triplicate.

2.3.6 Calibration of the PEDD flow cells with Bromocresol Green and Aniline Blue

A study was carried out involving the calibration of a change in colour intensity or concentration of pH indicator dyes, (A) bromocresol green at pH 7 in the single inlet PEDD flow cell [60] and (B) aniline blue in 0.1 M HCl in the dual inlet PEDD flow cell.

Bromocresol green and aniline blue were selected due to their large molar extinction coefficients of 1.2 x 10^4 and 7.5 x 10^4 $molL^{-1}cm^{-1}$ respectively. The light intensity transmitted in the flow cell was measured with an LED (λ_{max} 621 nm), which efficiently overlaps the absorbance spectra of bromocresol green (λ_{max} 616 nm) and aniline blue (λ_{max} 600 nm) as shown in Figure 2.4. The emission spectrum of the LED was obtained by using S2000 Ocean Optic spectrometer (OOIBase 32™, Ocean Optics, Inc., Dunedin, USA).

Procedure

Bromocresol Green

- Various concentrations of BCG were made up in pH 7 buffer solution.
- Each concentration was passed through the PEDD flow cell for ca. 4 minutes per sample, at a flow rate of 0.6 mL/min.
- All experiments were repeated 8 times.
- The data was captured as outlined in section 2.2.3.

Aniline Blue

- Various concentrations of aniline blue were made up in 0.1 M HCl.
- Each concentration was passed through the PEDD flow cell for ca. 4 minutes per sample, at a flow rate of 0.6 mL/min.
- All experiments were repeated 4 times.
- The data was captured as outlined in section 2.2.3.

2.3.7 Comparison of results with a platewell reader

As a comparison study the absorbance of the same bromocresol green and aniline blue concentrations (section 2.3.6) were acquired using the μQuant™ platewell reader (Bio – Tek Instruments, Inc., USA) [60].

Figure 2.10 200 μL aliquots of increasing concentrations from 0.5 μM-20.5 mM of BCG at pH 7 in a 96 plate well.

Procedure

- A 200 μL aliquot of each concentration ranging from 0.5 μM-20.5 mM for both bromocresol green and aniline blue were taken and added to a 96 plate well (Figure 2.10).
- Each concentration was added to the 96 plate well in triplicate.
- The absorbance was scanned from 400 – 700 nm.
- The data was captured using the μQuant™ software and saved as a text file for later analysis using Microsoft ™ Excel software.

2.3.8 Using PEDD to Monitor Colour Changes

The PEDD flow cell was used to monitor the pH-dependent colour change of BCG [60]. The pK_a of the BCG was also examined using this technique. A dye concentration of 40 μM was chosen to demonstrate this application as it has good colour density. Using the indicator dye bromocresol green (BCG) a range of pHs (2.26 – 8.10) were examined as shown in Figure 2.11.

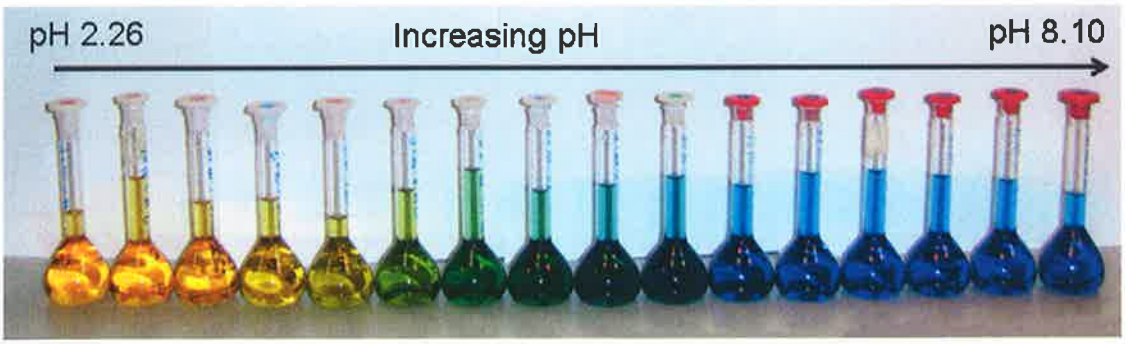

Figure 2.11 Range of pHs of 40 μM BCG from pH 2.26 to pH 8.10.

Procedure

- The pH of the 40 μM sample was varied by the dropwise addition of concentrated HCl or 4 M NaOH.
- The pH of the solution was monitored with the use of a pre-calibrated Metrohm pH meter (Metrohm Ireland Ltd., Tallaght, Dublin 24). The procedure for the calibration of the pH meter is outlined in the Appendix (section 7.1).
- After the addition of acid or base the solution was left to stir for approximately 3 minutes before passing through the PEDD flow cell.
- The measuring time was approximately 4 minutes for each pH examined.
- The data was captured as outlined in section 2.2.3.

2.4 Results and Discussion

2.4.1 Validation of the PEDD flow system

Experiments were carried out to verify the response characteristics of the LED light sensor. Figure 2.12 shows the linear relationship between increasing load (current limiting) resistance on an ultrabright LED emitter (λ_{max} 621 nm) and the resulting light intensity observed by a light dependent resistor (LDR). A maximum relative standard deviation (R.S.D.) of 1.33% was achieved. This demonstrates that the LDR response (R) is increased linearly with the current limiting resistance. The response of the LDR to varying light intensity is well established such that light intensity (i_{light}) is inversely proportional to the current limiting resistance, i.e. $i_{light} \alpha 1/R$.

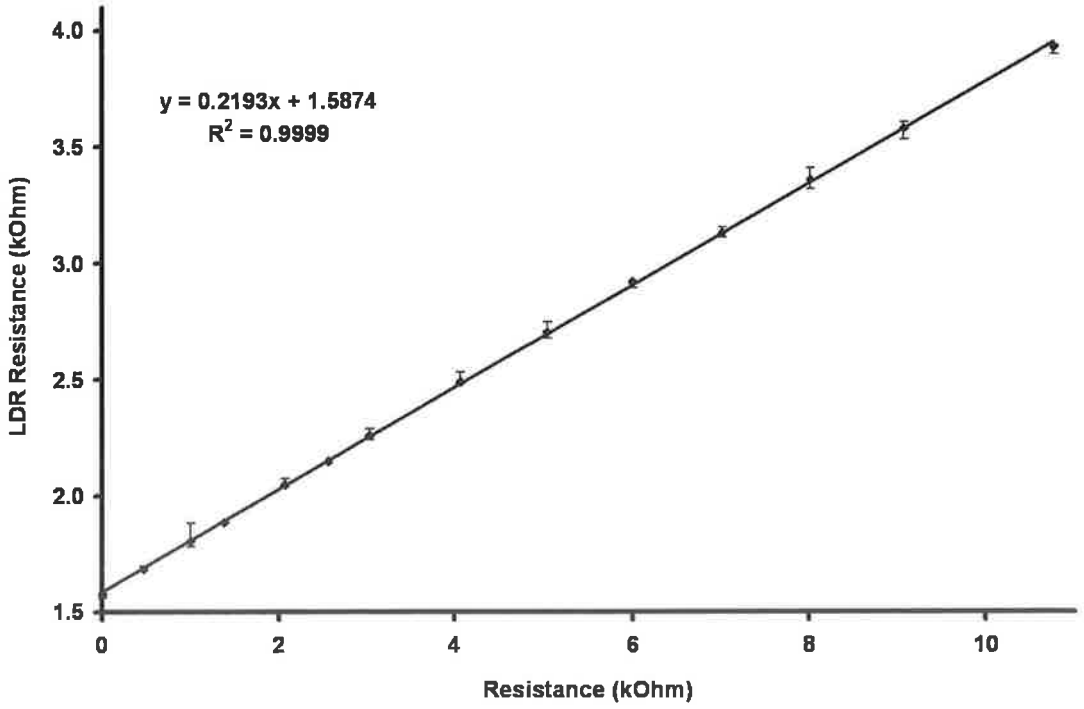

Figure 2.12 A linear plot obtained by increasing current limiting resistance applied to an LED emitter circuit which results in a change in light intensity measured with a light dependent resistor. The error bars represent the standard deviations for $n = 3$.

This experiment was repeated by substituting the LDR with an LED light sensor (λ_{max} 621 nm). Figure 2.13 shows that the discharge time t increases linearly with current limiting resistance, which may be expressed as the reciprocal of light intensity, and is therefore in agreement with equation (i.e. $t \propto 1/i_{light}$). A maximum R.S.D. of 2.1% was achieved. The increase in discharge time is not linear below 15 kΩ as the light intensity of the ultrabright red LED is too intense.

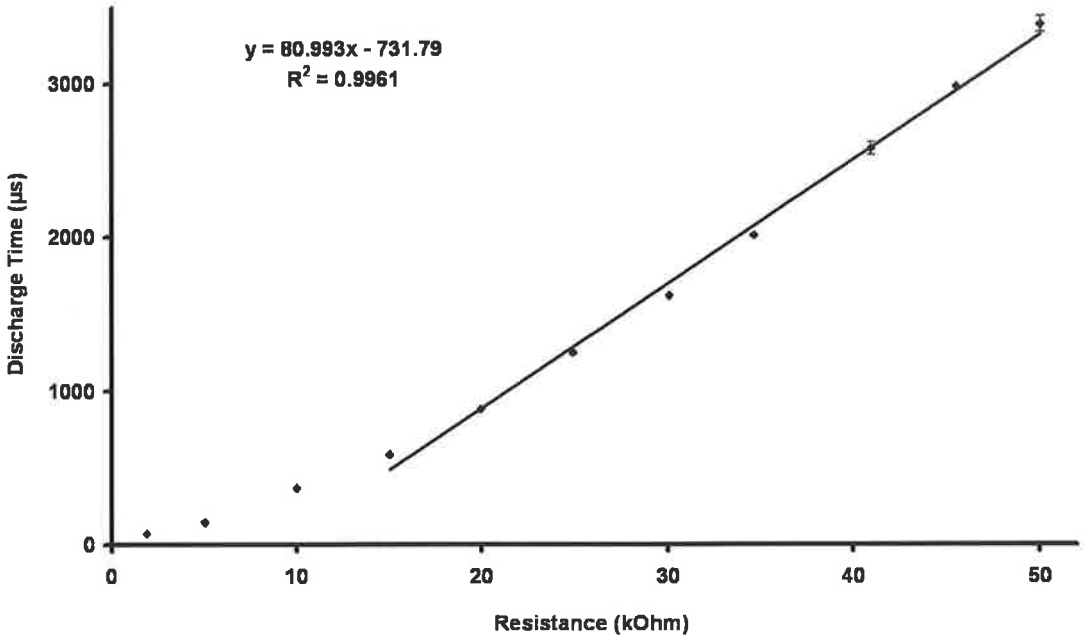

Figure 2.13 Discharge time of detector LED vs. the current limiting resistance used to control intensity of the emitter. The error bars represent the standard deviations for $n = 3$.

2.4.2 Optimisation of the PEDD light intensity

A study was carried out to investigate the effect of varying illumination intensity on the sensitivity of the detector. The emitter intensity was controlled by using a variable resistor connected directly to the emitter LED as the amount of electrical current passing to the emitter LED is directly proportional to its emission intensity. Various light intensities brought about by varying the resistance were examined and the results obtained were shown in Figure 2.14.

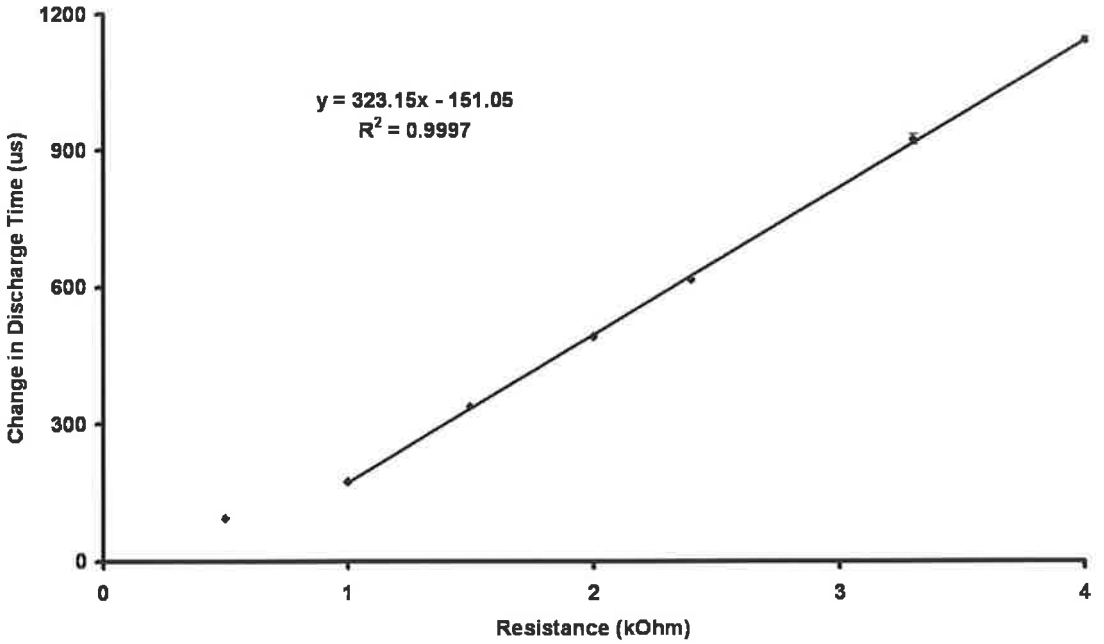

Figure 2.14 A plot to illustrate the effect of varying light intensity on the change in discharge time detected for 20 μM BCG and pH 7 buffer. The error bars represent the standard deviations for $n = 3$.

The data showed that increasing resistance to reduce light intensity resulted in a linear increase in the change of response obtained (Δt) from pH 7 buffer to 20 μM BCG. The largest R.S.D. (n = 3) shown in Figure 2.14 is ca. 5.5%. The maximum preset discharge time of the circuitry is 65504 μs. While decreasing the light intensity increases the change in discharge time (i.e. peak height), an increase in the baseline discharge time is also achieved. At resistances above 4 kΩ the circuitry has approached maximum discharge time.

Figure 2.15 shows a comparison of the reproducibility of the system with (1) minimal resistance (6 Ω) and (2) at 2 kΩ for 8 μM BCG at pH 7.

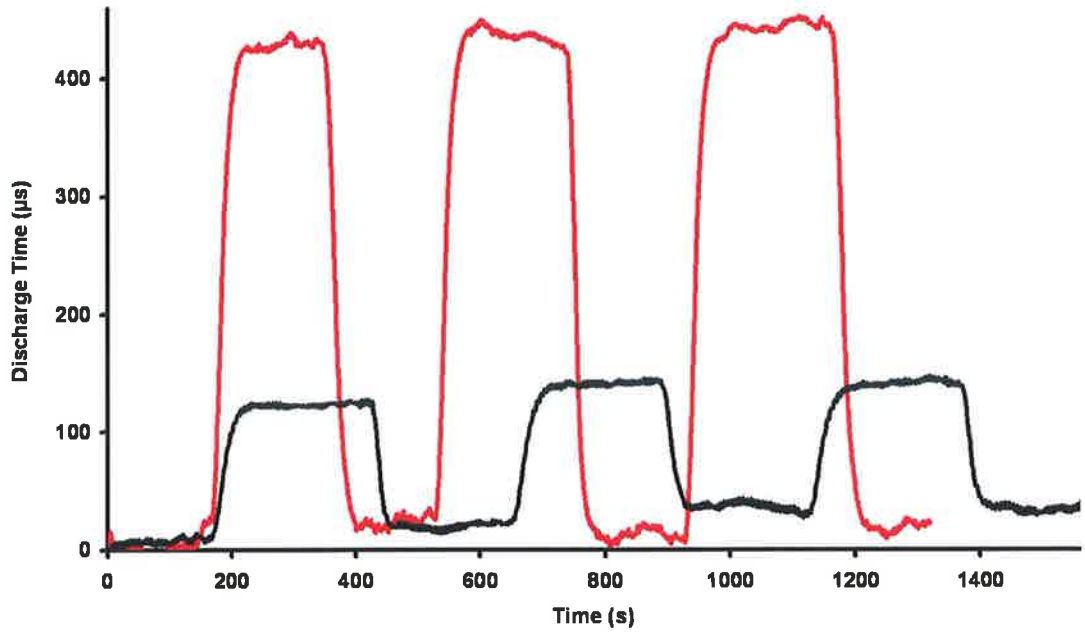

Figure 2.15 Real time traces obtained for 8 μM BCG solution buffered at pH 7 using 2 resistances (6 Ω, black line and 2 KΩ, red line).

The average response to 8 μM BCG obtained from (1) was 104.5 μs ± 1.9 μs (n = 3) whereas the average response from (2) was 416.2 μs ± 11.6 μs (n = 3). Increasing the resistance to 2 kΩ therefore improved the response by approximately a factor of 4.

Table 2.1 The effect of decreasing emitter LED light intensity (i.e. by applying resistance) on the baseline response. The experiment was repeated 3 times.

Resistance (kΩ)	*Baseline Std. Dev. (μs)*
0.5	1.3 ± 0.2
1.0	2.9 ± 0.5
1.5	5.8 ± 0.3
2.0	9.5 ± 1.8
2.4	12.3 ± 0.4
3.3	18.6 ± 1.4
4.0	26.0 ± 1.9

The data presented in Table 2.1 indicates that while decreasing the light intensity of the emitter LED increases the change in response achieved there is also an increase in the standard deviation of the baseline. A resistance of 2 kΩ was therefore selected as the compromise resistance as this improved the signal response while maintaining a smooth baseline.

2.4.3 Investigation of flow effect on the PEDD response

The effect of flow rate on the response obtained from the PEDD in a flow system was investigated. Figure 2.16 demonstrates the effect of flow on residence time and response.

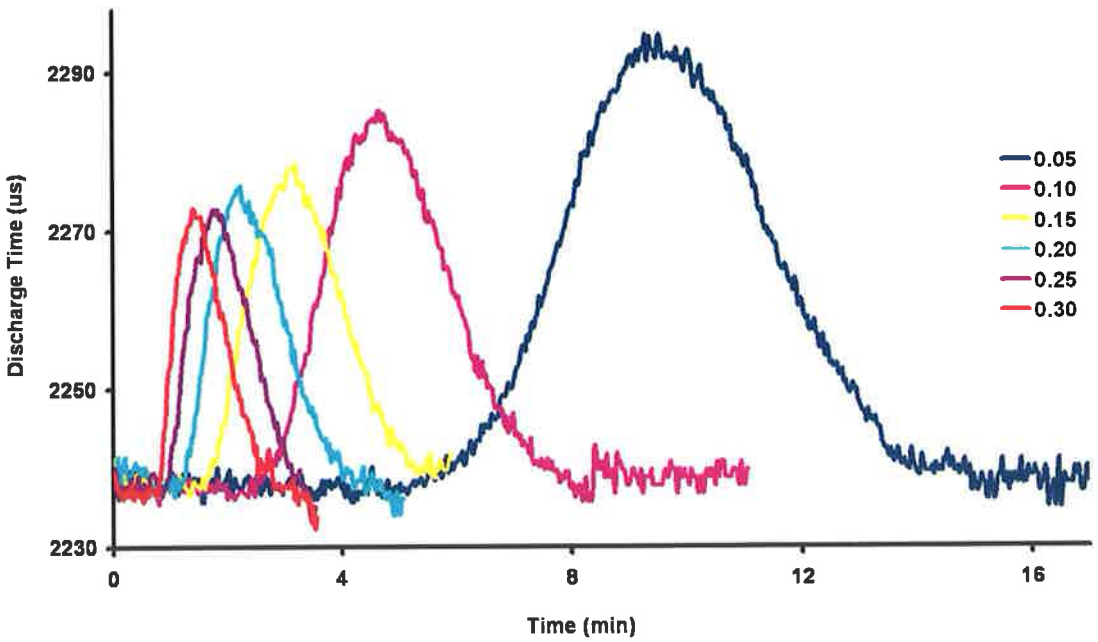

Figure 2.16 The effect on PEDD response was investigated by varying flow rates (0.05-0.3 mL/min) of 20 µM bromocresol green at pH 7. The sample volume used was 100 µl. The experiment was carried out in triplicate.

Increasing the flow rate decreased the residence time as presented in Table 2.2.

Table 2.2 Residence data for the effect of flow rate on response obtained for 20 µM BCG at pH 7.

Flow Rate (mL/min)	*Residence Time (min)*
0.05	9.3
0.10	4.5
0.15	3.1
0.20	2.3
0.25	1.7
0.30	1.3

Increasing the flow rate had a negligible effect on the response of the pH 7 buffer solution (i.e. baseline). The average maximum response obtained for the pH 7 was 2243.2 ± 3.5 µs, with an R.S.D. (n = 3) of 0.2%. Table 2.3 presents the effect of flow rate on the change in discharge time (µs).

Table 2.3 The effect on PEDD response was investigated by varying flow rates (0.05-0.30 mL/min) of 20 µM bromocresol green at pH 7. The sample volume used was 100 µl. The experiment was carried out in triplicate.

Flow Rate (mL/min)	*Change in Discharge Time (µs)*	*Std. Dev.*	*R.S.D.%*
0.05	56.3	0.6	1.0
0.10	50.0	1.3	2.6
0.15	41.3	1.1	2.7
0.20	35.7	1.5	4.2
0.25	35.2	1.8	5.1
0.30	35.4	1.5	4.3

The mean change in discharge time from pH 7 to 20 µM BCG at pH 7 decreased linearly with increasing pump speed from 0.05 – 0.20 mL/min as shown in Figure 2.17. This trend was no longer observed with flow rates above 0.20 mL/min.

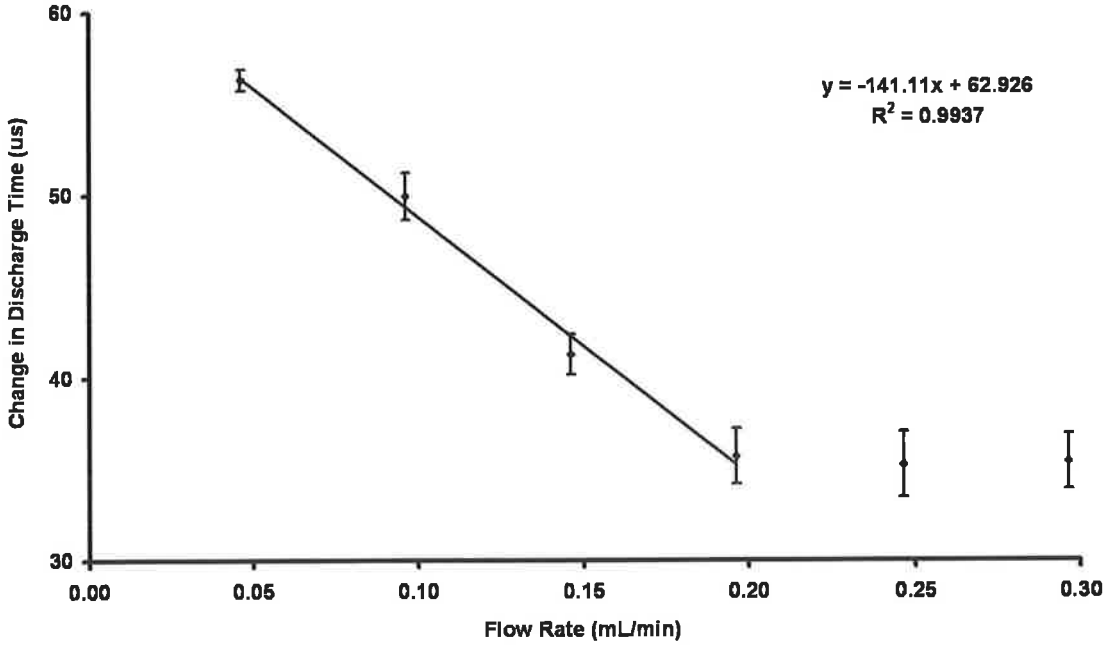

Figure 2.17 The effect of varying flow rates (0.05-0.30 mL/min) on the change in discharge time (μs) of 20 μM bromocresol green at pH 7 (n = 3).

2.4.4 Calibration of the PEDD flow cell

2.4.4.1 Bromocresol Green

The single inlet PEDD flow cell was calibrated with a range of bromocresol green solutions of varied dye concentration (Figure 2.18). All calibration standards were buffered to pH 7. The log of the discharge times (log t/μs) were plotted against dye concentration (C) in accordance with the model (eqn.2.4).

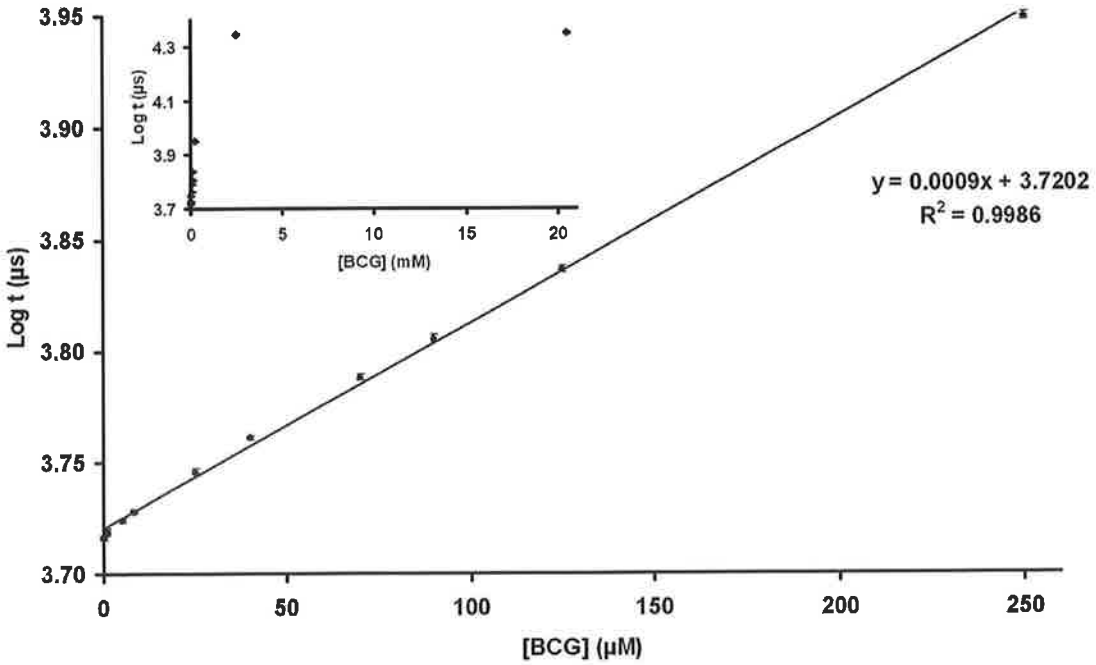

Figure 2.18 Linear calibration plot of log of the discharge times (t) versus BCG dye concentration at pH 7. The inset shows the full range of responses obtained from the calibration.

The inset in Figure 2.18 shows a large detection range from ca. 0.5 µM – 20.5 mM BCG from which a linear range of approximately 0.9 to 250 µM BCG (R^2 value 0.9986) was observed as shown in the main feature plot. The PEDD response levelled off from ca. 2.5 mM as shown in the inset. The relative standard deviation of the measurements (n = 8, shown as error bars) are very low (ca. 0.4%).

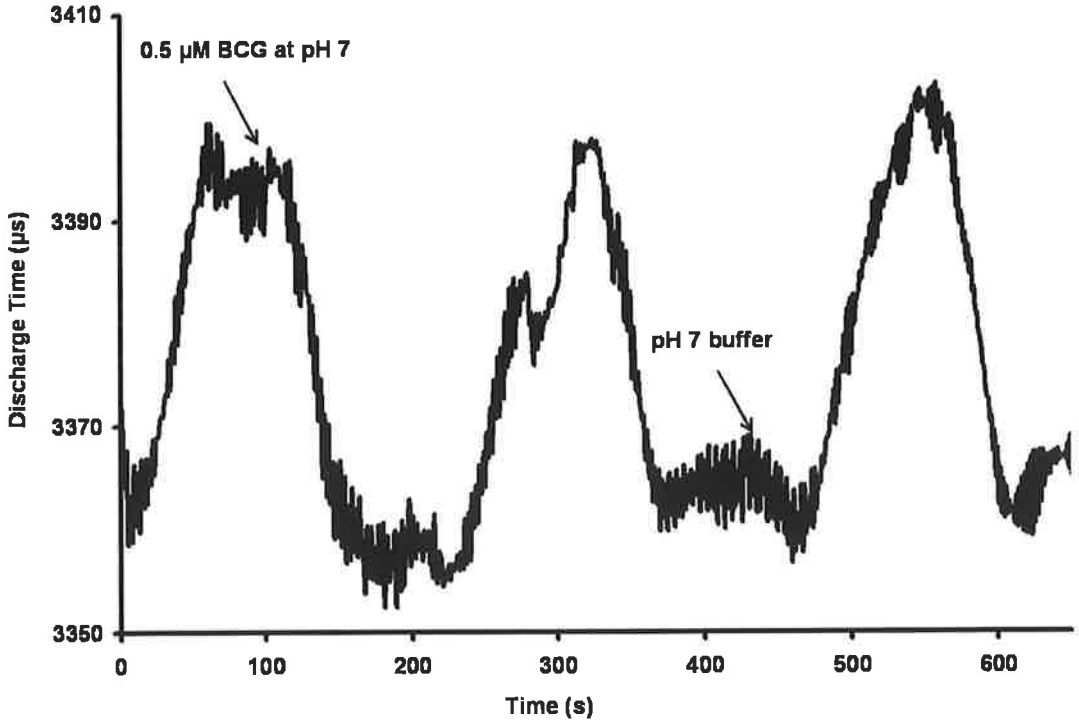

Figure 2.19 Determination of the LOD of BCG at pH 7. A concentration of 0.5 µM BCG at pH 7 was first passed through the PEDD flow cell for ca. 100 µs and then followed by pH 7 buffer. This was repeated in triplicate.

An LOD of 0.5 µM BCG at pH 7 was obtained as shown in Figure 2.19. The average discharge time obtained for the baseline (pH 7 buffer) 3361.9±3.4 µs (n = 3). The average change in discharge time between the pH 7 buffer and 0.5 µM BCG at pH 7 achieved was 31.2±5.5 µs (n = 3).

2.4.4.2 Aniline Blue

The longer path length dual inlet PEDD was calibrated using aniline blue. The molar extinction coefficient of aniline blue is higher than that of Bromocresol green. As a result a shorter dynamic range than that of BCG is obtained, however a lower LOD is achieved. The log of the discharge times (log t/µs) were plotted against dye concentration (C) in accordance with the model (eqn.2.4) and the result was presented in Figure 2.20.

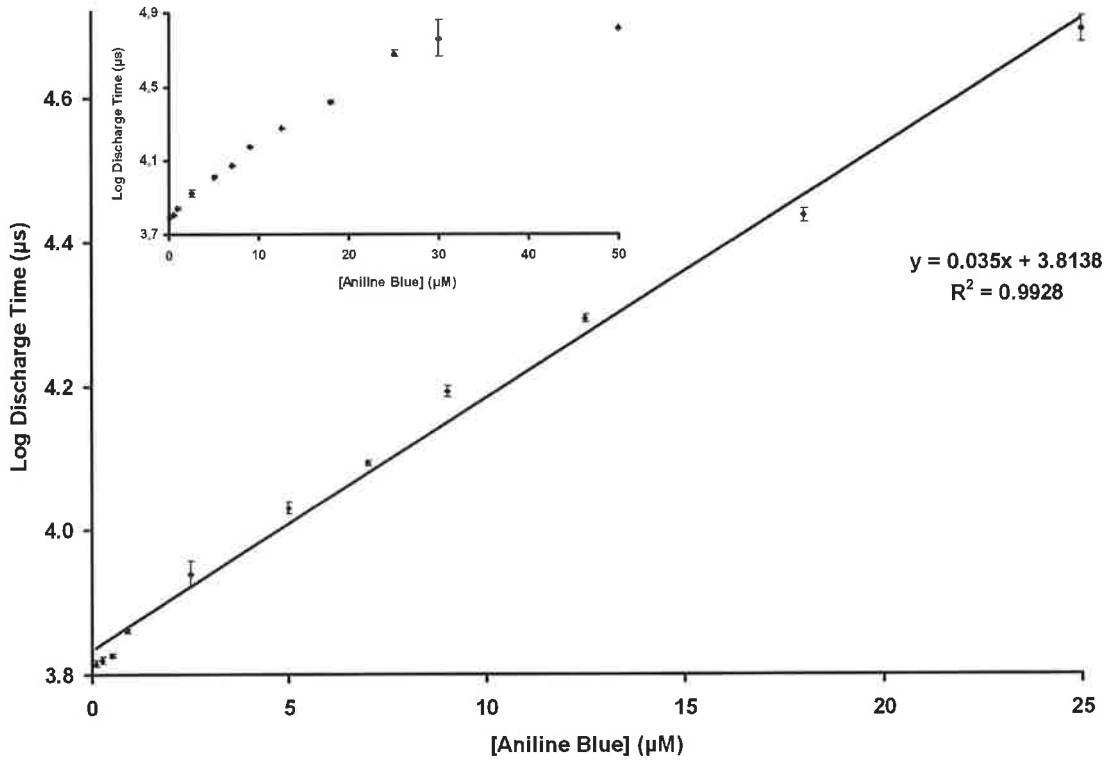

Figure 2.20 Linear calibration plot of log of discharge times (t) versus aniline blue dye concentration. The inset shows the full range of responses obtained from the calibration. The error bars represent the standard deviations (n = 3).

A dynamic range from ca. 0.1 – 30 µM aniline blue was achieved as shown in Figure 2.20 inset. A linear range of approximately 0.1 to 25 µM aniline blue (R^2 value 0.9928) was observed as shown in the main feature plot. The relative standard deviation of the measurements (n = 3, shown as error bars) are very low (ca. 0.5%) and an LOD of 0.25 µM was obtained as shown in Figure 2.21.

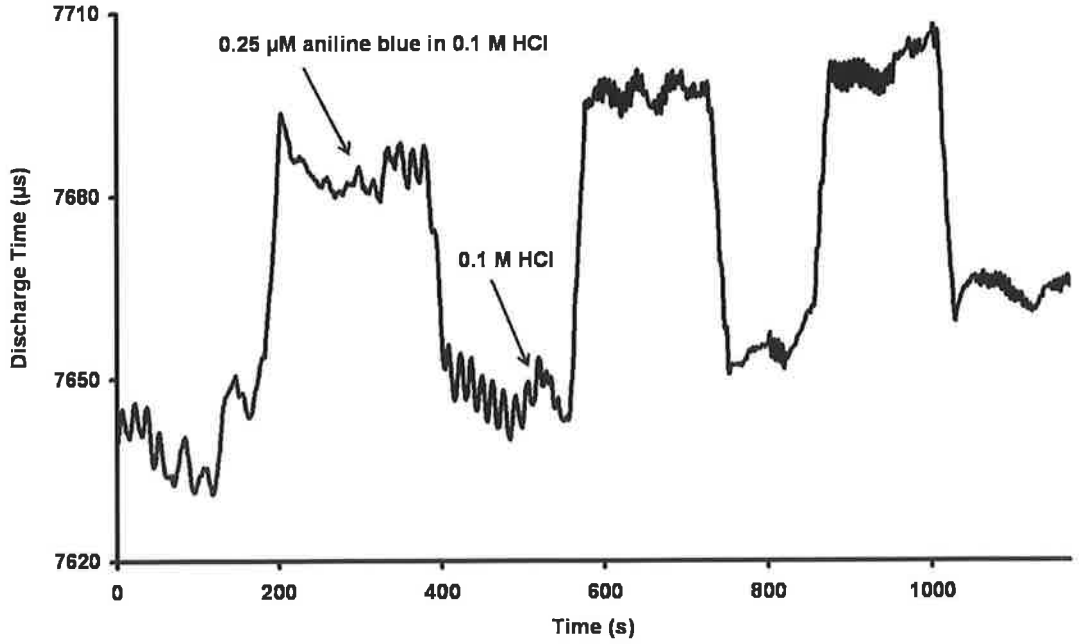

Figure 2.21 Determination of the LOD of aniline blue in 0.1 M HCl. A concentration of 0.25 µM aniline blue in 0.1 M HCl was first passed through the PEDD flow cell for ca. 100 µs and then followed by 0.1 M HCl. This was repeated in triplicate.

An LOD of 0.25 µM aniline blue in 0.1 M HCl was obtained. The average discharge time obtained for the baseline (0.1 M HCl) 7646.91±7.17 µs (n = 3). The average change in discharge time between the 0.1 M HCl and 0.25 µM aniline blue in 0.1 M HCl achieved was 47.02±3.61 µs (n = 3).

2.4.5 Comparison of results with a μQuant™ platewell reader

As a comparison study the absorbance of the same bromocresol green and aniline blue concentrations were acquired using the μQuant™ platewell reader (Bio – Tek Instruments, Inc., USA).

Bromocresol Green

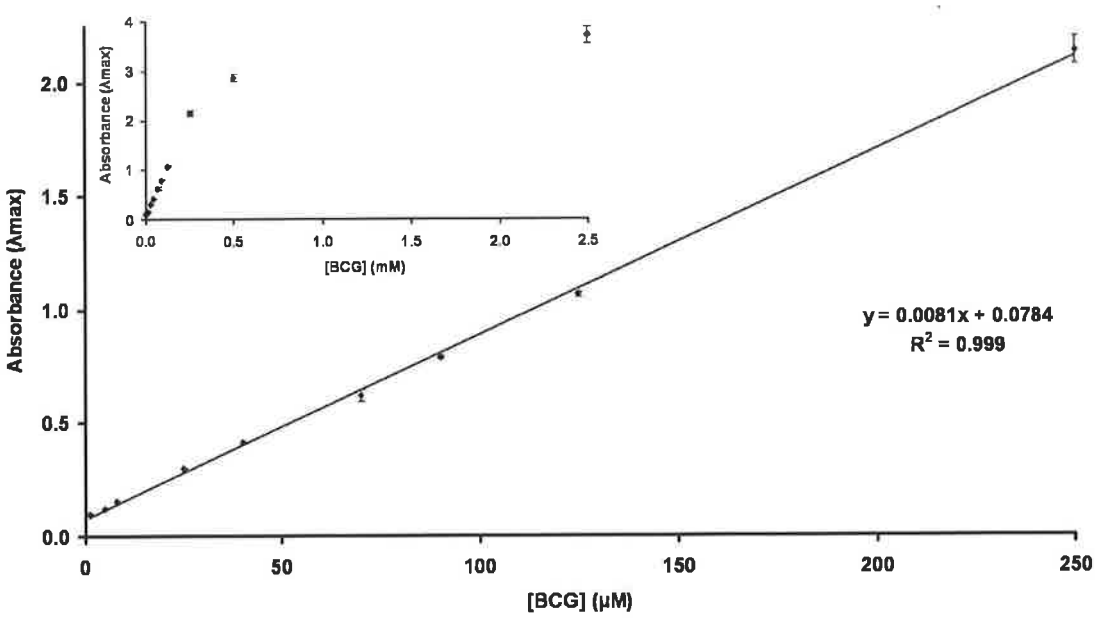

Figure 2.22 Calibration plot of absorbance at λ_{max} versus BCG dye concentration obtained using a platewell reader. The inset shows the dynamic range of the system. The error bars represent the standard deviations for $n = 3$.

As shown in Figure 2.22 the absorbance at λ_{max} were plotted against the dye concentration (C). Absorbance λ_{max} achieved for concentrations above 250 μM no longer increased linearly as shown in the inset. A linear range from 0.5 – 250 μM (R^2 value 0.999) was obtained, with an R.S.D. ($n = 3$) of 4% and an LOD of 0.9 μM.

Aniline Blue

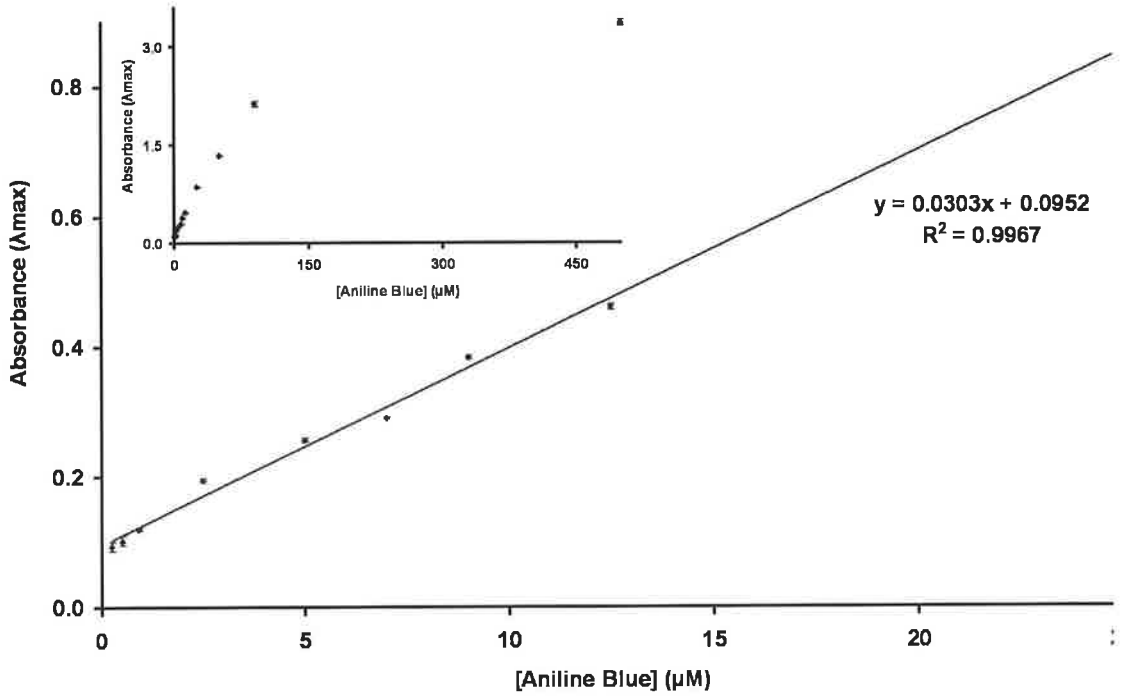

Figure 2.23 Calibration plot of absorbance at λ_{max} versus aniline blue dye concentration obtained using a platewell reader. The inset shows the dynamic range of the system. The error bars represent the standard deviations for $n = 3$.

Figure 2.23 presents the linear and dynamic range achieved for the indicator dye aniline blue in 0.1M HCl. A dynamic range of 0.25 – 90 μM aniline blue was achieved (shown in inset) from which a linear range of 0.25 – 25 μM (R^2 value 0.9967) was obtained, with an R.S.D. ($n = 3$) of 7% and an LOD of 0.5 μM.

Table 2.4 A comparative summary of the data obtained for the bromocresol green at pH 7 and aniline blue in 0.1 M HCl calibration using both a PEDD and a platewell reader.

	Bromocresol Green (pH 7)		*Aniline Blue (0.1 M HCl)*	
	PEDD (single inlet)	Platewell Reader	PEDD (dual inlet)	Platewell Reader
Dynamic Range	0.5 μM-20.5 mM	0.6-250 μM	0.1-30 μM	0.25-90 μM
Linear Range	0.9-250 μM	0.9-250 μM	0.1-25 μM	0.25-25 μM
LOD	0.5 μM	0.9 μM	0.25 μM	0.5 μM

It can be seen from the data presented in Table 2.4 that the performance of the simple LED based device matched that of a conventional bench top instrument. It has also been demonstrated than increasing the path length of the PEDD can further improve the sensitivity of the optical device.

2.4.6 Using PEDD to Monitor Colour Changes

The calibration studies discussed above employed BCG solutions at pH 7, however the PEDD flow cell has also been used to monitor the pH-dependent colour change of BCG.

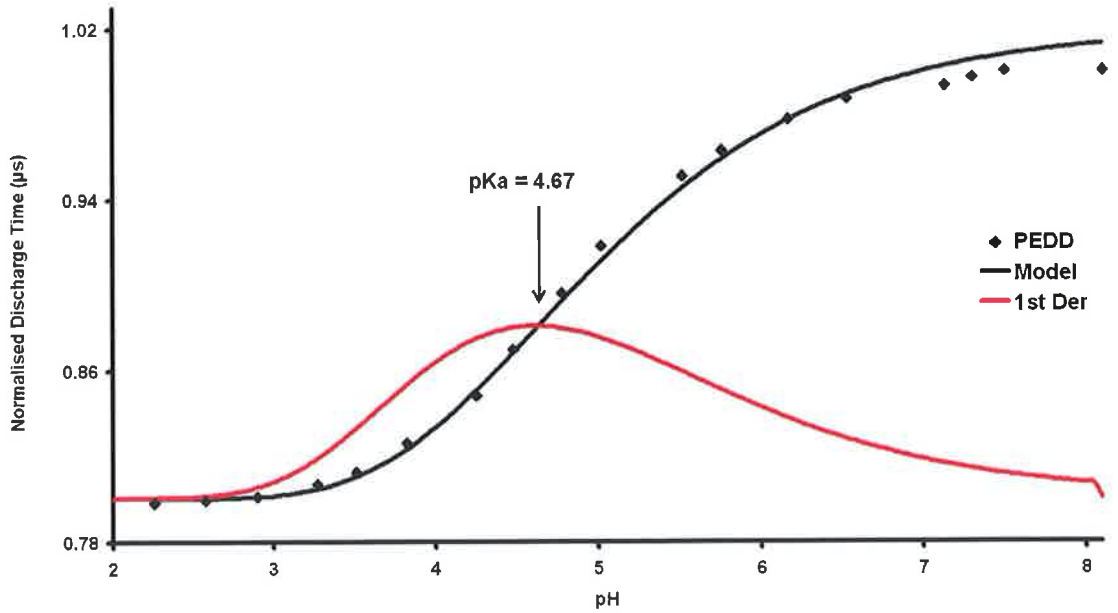

Figure 2.24 A plot to illustrate the change in pH of 40 µM BCG solution with the discharge time of the PEDD flow detector (◆). The 1st derivative (dashed line) of the best fit line (solid line) for the data gave an estimated pK_a value of 4.67.

The data presented in Figure 2.24 was normalised (0-1 range) by dividing each set of values by the maximum value achieved. The plot obtained from the PEDD (depicted in Figure 2.24 by the legend ◆) is sigmoidal in shape with a linear range between pH 3.82 to pH 5.76. Using Microsoft™ Excel solver and a method developed by

Diamond *et al.* [76] a best fit line was found for the experimental data (solid line). The pK_a was determined to be 4.67 using this method, which is slightly lower than the reported pK_a value of 4.74 for BCG at room temperature [77].

2.5 Conclusion

It can be concluded that the integrated PEDD flow analysis system is useful for the colorimetric analysis of indicator pH dyes such as bromocresol green and aniline blue and pH determination. The PEDD flow analysis system used had an emission λ_{max} of 621 nm as this efficiently overlapped with the indicator dyes used. A broad spectral range of LEDs are commercially available from ultraviolet to near-infrared (ca. 380 - 900 nm). This allows the PEDD to be used for a wider range of colorimetric analyses.

The single inlet PEDD flow analysis system was calibrated using bromocresol green, which obtained a linear range from 0.9 - 250 μM BCG at pH 7 (R^2 0.998) with a relative standard deviation of 0.4% (n = 8). An LOD of 0.5 μM BCG at pH 7 was achieved (Table 2.4). A comparison study carried out using a commercially available μQuant™ platewell reader (Bio – Tek Instruments, Inc., USA) also achieved a linear range of 0.9 - 250 μM BCG at pH 7 (R^2 0.999) with a relative standard deviation of 4% (n = 3), however an LOD of 0.9 μM BCG at pH 7 was obtained.
The device was also successfully employed for the determination of BCG pK_a. The reported pK_a of BCG is 4.74 [77]. The pK_a determined using the PEDD was 4.67.

The dual inlet PEDD flow analysis system with longer path length was calibrated using aniline blue. A linear range of 0.1-25 μM aniline blue in 0.1 M HCl (R^2 0.9928) with a relative standard deviation of 0.5% (n = 3) was achieved. An LOD of 0.25 μM aniline blue in 0.1 M HCl was determined using the PEDD. The samples were also investigated using the μQuant™ platewell reader as a comparative study. The results obtained provided a linear range of 0.25 – 25 μM aniline blue in 0.1 M HCl (R^2 0.9967) with a relative standard deviation of 7% (n = 3). An LOD of 0.5 μM aniline blue in 0.1 M HCl was achieved.

This system is small, compact and comprises of inexpensive optical and electronic components, while still providing high sensitivity and accuracy with detection limits at nanomolar concentrations. The power consumption required is extremely low and the sensor can be operated from a 9 V battery. The PEDD flow system is therefore very suitable for scale-up and field deployment in autonomous monitoring systems.

CHAPTER 3

Determination of Phosphate using a Highly Sensitive PEDD Photometric Flow Detector

3. Determination of Phosphate using a Highly Sensitive Paired Emitter-Detector Diode Flow Detector

3.1 Introduction

Phosphorus, specifically orthophosphate, is an essential nutrient used by plants and animals for growth and energy transport [78]. However elevated concentrations in aquatic ecosystems cause the phenomenon of eutrophication, which can result in algal bloom formation as shown in Figure 3.1 [79]. The rapid growth of aquatic vegetation in turn causes the death and decay of vegetation and aquatic life due to the decrease in dissolved oxygen levels. The resulting eutrophication of natural waters is a subject of utmost concern, and has been recognized by the European Union through legislation that stipulates 0.1 mg L^{-1} PO_4 as an indicator level for possible problematic algal growth in rivers [80].

Figure 3.1 Photograph of a river with algal growth

Spectrophotometric procedures for monitoring orthophosphate include the molybdenum blue method [78,80-84], the yellow vanadomolybdate complex method [30,31,85,86] and the malachite green method [87-92]. The malachite green method

has been shown to enhance sensitivity by approximately 4 times when compared to the aforementioned methods [87,93]. A significant advantage of the malachite green method is its lack of sensitivity to experimental conditions such as changes in heating, reagent addition sequence or reaction time [87,94]. Additional advantages include higher sensitivity compared to the molybdenum blue method and the longer optimum detection wavelength than the yellow method [95]. The malachite green method is based on the reaction at low pH between ammonium molybdate, polyvinyl alcohol (PVA) and malachite green (MG) as in the following equations [95]:

$$\underset{\text{(yellow)}}{H_3PMo_{12}O_{40}} + \underset{\text{(yellow, } \lambda_{max} \text{ 446 nm)}}{HMG^{2+}} \rightarrow \underset{\text{(green, } \lambda_{max} \text{ 640 nm)}}{\left(MG^+\right)\left(H_2PMo_{12}O_{40}^-\right)} + 2H^+ \quad \textbf{Equation 3.1}$$

$$\left(MG^+\right)\left(H_2PMo_{12}O_{40}^-\right) + HMG^{2+} \rightarrow \left(MG^+\right)_2\left(HPMo_{12}O_{40}^{2-}\right) + 2H^+ \quad \textbf{Equation 3.2}$$

$$\left(MG^+\right)_2\left(HPMo_{12}O_{40}^{2-}\right) + HMG^{2+} \rightarrow \left(MG^+\right)_3\left(PMo_{12}O_{40}^{3-}\right) + 2H^+ \quad \textbf{Equation 3.3}$$

In the presence of large excess of MG, the reactions (Equation 3.1-3.3) can occur, and the 3:1 ion associate formed in Equation 3.3 can easily precipitate in the acidic aqueous solution. To prevent the formation of the ion association reactions shown in Equations 3.2 and 3.3, and to stabilize the ion associate in the aqueous solution, PVA is added to the solution [89,95].

The optical detection employed in this research to determine orthophosphate via the malachite green method is a novel, highly sensitive, low cost paired emitter-detector diode (PEDD) photometric detector. The PEDD flow cell consists of two LEDs, whereby one is the light source and the second is the light detector. The LED light source is forward biased while the LED detector is reversed biased. The photon flux from the emitter LED strikes the detector LED, generating a small photocurrent (of the order of nanoamperes) that discharges the capacitor voltage over time. The photocurrent produced is not measured directly as this would require an expensive nanoamperometer. Instead, the parameter monitored is the decay time (μs) taken for the discharge process to go from an initial value of 5 V (logic 1) to a preset value of 1.7 V (logic 0) using a simple timer circuit, and a comparator which determines whether the remaining charge is above or below the set point (+1.7 V). The use of LEDs offer advantages such as low cost, compact form, availability across a broad

spectral range from UV to near-IR, robust and long lifetimes [15,19,20]. In most microanalytical systems the light source and the photodetector are normally separate units integrated with the microfluidic manifold [74], however in this case the PEDD is a single unit containing light source, fluid channel and detector for flow analysis [60,96,97].

3.2 PEDD and LED-PD

3.2.1 Analytical Model

Paired Emitter-Detector Diode (PEDD)

The PEDD analytical model is as described in section 2.2.1.

Light Emitting Diode-Photodiode Detector (LED-PD)

The reported absorbance (A) measurement was calculated according to Equation 3.4:

$$A = -\log\left(\frac{SampleIntensity}{BlankIntensity}\right) \qquad \textbf{Equation 3.4}$$

where sample intensity is the intensity of the light passing through the cell with sample solution and blank intensity is the intensity of the light passing through the cell with reference solution.

3.2.2 The Circuitry

PEDD

The circuitry employed to drive the PEDD was as described in section 2.2.2.

LED-PD

The circuitry used to drive the LED photodiode detector is illustrated in Figure 3.2.

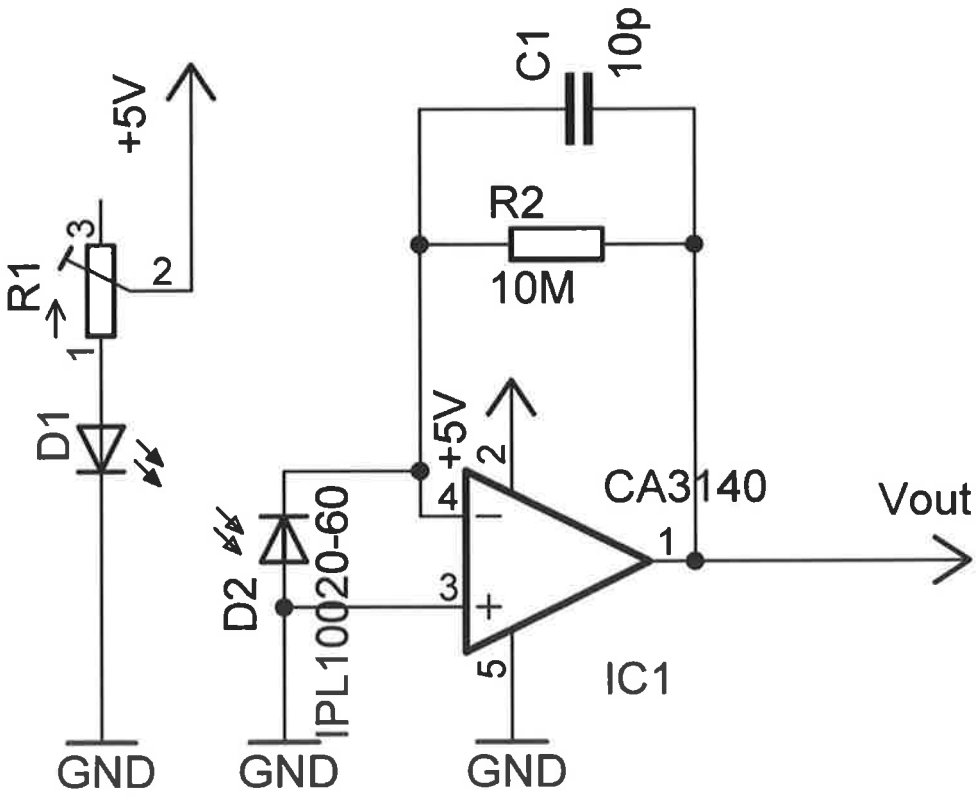

Figure 3.2 Electronic circuitry of the LED-photodiode detector. Capacitor (C1) = 10 pF, LED (D1) = Red LED, Photodiode (D2) = IPL10020BW, Resistor (R1) =10 KΩ, R2 = 40 MΩ and Operational Amplifier (IC1) = CA3140.

Figure 3.2 shows a light emitting diode (D1) illuminating a photodiode (D2) connected to a current to voltage converter. The voltage between V_{out} and GND is then measured by an analogue digital converter on a microcontroller. The current

through the LED is adjusted by a potentiometer (R1) thus controlling the illumination. The output current of a photodiode in reverse bias is linearly proportional to the light intensity. To condition the signal for the 10 bit ADC on a PIC16F876 microcontroller a current to voltage converter is employed. A circuit consisting of a FET input operational amplifier (IC1) and a resistor (R2) in feed back was constructed.

In the circuit the output voltage is determined by Equation 3.5:

$$V_{out} = -I_p \times R2, \qquad \textbf{Equation 3.5}$$

whereby output voltage is V_{out}, I_p is the current through the photodiode and R2 is a 40 MΩ resistor. A capacitor (C1) is not a requirement but was added to reduce noise. Although a circuit with enhanced performance can be constructed, the cost incurred for slight increases in sensitivity by using more precise components and/or higher resolution ADCs would not be justified on a low cost sensor.

3.2.3 Data Capture

PEDD

The data acquired from the PEDD was captured and analysed as per section 2.2.3.

LED-PD

The circuitry used to drive the LED-PD is shown in Figure 3.3. For this work the programmable interface controller (PIC) board was programmed to measure the current through the photodiode.

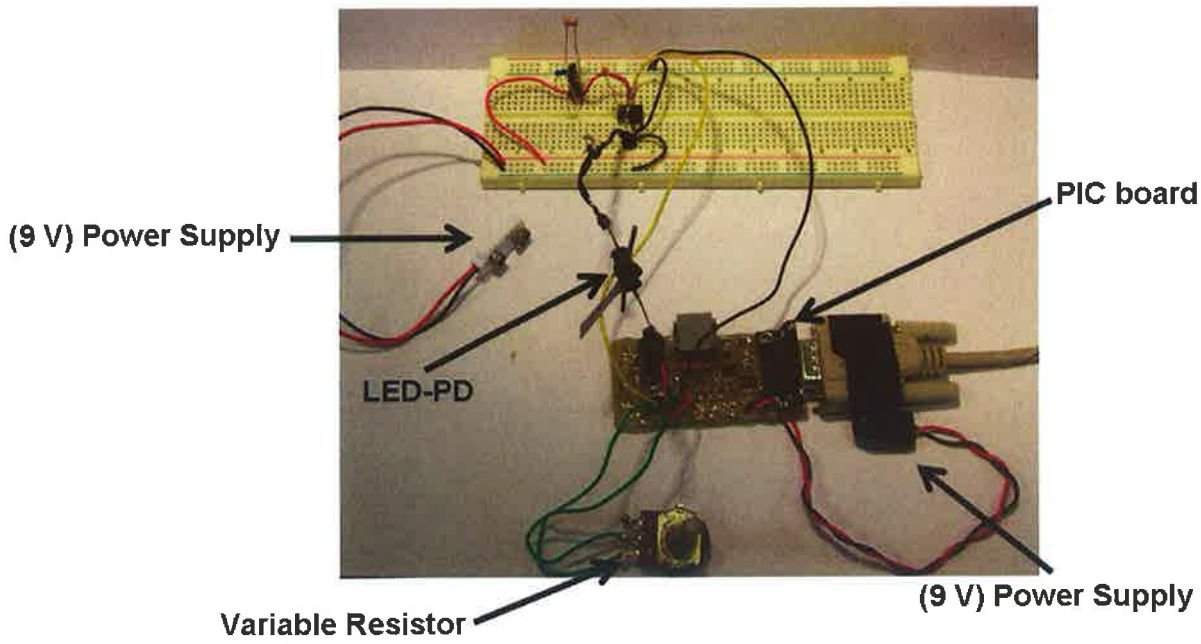

Figure 3.3 Photograph outlining the layout of the programmable interface controller (PIC) board, A/D converter and operational amplifier

The current was reported at a rate of 1.5 data point/second. Data is transferred to a PC via a RS232 port (Figure 3.3), and captured with the HyperTerminal software, and then saved as a text file for further analysis using Excel™ (Microsoft, Inc., USA).

3.2.4 Project Aim

The work presented here will demonstrate the detection of orthophosphate using this novel detector and a comparative study carried out using both a photodetector comprising of an LED as a light source and a photodiode as the detector and a commercially available platewell reader. The malachite green (MG) method employed for orthophosphate determination is based on the formation of a green molybdophosphoric acid complex, the intensity of which is directly related to orthophosphate concentration. Optimum conditions such as time allowed for colour formation, reagent to sample ratio and emitter wavelength and intensity were investigated for the spectrophotometric method. The dynamic range, sensitivity, limits of detection and linear range were determined. Under optimised conditions the low

cost PEDD detector (~$1) displayed higher sensitivity and improved precision compared to the commonly employed LED–photodiode detector and a commercially available platewell reader. As such it could provide a route to autonomous, very low cost, low power consuming, highly sensitive, field deployable analytical measurements, which would form the basis of widely deployed chemosensor networks [18].

3.2.5 Fabrication of PEDD and LED-PD flow cell detectors

PEDD

The integrated detector cell was fabricated as previously described in section 2.2.5 using two 5 mm LEDs (Kingbright, Ireland) as shown in Figure 3.4.
The detector used was a red LED (λ_{max} at 660 nm) which can detect any wavelength below this point. A red LED (λ_{max} at 636 nm) was used as the emitter LED. The PEDD flow cell was operated as described in section 2.2.2 and the data was captured and saved according to section 2.2.3.

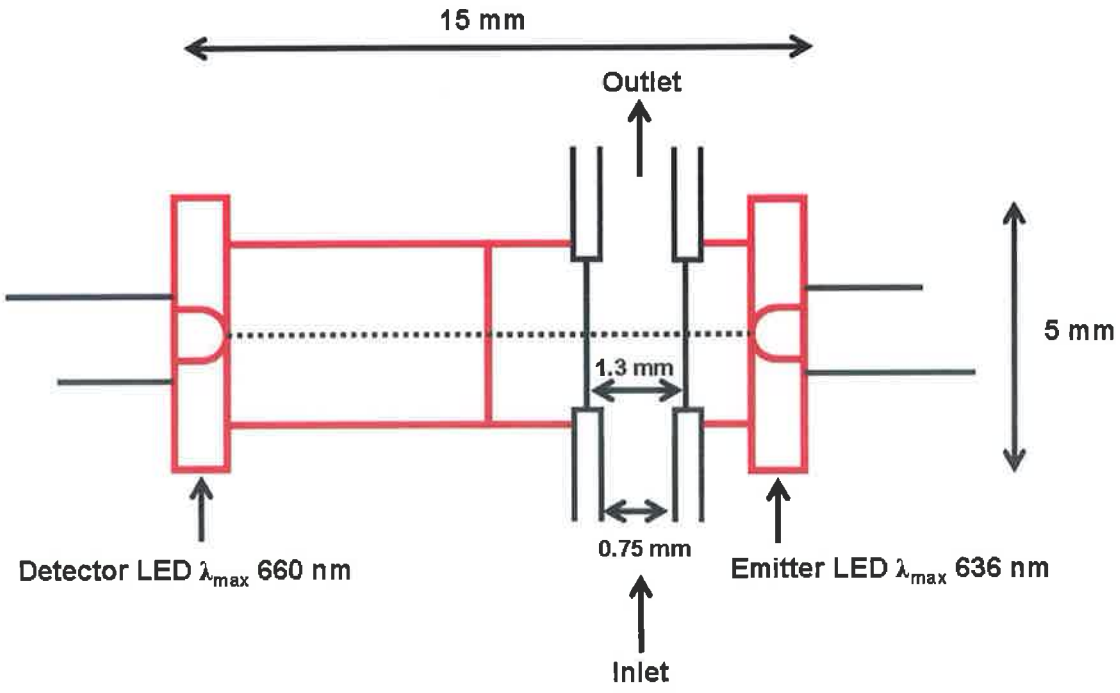

Figure 3.4 A schematic of the integrated PEDD flow analysis device used for colorimetric detection.

LED-PD

As shown in Figure 3.5 the LED-photodiode detector was fabricated similarly to the PEDD. A red LED (λ_{max} at 636 nm) was used as the emitter LED with a pathlength of 1.3 mm. The LED detector was replaced with a Si photodiode, IPL10020BW (Thales Optronics, UK) detector and bonded in the same way as the PEDD.

The LED-PD flow cell was operated as described in section 3.2.2 and the data was captured and saved according to section 3.2.3.

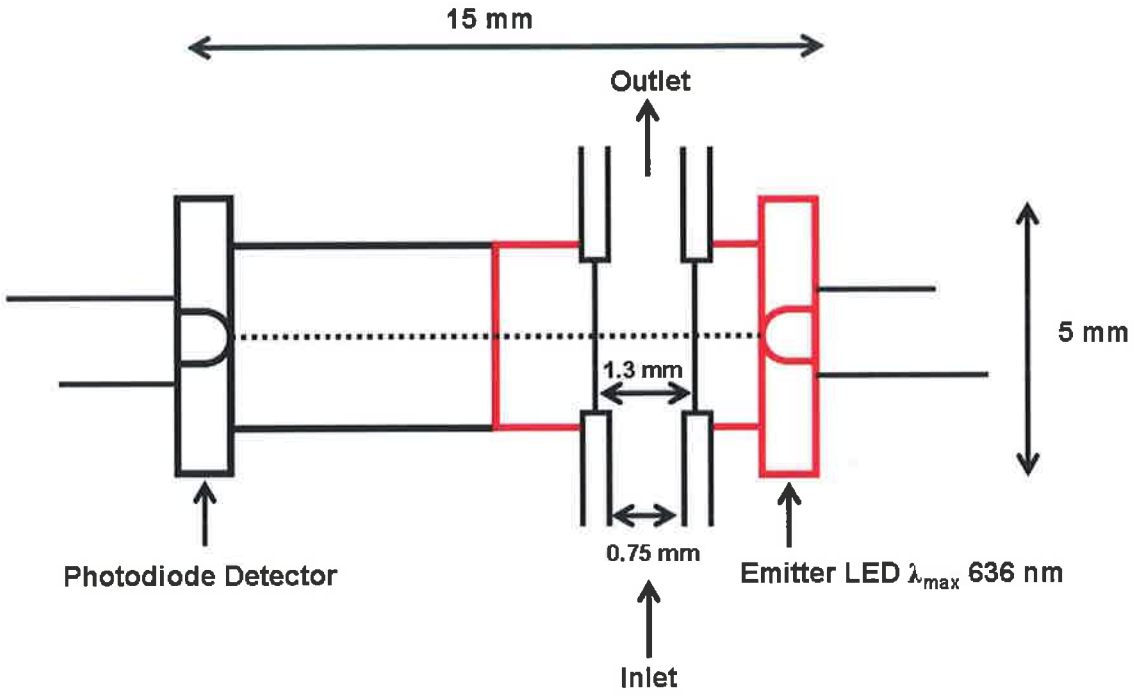

Figure 3.5 A schematic of the LED-PD flow analysis device used for colorimetric detection.

3.3 Experimental Procedure

3.3.1 Equipment

A Gilson (MiniPlus 3) peristaltic pump, (Anachem, UK) was used to deliver the premixed sample and reagent at a flow rate setting of 0.6 mL/min. A single channel PEDD flow cell (Emitter λ_{max} 623 nm, Detector λ_{max} 660 nm) was used in combination with the LED-PD.

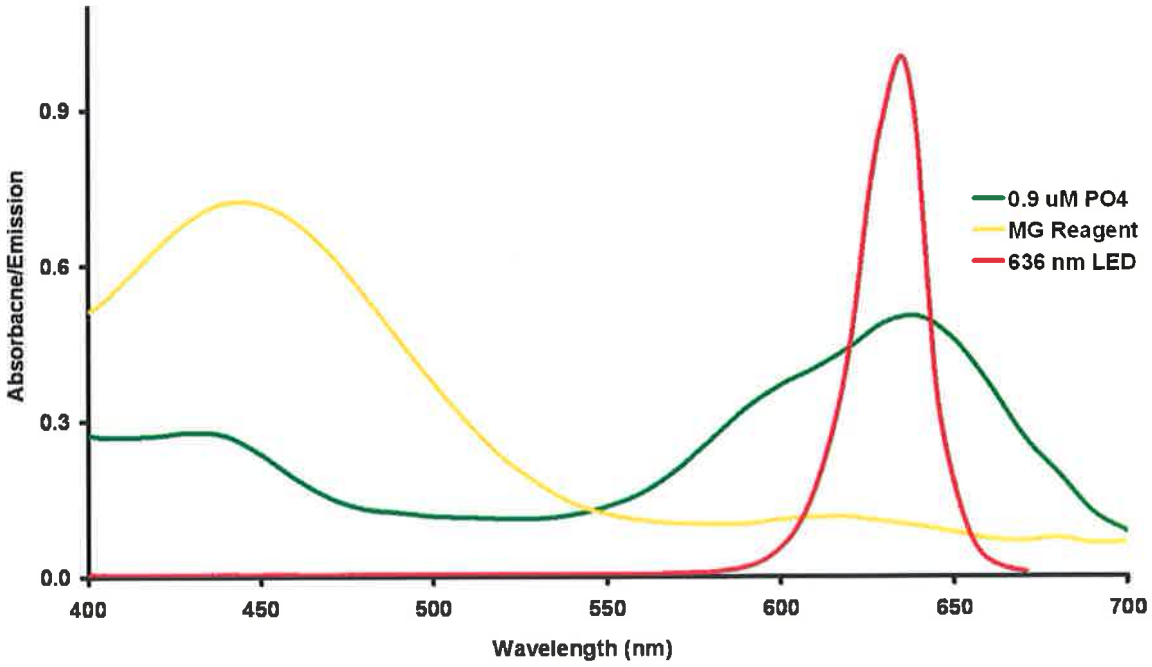

Figure 3.6 Emission spectrum (λ_{max} 636 nm) of the emitter LED (red line) used in the integrated PEDD flow analysis device, the absorption spectrum (λ_{max} 640 nm) of 0.9 µM PO_4 and MG reagent (green line) and (λ_{max} 450 nm) MG reagent (yellow line).

Figure 3.6 shows that the absorption spectrum of malachite green-molybdphosphate complex overlaps with the emission spectrum of the PEDD device. The emission spectrum of the red emitter LED was obtained by using an Ocean Optic spectrometer (OOIBase 32™, Ocean Optics Inc., Dunedin, USA). The absorbance spectrum of malachite green-molybdphosphate complex was acquired using the µQuant™ platewell reader (Bio – Tek Instruments, Inc., USA). The overlap between absorbing

species and the light source provide high sensitivity for the detection of malachite green-molybdphosphate complex.

3.3.2 Chemicals

- Sulphuric acid (H_2SO_4, 98%, Fisher Scientific UK Ltd)
- Ammonium molybdate ($(NH_4)_6Mo_7O_{24}.7H_2O$, Fluka, Dublin, Ireland)
- Malachite green oxalate ($C_{25}H_{22}N_2O_4$) (Baltimore Biological Laboratory, Baltimore, Md.)
- Polyvinyl alcohol (PVA) (Sigma Aldrich, Dublin, Ireland)
- Milli-Q water (Millipore Ireland B.V., Cork)
- Potassium phosphate dibasic (K_2HPO_4, Sigma Aldrich, Dublin, Ireland)

3.3.3 Reagents and Solutions

All solutions were prepared from analytical grade chemicals. Deionised water obtained from a Millipore Milli-Q water purification system was used for all analysis.

Malachite green Reagent

A stock malachite green reagent was prepared by slowly adding 100 mL concentrated sulphuric acid (H_2SO_4, 98%, Fisher Scientific UK Ltd) to approximately 400 mL of deionised water. The solution was allowed to cool to room temperature before adding 27 g of ammonium molybdate ($(NH_4)_6Mo_7O_{24}.7H_2O$, Fluka, Dublin, Ireland). Malachite green oxalate ($C_{25}H_{22}N_2O_4$) (Baltimore Biological Laboratory, Baltimore, Md.) (0.135 g) was then added to the solution and stirred until dissolved. The solution was then made up to 1 L, vacuum filtered (0.45 µm Nylaflo®, VWR International, Meath, Ireland) and stored at 4 °C.

0.1% (w/v) polyvinyl alcohol (PVA)

A stock solution of 0.1% (w/v) polyvinyl alcohol (PVA) (Sigma Aldrich, Dublin, Ireland) was prepared by dissolving 5 g in 500 mL. To assist the dissolution process,

the solution was heated to near boiling point while being stirred continuously. Both stock solutions were stored in the dark at 4 °C.

Malachite green and PVA solution

The colour reagent was prepared daily by mixing equal amounts of each stock reagent.

Orthophosphate standards

Standard solutions of phosphorus (P) were prepared daily from a stock solution of 1 mM potassium phosphate dibasic (K_2HPO_4, Sigma Aldrich, Dublin, Ireland). The stock solution was prepared by dissolving 0.0175 g K_2HPO_4 in 100 mL deionised water. A new stock solution was prepared weekly.

Sample and Reagent

The colour reagent (1 mL) was added to the samples (6 mL) and the solution was left to stand at room temperature for ca. 30 minutes for colour development.

3.3.4 Measurement Procedure

Various concentrations of orthophosphate (PO_4) were made up in Milli-Q water and 1 mL of the colour reagent was added to the samples (6 mL). The solution was left to stand at room temperature for ca. 30 minutes for colour development. The solution was delivered using a Gilson (MiniPlus 3) peristaltic pump at a flow rate of 0.6 mL/min. The analytes were first detected using the PEDD flow cell. The same solutions were then analysed using the LED-PD flow cell. All experiments were carried out in triplicate (n = 3). The data acquired from the PEDD and the LED-PD flow cells were transported to a PC via RS232 port and captured with HyperTerminal software (Microsoft Inc., USA), saved as a text file and then analysed using Excel™ (Microsoft Inc., USA).

3.3.5 Optimisation of Standard Procedure

Optimisation of the experimental parameters such as wavelength and light intensity of the emitter LED, reagent to sample ratio and colour formation time were investigated. A sample concentration of 0.9 μM PO_4 was selected to carry out the study as it provided reproducible responses.

Wavelength

The optimum wavelength to monitor the malachite green-molybdphosphate complex has been variously reported in the literature, typically citing the λ_{max} in the range ca. 600 to 650 nm [87,88,98]. The λ_{max} was therefore determined under our experimental conditions by obtaining the absorbance spectrum of 0.9 μM PO_4 using the μQuant™ platewell reader (Bio-Tek Instruments, Inc., USA).

Procedure

- 200 μL aliquots of 0.9 μM PO_4 and colour reagent were placed into a 96 platewell.
- The samples were monitored in the range of 400-700 nm.
- The data was captured using the μQuant™ software and saved as a text file for later analysis using Microsoft ™ Excel software.
- All experiments were carried out in triplicate.

Light Intensity

Previous studies have shown the need to optimise the emitter LED light intensity [60,96], as the change in discharge time (i.e. the resolution) can be improved by up to a factor of 8. As LEDs vary with regard to their light intensity it was necessary to determine the optimum resistance required for a 636 nm LED. The optimization of the light intensity was carried out as previously described using a (0–10 kΩ) variable resistor [96].

Procedure

- A blank solution was passed through the flow cell for ca. 1 minute at a flow rate of 0.6 mL/min.
- This was then followed by 0.9 μM PO_4 solution for ca. 1 minute at a flow rate of 0.6 mL/min.
- Various light intensities brought about by varying the resistance on the emitter LED as in section 2.3.3 were examined
- The data was captured as described in section 2.2.3
- All experiments were carried out in triplicate.

Reagent Ratio

The optimum reagent to sample ratio was determined by preparing a range of samples at a concentration of 2 μM PO_4 with varying volumes of reagent (0.1 – 2 mL) added. The normalized maximum absorbance (R/R_{max}) of each sample was recorded after 40 minutes and plotted against the volume of reagent added to 6 mL of sample.

Procedure

- Various ratios of reagent:sample were examined
- The sample solutions were allowed to stand at room temperature for ca. 40 minutes
- Aliquots of 200 μL were taken and placed into a 96-plate
- The absorbance spectrum was taken using the μQuant platewell reader
- All experiments were carried out in triplicate.

Kinetic Study

Linge *et al.* [87] reported a stand time for sample and reagent colour development of approximately 30 minutes. The development of the 0.5 μM malachite green-molybdphosphate colour intensity was monitored using the μQuant™ platewell reader by taking an absorbance measurement every 2 minutes for 5 hours. Figure 3.7 shows the colour development of 0.5 μM malachite green-molybdphosphate at time (T) 0 minutes and 30 minutes.

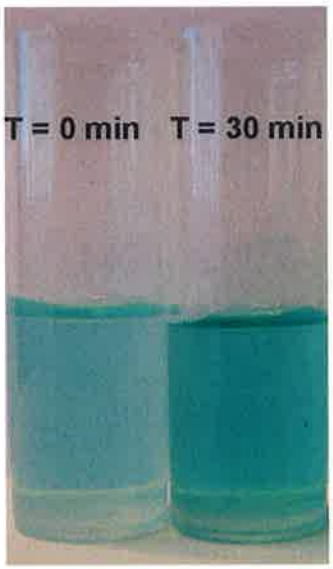

Figure 3.7 Photograph of 0.5 μM malachite green-molybdphosphate complex at (A) T = 0 minutes and (B) T = 30 minutes.

Procedure

- 200 μL aliquots of 0.5 μM PO_4 and colour reagent were placed into a 96 platewell
- The wavelength selected to monitor was 640 nm
- An absorbance reading was taken every 2 minutes
- The data was captured using the μQuant™ software and saved as a text file for later analysis using Microsoft ™ Excel software.
- All experiments were carried out in triplicate.

3.3.6 Calibration using the PEDD and LED-PD flow cell

Working calibration solutions between 0.002 and 20 μM were prepared from the stock standard. The malachite green method has a limited range of up to 20 μM before precipitation of MG occured. As a comparison study, the absorbance of the same malachite green-molybdphosphate complex concentrations were acquired employing both the commonly used LED-photodiode detector and a μQuant™ platewell reader.

PEDD/LED-PD

Procedure

- Various concentrations of orthophosphate were prepared in deionised water.
- 1 mL of reagent was added to each sample and allowed to stand for ca. 30 minutes to allow colour development.
- Each concentration was passed through the PEDD/LED-PD flow cell for ca. 4 minutes per sample, at a flow rate of 0.6 mL/min.
- **PEDD:** The log of the discharge times (log t, μs) was plotted against malachite green-molybdphosphate complex concentration (C) in accordance with the model (Equation 2.4).
- **LED-PD:** The absorbance was plotted against malachite green-molybdphosphate complex concentration (C) in accordance with Equation 3.4.
- All experiments were carried out in triplicate.
- The data was captured as outlined in section 2.2.3 (PEDD) and 3.2.3 (LED-PD).

μQuant™ platewell reader

Procedure

- A 200 μL aliquot of each concentration ranging from 0.002 and 20 μM were taken and added to a 96 plate well.
- Each concentration was added to the 96 plate well in triplicate.
- The absorbance was scanned from 400 – 700 nm.
- The data was captured using the μQuant™ software and saved as a text file for later analysis using Microsoft ™ Excel software.

3.4 Results and discussion

3.4.1 Optimisation Standard Procedure

Wavelength

The λ_{max} of the sample was found to be 640 nm. An emitter LED with a λ_{max} of 636 nm was therefore selected. The light intensity transmitted from the emitter LED (λ_{max} 636 nm) was measured with a detector LED that had a slightly smaller bandgap (λ_{max} 660 nm). The absorbance of the malachite green-molybdphosphate species (λ_{max} 640 nm) as shown in Figure 3.6 efficiently overlaps with the emission spectrum of the emitter red LED and will therefore allow high sensitivity.

Light Intensity

As previously mentioned studies carried out in chapter 2 have shown the need to optimise the emitter LED light intensity [60,96], as the change in discharge time (i.e. the resolution) can be improved by up to a factor of 8. The optimization of the light

intensity was carried out as previously described using a (0–10 kΩ) variable resistor in section 2.3.3. A resistance of 1.58 kΩ was found to provide the optimum light source intensity resulting in high sensitivity, while maintaining a smooth baseline without drift. A 12-pt moving average was applied to the data shown in Figure 3.8. The effects of decreasing the light intensity on the response are clearly demonstrated in Figure 3.8. For example, at a resistance of 0.004 kΩ, the difference in discharge time (Δt) i.e. peak height was 4.78 ± 0.19 μs with an R.S.D. (n = 3) of 3.90%. At an additional applied resistance of 1.58 kΩ the peak height obtained was 32.59 ± 0.44 μs with 1.35% R.S.D. (n = 3). The standard deviation (n = 3) of the baseline was 6.95 μs. At a resistance of 6.02 kΩ the peak height achieved was 144.87 ± 0.78 μs with 0.54% R.S.D. (n = 3). Increasing the resistance to 6.02 kΩ further improved the change in discharge time but the standard deviation (n = 3) of the baseline deteriorated to 29.37 μs.

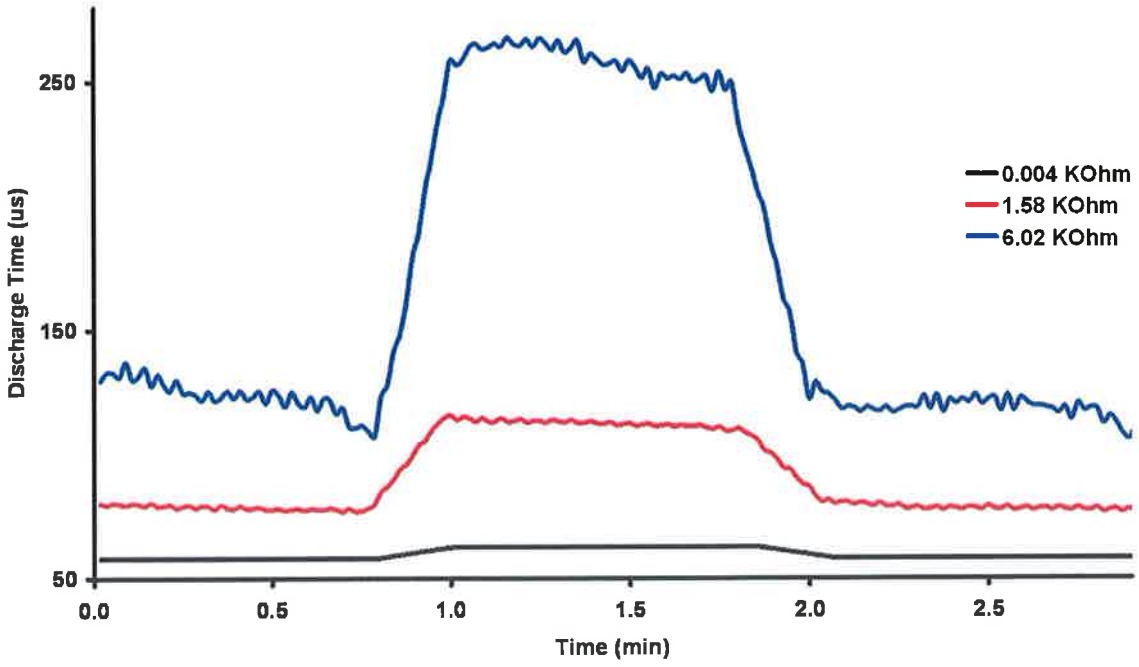

Figure 3.8 Plot obtained for 0.5 μM malachite green-molybdphosphate complex using 0.004 kΩ, 1.58 kΩ and 6.02 kΩ.

Further increases in resistance increased the peak height even more, but caused more baseline drift and higher R.S.D. values as shown in Figure 3.8. Applying a moving average to the data set can compensate for the increase in baseline noise and drift. An additional disadvantage however of over-increasing the emitter resistance is that the

resulting decrease in emitted light intensity can lead to a reduction in the dynamic range.

Table 3.1 Data outlining the effect of decreasing emitter light intensity on 0.5 μM malachite green-molybdphosphate complex peak height (i.e. change in discharge time), standard deviation of the baseline and S/N (n = 3).

Resistance (KΩ)	Peak Height (μs)	Baseline Std Dev (μs)	S/N
0.004	4.78	0.14	33.83
0.55	8.81	0.64	13.69
1.15	22.15	3.45	6.43
1.58	32.59	6.95	4.69
2.00	47.27	10.46	4.52
3.02	70.27	22.25	3.16
4.09	90.50	34.02	2.66

The data presented in Table 3.1 shows that while decreasing the emitter light intensity (i.e. by increasing the resistance applied to the emitter LED) results in an increase in the change in discharge time (μs) it also brings about an increase in the standard deviation of the baseline, which ultimately decreases the signal to noise ratio (S/N) calculated. The change in discharge time (μs) achieved applying a minimal resistance (0.004 KΩ) obtained an excellent S/N, however the lower limit of the dynamic range at this light intensity is significantly reduced. This is due to the strength of the emitter light intensity. The detector LED is discharged from logic 1 (5 V) to logic 0 (1.7 V) so rapidly that changes in low level malachite green-molybdphosphate concentrations (sub μM) are negligible. Selecting an optimum resistance to apply to the emitter LED is a compromise between decreasing the lower limit of the dynamic range while maintaining a good S/N.

Reagent Ratio

The optimum reagent to sample ratio was determined by preparing a range of samples at a concentration of 2 μM PO_4 with varying volumes of MG reagent (0.1 – 2 mL) added. The normalized maximum absorbance (R/R_{max}) of each sample was recorded after 40 minutes and plotted against the volume of reagent added to 6 mL of sample, see Figure 3.9.

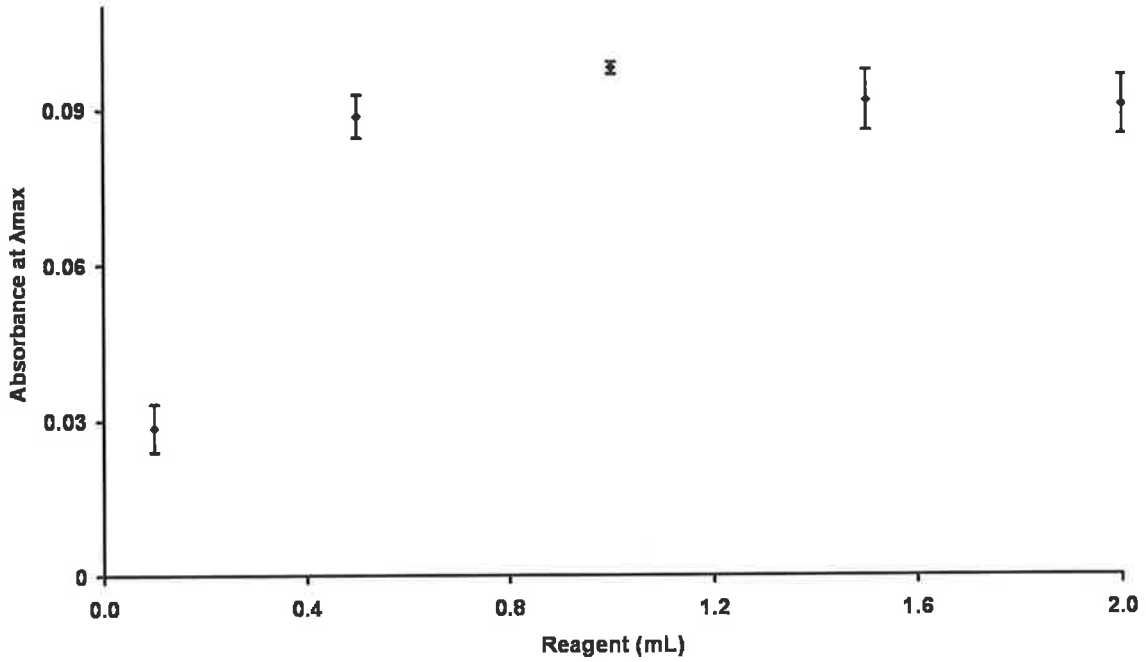

Figure 3.9 Determination of optimum reagent to sample (2 μM PO_4) ratio. The error bars represent the standard deviations for n = 3.

As shown in Figure 3.9 the reagent volume that provides the highest R/R_{max} i.e. the most intense colour was the 6:1 v/v sample to reagent ratio (i.e. 6 mL of sample to 1 mL reagent). This was the sample to reagent ratio adopted throughout all remaining experiments.

Kinetic Study

Linge *et al.* [87] reported a stand time for sample and reagent colour development of approximately 30 minutes. The development of the malachite green-molybdphosphate colour intensity with 0.5 μM PO_4 was monitored using the μQuant™ platewell reader by taking an absorbance measurement every 2 minutes.

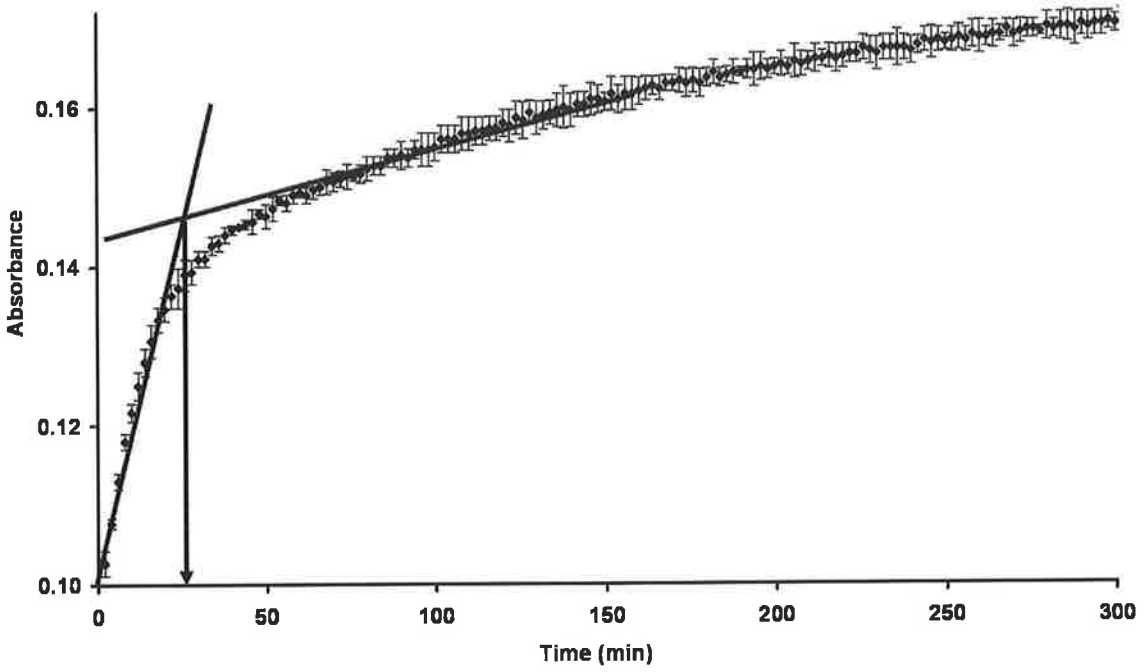

Figure 3.10 Kinetic study of the colour formation between 0.5 μM PO_4 and MG reagent (n = 3).

As shown in Figure 3.10 the colour formation increased rapidly until approximately 27 minutes after which the rate of increase decreased to a much slower stage. This was in agreement with the time allowed for colour developed outlined by Linge *et al.* [87]. A colour formation time of approximately 30 minutes was adopted for experimental investigations.

3.4.2 Calibration using the PEDD flow cell and the UV-vis spectrophotometer

PEDD

Working calibration solutions between 0.002 and 20 μM were prepared from the stock standard. The malachite green method has a limited range of up to 20 μM before precipitation of MG occurs. Various concentrations of orthophosphate were prepared in deionised water and passed through the PEDD flow cell for ca. 4 minutes per sample, at a flow rate of 0.6 $mLmin^{-1}$. The log of the discharge times (log t, μs) was plotted against malachite green-molybdphosphate complex concentration (C) in accordance with the model (Equation 2.4) and the result is presented in Figure 3.11. The inset plot shows a large dynamic range from ca. 0 to 20 μM malachite green-molybdphosphate complex from which a linear range of approximately 0.02 – 2 μM malachite green-molybdphosphate (R^2 value 0.9964) was observed as shown in main feature plot.

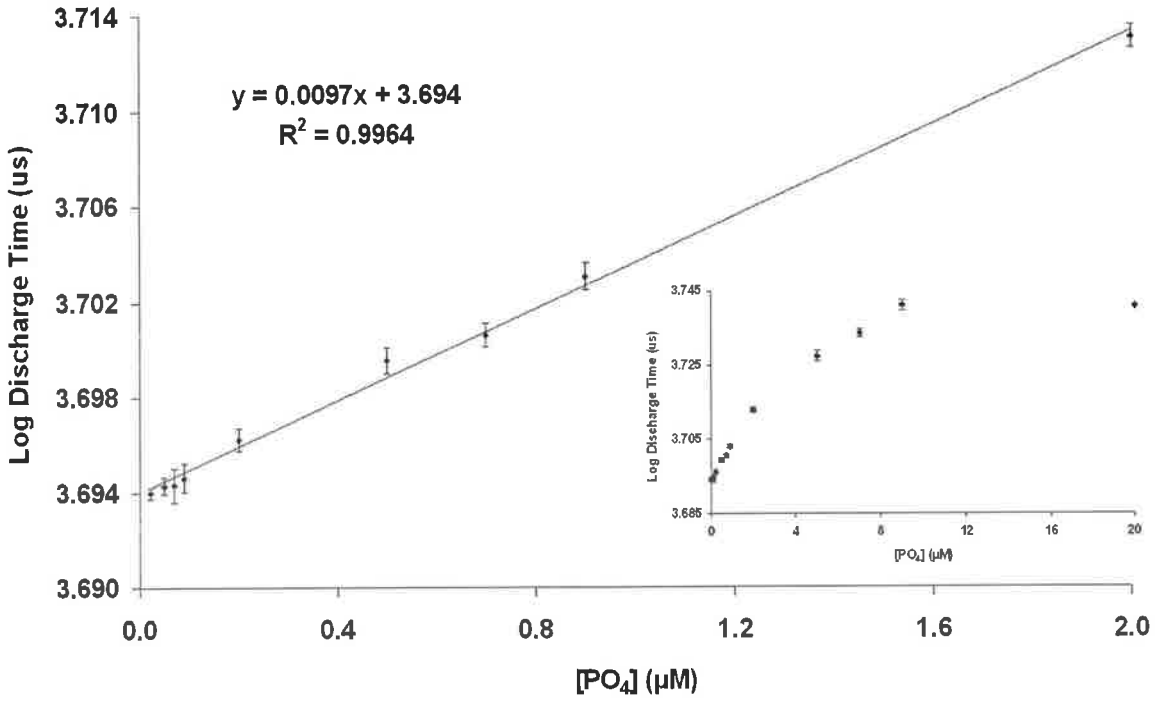

Figure 3.11 Log of the discharge times (t) obtained using a PEDD versus malachite green-molybdphosphate complex concentration. The error bars represent the standard deviations for n = 3. The inset shows the dynamic range of responses obtained from the calibration.

The relative standard deviation of the measurements (n = 3, shown as error bars) is very low (ca. 0.05%).

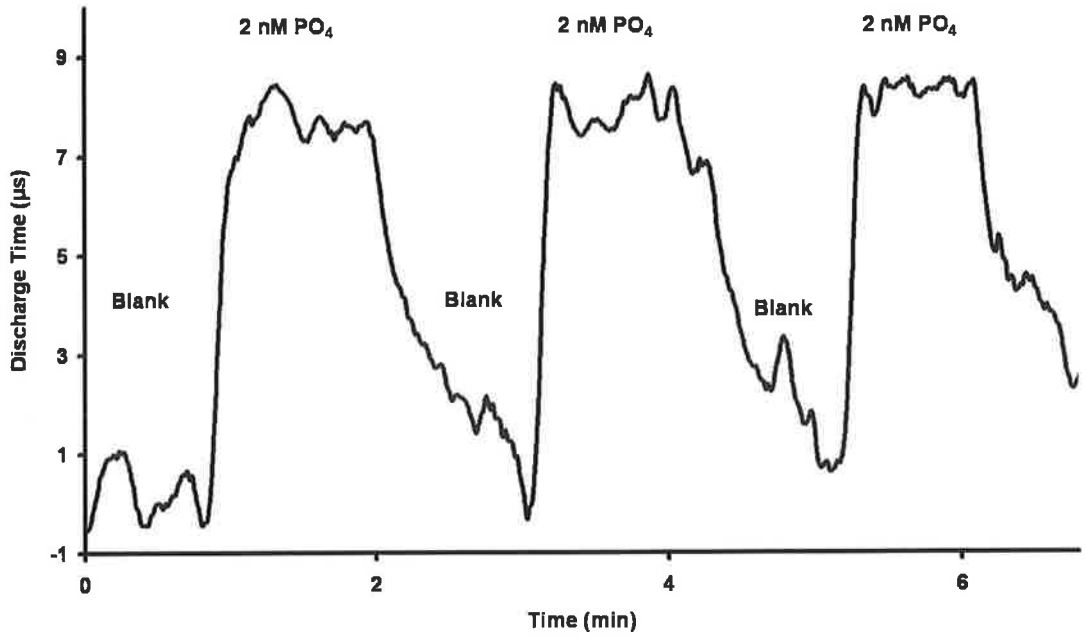

Figure 3.12 Determination of the LOD of the malachite green-molybdphosphate complex concentration (2 nM).

An LOD of ca. 2 nM of the malachite green-molybdophosphate complex as shown in Figure 3.12. A blank containing deionised water and the malachite green reagent mixture was passed through the flow cell for approximately 1 minute. This was then followed by a 2 nM malachite green-molybdphosphate complex. The procedure was repeated 3 times. The response (change in discharge time, µs) obtained was 8.49 ± 0.82 µs with an RSD of 9% (n = 3).

LED-PD

A low cost LED-photodiode detector was investigated to compare its performance with that of the PEDD (Table 3.2). As shown in Figure 3.13 the mean change in absorbance, i.e. peak height was plotted against malachite green-molybdphosphate complex concentration (C) resulting in a dynamic range of 0.9 – 10 µM. A linear range of (R^2 value 0.9816) of 2 – 10 µM was achieved, with an R.S.D. (n = 3) of

6.4%. A significantly higher LOD of 2 μM was determined using this comparative LED-photodiode detector.

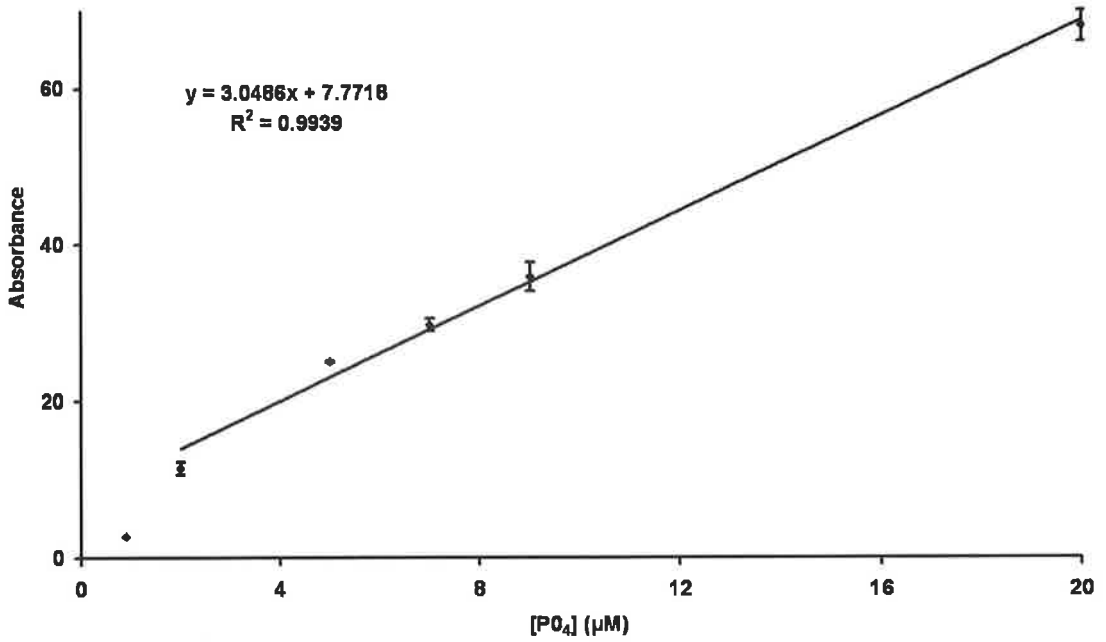

Figure 3.13 Calibration plot of absorbance obtained using an LED-photodiode detector versus malachite green-molybdphosphate complex concentration. The error bars represent the standard deviations for *n*=3.

μQuant™ Platewell Reader

As a comparison study (Table 3.2), the absorbance of the same malachite green-molybdphosphate complex concentrations was acquired employing a μQuant™ platewell reader. As shown in Figure 3.14 the mean normalized maximum absorbance (R/R_{max}) was plotted against malachite green-molybdphosphate complex concentration (C) resulting in a dynamic range of 0.2 – 20 μM. A linear range of (R^2 value 0.9947) of 0.2 – 2 μM was achieved, with an R.S.D. (n = 3) of 8.7%. A significantly higher LOD of 0.2 μM was determined using the μQuant™ platewell reader.

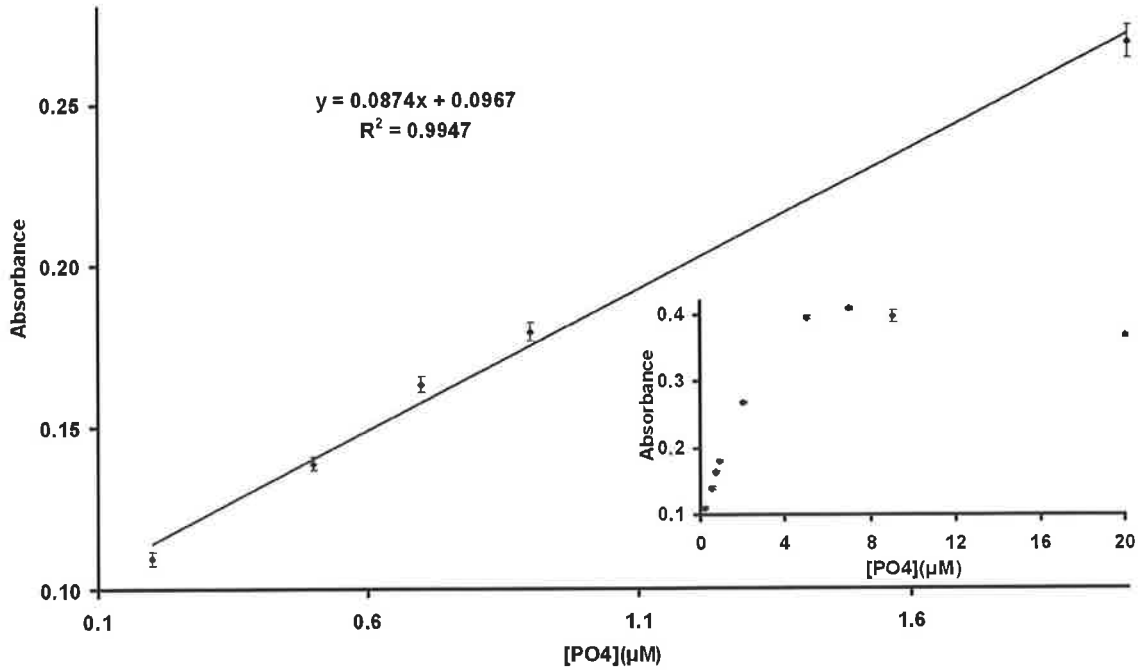

Figure 3.14 Calibration plot of absorbance at λ_{max} obtained using a µQuant™ platewell reader versus malachite green-molybdphosphate complex concentration. The error bars represent the standard deviations for n=3.

Table 3.2 A comparative summary of the data obtained for the detection of malachite green-molybdphosphate complexes using a PEDD, LED-PD and a µQuant™ platewell reader (n = 3).

	PEDD (λ_{max} 636 nm)	LED-PD (λ_{max} 636 nm)	µQuant™ platewell reader (λ_{max} 640 nm)
Dynamic Range	2 nM-20 µM	0.9-10 µM	0.2-20 µM
Linear Range	0.002-2 µM	2-10 µM	0.2-2 µM
LOD	2 nM	2 µM	0.2 µM

3.5 Conclusions

The results obtained employing the low cost, miniaturized PEDD flow analysis system exhibits high sensitivity for the detection of orthophosphate. Under optimised conditions the PEDD detector offered a linear range of 0.02 – 2 μM and an LOD of 2 nM. For comparative purposes a simple, low cost LED-photodiode detector and a μQuant™ platewell reader were investigated. The LED-photodiode detector achieved an LOD in the micromolar range (2 μM). Enhanced performance of the LED-photodiode can be achieved by using more precise components and/or higher resolution ADCs, however, the cost incurred for slight increases in sensitivity would not be justified on a low cost sensor. The PEDD device exhibited sensitivity in the nanomolar concentration range, which was approximately 100 times lower than that of the commercially available bench top platewell reader. The PEDD offers advantages of extremely low power consumption, no requirement for an A/D converter or operational amplifier and the sensor can be operated from a 9 V battery. There are however limitations to the method investigated with regard to its potential use in field deployment. The reaction between the orthophosphate and the malachite green reagent mixture takes approximately 30 minutes for colour formation. To improve this reaction time in the field would require additional instrumentation to heat the reaction coil for example. Furthermore the reagents are not stable beyond 24 hours and need to be stored at a temperature of 4^0C. Irrespective of the limitations, the low levels of orthophosphate detected using the malachite green method in conjunction with the PEDD photometric detector show that the system offers huge potential for field deployable analysis. An alternate method which could be investigated to address some of these issues is the employment of the molybdenum blue method which is the standard method for the detection of orthophosphate. The sensitivity reported with the use of this method are slightly lower than that of the malachite green method however it posses advantages of stable reagents, fast kinetics and reproducible method. The use of the molybdenum blue method has been widely reported for field analysis and when used in combination with the PEDD could provide a highly sensitive autonomous system for remote monitoring of orthophosphate levels in-situ.

CHAPTER 4

NOVEL INTEGRATED PEDD AS A MINIATURIZED PHOTOMETRIC DETECTOR IN LC SYSTEMS

4. Novel Integrated PEDD as a Miniaturized Photometric Detector in HPLC

4.1 Introduction

Sensor research is driven by the need to generate a selective response to a particular analyte [18]. Separation prior to detection essentially eliminates the need for highly selective detection for many applications [99]. HPLC as a separation technique offers excellent selectivity through well established combinations of stationary phase and mobile phase and this is often the method of choice for routine Lab-based assays [100]. During the last decade there has been a general trend towards the miniaturization of separation techniques. There are significant advantages that include increased chromatographic resolution, reduced sample volume and reduced solvent consumption [101,102]. These characteristics are also essential criteria for making chromatography instrumentation field-deployable. Coupled with wireless communication, miniaturized field deployable HPLC systems will have an important role in the future realisation of widely distributed environmental monitoring networks [17].

However, there are considerable challenges associated with the miniaturization of all components including pumps, columns and detectors into fully integrated systems. Significant advances have been made in recent years in the development of innovative fluid handling based on electro-osmotic [103] and micro pumps [102,104,105] and of short columns[106]. Comparatively fewer advances have been made in optical detection and UV-vis photodiode array detectors are still the most commonly used detectors in HPLC. They are expensive (> $3,500), relatively large (32 x 21 cm) as shown in Figure 4.1, have high power consumption and are therefore not suitable for field deployment.

Figure 4.1 1050 series Hewlett Packard variable wavelength Detector.

Basic components in a chromatographic separation system include the sample introduction port, the separation column, connecting tubing, fluid control systems (pump, valves), and detector. For miniaturized systems, components should ideally be integrated, small, low reagent consumption, low power and low cost. The work presented here focuses on developing a miniaturized optical detector for HPLC. LEDs provide convenient source of light illumination in almost the entire visible spectral range [15] and have long been used as light sources because they offer the advantages of being inexpensive, small in size (available as surface mount), cover a broad spectral range from UV to near-IR, robust and exhibit long lifetimes [22]. In sensor research LEDs to date have been primarily used as light sources in optical sensors. Hauser [38-40,55] has long advocated the advantages of using LEDs and was the first to report the use of a blue LED as a spectrophotometric source coupled with a photodiode as a detector. Photodiodes are one of the most commonly used detectors in optical sensors [20,39,50,51].

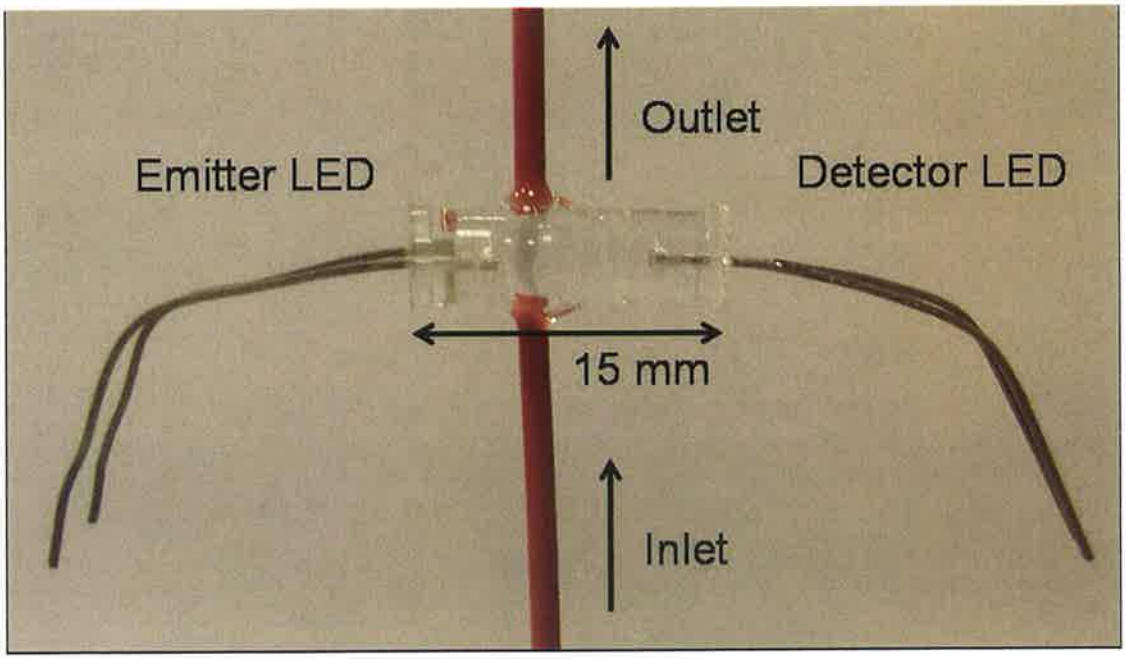

Figure 4.2 Photograph of paired emitter-detector diode (PEDD)

In most microanalytical systems the light source and the photodetector are normally separate units integrated with the microfluidic manifold [74]. We have previously demonstrated the use of the integrated PEDD device for colour and pH measurements in static solution [58,59] and subsequently fabricated a single unit containing light source, fluid channel and detector for flow analysis [60]. The PEDD integrated flow cell detector is highly sensitive (detection limits in the sub micromolar range), low power, extremely low cost (< $1) and small in size (Figure 4.2).

4.1.1 Project Aim

The work presented here will demonstrate for the first time the use of an integrated PEDD flow cell as a simple, small, highly sensitive, low cost photometric detector for HPLC. Using a post column colorimetric detection method commonly used for transition metal ions [107], manganese and cobalt were separated on a miniature Nucleosil 100-7 IDA functionalized column [108]. The coloured metal complexes formed by reacting the transition metal ions with a post column reagent (PCR) mixture containing 4-(2-pyridylazo) resorcinol (PAR) and ammonia were detected inline by the HPLC variable wavelength detector and the PEDD device.

Spectrophotometric detection of metal complexes with PAR is a rapid, sensitive and convenient technique used for quantitative metal analyses [109,110]. The colour forming reaction is rapid and so can be carried out by direct mixing of the PCR reagent and eluent in a simple mixing tee-piece [111].

Employing a post-column reagent method, a Nucleosil 100-7 (functionalised with iminodiacetic acid (IDA) groups) column was used to separate a mixture of transition metals, manganese (II) and cobalt (II). All optical measurements were taken by using both the HPLC variable wavelength detector and the proposed paired-emitter-detector-diode (PEDD) optical detector configured in-line for data comparison. The concentration range investigated using the PEDD was found to give a linear response to the Mn (II) and Co (II) PAR complexes. The effects of flow rate and emitter LED light source intensity were investigated. Under optimised conditions the PEDD detector offered higher sensitivity and improved precision compared to the variable wavelength detector.

4.2 Experimental Procedure

4.2.1 Equipment

A Hewlett Packard series 1050 HPLC system (Agilent Technologies., Dublin) was used to deliver the eluent at a flow rate of 0.7 mL/min. Samples were injected using an automated injector with a sample loop of 100 μL. A Nucleosil 100-7 column covalently functionalised with IDA groups of 4 x 14 mm in size was used for the ion separation. A Gilson (MiniPlus 3) peristaltic pump, (Anachem, UK) at a flow rate setting of 0.38 mL/min was used for the introduction of the post-column reagent (PCR), which was mixed at room temperature with the eluent using 0.5 m of PEEK reaction coil (0.25 mm i.d., VICI® AG International, Switzerland). A single channel PEDD flow cell (Emitter λ_{max} 500 nm, Detector λ_{max} 621 nm, Figure 4.2) was used inline with the Hewlett Packard (series 1050) UV-vis variable wavelength detector (Agilent Technologies, Dublin) for the detection of the metal complexes.

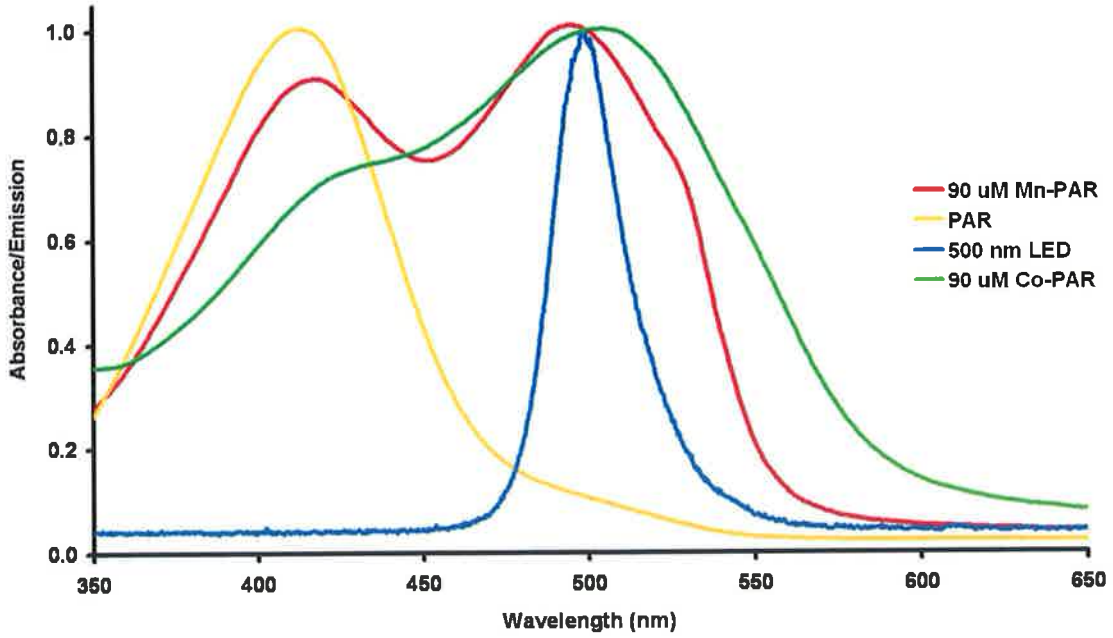

Figure 4.3 Emission spectrum (λ_{max} 500 nm) of the emitter LED (blue line) used in the integrated PEDD flow analysis device and the absorption spectra (λ_{max} 500 nm) of 90 µM Mn-PAR (red line), (λ_{max} 510 nm) 90 µM Co-PAR (green line) and (λ_{max} 420 nm) PAR (gold line).

Figure 4.3 shows that the absorption spectra of manganese (II) and cobalt (II) PCR complexes overlap with the emission spectrum of the PEDD device. The emission spectrum of the green emitter LED was obtained by using an Ocean Optic spectrometer (OOIBase 32™, Ocean Optics. Inc., Dunedin, USA). The absorbance spectra of manganese (II) and cobalt (II) PAR complexes were acquired using the µQuant™ platewell reader (Bio – Tek Instruments, Inc., USA). The overlap between absorbing species and the light source provide high sensitivity for the detection of Mn-PAR and Co-PAR.

4.2.2 Chemicals

- 4-(2-pyridylazo) resorcinol monosodium salt hydrate (PAR) (Sigma Aldrich, Dublin)
- Ammonia (35%, BDH, Poole, England)
- Manganese chloride tetrahydrate (Sigma Aldrich, Dublin)

- Cobalt (II)-nitrate hexahydrate (Sigma Aldrich, Dublin)
- Milli-Q water (Millipore Ireland B.V., Cork)
- Nitric acid (70%, East Anglia Chemicals, Suffolk, England)

4.2.3 Reagents and Solutions

All solutions were vacuum filtered through a 0.45 μm filter and degassed by sonication. The mobile phase, stock solutions and standard solutions were prepared using water from a Millipore Milli-Q water purification system.

Post Column Reagent (PCR)

The PCR reagent used for the detection of the transition metal ions consisted of a mixture of 0.4 mM 4-(2-pyridylazo) resorcinol monosodium salt hydrate (PAR and 0.5 M ammonia, which was adjusted to pH 10.5. A concentration of 0.4 mM was prepared by dissolving 0.09488 g of PAR in 1 L of 0.5 M ammonia.

Mobile Phase (3 mM nitric acid)

The 3 mM nitric acid mobile phase was prepared by diluting 270 μL of 70% nitric acid to 1 L with Milli-Q ultrapure water.

Manganese and Cobalt standards

A stock solution was of 1 mM manganese chloride tetrahydrate and cobalt (II)-nitrate hexahydrate was prepared by dissolving 0.0495 g of manganese and 0.0325 g of cobalt in a 250 mL volumetric flask. Dilutions were prepared daily from the 1 mM stock solution.

4.2.4 Fabrication and operation of integrated PEDD flow cell detector

The integrated detector cell was fabricated as previously described [60] using two 5 mm LEDs (Kingbright, Ireland) as shown in Figure 4.4. The detector used was a red LED with a λ_{max} at 621 nm. A green LED with a λ_{max} at 500 nm was used as the emitter.

The PEDD flow cell was operated as described in section 2.2.2 and the data was captured and saved according to section 2.2.3.

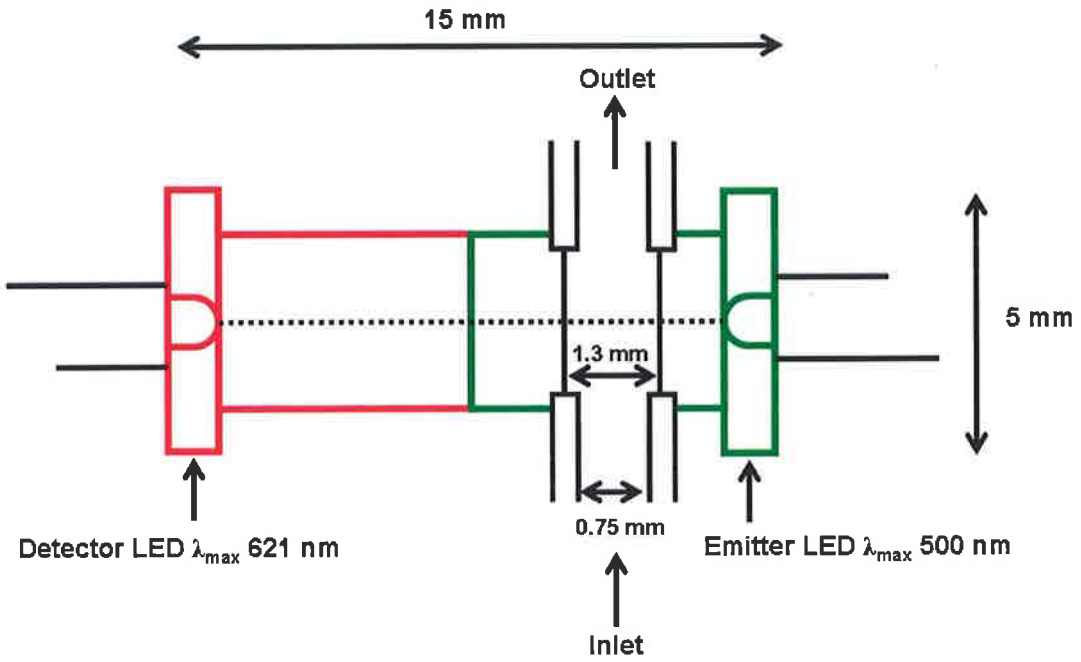

Figure 4.4 A schematic of the integrated PEDD flow analysis device used for colorimetric detection.

4.2.5 Measurement Procedure

Various concentrations of Mn (II) and Co (II) were made up in Milli-Q water and 100 µl aliquots of sample were injected onto the Nucleosil 100-7 column at a flow rate of 0.7 mL/min. The analytes were first detected using the UV-vis detector at a wavelength of 500 nm followed directly by the PEDD flow cell. All experiments were carried out in triplicate (n = 3). The chromatograms obtained from the UV-vis

spectrophotometric detector were analysed using Agilent Chemstation for LC and LC/MS systems software. The data acquired from the PEDD was transported to a PC via RS232 port and captured with HyperTerminal software (Microsoft Inc., USA), saved as a text file and then analysed using Excel™ (Microsoft Inc., USA).

4.2.6 Optimisation of HPLC and PEDD flow cell conditions

Optimisation of HPLC and PEDD parameters such as flow rate and light intensity were carried out. A concentration of 2 μM manganese (II) solution was selected to carry out the study as it provided reproducible responses and good peak size and shape.

Light Intensity

Procedure

- The peristaltic pump delivering the PCR was set at 0.26 mL/min
- The mobile phase was delivered at a flow rate of 0.7 mL/min
- A 100 μL injection of 2 μM Mn (II) was made
- Various light intensities brought about by varying the resistance on the emitter LED were examined
- The data was captured as outlined in section 3.2.5
- Each injection was carried out in triplicate

PCR Flow Rate

Procedure

- The mobile phase was delivered at a flow rate of 0.7 mL/min
- A 100 μL injection of 2 μM Mn (II) was made

- Various flow settings of the peristaltic pump delivering the PCR were examined
- A resistance of 1.5 kΩ was applied to the emitter LED
- The data was captured as outlined in section 3.2.5
- Each injection was carried out in triplicate

4.2.7 Separation and Detection of Manganese (II) and Cobalt (II) PAR complexes

A study was carried out to investigate whether the PEDD flow cell caused additional peak broadening to the detection of manganese (II) and cobalt (II) PAR complexes.

Procedure

- A 100 µL injection of 5 µM manganese and cobalt was made
- The mobile phase was delivered at a flow rate of 0.7 mL/min
- The PCR was delivered at a pump setting of 0.38 mL/min
- A resistance of 1.5 kΩ was applied to the emitter LED
- Data was captured as outlined in section 3.2.5

4.2.8 Calibration using the PEDD flow cell and the UV-vis spectrophotometer

A study was carried out involving the calibration of a change in concentration of manganese and cobalt PAR complexes.

Procedure

- 100 µL injections at various concentrations of manganese and cobalt were made

- The mobile phase was delivered at a flow rate of 0.7 mL/min
- The PCR was delivered at a pump setting of 0.38 mL/min
- A resistance of 1.5 kΩ was applied to the emitter LED
- Data was captured as outlined in section 3.2.5 using both the PEDD flow cell and a UV-vis spectrophotometer
- All injections were carried out in triplicate

4.3 Results and discussion

4.3.1 Optimisation of HPLC and PEDD flow cell conditions

The data obtained by the PEDD is based on the theoretical model derived by Lau *et al.* as discussed in section 2.2.1 [58,59].

$$\mathbf{Log}\ (t) = \varepsilon Cl + \mathbf{log}\ (t_0) \qquad \textbf{Equation 4.1}$$

Optimisation of HPLC and PEDD parameters such as flow rate and light intensity were carried out. Optimal separation conditions were determined to be: eluent flow rate of 0.7 mL/min and peristaltic pump rate setting of 0.38 mL/min. Previous studies have shown that on decreasing the light intensity of the emitter LED, sensitivity can be improved by a factor of 4 [60]. LED light intensity varies with make and wavelength therefore optimisation of the 500 nm PEDD flow cell light intensity was required. A (0-10 kΩ) variable resistor was used to determine the optimum light intensity of the green emitter LED to achieve optimum sensitivity i.e. by varying the electrical current applied to the emitter LED. As shown in Figure 4.5 the detector response increases with an increase in electrical resistance at the LED emitter.

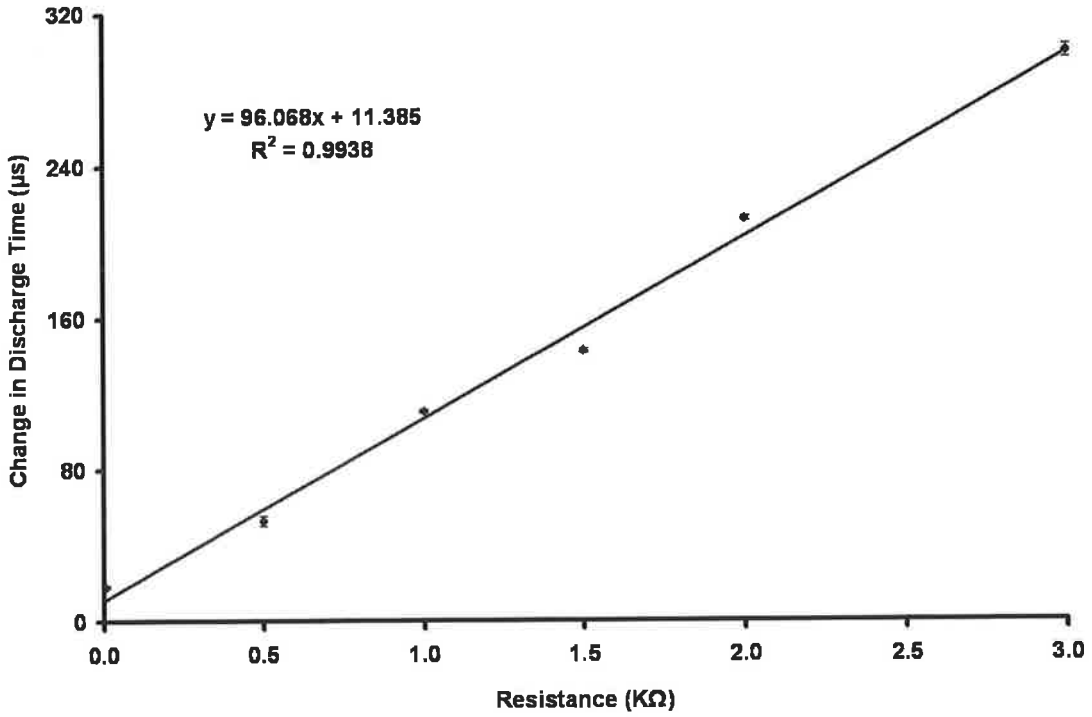

Figure 4.5 The effect of varying light intensity on the change in discharge time detected from baseline (PAR) to 2 µM Mn-PAR by changing the resistance of the variable resistor connecting to the emitter LED. The error bars represent the standard deviations (*n*=3).

A resistance of 1.5 kΩ was found to provide the optimum light source intensity giving high sensitivity, while maintaining a smooth baseline without drift. These effects are clearly demonstrated in Figure 4.6. For example, at a resistance of 0.005 kΩ, the difference in discharge time (Δt) i.e. peak height was 18.33 ± 0.58 µs with an R.S.D. (n = 3) of 3.15%. At an additional applied resistance of 1.5 kΩ the peak height obtained was 142.67 ± 1.15 µs with 0.81% R.S.D. (n = 3). At a resistance of 4 kΩ the peak height achieved was 457.33 ± 13.20 µs with 2.89% R.S.D. (n = 3).

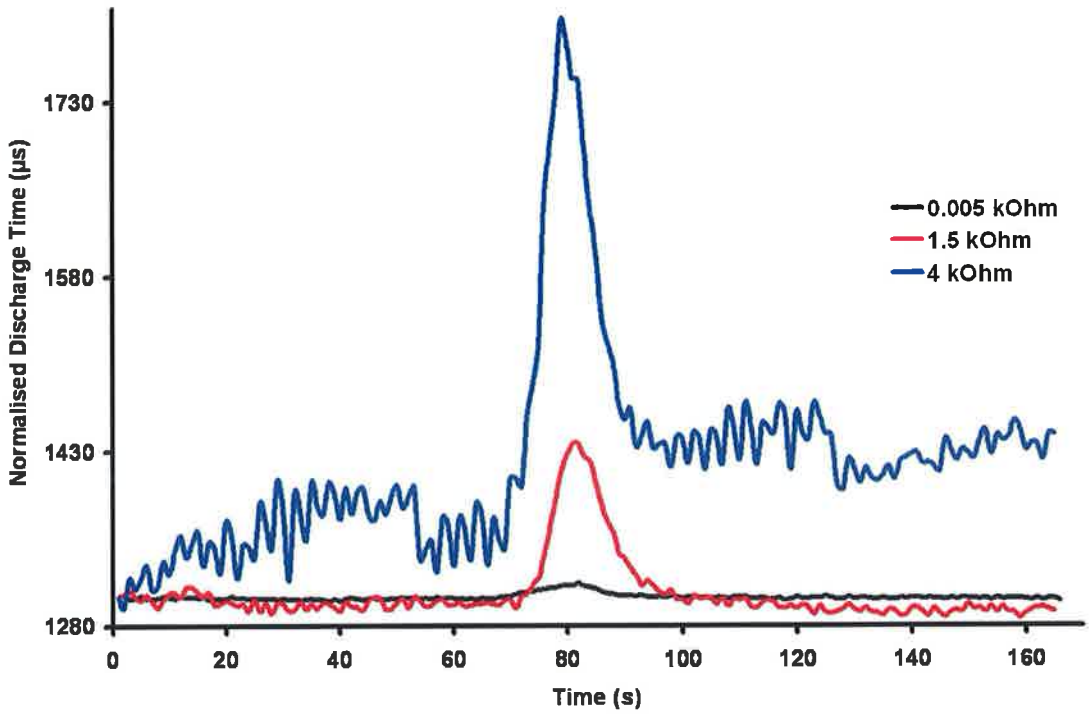

Figure 4.6 Real time traces obtained for 100 µL injections of 2 µM Mn-PAR sample using 3 resistances (0.005 kΩ, bold line, 1.5 kΩ, dashed line and 4 kΩ, solid line). The PCR flow setting used was 0.38 mL/min.

As the data shows, on increasing the resistance the baseline discharge time also increases. This in turn reduces the dynamic range of the PEDD system as the maximum discharge time of 65504 µs is now approached. A resistance of 1.5 kΩ was selected as the compromise resistance as this improved the peak height by a factor of 8. Further increase in resistance increased the peak height even more, but caused more baseline drift and higher R.S.D. values as shown in Figure 4.6 and Table 4.1. Higher resistances also reduced the dynamic range significantly.

Table 4.1 Effect of varying light intensity on the baseline (PAR) stability (n = 3).

Resistance (kΩ)	PAR	Standard Deviation	R.S.D.%
0.005	1303.36	0.91	0.07
0.5	4376.46	5.66	0.13
1.0	6904.75	4.08	0.06
1.5	9651.47	5.68	0.06
2.0	11868.85	8.21	0.07
3.0	17239.35	6.48	0.04
4.0	25859.73	30.48	0.12

The optimal PCR delivery rate was determined experimentally as 0.38 mL/min as this achieved the highest response for the detection of 2 μM Mn-PAR. This setting was used in subsequent experiments.

4.3.2 Separation and Detection of Manganese (II) and Cobalt (II) PAR complexes

To investigate whether the PEDD flow cell caused additional peak broadening a 5 μM mixture of manganese (II) and cobalt (II) was prepared and injected (n = 3). The chromatogram obtained from the UV-vis spectrophotometric detector shown in Figure 4.7 (A) shows two well-resolved peaks (Table 4.2) with retention times of 1.3 and 2.1 minutes for manganese (II) and cobalt (II) PAR complexes respectively. The average peak area calculated for Mn-PAR and Co-PAR had relative standard deviations of 0.29% and 2.71% respectively.

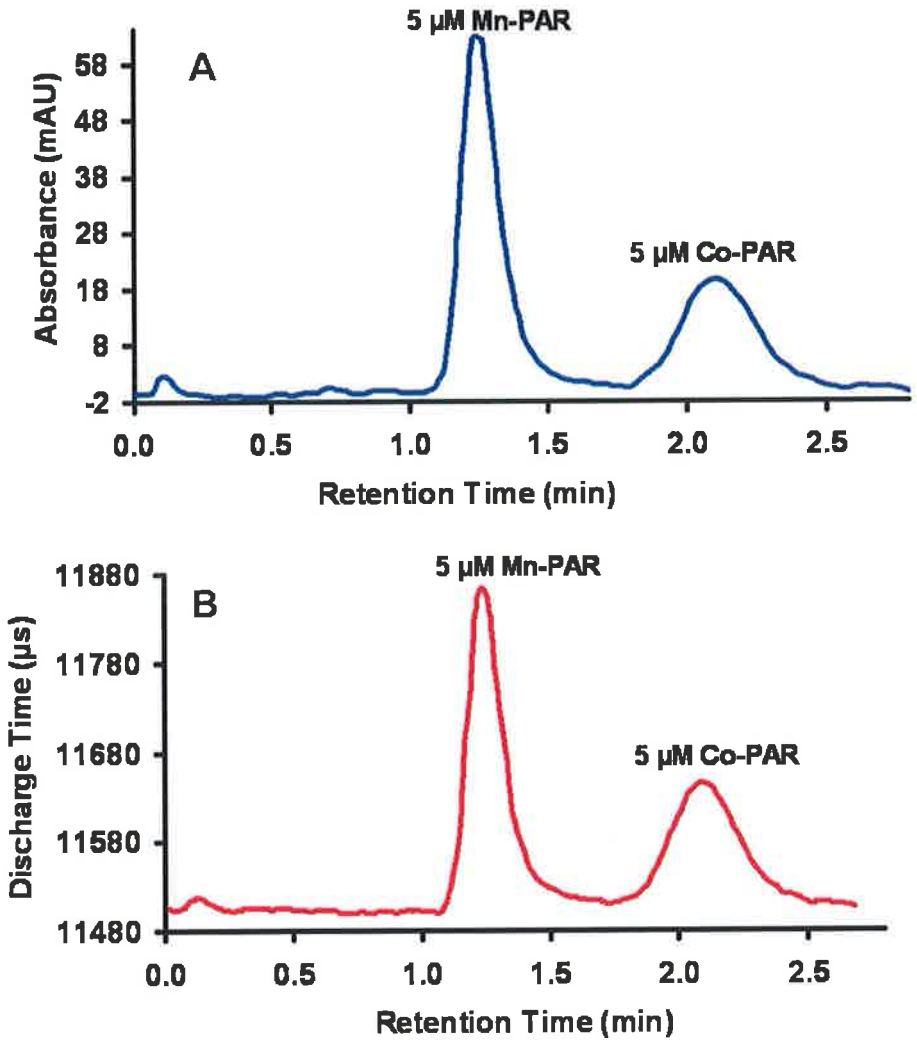

Figure 4.7 A comparison of the chromatograms obtained for the detection of 5 µM Mn (II) and Co (II) PAR complexes using the spectrophotometric detector (A) and the PEDD flow device (B).

The PAR complex detection data (discharge time *t*/µs) was plotted against retention time (minutes) and presented in Figure 4.7 (B). As shown in Figure 4.7 (B) the plot obtained from the PEDD shows identical retention times to that acquired from the UV-vis spectrophotometric detector. The mean peak height (discharge time/µs) calculated for Mn (II) and Co (II) PAR complexes both had a relative standard deviation of 0.04% (n = 3). The peak efficiencies calculated for both the UV-vis variable wavelength and the PEDD flow device are presented in Table 4.2. The results obtained show similar peak efficiencies and indicate that the PEDD flow device does not cause additional peak broadening to the sample peaks.

Table 4.2 Retention data for transition metal PCR complexes on a Nucleosil 100-7 (functionalized with IDA) column. The efficiency was calculated from: $5.54(t_R/W_{½})^2$.

	PEDD (500 nm)	VWD (500 nm)
Resolution	2.05	1.98
Mn-PAR efficiency, *N*	365.73	365.73
Co-PAR efficiency, *N*	311.63	224.35

4.3.3 Calibration using the PEDD flow cell and the UV-vis spectrophotometer

Mixtures containing various concentrations of manganese (II) and cobalt (II) were passed through the HPLC system using the optimal conditions (carrier flow rate of 0.7 mL/min, PCR flow setting of 0.38 mL/min and a 1.5 kΩ current limiting resistor on the emitter LED). Each injection was carried out in triplicate (n = 3). Results were acquired simultaneously using both a UV-vis spectrophotometric detector in-line with the PEDD flow cell.

Figure 4.8 shows results obtained from the PEDD flow cell. The peak heights (log $t/\mu s$) of each transition metal complex detected were plotted against the input ion concentration (C) in accordance with the model (Eqn. 4.1).

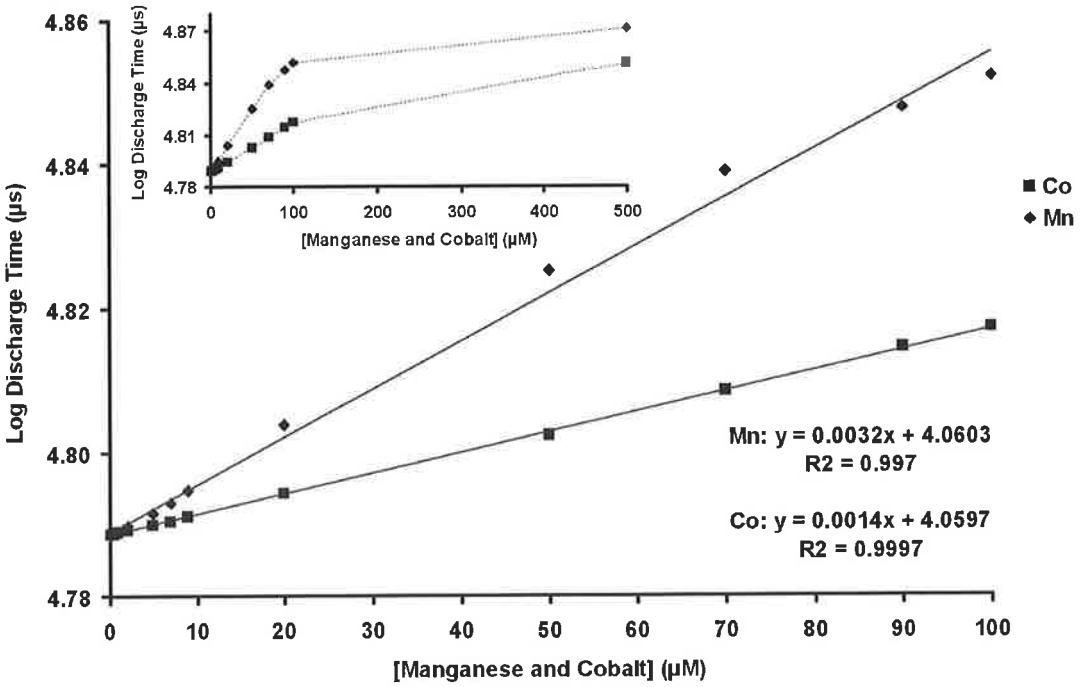

Figure 4.8 Log of the discharge times (t) obtained using a PEDD versus Mn (II) and Co (II) PAR complex concentration. The error bars represent the standard deviations for n=3. The inset shows the dynamic range of responses obtained from the calibration.

A large detection range (shown in the inset) from 0.09 µM to 500 µM with linear ranges of 0.9 – 100 µM for Mn-PAR (R^2 = 0.997) and 0.2 – 100 µM Co-PAR (R^2 = 0.9997) were obtained. It can be seen from Figure 4.8 that the relative standard deviation of the measurements (n = 3, shown as error bars) were very low (<0.08%).

Experimental runs at the minimum detectable concentration for both Mn-PAR and Co-PAR are shown in Figure 4.9 for both the PEDD and the UV-vis detectors to emphasize the improved sensitivity provided by the PEDD. The PEDD achieved an LOD of approximately 0.09 µM for both Mn-PAR and Co-PAR.

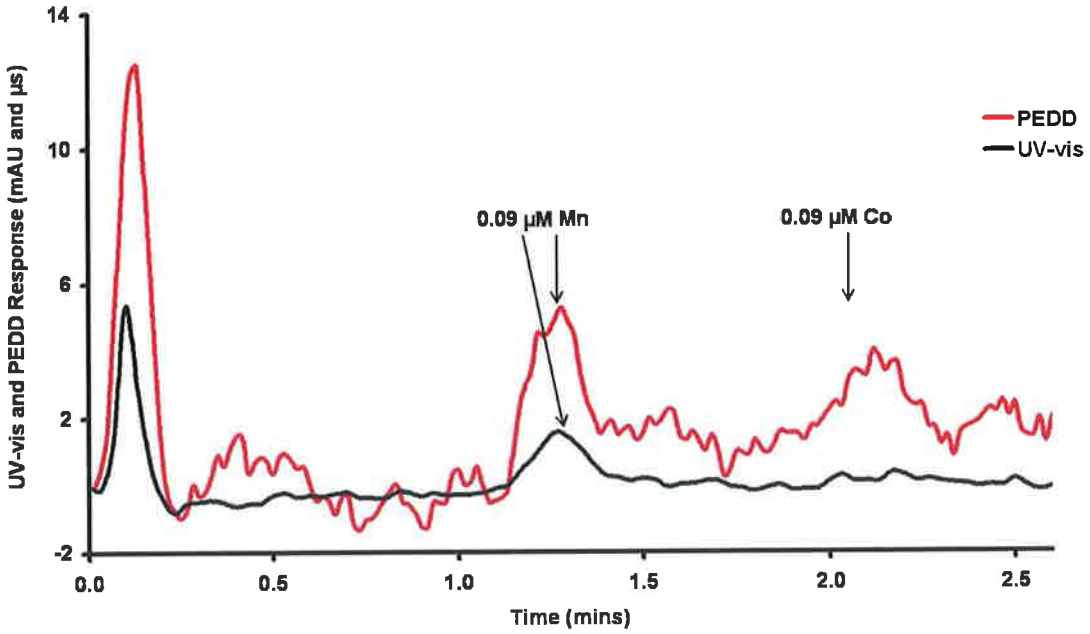

Figure 4.9 Real time traces of the experimental runs carried out at the LOD concentration of 0.09 µM Mn-PAR and Co-PAR from the PEDD flow device (red line) and the variable wavelength detector (black line).

For the data obtained from the UV-vis detector, the peak area was plotted against concentration (C) and the results were presented in Figure 4.10 for both manganese and cobalt complexes. A similar detection range from 0.09 µM to 500 µM (Inset, Figure 4.10) was achieved for Mn-PAR. A detection range of 0.7 µM to 500 µM was obtained for Co-PAR (inset). The linear ranges obtained were 0.9 – 100 µM for Mn-PAR (R^2 = 0.9981) and 0.7 – 100 µM for Co-PAR (R^2 = 0.9997). An LOD of 0.09 µM was obtained for Mn-PAR but a much higher LOD value of 0.7 µM was achieved for Co-PAR. It can be seen from the inset of Figure 4.10 that the relative standard deviations of the measurements (n = 3, shown as error bars) are in the region of ca. 10%.

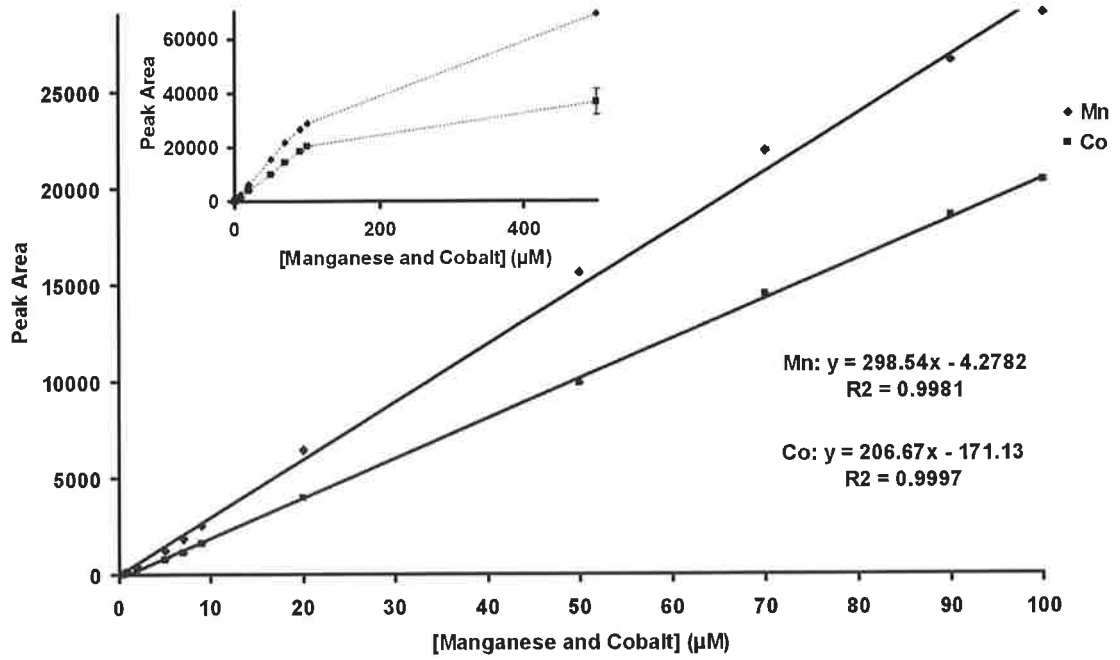

Figure 4.10 Linear calibration plot achieved using the variable wavelength detector of absorbance (mAU) versus Mn (II) and Co (II) PAR complex concentration. The error bars represent the standard deviations for *n*=3. The inset shows the dynamic range of responses obtained from the calibration.

The simple PEDD flow cell was successful as a post column detector for HPLC. The data obtained from this inexpensive, small, power efficient optical detector were comparable to those obtained from the HPLC UV-vis spectrophotometric detector and sensitivity is significantly higher. For the detection of the Co-PAR complex the PEDD response was 6 times more sensitive and for the detection of the Mn-PAR complex the PEDD matched the UV-vis spectrophotometer as shown in Table 4.3.

Table 4.3 A comparative summary of the data obtained for the detection of manganese and cobalt PAR complexes using both a PEDD and a variable wavelength detector (VWD).

	Mn-PAR		*Co-PAR*	
	PEDD	**VWD**	**PEDD**	**VWD**
Dynamic Range	0.09-500 μM	0.09-500 μM	0.09-500 μM	0.7-500 μM
Linear Range	0.9-100 μM	0.9-100 μM	0.9-100 μM	0.7-100 μM
LOD	0.09 μM	0.09 μM	0.09 μM	0.7 μM

4.4 Conclusions

The results obtained using the integrated PEDD flow analysis cell have demonstrated that this simple low cost, low power device can be used as a photometric detector in HPLC. The PEDD flow analysis device was successfully applied to the detection of transition metals manganese and cobalt coupled with the post column reagent PAR. The PEDD flow cell can detect lower concentration levels of Co-PAR than that of an expensive, commercially available bench top instrument.

This optical sensor has the potential for very broad analytical applications, given that it offers high sensitivity and precision with excellent signal-to-noise characteristics. The PEDD flow cell is therefore ideal for detection of multiple analytes when operated in conjunction with a separation technique. A simple PEDD detector cannot replace the existing variable wavelength detector because of the limited bandwidth a single LED can cover, however, a more sophisticated PEDD device with multiple LED sources covering a wider range of wavelengths could make this possible. For specific applications where an appropriate operation wavelength can be selected for the analytes a single PEDD flow detector is ideal and preferable to a more complex multi-source detector.

This small flow detector when coupled with a miniature low pressure separation column, such as the one used in this work, and a pressure/pumping unit, such as a small gas cylinder, could form a complete miniature HPLC system suitable for rapid small sample analysis. Apart from working as a small bench top analytical device, such a system may also be developed as a field deployable autonomous monitoring device.

CHAPTER 5

Limit of Detection Improvements in HPLC Employing a PEDD Dual Wavelength Monitoring Procedure

5. Limit of Detection Improvements in HPLC Employing a PEDD Dual Wavelength Monitoring Procedure

5.1 Introduction

A common method employed in liquid chromatography to convert non-absorbing or weakly absorbing analytes of interest to strongly absorbing analytes is the use of post column derivatisation. There are many colorimetric reactions which can be applied post column as outlined in Table 5.1. Although widely used in certain liquid chromatography applications, post column reactions (PCR) do possess some disadvantages such as the increased cost and complexity due to the requirement of an additional pump. The main disadvantage, however, is the increase in baseline noise. This can be accounted for due to (A) mixing noise arising from imperfect mixing of the eluent and the PCR reagent, (B) cell noise due to the background eluent flowing through the detector, which (in the absence of analyte) produces a finite detector signal and (C) any variations in the mixing profiles of the PCR reagent and eluent will cause baseline noise in the detector [110]. These factors adversely affect the limit of detection (LOD) as it is typically calculated as three times the standard deviation of the baseline (Figure 5.1).

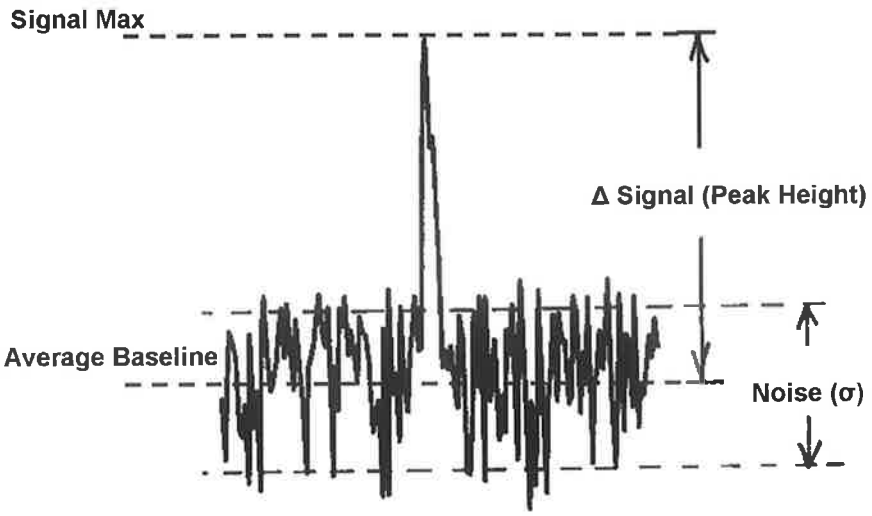

Figure 5.1 Limit of Detection (LOD) is commonly determined as three times the standard deviation (σ) of the baseline [112].

Table 5.1 Examples of post-column reactions (PCR) in liquid chromatography [110,111].

Solutes	*Post-column Reagent*
Cations	
Thorium (IV)	Arsenazo III, PAR
Zirconium (IV)	Arsenazo III, PAR
Aluminium (III)	Arsenazo III
Lanthanides (III)	Arsenazo III
Iron (II and III)	PAR
Manganese (II)	PAR
Cobalt (II)	PAR, Luminol
Copper (II)	Arsenazo III, PAR
Magnesium (II)	Arsenazo I
Calcium (II)	Arsenazo I, Arsenazo III
Anions	
NO_2^-, NO_3^-	Ce (IV) in H_2SO_4
HPO_4^{2-}, $H_2PO_2^-$, HPO_3^{2-}, $H_2PO_4^{2-}$,	Mo (V)-Mo (VI)
EDTA, NTA, SO_4^{2-}, citrate	$Fe(ClO_4)_3$

In chromatography response (e.g. peak height) can be a misleading measure of sensitivity. As shown in Figure 5.2, chromatogram A displays a larger response for peak 1 and 2 than that of peak 3 and 4 in chromatogram B. The baseline noise however is much greater in chromatogram A than chromatogram B. The signal to noise ratios calculated for peak 1 and 2 in chromatogram A are 28 and 6 respectively. The signal to noise ratios calculated for peak 3 and 4 in chromatogram B are 75 and 10 respectively.

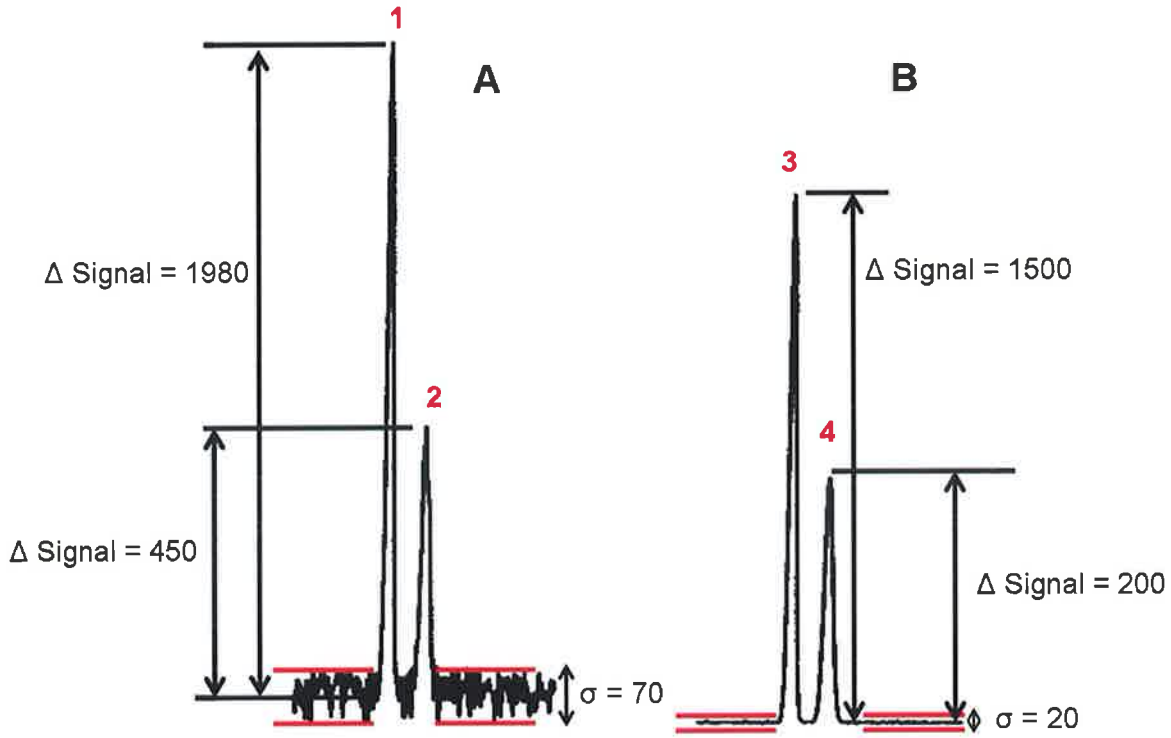

Figure 5.2 Comparison of chromatograms with different background noise [112].

To improve limit of detection values in chromatograms such as Figure 5.2 (A), two approaches can be adopted. The first is to increase the absorbance of the analyte of interest, which will result in an increase in the peak height achieved. The second approach is to reduce the baseline noise. The first approach can be achieved by optimising the wavelength at which the analyte is monitored at. When employing an LED as the light source in a detector it is important that an LED of narrow bandwidth with an emission λ_{max} as close to the analyte absorbance λ_{max} is selected.

The second approach to reduce baseline noise can be achieved by employing a dual wavelength monitoring procedure. In flow injection analysis (FIA) applications, a difference in refractive index (RI) between the sample and the carrier is common, which can lead to an artefact in the absorbance signal often referred to as the Schlieren effect [51]. An additional problem with detection in FIA occurs when samples have any degree of turbidity. Hooley *et al.* proposed the use of an LED combined with a beam splitter and two photodiodes for the correction of drift from the light source [113]. Alternatively, the use of two LEDs first introduced by Worsfold *et al.* in 1987 [50] allows for the correction of colour change, RI or turbidity [51,52,57,114,115].

Jones applied the method of dual wavelength monitoring to improve sensitivity in ion chromatography employing post-column reactions [116]. This was achieved by monitoring at two wavelengths simultaneously using a spectral array detector. The first wavelength selected was the λ_{max} of the analyte, while the second was selected at a wavelength close to the isosbestic point. Employing simple post run processing to manipulate the data the pump noise was subtracted from the analyte baseline, allowing an improved LOD.

5.1.1 Project Aim

The work presented here will demonstrate improved LOD of transition metals in ion chromatography than previously achieved in Chapter 4. The improved LODs for manganese (II) and cobalt (II) PAR complexes were achieved as a result of two methods.

Firstly, the optimum wavelength selected to monitor the analytes of interest was investigated to improve peak response. The fabrication process of PEDD flow cells was validated by determining the reproducibility of the flow cells within a batch. The reproducibility of the detector was investigated for both intra- and inter-day chromatograms.

Secondly, further sensitivity improvements were achieved employing a dual wavelength monitoring procedure described by Jones [116] to reduce baseline noise.

Using a post column colorimetric detection method commonly used for transition metal ions [107], Mn (II) and Co (II) PAR complexes were separated on a miniature Nucleosil 100-7 IDA functionalized column [108]. The coloured metal complexes formed by reacting the transition metal ions with a post column reagent (PCR) mixture containing 4-(2-pyridylazo) resorcinol (PAR) and ammonia were detected as previously described in chapter 4 using a HPLC variable wavelength detector and the PEDD flow cell for data comparison. The optimum experimental procedure determined in chapter 4 was adopted throughout the experiments carried out in this work. The concentration range investigated using the PEDD was found to give a linear response to Mn (II) and Co (II) PAR complexes. Under optimised conditions the PEDD detector offered lower limits of detection and improved precision compared to the variable wavelength detector.

5.2 Experimental Procedure

5.2.1 Equipment

The system was set up as previously described in section 4.2.1, employing a Hewlett Packard series 1050 HPLC system (Agilent Technologies., Dublin) to deliver the eluent at a flow rate of 0.7 mL/min. Samples were injected using an automated injector with a sample loop of 100 µL. A Nucleosil 100-7 column covalently functionalised with IDA groups of 4 x 14 mm in size was used for the ion separation. A Gilson (MiniPlus 3) peristaltic pump, (Anachem, UK) set at a flow rate setting of 0.38 mL/min was used for the introduction of the post-column reagent (PCR), which was mixed at room temperature with the eluent using a 0.5 m PEEK reaction coil (0.25 mm i.d., VICI® AG International, Switzerland).

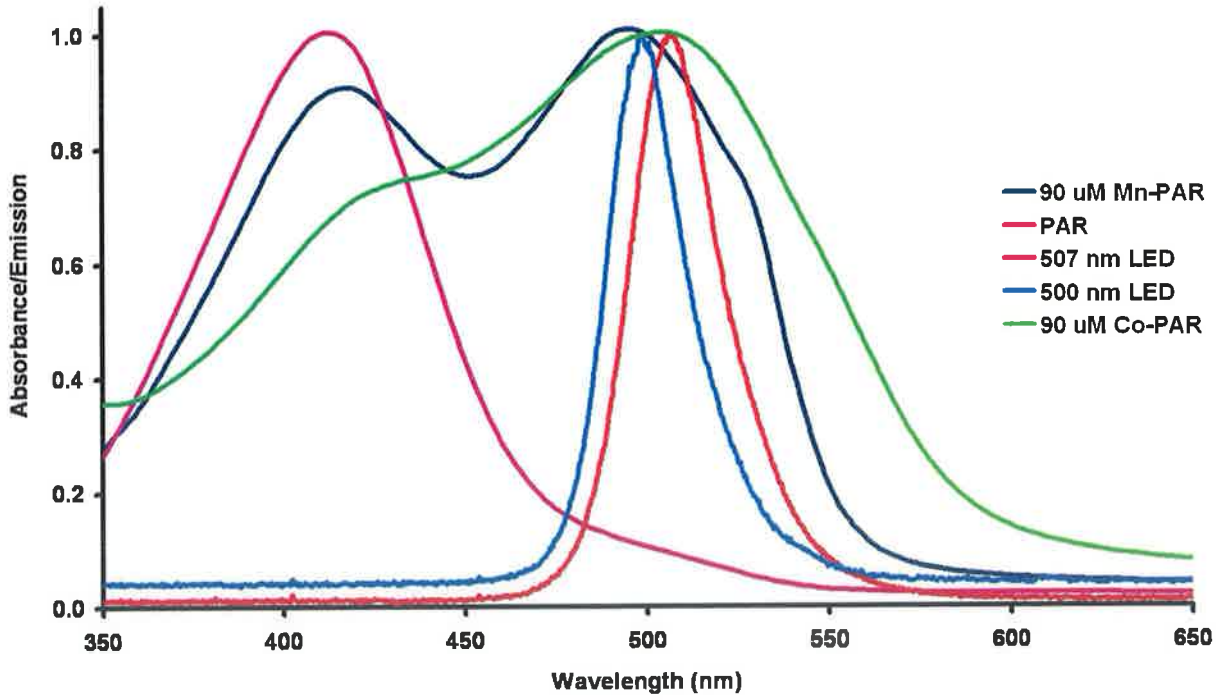

Figure 5.3 Emission spectra (λ_{max} 500 nm (blue line) and λ_{max} 507 nm (red line)) of the emitter LEDs used in the integrated PEDD flow analysis device and the absorption spectra (λ_{max} 500 nm) of 90 µM Mn-PAR (navy line), (λ_{max} 510 nm) 90 µM Co-PAR (green line) and (λ_{max} 420 nm) PAR (pink line).

PEDD flow cells of varying emitter wavelengths were investigated. The PEDD was placed inline with the Hewlett Packard (series 1050) UV-vis variable wavelength detector (Agilent Technologies, Dublin) for the comparative detection of the metal complexes.

Figure 5.3 shows that the absorption spectra of Mn-PAR, Co-PAR and PAR overlap with the emission spectra of the PEDD device. The emission spectra of the green emitter LEDs were obtained using an Ocean Optic spectrometer (OOIBase 32™, Ocean Optics. Inc., Dunedin, USA). The absorbance spectra of manganese (II) and cobalt (II) PAR complexes were acquired using the μQuant™ platewell reader (Bio – Tek Instruments, Inc., USA). The overlap between absorbing species and the light source provide high sensitivity for the detection of Mn-PAR and Co-PAR. To facilitate comparison, the emission and absorption spectra were normalized to a 0-1 range by dividing values by the maximum emission and absorbance achieved.

5.2.2 Chemicals

- 4-(2-pyridylazo) resorcinol monosodium salt hydrate (PAR) (Sigma Aldrich, Dublin)
- Ammonia (35%, BDH, Poole, England)
- Manganese chloride tetrahydrate (Sigma Aldrich, Dublin)
- Cobalt (II)-nitrate hexahydrate (Sigma Aldrich, Dublin)
- Milli-Q water (Millipore Ireland B.V., Cork)
- Nitric acid (70%, East Anglia Chemicals, Suffolk, England)

5.2.3 Reagents and Solutions

All solutions were vacuum filtered through a 0.45 μm filter and degassed by sonication. The mobile phase, stock solutions and standard solutions were prepared using water from a Millipore Milli-Q water purification system.

Post Column Reagent (PCR)

The PCR reagent used for the detection of the transition metal ions consisted of a mixture of 0.4 mM 4-(2-pyridylazo) resorcinol monosodium salt hydrate (PAR and 0.5 M ammonia, which was adjusted to pH 10.5. A concentration of 0.4 mM was prepared by dissolving 0.09488 g of PAR in 1 L of 0.5 M ammonia.

Mobile Phase (3 mM Nitric Acid)

The 3 mM Nitric acid mobile phase was prepared by diluting 270 µL of 70% nitric acid to 1 L with Milli-Q ultrapure water.

Manganese and Cobalt standards

A stock solution was of 1000 ppm manganese chloride tetrahydrate and cobalt (II)-nitrate hexahydrate was prepared by dissolving 0.18013 g of manganese and 0.110165 g of cobalt in a 50 mL volumetric flask. Dilutions were prepared daily from the 1000 ppm stock solution.

5.2.4 Fabrication and operation of integrated PEDD flow cell detector

Single Wavelength PEDD

The integrated detector cell was fabricated as previously described in section 2.2.5 using two 5 mm LEDs (Kingbright, Ireland) (Figure 5.4). As shown in Figure 5.3 Mn and Co PAR complexes have an absorbance λ_{max} of 500 nm and 510 nm respectively. Previously an LED with a λ_{max} of 500 nm was employed to detect Mn and Co PAR complexes. In an attempt to improve the absorbance of the Mn and Co PAR complexes two PEDDs were investigated, whereby one employed a green LED with a λ_{max} at 500 nm and the other a λ_{max} at 507 nm as the emitter (Figure 5.3). The detector used was a red LED with a λ_{max} at 660 nm.

The PEDD flow cell was operated as described in section 2.2.2 and the data was captured and saved according to section 2.2.3.

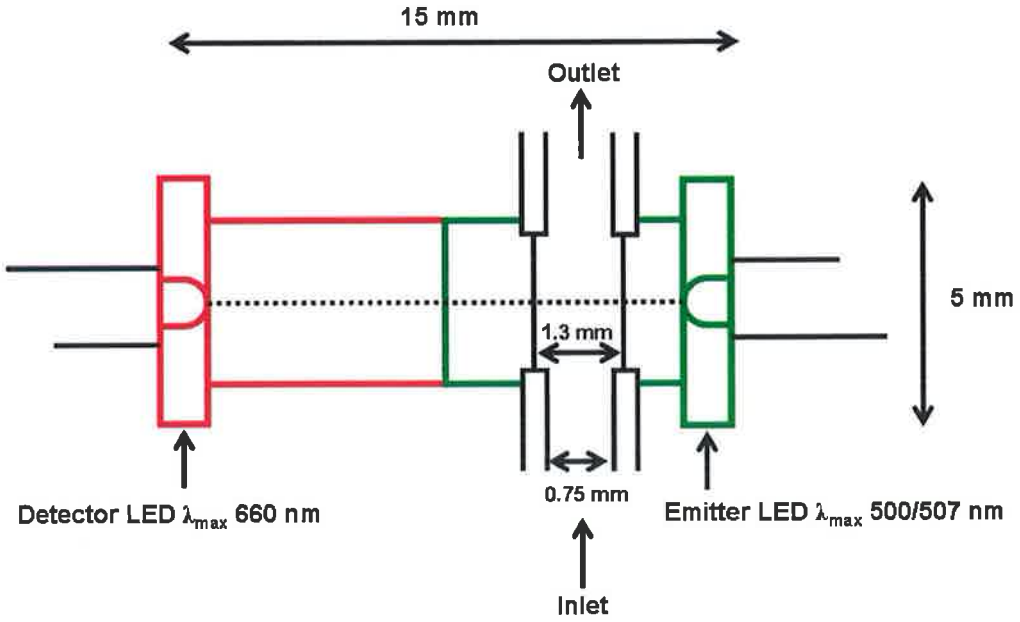

Figure 5.4 A schematic of the single wavelength PEDD flow analysis device used for colorimetric detection.

Dual Wavelength PEDD

The dual wavelength PEDD was fabricated similarly to the single wavelength PEDD previously described. The first PEDD employed a green LED with a λ_{max} at 507 nm as the light source and a red LED with a λ_{max} at 660 nm as the light detector. The second PEDD monitored at wavelength near the isosbestic point, which were ca. 340 nm and 450 nm (Figure 5.14). Several LEDs of varying wavelengths were investigated for this experiment. Figure 5.5 shows an LED with a λ_{max} at 627 nm as the light source monitoring at the reference point with a red LED (λ_{max} at 660 nm) as the light detector. The two PEDDs are joined by PEEK tubing of ca. 1 cm in length.

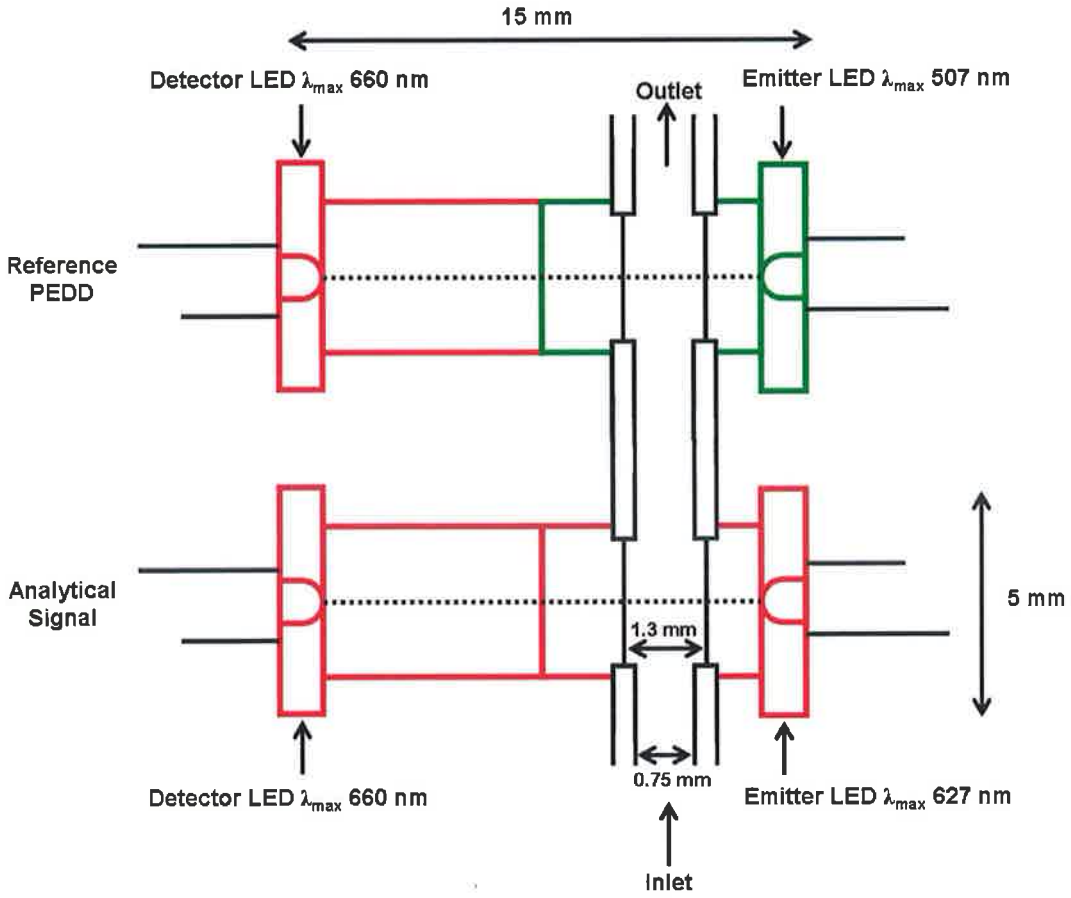

Figure 5.5 A schematic of the integrated dual wavelength PEDD flow analysis device used for colorimetric detection.

The dual wavelength PEDD flow cell was operated as described in section 2.2.2 and the data was captured and saved according to section 2.2.3.

5.2.5 Measurement Procedure

Various concentrations of Mn (II) and Co (II) were made up in Milli-Q water and 100 µl aliquots of sample were injected onto the Nucleosil 100-7 column at a flow rate of 0.7 mL/min. The analytes were first detected using the UV-vis spectrophotometric detector at a wavelength of 500 nm followed directly by the single/dual wavelength PEDD flow cell. All experiments were carried out in triplicate (n = 3). The chromatograms obtained from the UV-vis spectrophotometric detector were analysed using Agilent Chemstation for LC and LC/MS systems software. The data acquired from the PEDD was transferred to a PC via RS232 port and captured with

HyperTerminal software (Microsoft Inc., USA), saved as a text file and then analysed using Excel™ (Microsoft Inc., USA).

5.2.6 Optimisation of Single Wavelength PEDD flow cell detector

Wavelength

The optimum wavelengths to monitor the Mn and Co PAR complexes have been variously reported in the literature, typically citing the λ_{max} in the range of ca. 495-520 nm [107,108,116,117]. Under the optimised experimental conditions determined in chapter 4 the absorbance spectra of 90 μM Mn and Co PAR complexes were acquired using the μQuant™ platewell reader (Bio-Tek Instruments, Inc., USA). A λ_{max} of 500 nm and 510 nm were obtained for 90 μM Mn and Co PAR complexes respectively (Figure 5.3). To determine if improved analyte response with respect to that previously reported could be obtained a PEDD with a λ_{max} of 510 nm was investigated. Manufacturers' descriptions of LEDs can be inaccurate as they vary between batches. 510 nm LEDs obtained for these experiments on investigation actually had a λ_{max} of 507 nm.

Procedure

- The peristaltic pump delivering the PCR was set at 0.38 mL/min
- The mobile phase was delivered at a flow rate of 0.7 mL/min
- A 100 μL injection of 0.25 ppm Mn (II) and Co (II) was made
- 4 PEDDs with a λ_{max} of 500 nm were investigated
- 4 PEDDs with a λ_{max} of 507 nm were investigated
- The data was captured as outlined in section 2.2.3
- Each injection was repeated ten times per PEDD investigated

5.2.7 Validation of Single Wavelength PEDD flow cell detector

Intra/Inter-Day Reproducibility

The reproducibility of the detector was investigated for intra and inter-day experiments. For the purpose of these experiments a single (λ_{max} 507 nm) PEDD was selected. The detection of 0.25 ppm Mn and Co PAR complexes was also obtained using a VWD for comparison.

Procedure

- The peristaltic pump delivering the PCR was set at 0.38 mL/min
- The mobile phase was delivered at a flow rate of 0.7 mL/min
- A 100 µL injection of 0.25 ppm Mn (II) and Co (II) was made
- A PEDD with a λ_{max} of 507 nm was investigated
- The data was captured as outlined in section 2.2.3
- **Intra-Day reproducibility**: Each injection was repeated ten times
- **Inter-Day reproducibility**: Each injection was repeated ten times for 3 consecutive days

5.2.8 Calibration using the Single Wavelength PEDD flow cell and UV-vis spectrophotometer

A study was carried out involving the calibration of a change in concentration of manganese and cobalt PAR complexes.

Procedure

- 100 µL injections at various concentrations of manganese and cobalt were made

- The mobile phase was delivered at a flow rate of 0.7 mL/min
- The PCR was delivered at a pump setting of 0.38 mL/min
- A resistance of 1.5 kΩ was applied to the emitter LED
- Data was captured as outlined in section 2.2.3 using both the single wavelength PEDD flow cell and a UV-vis spectrophotometer
- All injections were carried out in triplicate

5.2.9 Optimisation of Dual Wavelength PEDD flow cell detector

As mentioned previously post-column reaction systems can add substantially to the baseline noise in liquid chromatography. A dual wavelength monitoring procedure was investigated to improve limits of detection in ion chromatography employing post column reactions by reducing the background noise. The procedure entailed monitoring at two wavelengths simultaneously. The (λ_{max} 507 nm) PEDD was selected to monitor at λ_{max} of the analyte, while the second was selected at a wavelength close to the isosbestic point. To determine which wavelength was required to monitor at the isosbestic point, it was necessary to determine experimentally the isosbestic points for the transistion metals and PAR complexes.

Determination of Isosbestic Point

Procedure

- A 200 µL aliquot of each concentration ranging from 0.2 µM - 1 mM for Co-PAR complex was taken and added to a 96 plate well
- Each concentration was added to the 96 plate well in triplicate.
- The absorbance was scanned from 300 – 700 nm.
- The data was captured using the µQuant™ software and saved as a text file for later analysis using Microsoft ™ Excel software.

Selection of LED to Monitor at Isosbestic Point

The isosbestic point for Co (II) and PAR was experimentally determined to be approximately 450 nm (Figure 5.14). LEDs are not monochromatic, typically citing bandwidths at half maximum (BWHM) of approximately 10-30 nm. LEDs in the region of 410–480 nm are particularly broad citing BWHM of approximately 90 nm (Figure 5.6).

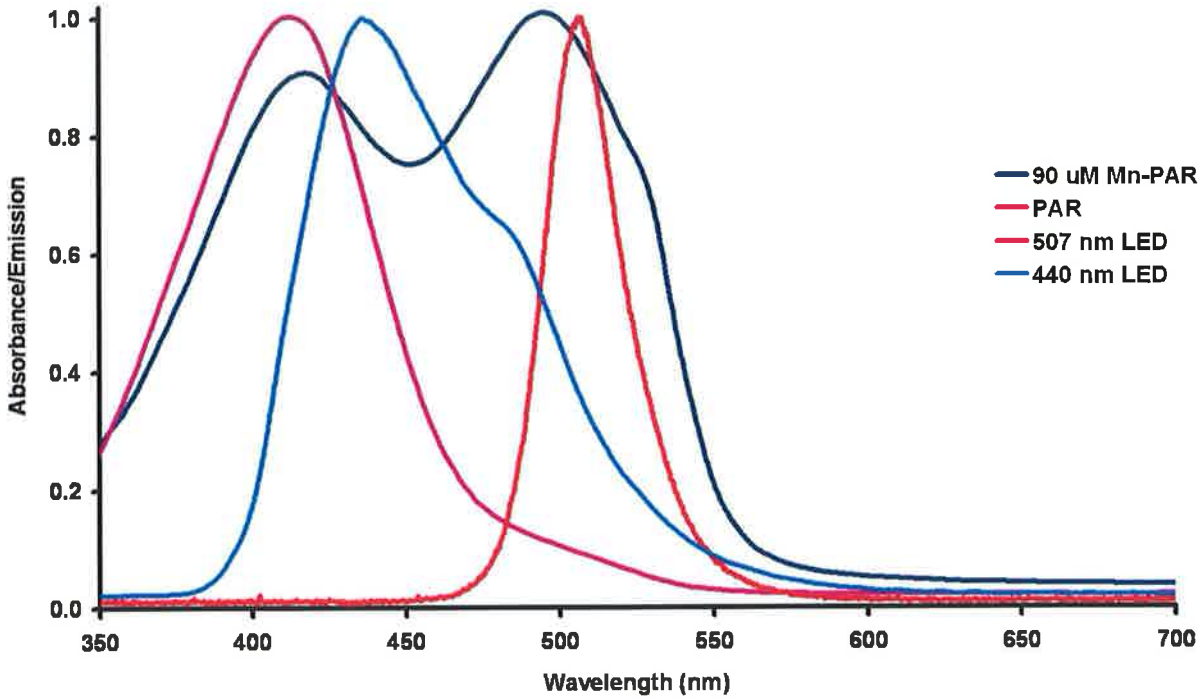

Figure 5.6 Emission spectra (λ_{max} 440 nm (blue line) and λ_{max} 507 nm (red line)) of the emitter LEDs used in the dual wavelength PEDD flow analysis device and the absorption spectra (λ_{max} 500 nm) of 90 μM Mn-PAR (navy line) and (λ_{max} 420 nm) PAR (pink line).

As shown in Figure 5.6 the 450 nm isosbestic point could not be monitored as LEDs available in this region cover the absorbance spectra of the Mn and Co PAR complexes also. The appropriate LED wavelength to monitor the isosbestic point was determined by preparing PEDDs of varying wavelengths.

Procedure

- The peristaltic pump delivering the PCR was set at 0.38 mL/min
- The mobile phase was delivered at a flow rate of 0.7 mL/min
- A 100 μL injection of varying concentration of Mn (II) and Co (II) were made
- PEDDs of varying wavelength were investigated
- The data was captured as outlined in section 2.2.3
- Each injection was repeated in triplicate

5.3 Results and discussion

5.3.1 Optimisation of Single Wavelength PEDD flow cell detector

Wavelength

Previously the detection of transition metal complexes were obtained using a PEDD with a λ_{max} of 500 nm. Absorbance spectra obtained for Mn and Co-PAR complexes show a λ_{max} of 500 nm and 510 nm respectively (Figure 5.3). To determine if improved sensitivity could be acquired a PEDD with a λ_{max} of 507 nm was investigated. A 0.25 ppm mixture of manganese (II) and cobalt (II) was prepared and injected (n = 10). The mean peak height (change in discharge time, μs) calculated for Mn and Co PAR complexes from both PEDDs (λ_{max} 500 nm and 507 nm) are shown in Table 5.2.

Table 5.2 Comparison peak height (change in discharge time) data acquired from PEDDs with a λ_{max} of 500 nm and 507 nm for the detection of 0.25 ppm Mn and Co PAR complexes (n = 10)

	507 nm Peak Height (µs)		500 nm Peak Height (µs)	
0.25 ppm	**Mn-PAR**	**Co-PAR**	**Mn-PAR**	**Co-PAR**
Average (n = 10)	898.4	375.1	404.9	114.1
Std Dev (n = 10)	31.1	14.2	5.0	3.4
RSD%	3.5	3.8	1.2	3.0

As shown in Figure 5.7 the average peak height obtained employing the (λ_{max} 507 nm) PEDD for 0.25 ppm Mn and Co PAR complexes were respectively 2.2 and 3.3 times greater than that measured with the (λ_{max} 500 nm) PEDD.

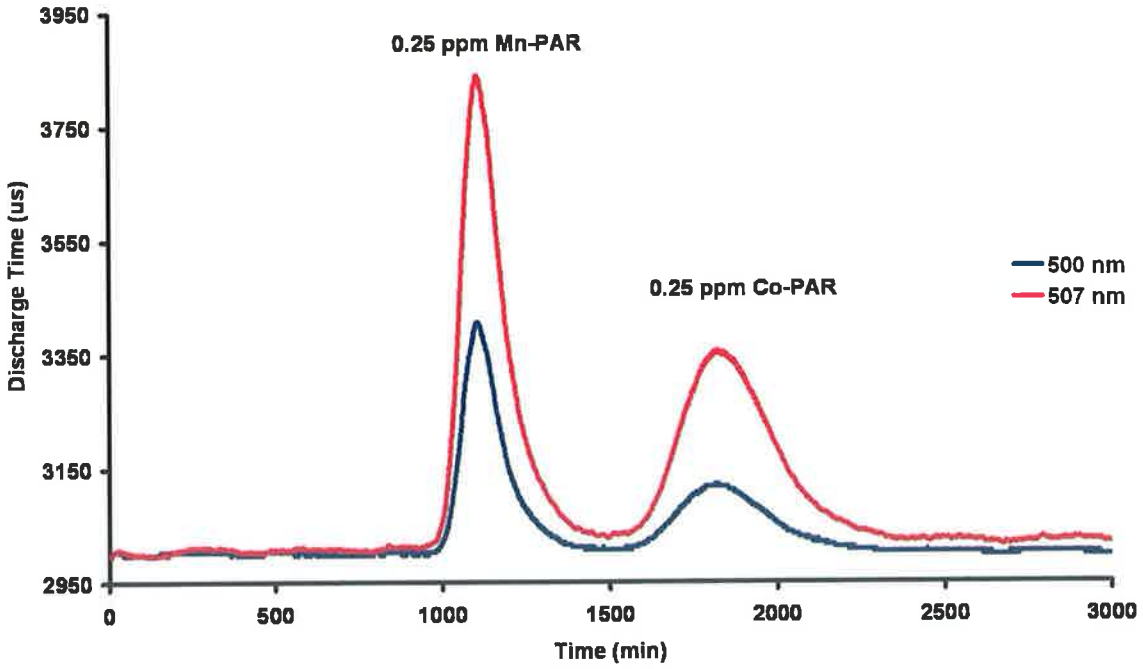

Figure 5.7 Comparison of average traces acquired from two PEDDs (A) λ_{max} of 500 nm and (B) λ_{max} of 507 nm for the detection of 0.25 ppm Mn and Co PAR complexes (n = 10).

To prove experimentally that the PEDD with a λ_{max} of 507 nm was the optimum wavelength for the detection of Mn and Co PAR complexes due to the efficient

overlap of the emission and absorption spectra and not due merely to an improvement in the fabrication of the PEDD, 4 PEDDs of each wavelength were prepared.

A mixture of 0.25 ppm Mn and Co were injected onto the column (n = 10) and were monitored with (A) 4 individual (λ_{max} 500 nm) PEDDs, (B) 4 individual (λ_{max} 507 nm) PEDDs and (C) a VWD (500 nm). The 0.25 ppm Mn and Co mixture was injected ten times for each PEDD. The experiments were carried out over a period of 3 months. The results shown in Table 5.3 were obtained by calculating the average peak heights (change in discharge time, μs) from the ten injections for each (λ_{max} 500 nm) PEDD. An overall average for the 4 (λ_{max} 500 nm) PEDDs was then calculated. This was repeated for the 4 (λ_{max} 507 nm) PEDDs investigated. The average peak heights (change in discharge time, μs) measured using the (λ_{max} 507 nm) PEDDs (Figure 5.8 A) for 0.25 ppm Mn and Co PAR complexes are approximately 2 times that of the average peak heights measured using the (λ_{max} 500 nm) PEDDs Figure 5.8 B.

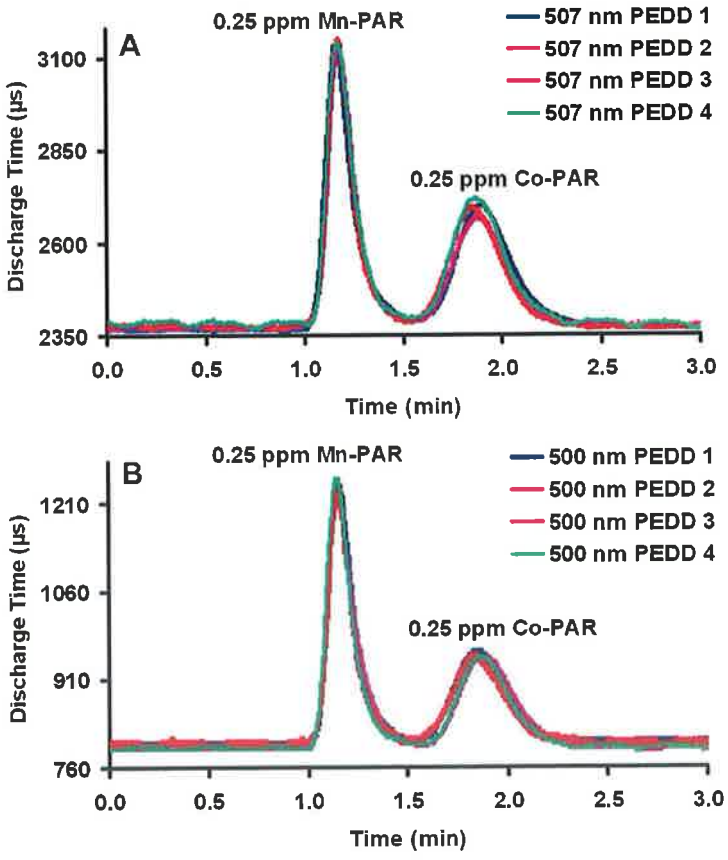

Figure 5.8 Overlaid traces for the detection of 0.25 ppm Mn-PAR and Co-PAR using (A) 4 x (λ_{max} 507 nm) PEDDs and (B) 4 x (λ_{max} 500 nm) PEDDs. Each trace is an average of 10 injections.

The average peak height measured for 0.25 ppm Mn and Co PAR complexes using the VWD (λ_{max} 500 nm) as outlined in Table 5.3 had a R.S.D.% of 3.7 and 6.1% respectively. The reproducibility of the peak heights achieved for the metal complexes using the 4 individual (λ_{max} 500 nm) PEDDs and the 4 individual (λ_{max} 507 nm) PEDDs were good with a highest R.S.D. of 4.8% measured.

Table 5.3 Determination of the reproducibility of detectors (A) (λ_{max} 500 nm) PEDD, (B) (λ_{max} 507 nm) PEDD and (C) VWD (n = 4).

	Peak Height (n = 4)	*Std Dev*	*R.S.D.%*
PEDD (λ_{max} 500 nm)			
0.25 ppm Mn-PAR	441.1 µs	21.0 µs	4.8
0.25 ppm Co-PAR	151.5 µs	4.1 µs	2.7
PEDD (λ_{max} 507 nm)			
0.25 ppm Mn-PAR	826.7 µs	23.2 µs	2.8
0.25 ppm Co-PAR	351.4 µs	12.1 µs	3.4
VWD (λ_{max} 500 nm)			
0.25 ppm Mn-PAR	1290.7	48.3	3.7
0.25 ppm Co-PAR	450.9	27.6	6.1

The same VWD at the same wavelength was employed throughout the experiments The VWD exhibited a higher R.S.D. of 6.1% for the detection of 0.25 ppm Co-PAR in comparison to the 2.7 and 3.4% R.S.D. obtained using the (λ_{max} 500 nm) PEDDs and the (λ_{max} 507 nm) PEDDs respectively. These results demonstrate that the PEDD can be fabricated reproducibly, providing a reliable response over a long period of time (3 months). This is of utmost importance if the PEDD is a viable detector in field deployable systems and sensor networks.

5.3.2 Validation of Single Wavelength PEDD flow cell detector

Intra/Inter-Day Reproducibility

Reproducibility is an important characteristic for a field deployable device. To demonstrate the intra and inter-day reproducibility within an individual PEDD flow

cell a mixture of 0.25 ppm manganese (II) and cobalt (II) was injected on the column. The separation was monitored using a PEDD (λ_{max} 507 nm) and a VWD (500 nm) for comparison. The same PEDD was used for all experiments to determine the reproducibility within an individual PEDD.

Intra-Day Reproducibility

Figure 5.9 shows an overlay of the ten chromatograms obtained using (A) the UV-vis spectrophotometer detector and (B) the (λ_{max} 507 nm) PEDD. As shown in Figure 5.9 A the chromatogram achieved from the UV-vis spectrophotometer detector demonstrates good reproducibility with relative standard deviations of 1.5% and 2.0%, n = 10 (Table 5.4) for 0.25 ppm Mn and Co PAR complexes respectively.

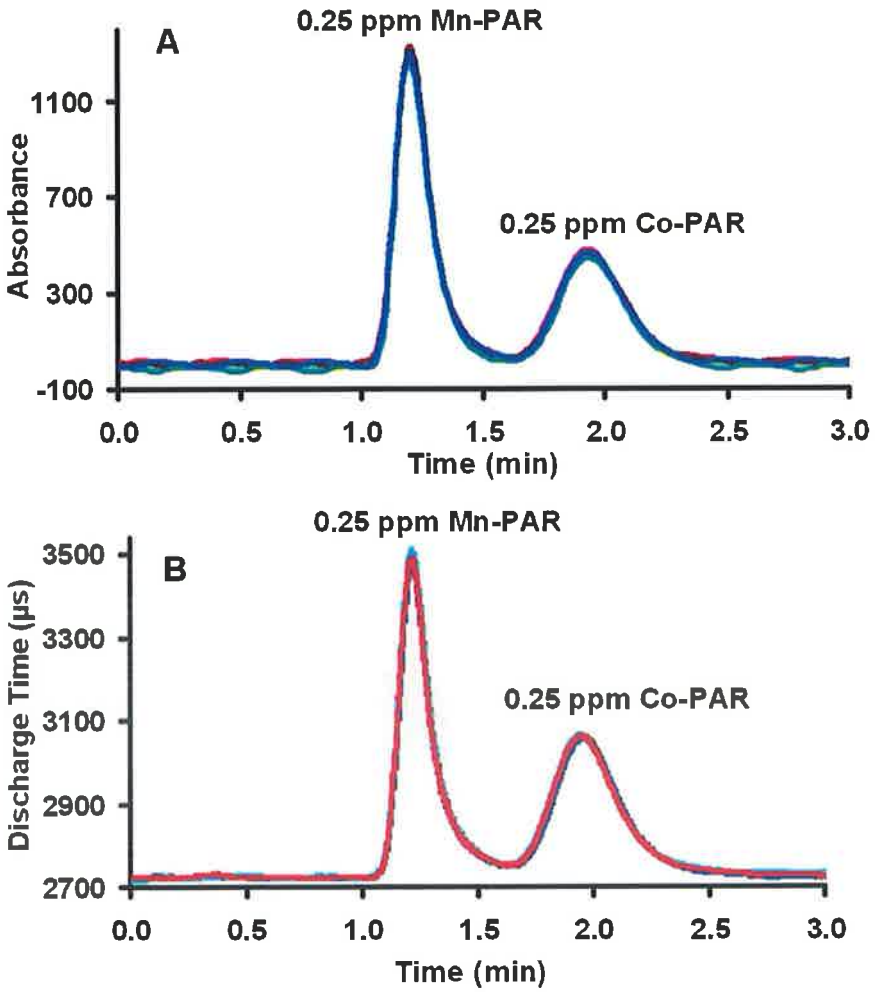

Figure 5.9 Reproducibility of (A) VWD (500 nm) and (B) PEDD (λ_{max} 507 nm) for the detection of 0.25 ppm Mn and Co PAR complexes (n = 10)

The results obtained from the PEDD are presented in Figure 5.9 B. The peak height (change in discharge time, μs) was plotted against retention time (minutes). As shown in Figure 5.9 B the plot obtained from the PEDD matches the reproducibility of the UV-vis spectrophotometer detector. The PEDD demonstrated relative standard deviations of 1.6% and 0.9%, n = 10 (Table 5.4) for 0.25 ppm Mn and Co PAR complexes respectively. The signal to noise ratios calculated using the (λ_{max} 507 nm) PEDD for the detection of 0.25 ppm Mn-PAR and Co-PAR complexes were ca. 1.8 and 2.3 times higher than those calculated using the VWD.

Table 5.4 Comparison data for the determination of the intra-day reproducibility within an individual (λ_{max} 507 nm) PEDD and a VWD (500 nm) (n = 10).

n = 10	PEDD (λ_{max} 507 nm)		VWD (500 nm)	
0.25 ppm	**Mn-PAR**	**Co-PAR**	**Mn-PAR**	**Co-PAR**
Peak Height	786.7 ± 12.6 μs	337.3 ± 3.2 μs	1302.6 ± 19.9	440.8 ± 9.0
RSD%	1.6	0.9	1.5	2.0
Baseline Noise (σ)	2.0 μs	2.0 μs	6.0	6.0
S/N	400.7	171.8	217.0	73.4

Inter-day Reproducibility

To investigate the inter-day reproducibility of a PEDD flow cell, a single (λ_{max} 507 nm) PEDD was selected and a 100 μL injection of 0.25 ppm manganese (II) and conbalt (II) was made onto the column (n = 10). This was repeated for three consecutive days employing the same PEDD and experimental conditions. The data obtained from the (λ_{max} 507 nm) PEDD and the UV-vis spectrophotometer detectors are given in Table 5.5. The UV-vis spectrophotometer detector achieved peak height relative standard deviations of 1.0% and 2.1% for 0.25 ppm Mn and Co PAR complexes (n = 3) respectively.

Table 5.5 Comparison data for the determination of the inter-day reproducibility within an individual (λ_{max} 507 nm) PEDD and a VWD (500 nm) (n = 10) for 3 consecutive days.

0.25 ppm	Mn-PAR (n = 10)	Co-PAR (n = 10)	Mn-PAR (n = 10)	Co-PAR (n = 10)
Day	(λ_{max} 507 nm) PEDD Peak Height (μs)		(500 nm) VWD Peak Height	
1	868.0 ± 2.6	366.3 ± 2.9	9497.8 ± 2.9	435.3 ± 1.5
2	881.4 ± 14.0	386.8 ± 5.1	9681.0 ± 9.3	422.8 ± 1.7
3	855.7 ± 12.2	381.5 ± 6.1	9553.6 ± 10.8	417.5 ± 1.7
Average	868.4 ± 12.9	378.2 ± 10.6	9577.5 ± 94.0	425.2 ± 9.1
R.S.D.%	1.5	2.8	1.0	2.1

The peak height (change in discharge time, μs) measured using the (λ_{max} 507 nm) PEDD demonstrated relative standard deviations of 1.5% and 2.8% for 0.25 ppm Mn and Co PAR complexes (n = 3) respectively. To facilitate comparison, the peak heights measured for 0.25 ppm Mn and Co PAR complexes using both the PEDD and the VWD were normalized to a 0-1 range by dividing values by the maximum peak heights achieved (Figure 5.10). The relative standard deviations (shown as error bars in Figure 5.10) calculated employing the PEDD are comparable to those achieved from the UV-vis spectrophotometer.

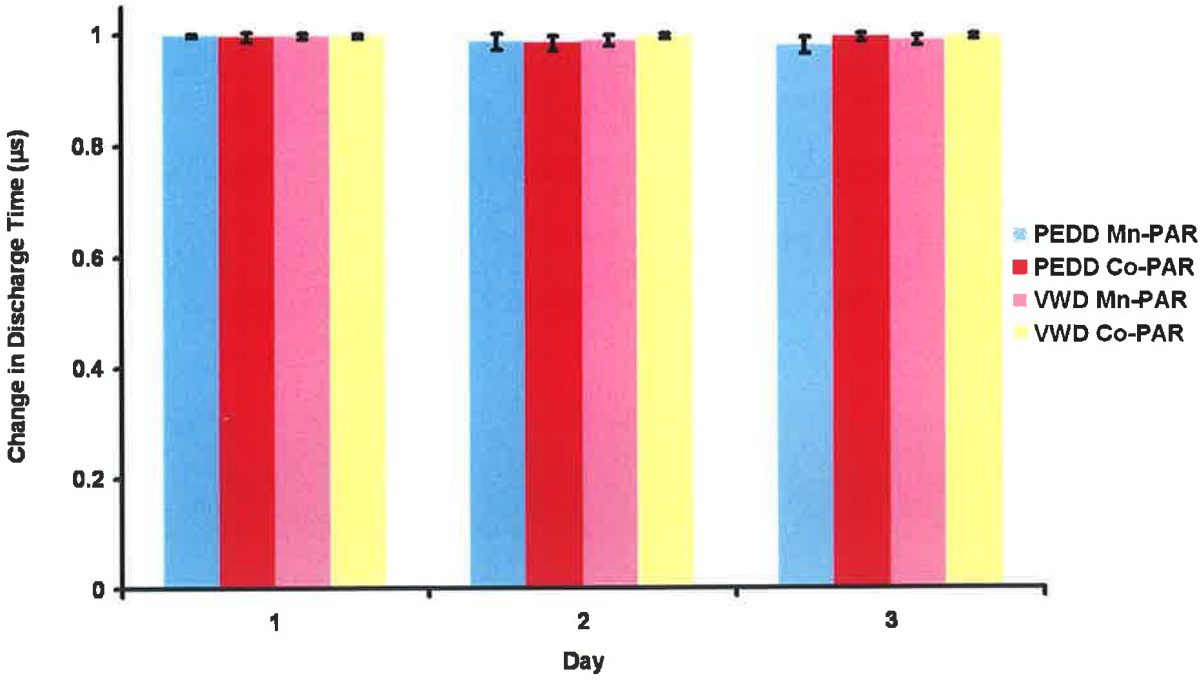

Figure 5.10 Plot comparing the average peak heights measured over 3 days for 0.25 ppm Mn and Co PAR complexes using a (λ_{max} 507 nm) PEDD and a VWD (500 nm). Each bar represents the average peak height measured for ten injections. The standard deviations are shown as error bars (n = 10).

5.3.3 Calibration using the Single Wavelength PEDD flow cell and UV-vis spectrophotometer

A study was carried out involving the calibration of a change in concentration of manganese and cobalt PAR complexes. Mixtures of the two metals were passed through the HPLC system using the optimal conditions previously determined in chapter 4 (carrier flow rate 0.7 mL/min, PCR flow setting of 0.38 mL/min). Each injection was carried out in triplicate (n = 3). The chromatograms obtained from both detectors were acquired simultaneously.

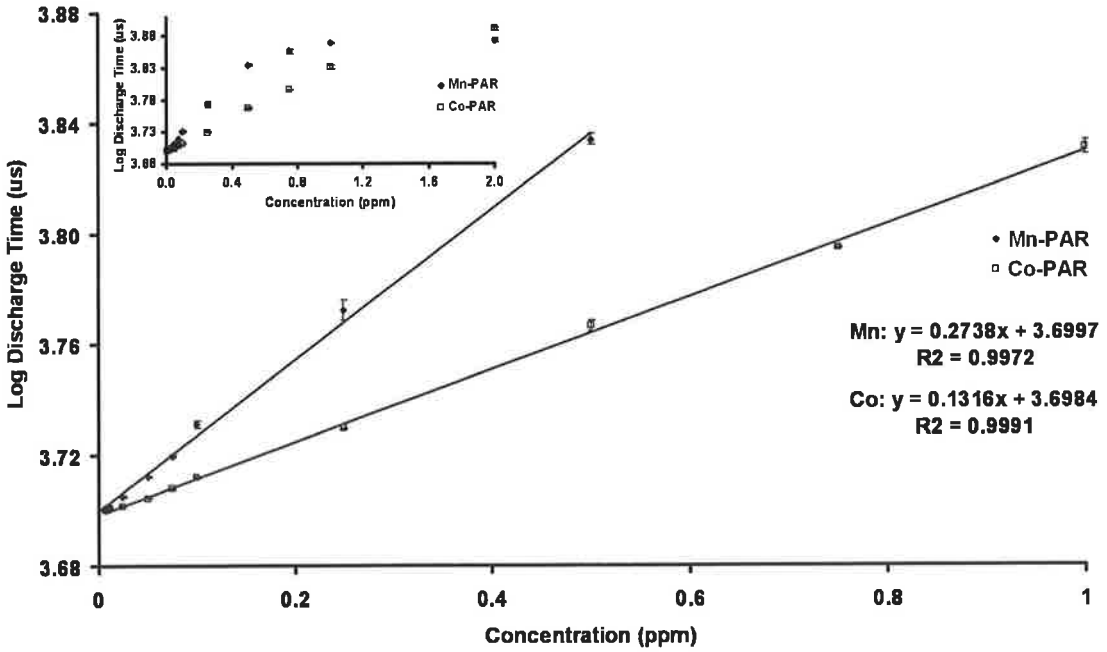

Figure 5.11 Log of the discharge times (*t*, µs) obtained using a PEDD versus Mn (II) and Co (II) PAR complex concentration (ppm). The error bars represent the standard deviations for n = 3. The inset shows the dynamic range of responses obtained from the calibration.

Figure 5.11 shows the results obtained from the single (λ_{max} 507 nm) PEDD flow cell. The log of the discharge times, t (µs) for manganese and cobalt PAR complexes were plotted against the metal concentration (ppm) in accordance with the model (Equation 2.4). A dynamic range (shown in inset Figure 5.11) from 1 ppb to 2 ppm for Mn-PAR and 7.5 ppb to 2 ppm for Co-PAR were achieved. Linear ranges of 5 ppb to 0.5 ppm for Mn-PAR (R^2 = 9972) and 7.5 ppb to 1 ppm for Co-PAR (R^2 = 9991) were obtained (Table 5.6). As shown in Figure 5.11 the relative standard deviation of the measurements made with the PEDD (n = 3, shown as error bars) are very low (< 0.09%).

A limit of detection of 1 ppb Mn-PAR was achieved using the single (λ_{max} 507 nm) PEDD flow cell. A peak height (change in discharge time, µs) of 23.6 µs ± 2.5 µs (n = 3) was calculated for 1 ppb Mn-PAR. Three times the standard deviation of the baseline (3σ) was calculated as 17.4 µs. A limit of detection of 7.5 ppb Co-PAR was measured using the single (λ_{max} 507 nm) PEDD flow cell. A peak height (change in discharge time, µs) of 15.7 µs ± 0.32 µs (n = 3) was achieved for 7.5 ppb Co-PAR (3σ = 13.2 µs).

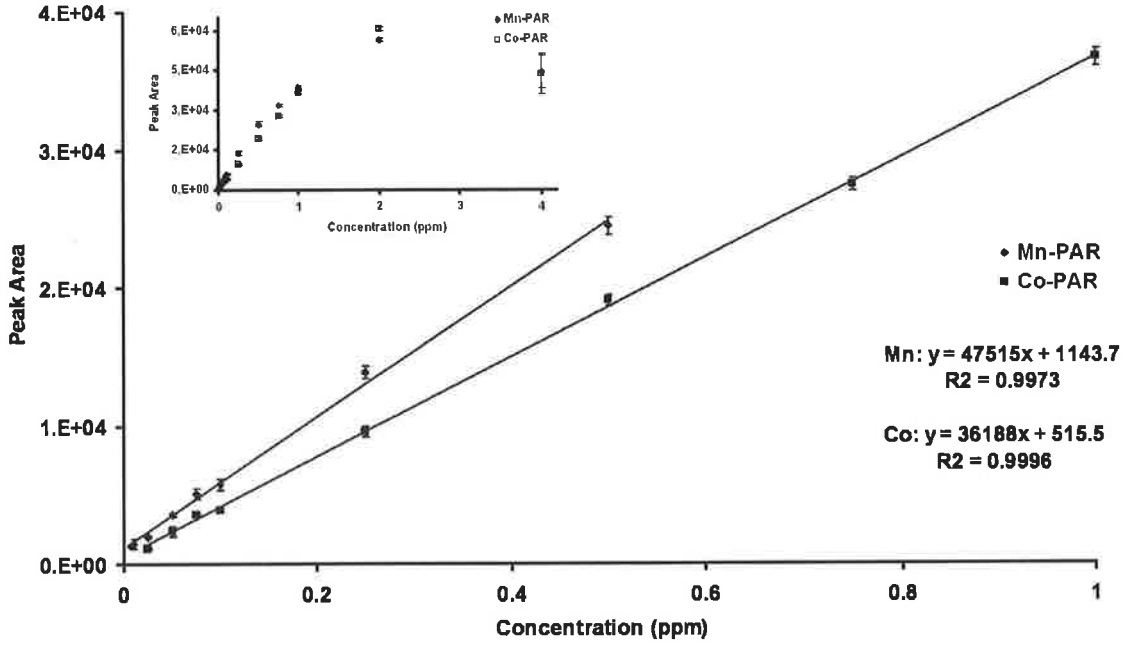

Figure 5.12 Linear calibration plot achieved using the variable wavelength detector of peak area versus Mn (II) and Co (II) PAR complex concentration. The error bars represent the standard deviations for n = 3. The inset shows the dynamic range of responses obtained from the calibration.

Figure 5.12 shows the results obtained from the variable wavelength detector (500 nm). The peak areas measured for manganese and cobalt PAR complexes were plotted against the metal concentration (ppm). A dynamic range (shown in inset Figure 5.12) from 7.5 ppb to 2 ppm for Mn-PAR and 25 ppb to 2 ppm for Co-PAR were achieved. Linear ranges of 7.5 ppb to 0.5 ppm for Mn-PAR (R^2 = 9973) and 25 ppb to 1 ppm for Co-PAR (R^2 = 9996) were obtained (Table 5.6). As shown in Figure 5.12 relative standard deviations of ca. 6% were calculated (n = 3, shown as error bars).

A limit of detection of 7.5 ppb Mn-PAR was achieved using the VWD (500 nm). A peak area of 1304.1 ± 110.0 (n = 3) was calculated for 7.5 ppb Mn-PAR. A limit of detection of 25 ppb Co-PAR was measured using the VWD. A peak area of 1107.7 ± 70.7 (n = 3) was achieved for 25 ppb Co-PAR.

Table 5.6 A comparative summary of the data obtained for the detection of manganese and cobalt PAR complexes using both a PEDD (λ_{max} 507 nm) and a variable wavelength detector (VWD) ($n = 3$).

	Mn-PAR		Co-PAR	
	PEDD	VWD	PEDD	VWD
Dynamic Range	1 ppb-2 ppm	7.5 ppb – 2 ppm	7.5 ppb – 2 ppm	25 ppb – 2 ppm
Linear Range	5 ppb – 0.5 ppm	7.5 ppb – 0.5 ppm	7.5 ppb – 1 ppm	25 ppb – 1 ppm
LOD	1 ppb	7.5 ppb	7.5 ppb	25 ppb

5.3.4 Optimisation of Dual Wavelength PEDD flow cell detector

Applying a moving average is a common method employed to reduce baseline noise in chromatography. A moving average was applied to a chromatogram obtained from a single (λ_{max} 507 nm) PEDD for the detection of 0.01 ppm Mn and Co Par complex, in an attempt to reduce the baseline noise. A 4 pt-MA was applied to the data set. While this improved the plot marginally, the standard deviation was still too high. Increasing the moving average amount by a factor of one resulted in a linear decrease in baseline noise and peak height (change in discharge time, μs) up to a maximum of 8 pt-MA. Beyond this point the baseline noise and peak height ceased to decrease linearly as shown in Figure 5.13 (A) 0.01 ppm Mn-PAR and (B) 0.01 ppm Co-PAR.

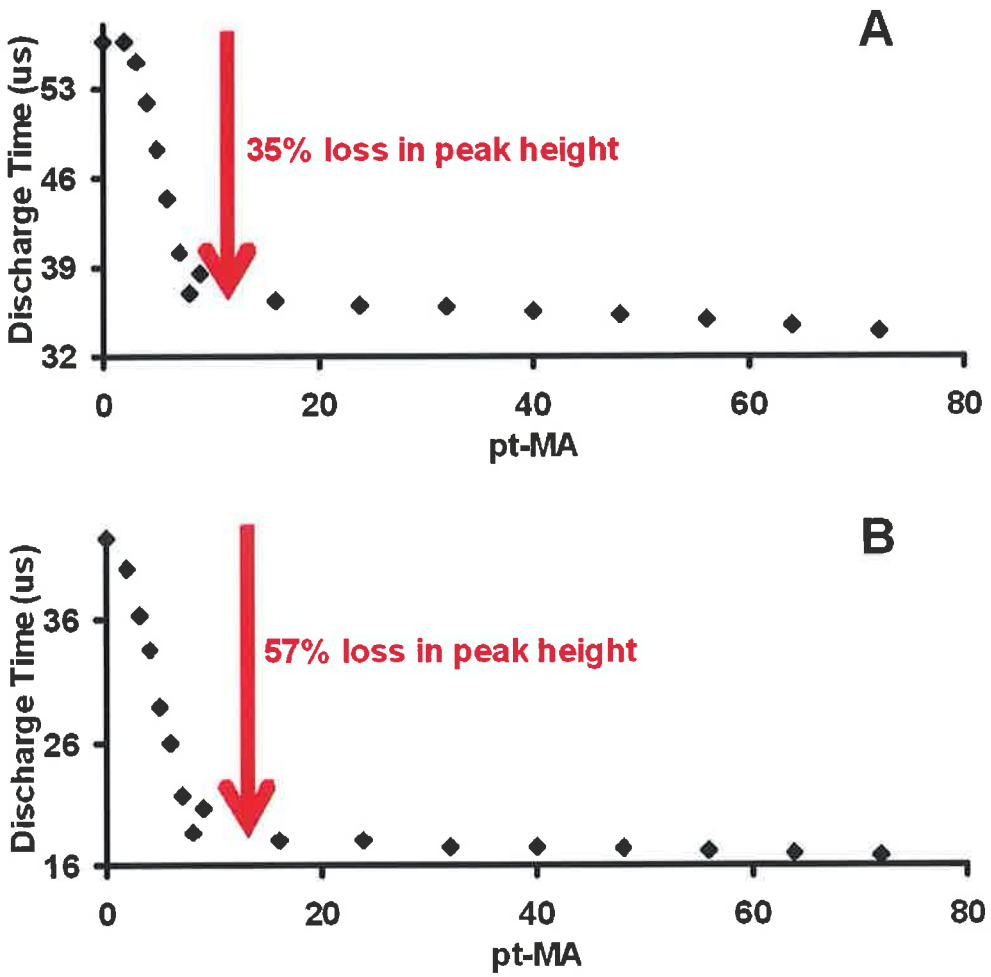

Figure 5.13 Plot showing the effect of applying a moving average (pt-MA) to the response achieved for 0.01 ppm (A) Mn-PAR and (B) Co-PAR.

Figure 5.13 (A) and (B) show a 35% and 57% loss in peak height calculated for 0.01 ppm Mn-PAR and Co-PAR respectively with an 8 pt-MA. While applying a moving average resulted in a loss in peak height, a linear increase in the signal to noise ratio was achieved up to a limit of 8 pt-MA. Using an 8 pt-MA resulted in an increase in the signal to noise ratio calculated from 3.3 to 6.5 and 2.5 to 3.3 for 0.01 ppm Mn and Co PAR complexes respectively. Applying a moving average of greater than 8 data points no longer resulted in a linear increase in signal to noise ratio.

Wavelength

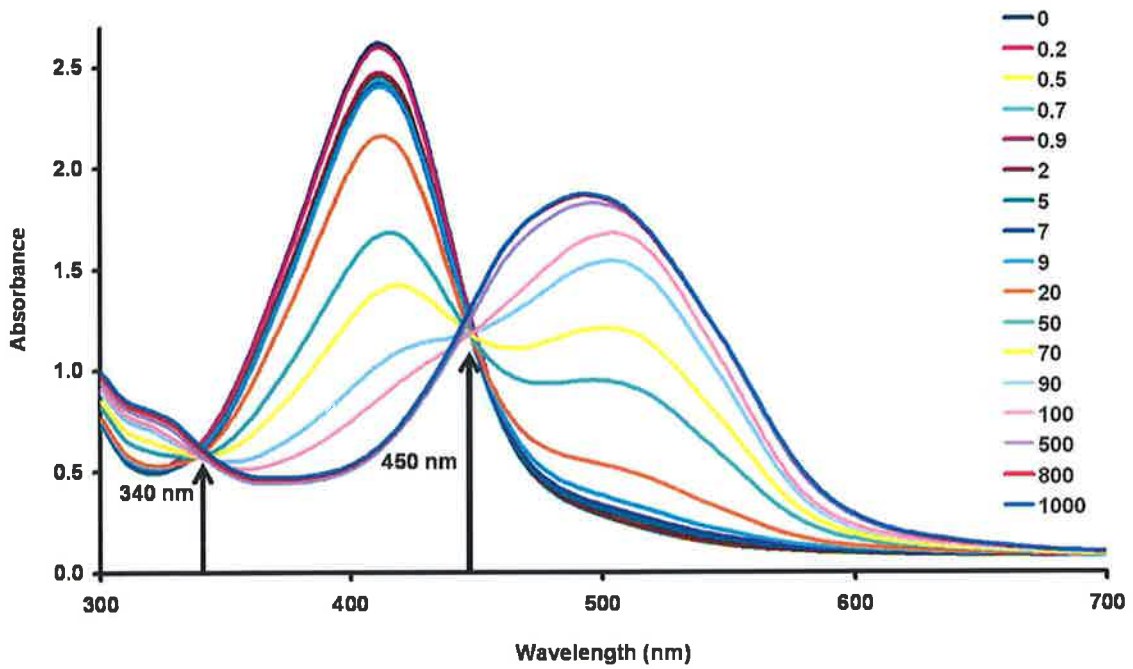

Figure 5.14 Determination of isosbestic points from absorbance spectra of a range of concentrations (μM) of Co-PAR complex (n = 3)

The isosbestic point was determined by obtaining the absorbance spectra of increasing concentrations of cobalt, as shown in Figure 5.14. The ideal isosbestic point to monitor at was determined as 450 nm, however as shown in Figure 5.6 commercially available LEDs in this region typically have an emission spectrum possessing a band width at half height of approximately 90 nm. Alternatively an LED with a λ_{max} of 627 nm was investigated as the wavelength to monitor the baseline noise. This wavelength was selected as it had an emission spectrum which overlapped with a region in the absorption spectrum where relatively little absorption was occurring. Various concentrations of manganese and cobalt were injection on the column and monitored using the dual wavelength PEDD (Analyte Signal: λ_{max} 507 nm and Reference Signal: λ_{max} 627 nm). Each concentration was injected 3 times.

Dual PEDD (Analyte Signal: λ_{max} 507 nm and Reference Signal: λ_{max} 627 nm)

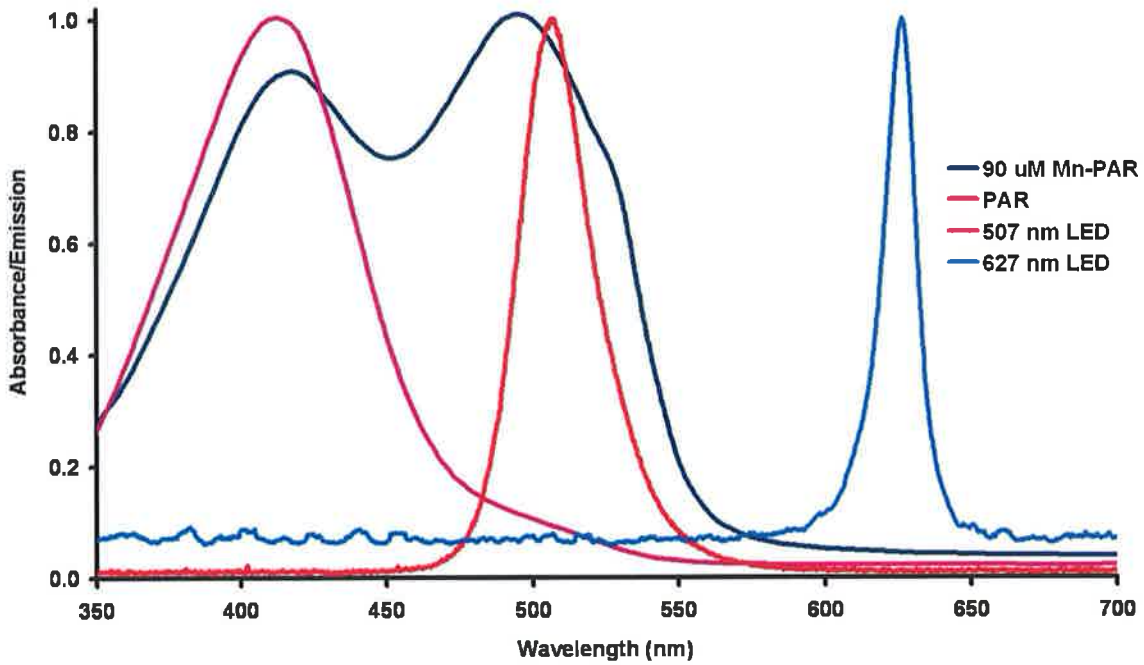

Figure 5.15 Emission spectra (λ_{max} 627 nm (blue line) and λ_{max} 507 nm (red line)) of the emitter LEDs used in the integrated PEDD flow analysis device and the absorption spectra (λ_{max} 500 nm) of 90 µM Mn-PAR (navy line) and (λ_{max} 420 nm) PAR (pink line).

Figure 5.15 shows the absorption spectra of 90 µM Mn-PAR and PAR, and the emission spectra of the green LED (λ_{max} 507 nm) which will monitor the analytes and the red LED (λ_{max} 627 nm) which will monitor the baseline noise. The emission spectra of the LEDs were obtained using an Ocean Optic spectrometer (OOIBase 32™, Ocean Optics. Inc., Dunedin, USA). The absorbance spectra of manganese (II) PAR complex and PAR were acquired using the µQuant™ platewell reader (Bio – Tek Instruments, Inc., USA).

The two PEDDs were driven from the same circuit board with a data output rate of 16 data points per second. The data manipulation was carried out post run. On acquiring the data from the (λ_{max} 627 nm) PEDD which was monitoring the baseline only, the amplitude of the baseline noise was normalised and subtracted from the (λ_{max} 507 nm)

PEDD Mn and Co Par data set. A 9 pt moving average was then applied to the data. The experiment was repeated three times.

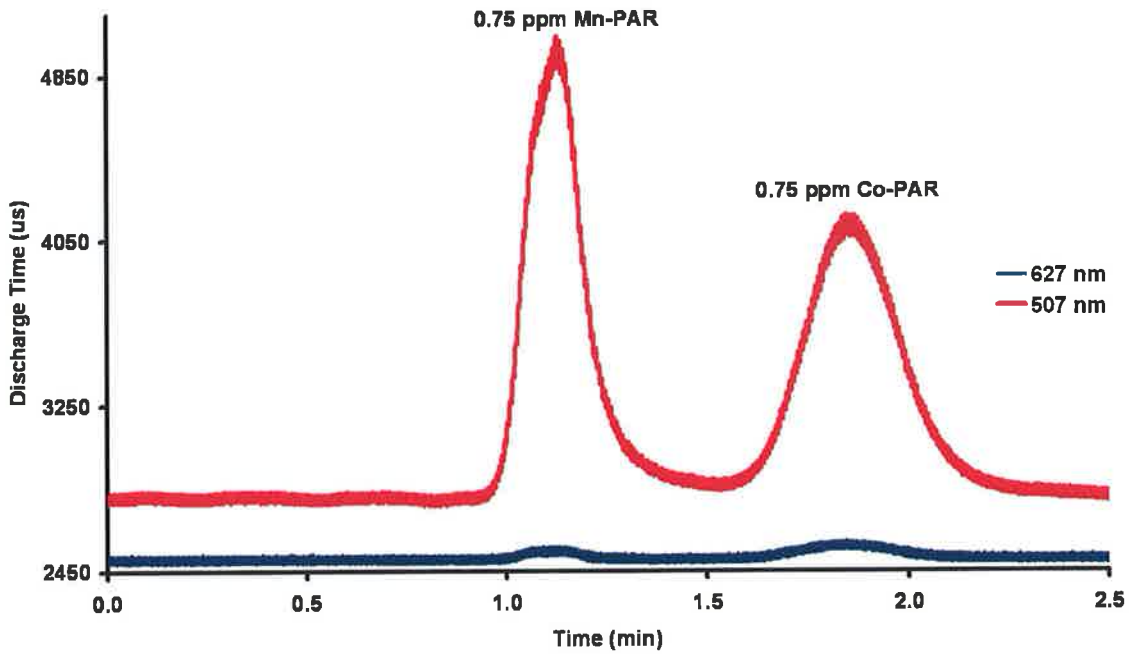

Figure 5.16 Comparison data acquired from the dual wavelength PEDD (λ_{max} 627 nm (navy line) and 507 nm (red line)) for the detection of 0.75 ppm Mn and Co PAR complexes (n = 3).

As shown in Figure 5.16 for the detection of 0.75 ppm Mn and Co PAR complexes the (λ_{max} 627 nm) PEDD which is intended to monitor the baseline noise only is detecting the transition metal PAR complexes.

Figure 5.17 shows a comparison of the S/N data achieved for the detection of 0.75 ppm Mn and Co PAR complexes using the single and dual wavelength monitoring procedure. The bars shown in blue were calculated from the data collected with the single wavelength PEDD (λ_{max} 507 nm) and the bars shown in purple were calculated from the data obtained by subtracting the baseline monitored using the (λ_{max} 627 nm) PEDD from the data captured with the (λ_{max} 507 nm) PEDD.

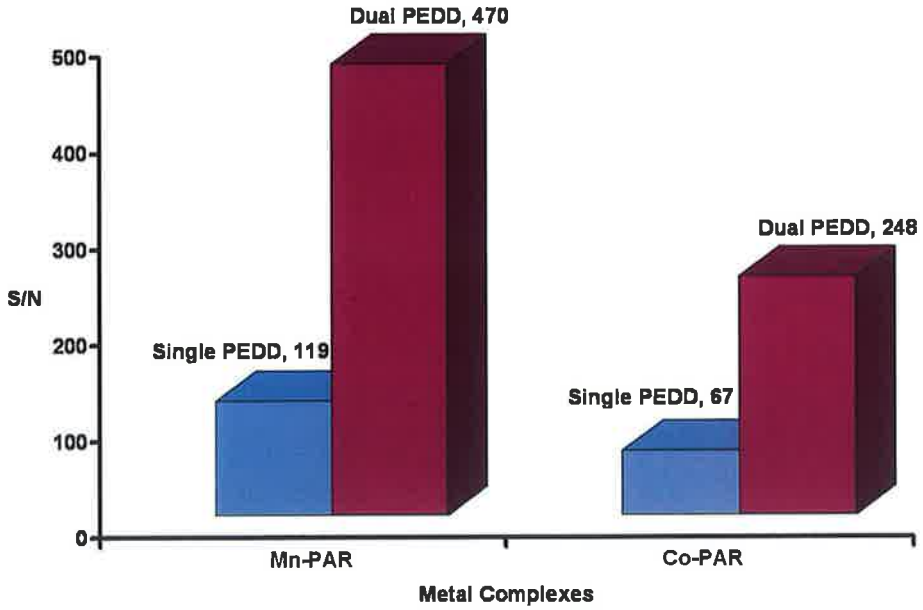

Figure 5.17 Comparison of S/N data acquired from the single wavelength PEDD (λ_{max} 507 nm) (blue bar) and the dual wavelength PEDD (λ_{max} 507 nm - 627 nm) (purple bar) for the detection of 0.75 ppm Mn and Co PAR complexes (n = 3).

The signal to noise ratios calculated for the detection of 0.75 ppm Mn and Co PAR complexes using the dual PEDD (λ_{max} 507 nm- λ_{max} 627 nm) was ca. 4 times the signal to noise ratios calculated for both 0.75 ppm Mn and Co PAR complexes using the single wavelength (λ_{max} 507 nm) PEDD. This demonstrated for the detection of 0.75 ppm Mn and Co PAR complexes approximately a 395% and 370% increase in the signal to noise ratios calculated respectively, using the dual wavelength procedure in comparison to the signal to noise ratios calculated without the dual wavelength monitoring procedure.

As outlined in Table 5.7 the average peak height calculated using single wavelength PEDD (λ_{max} 507 nm) was 2221 μs for Mn-PAR and 1238 μs for Co-PAR. The peak height calculated using just the dual wavelength (λ_{max} 507 nm – 627 nm) PEDD was 2254 μs for Mn-PAR and 1191 μs for Co-PAR.

Table 5.7 Comparative data for the detection of 0.75 ppm Mn and Co PAR complexes with (A) a single (λ_{max} 507 nm) PEDD and (B) dual wavelength PEDD (λ_{max} 507 nm - λ_{max} 627 nm) (n = 3).

	Peak Height (µs)		*S/N*	
PEDD (0.75ppm)	*Mn-PAR*	*Co-PAR*	*Mn-PAR*	*Co-PAR*
507 nm	2221	1238	119	67
507 nm - 627 nm	2254	1191	470	248

To demonstrate the dual wavelength monitoring method at a lower concentration a 10 ppb mixture of Mn and Co was selected. The dual PEDD (λ_{max} 507 nm and λ_{max} 627 nm) detector was used for the experiment. The 100 µL injection of the sample was carried out in triplicate. Figure 5.18 shows the data obtained from the single (λ_{max} 507 nm) PEDD with no moving average.

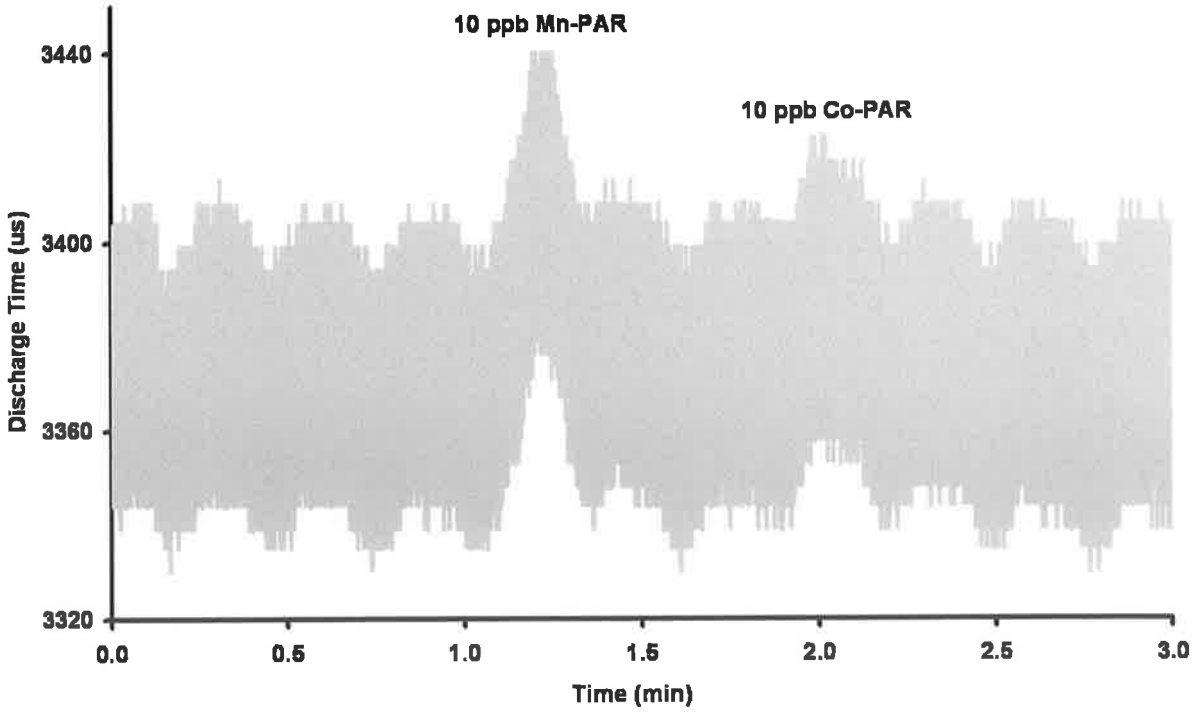

Figure 5.18 Plot of discharge time (µs) versus retention time (minutes) obtained for the detection of 10 ppb Mn and Co PAR complexes using a single wavelength (λ_{max} 507 nm) PEDD. No moving average has been applied to the data.

It is important to note that the plot in Figure 5.18 appears excessively noisy due to the programme employed on the PIC for this work. The data output rate was increased by removing the averaging normally carried out by the PIC. This does not affect the data as the averaging can be performed post run. On applying a 9 pt-MA to the data acquired using the single (λ_{max} 507 nm) PEDD an average peak height of 31.5 µs ± 5.1 µs and 13.8 µs ± 2.6 µs was calculated for 10 ppb Mn-PAR and Co-PAR respectively (Table 5.8). The average standard deviation of the baseline calculated was 4.5 µs (n = 3). A signal to noise ratio of 6.9 and 3.0 was achieved for Mn and Co PAR complexes respectively.

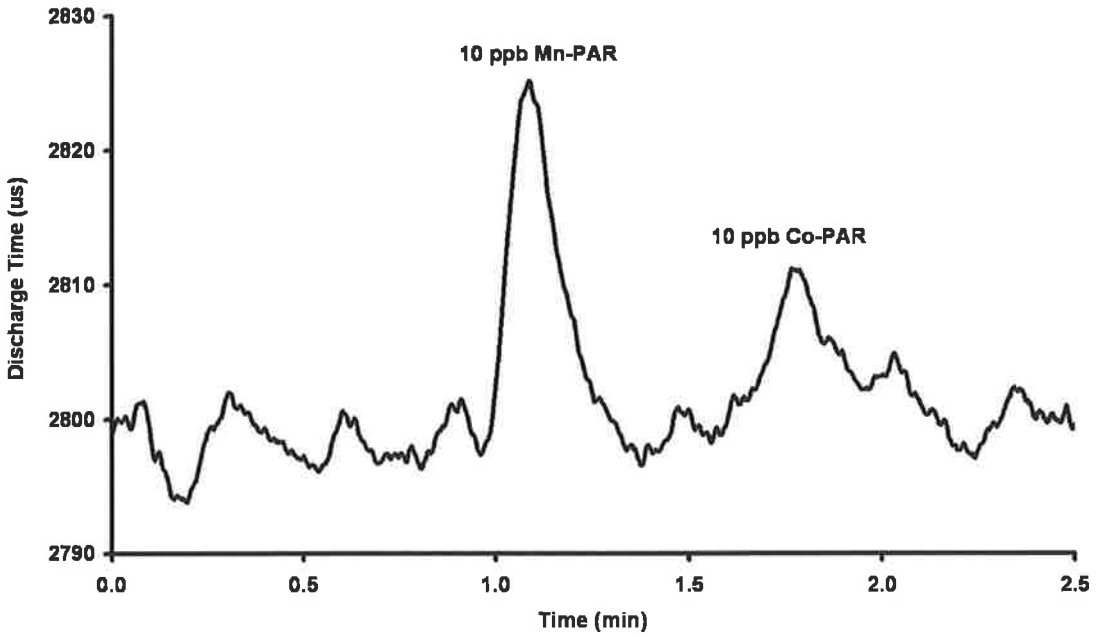

Figure 5.19 Plot of discharge time (µs) versus retention time (minutes) obtained for the detection of 10 ppb Mn and Co PAR complexes using dual wavelength monitoring procedure. A PEDD (λ_{max} 507 nm) was employed to detect the analytes and a PEDD (λ_{max} 627 nm) to monitor the baseline (n = 3).

Figure 5.19 shows the average (n = 3) plot measured for the detection of 10 ppb Mn and Co PAR complexes using the dual (λ_{max} 507 nm - λ_{max} 627 nm) PEDD. The average peak height (change in discharge time, µs) calculated for both the Mn and Co PAR complexes were 30.4 µs ± 1.6 µs and 15.0 µs ± 1.5 µs. The average standard deviation of the baseline calculated was 3.8 µs (n = 3). A signal to noise ratio of 8 and 4 were achieved for Mn and Co PAR complexes respectively. This showed an

increase of 17% in the signal to noise ratio calculated for the detection of Mn-PAR and a 33% increase for the detection of Co-PAR in comparison to the data calculating using the single PEDD (λ_{max} 507 nm) as outlined in Table 5.8.

Table 5.8 Comparative data for the detection of 10 ppb Mn and Co PAR complexes with (A) a single PEDD (λ_{max} 507 nm) and (B) dual PEDD (λ_{max} of 507 nm - 627 nm) (n = 3).

	10 ppb Mn-PAR		10 ppb Co-PAR	
PEDD	**507 nm**	**507 nm – 627 nm**	**507 nm**	**507 nm – 627 nm**
Peak Height (μs)	31.5 ± 5.1	30.4 ± 1.6	13.8 ± 2.6	15.0 ± 1.5
Baseline Std Dev (3σ) (μs)	5.0	3.8	5.0	3.8
S/N	6.9	8	3.0	4.0

5.4 Conclusions

The results obtained using the integrated single and dual wavelength PEDD flow cell have demonstrated improved sensitivity than previously reported in chapter 4 for the detection of transition metals manganese and cobalt coupled with the post-column reagent PAR. This was achieved through two approaches. Firstly by optimising the wavelength in which to monitor the transition metal PAR complexes and secondly by employing a dual wavelength monitoring procedure.

It was determined that monitoring the analytes with a single wavelength (λ_{max} 507 nm) PEDD resulted in an increase in response i.e. peak height (change in discharge time, μs) ca. 2 times that of the peak height measured using a single wavelength (λ_{max} 500 nm) PEDD. The fabrication process of the PEDD was validated by preparing 4 PEDDs of each wavelength (λ_{max} 500 nm and 507 nm) and measuring the reproducibility for the detection of 0.25 ppm Mn and Co PAR complexes. Standard deviations of 4.8% (Mn-PAR) and 2.7% (Co-PAR) were calculated for the λ_{max} 500 nm PEDD and 2.8% (Mn-PAR) and 3.4% (Co-PAR) 507 nm PEDD respectively. For comparative studies the 0.25 ppm mixture of Mn and Co was also monitored using the UV-vis spectrophotometer at a wavelength of 500 nm. This demonstrated that some of the relative standard deviation measured can be accounted to deviations in the chromatography itself. Relative standard deviations of 3.7% and 6.1% were calculated for the detection of 0.25 ppm Mn and Co PAR complexes respectively using the UV-vis spectrophotometer.

Intra and inter-day reproducibility within an individual single wavelength (λ_{max} 507 nm) PEDD was investigated. The intra-day reproducibility was determined to have a relative standard deviation of 1.6% and 0.9% for 0.25 ppm mixture of Mn and Co PAR respectively. The results acquired from the single wavelength (λ_{max} 507 nm) PEDD were comparable to the relative standard deviations of 1.5% and 2.0% calculated using the VWD for 0.25 ppm mixture of Mn and Co PAR respectively. The signal to noise ratios calculated for the single wavelength (λ_{max} 507 nm) PEDD were ca. 2 times those calculated using the VWD.

The inter-day reproducibility determined using the single wavelength (λ_{max} 507 nm) PEDD obtained a relative standard deviation of 1.5% and 2.8% for the detection of 0.25 ppm mixture of Mn and Co PAR respectively.

The PEDD flow cell can detect lower concentration levels of Mn and Co PAR complexes than that of an expensive, commercially available bench top instrument. The single wavelength (λ_{max} 507 nm) PEDD obtained a limit of detection (LOD) of 1 ppb Mn-PAR and 7.5 ppb Co-PAR. The LOD achieved using the UV-vis spectrophotometer detection was 7.5 ppb Mn-PAR and 25 ppb Co-PAR.

The employment of a dual wavelength monitoring procedure for the detection of the transition metal PAR complexes was carried out. Using the dual (λ_{max} 507 nm - λ_{max} 627 nm) PEDD achieved a signal to noise ratio of 8 and 4 for the detection of 10 ppb Mn and Co PAR complexes. This demonstrated a 17% and 33% increase in the signal to noise ratios measured using a single wavelength (λ_{max} 507 nm) PEDD for 10 ppb Mn and Co PAR respectively. While the dual wavelength PEDD (λ_{max} 507 nm – 627 nm) increased the signal to noise ratio the LED selected as the reference wavelength (λ_{max} 627 nm) is not the optimum wavelength to perform dual wavelength monitoring. As shown in Figure 5.16 the reference PEDD (λ_{max} 627 nm) which should only monitor the baseline noise can detect the Mn and Co PAR complexes and therefore on subtraction from the data collected using analyte monitoring PEDD (λ_{max} 507 nm) a loss in peak height occurs. Further investigation with regard to the optimum LED to employ as the reference wavelength will be carried out. An LED which could monitor at the second isosbestic point 340 nm or possibly an LED monitoring at an even longer wavelength (> 627 nm) will be investigated. The results presented within in this work however, show huge potential for the use of a dual wavelength PEDD for the purpose of improving limit of detection by reducing baseline noise in post column reaction systems.

This optical sensor has the potential for very broad analytical applications, given that it offers high sensitivity and precision with excellent signal-to-noise characteristics. The PEDD flow cell is therefore ideal for detection of multiple analytes when operated in conjunction with a separation technique. The optical sensor cannot replace the UV-vis spectrophotometer, however it offers many advantages such as its low cost, versatility, simplicity, ease of use, low power consuming, small in size and can be easily integrated into a field deployable liquid chromatography system.

CHAPTER 6

FUTURE WORK

6. Overview and Future Work

The results obtained using the integrated PEDD flow analysis system has demonstrated that this simple low cost device can be used as an optical sensor for colorimetric flow analysis. This optical sensor has shown the ability of detecting low concentrations levels (nanomolar).

A highly sensitive optical sensor was developed based on a novel concept of employing an LED as both the light source and detector in chemical flow analysis. A comprehensive review was provided in Chapter 1 of the background to the work performed in the thesis. Areas that were covered included the fundamentals of molecular absorption, UV-vis spectroscopy and LEDs. Various applications of LED based optical sensors were discussed, with an emphasis on the typical detectors employed in combination with LED light sources in optical sensors. LEDs are extremely versatile and can be configured in a variety of ways which were discussed in Chapter 1. The overall aim of this chapter was to introduce the reader to the concept of LED based optical sensors in chemical analysis.

Chapter 2 detailed the development of a novel integrated PEDD flow analysis system. The emitter LED is forward biased while the detector LED is reverse biased. Instead of measuring the photocurrent directly, a simple timer circuit is used to measure the time taken for the photocurrent generated by the emitter LED to discharge the detector LED from 5 V (logic 1) to 1.7 V (logic 0) to give digital output directly without using an A/D converter. Two PEDDs were developed whereby one had a single inlet and the second had a dual inlet design. The dual inlet has an increased path length in comparison to the single inlet PEDD. Calibration of the PEDDs using pH indicator dyes bromocresol green and aniline blue showed the optical devices have a lower LOD (at 3σ) of 0.5 μM BCG at pH 7 (single inlet PEDD) and 0.25 μM aniline blue in 0.1 M HCl (dual inlet PEDD) in comparison to 0.9 μM BCG at pH 7 and 0.5 μM aniline blue in 0.1 M HCl achieved using a commercially available μQuant™ platewell reader (Bio – Tek Instruments, Inc., USA. The device was also successfully employed for the determination of BCG pK_a. A linear range from 0.9 - 250 μM BCG at pH 7 (R^2 0.998) with a relative standard deviation of 0.4% (n = 8) was achieved

using the single inlet PEDD and a linear range of 0.1-25 μM aniline blue in 0.1 M HCl (R^2 0.9928) with a relative standard deviation of 0.5% (n = 3) was obtained using the dual inlet PEDD.
The reported pK_a of BCG is 4.74 [77]. The pK_a determined using the PEDD was 4.67. On the basis of these results the PEDD was proposed as a sensitive optical device for the detection of orthophosphate.

Chapter 3 demonstrated the application of the PEDD as an optical device in chemical flow analysis for the detection of orthophosphate. Conditions such as LED emitter light intensity were investigated as this had proven in chapter 2 to be an important factor on analyte response. Under optimised conditions the PEDD detector offered a linear range of 0.02 – 2 μM and an LOD of 2 nM. For comparative purposes a simple, low cost LED-photodiode detector and a μQuant™ platewell reader were investigated. The LED-photodiode detector achieved an LOD in the micromolar range (2 μM). The PEDD device exhibited sensitivity in the nanomolar concentration range, which was approximately 100 times lower than that of the commercially available bench top platewell reader.

Chapter 4 investigated the viability of the PEDD as a sensitive detector in HPLC. The PEDD flow analysis device was successfully applied to the detection of transition metals manganese and cobalt coupled with the post-column reagent PAR. The PEDD flow cell can detect lower concentration levels of Co-PAR than that of an expensive, commercially available bench top instrument. An LOD of 90 nM was achieved for both Mn and Co Par complexes employing a (λ_{max} 500 nm) PEDD. An LOD of 90 nM and 0.7 μM was achieved for Mn and Co PAR complexes respectively using a variable wavelength detector. A simple PEDD detector cannot replace the existing variable wavelength detector because of the limited bandwidth a single LED can cover, however, for specific applications where an appropriate operation wavelength can be selected for the analytes a single PEDD flow detector is ideal and preferable to a more complex multi-source detector.

Chapter 5 took the detection of transition metals manganese and cobalt employing a PEDD several steps forward by improving the change in response (i.e. peak height), reducing the background noise, and hence improving the LOD. In Chapter 4 the

PEDD selected to monitor the transition metal complexes had a λ_{max} at 500 nm. The optimum wavelength to monitor the analytes was investigated and found to provide an improved change in response employing a PEDD with a λ_{max} at 507 nm (ca. 2 times that obtained using the (λ_{max} at 500 nm) PEDD).

The fabrication process of the PEDD was validated by preparing 4 PEDDs of each wavelength (λ_{max} 500 nm and 507 nm) and measuring the reproducibility for the detection of 0.25 ppm Mn and Co PAR complexes. Standard deviations of 4.8% (Mn-PAR) and 2.7% (Co-PAR) were calculated for the λ_{max} 500 nm PEDD and 2.8% (Mn-PAR) and 3.4% (Co-PAR) 507 nm PEDD respectively. For comparative studies the 0.25 ppm mixture of Mn and Co was also monitored using the UV-vis spectrophotometer at a wavelength of 500 nm. This demonstrated that some of the relative standard deviation measured can be accounted to deviations in the chromatography itself. Relative standard deviations of 3.7% and 6.1% were calculated for the detection of 0.25 ppm Mn and Co PAR complexes respectively using the UV-vis spectrophotometer.

Intra and inter-day reproducibility within an individual single wavelength (λ_{max} 507 nm) PEDD was investigated. Good reproducibility was demonstrated using the PEDD achieving relative standard deviations of 1.6% and 0.9% (Intraday) and 1.5% and 2.8% (Interday) for the detection of 0.25 ppm Mn and Co PAR respectively. The results acquired from the single wavelength (λ_{max} 507 nm) PEDD were comparable to the relative standard deviations of 1.5% and 2.0% calculated using the VWD for 0.25 ppm mixture of Mn and Co PAR respectively.

The PEDD flow cell can detect lower concentration levels of Mn and Co PAR complexes than that of an expensive, commercially available bench top instrument. The single wavelength (λ_{max} 507 nm) PEDD obtained a limit of detection (LOD) of 1 ppb Mn-PAR and 7.5 ppb Co-PAR. The LOD achieved using the UV-vis spectrophotometer detection was 7.5 ppb Mn-PAR and 25 ppb Co-PAR.

The employment of a dual wavelength monitoring procedure for the detection of the transition metal PAR complexes was carried out. Using the dual (λ_{max} 507 nm - λ_{max} 627 nm) PEDD achieved a signal to noise ratio of 8 and 4 for the detection of 10 ppb Mn and Co PAR complexes. This demonstrated a 17% and 33% increase in the signal to noise ratios measured using a single wavelength (λ_{max} 507 nm) PEDD for 10 ppb Mn and Co PAR respectively.

This novel integrated optical flow analysis device has the potential for very broad analytical applications, given that it offers high sensitivity and precision with excellent signal-to-noise characteristics. The optical sensor cannot replace the UV-vis spectrophotometer, however it offers many advantages such as it's low cost, versatility, simplicity, ease of use, low power consuming, small in size, and can be easily integrated into a field deployable autonomous systems. The PEDD has been demonstrated as a sensitive detector in flow analysis systems and for the detection of multiple analytes when operated in conjunction with a separation technique in liquid chromatography. Due to the broad possibilities of analytical applications of the PEDD, a number of areas can be targeted for future works in this project.

Future work will include further investigation and development of the PEDD as a possible field deployment sensor for the detection of orthophosphate. The method discussed within the work presented in chapter 3 achieved extremely low limits of detection when used in the lab however, would not translate to a field deployable sensor without addressing issues such as reagent stability, reaction time and reagent storage. A more critical evaluation of the performance of the PEDD using existing methods will be carried out.

The use of the molybdenum blue method, which is the standard method for the detection of orthophosphate, will be investigated as this offers similar sensitivity without the drawback of poor reagent stability and reaction time. The use of the dual inlet flow cell will allow reagent mixing within the channel. This will enable chemical analyses, which require multiple reagents such as those required in the molybdenum blue method. Preliminary work carried out on the detection of nitrite using the Griess method [118] in combination with the PEDD, has also achieved detection limits in the nanomolar range. The main focus of the future work will be to build an autonomous system which will consist of multiple PEDD sensors allowing the detection of a variety of water pollutants. Limitations such as power supply and wireless communication have already been addressed by work carried out within the Adaptive Sensors Group.

Additional future work will be the investigation in optimising the sensitivity of the PEDD photometric detector. Results obtained from the longer path length dual inlet PEDD in Chapter 1 demonstrated higher sensitivity over the shorter path length single

inlet PEDD. Investigation into further improvement of sensitivity by increasing the path length will be carried out.

Alternative methods of improving sensitivity of the PEDD for example with regard to the detection of transition metals is to employ a detector LED with a λ_{max} of 590 nm. Previous work utilized a detector LED with a λ_{max} of 660 nm. Some preliminary results have shown that an LED with a λ_{max} of 590 nm can only detect wavelengths below ca. 520 nm. This would eliminate any interference from ambient light, which will improve sensitivity.

To develop the PEDD as a photometric detector for HPLC or any flow analysis system further improvement of sensitivity and selectivity will be investigated with the use of multi-LED systems. Multi-wavelength LEDs are already commercially available in a variety of shapes and sizes. With the use of surface mount LEDs a photometric detector covering almost the entire UV-vis range would allow the detection of multiple components as part of a mixture or separately (Figure 6.1).

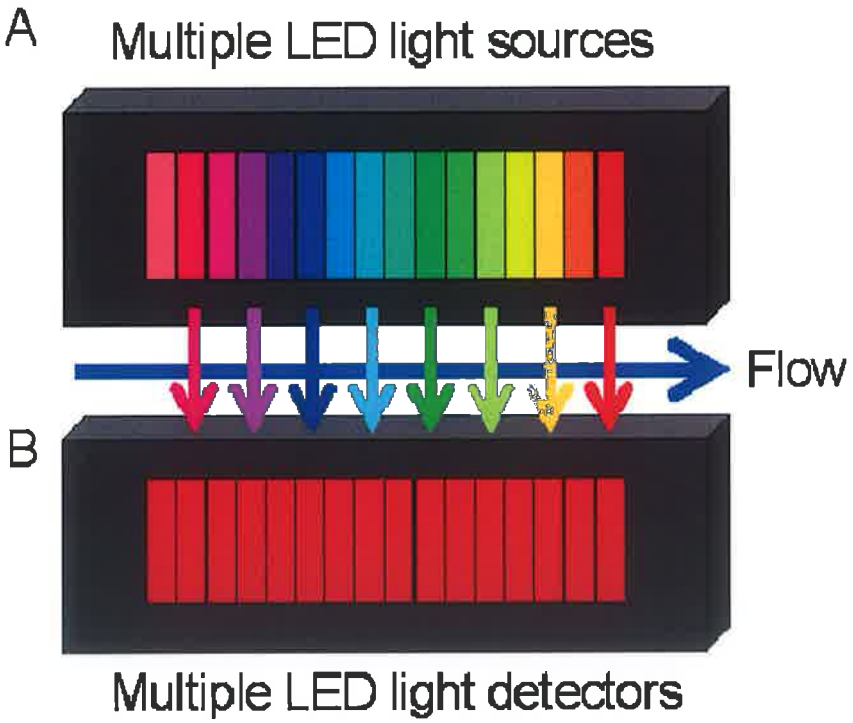

Figure 6.1 Schematic of a multi-wavelength PEDD. (A) Emitter LEDs covering entire spectral range commercially available, and (B) Red detector LEDs which align perfectly with the emitter LEDs.

One possible configuration for the multi-wavelength PEDD is shown in Figure 6.1, whereby the emitter (A) and detector (B) LEDs are aligned either side a microfluidics flow cell. The flow cell can consist of one or more inlets possibly allowing reagent mixing within the cell. The main objective in developing the PEDD as a detector is the realisation of a field deployable autonomous liquid chromatography system.

This sensing approach therefore has numerous potential for analytical applications, given that it has the advantages of very low cost, low power consumption and offers high sensitivity with excellent signal-to-noise characteristics.

APPENDIX

A Appendix

A1 Calibration of the pH meter

The pH meter was calibrated as follows [119]:

- Rinse the electrode (glass probe) and area around it twice with distilled water using a squeeze bottle and blot dry with a soft tissue after each rinse. Rinse into a discard beaker or sink, not into the pH buffer solution and do not touch the electrode with your fingers.
- Turn on the meter, push the CAL button to indicate that you will be calibrating the instrument.
- Immerse the electrode in the pH 7.0 buffer solution, making sure that the electrode is entirely immersed. Do not immerse the instrument further than is necessary.
- Gently stir the buffer solution with the electrode and wait for the display value to stabilize. Once the reading has stabilized, press the HOLD/CON button to accept the value and complete the calibration. If the electrode is still immersed in the buffer, the display will read the same value as the pH of the buffer (i.e. 4, 7, or 10).
- Remove the pH tester from the buffer solution, rinse the electrode with distilled water, and blot dry with soft tissue.
- Repeat steps 3 and 6 using the pH 4 buffer and then using the pH 10 buffer.
- Set the tester aside on a paper towel; turn the meter off by pushing the ON/OFF button.
- Pour the buffer solution into their labelled bottles and cap them tightly.
- Leave electrode immersed in distilled water to prevent drying up.

A2 Indicator Dye Used

Bromocresol green

Bromocresol green has a visual transition interval from pH 3.8 (yellow) to pH 5.4 (blue-green) with a pK_a of 4.74.

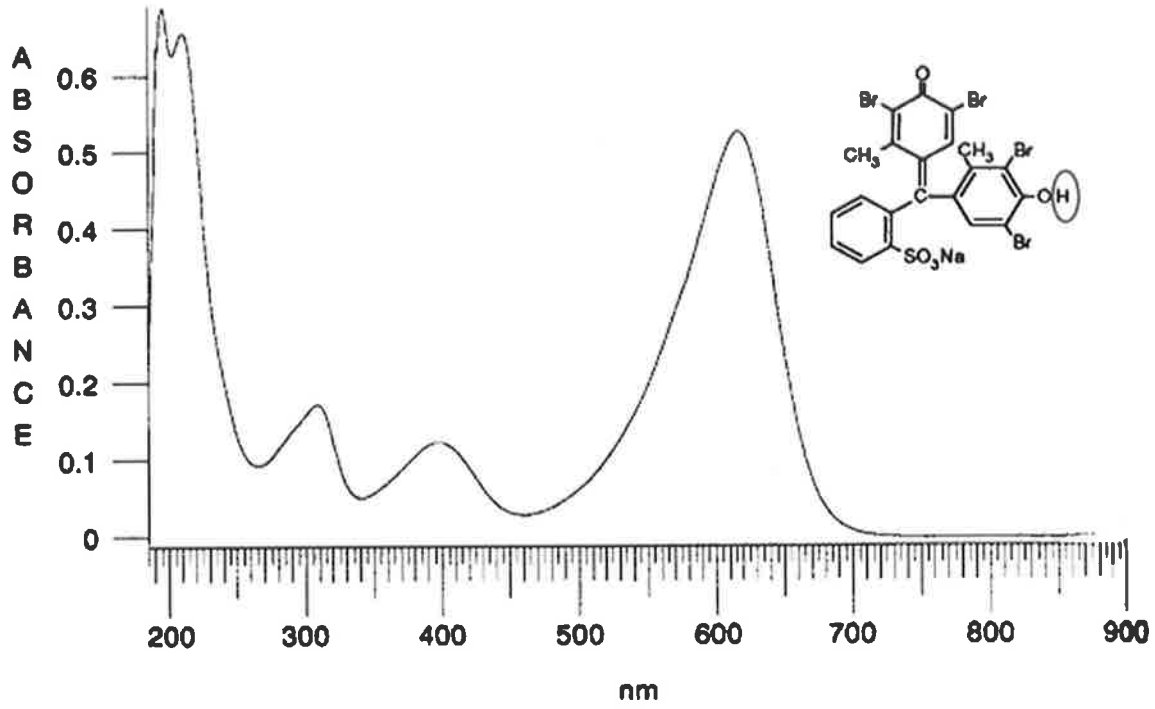

Figure A.1 Deprotonation of bromocresol green shifts the dye from its yellow form (450 nm) to its blue form (610 nm) [120]

Aniline blue

Aniline blue has a visual transition interval from pH 10 (blue) to pH 13 (orange) with a pK_a of 11.

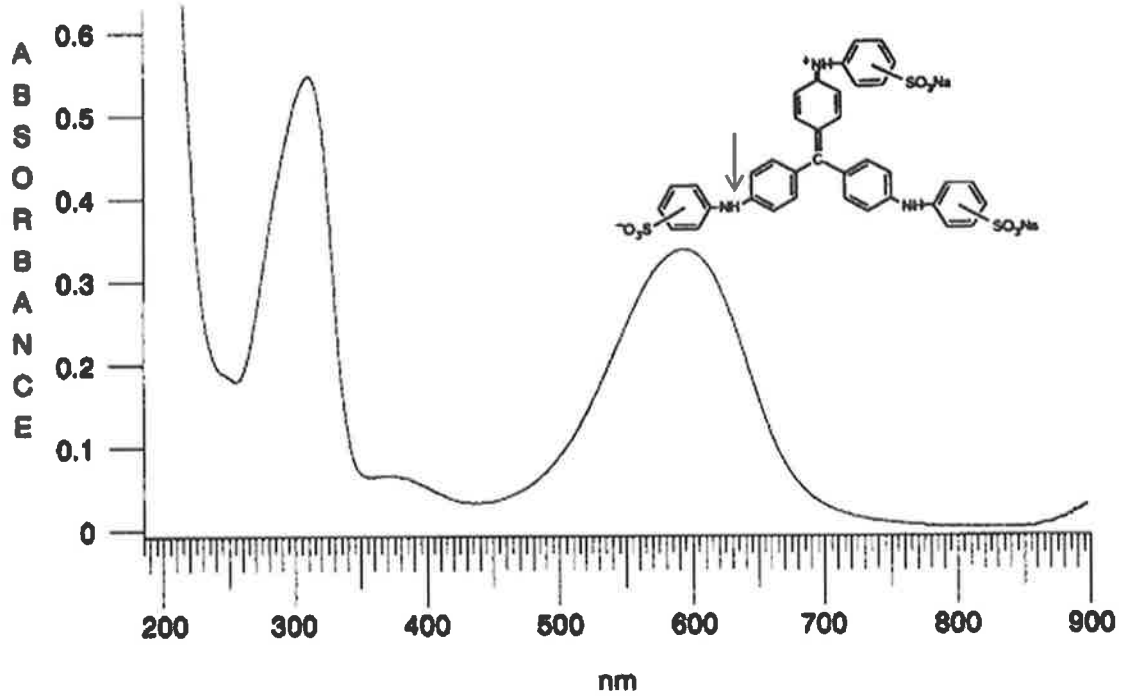

Figure A.2 Deprotonation of aniline blue shifts the dye from its blue form (300 nm) to its orange form (600 nm) [120].

References

[1] http://www.lbl.gov/MicroWorlds/ALSTool/EMSpec/

[2] G.D. Christian, J.E. O'Reilly, *Instrumental Analysis*, Boston : Allyn and Bacon, 1986.

[3] R. Kellner, J.-M. Mermet, M. Otto, H.M. Widmer, *Analytical Chemistry*, WILEY-VCH, 1997.

[4] http://www.colourware.co.uk/cpfaq/q1-1.htm

[5] E.D. Olsen, *Modern Optical Methods of Analysis*, McGrath-Hill Book Company, 1975.

[6] http://www.shu.ac.uk/schools/sci/chem/tutorials/molspec/uvvisab1.htm

[7] H.-H. Perkampus, *UV-VIS Spectroscopy and Its Applications*, Springer Laboratory, 1992.

[8] D. Diamond, *Principles of chemical and biological sensors*, New York : Wiley, 1998.

[9] J. Cazes, *Ewing's Analytical Instrumentation Handbook*, 2005.

[10] www.ssi.shimadzu.com/servicesupport/pdfs/baselines.pdf

[11] http://www.chem.agilent.com/Scripts/PDS.asp?lPage=255

[12] E. Katz, R. Eksteen, Schoenmakers, N. Miller, *Handbook of HPLC*, Marcel Dekker, Inc., 1998.

[13] D.C. Giancoli, *Physics : Principles with Applications*, Prentice Hall, 1998.

[14] A.A. Mitrani, M.L. Gonzalez, M.T. O'Connell, J. Guerra, R.B. Harwood, L.B. Gardner, *The American Journal of Surgery* **161** (1991) 646-650.

[15] A. Zukauskas, M.S. Shur, R. Gaska, *Introduction to Solid-State Lighting*, John Wiley & Sons, Inc., 2002.

[16] T.E. Jenkins, *Optical Sensing Techniques and Signal Processing*, Prentice/ Hall International, 1987.

[17] M. Sequeira, D. Diamond, A. Daridon, J. Lichtenberg, S. Verpoorte, N.F.d. Rooij, *Trends in Analytical Chemistry* **21** (2002) 816-827.

[18] D. Diamond, *Analytical Chemistry* **76** (2004) 279A-286A.

[19] Y. Taniyasu, M. Kasu, T. Makimoto, *Nature* **441** (2006) 325-328.

[20] P.K. Dasgupta, I.-Y. Eom, K.J. Morris, J. Li, *Analytica Chimica Acta* **500** (2003) 337-364.

[21] J. Kovac, L. Peternai, O. Lengyel, *Thin Solid Films* **433** (2003) 22-26.

[22] H. Flaschka, C. McKeithan, R. Barnes, *Analytical Letters* **6** (1973) 585-594.

[23] T. Anfalt, A. Graneli, M. Strandberg, *Analytical Chemistry* **48** (1976) 357-360.

[24] D. Betteridge, E.L. Dagless, B. Fields, N.F. Graves, *The Analyst* **103** (1978) 897-908.

[25] G.M. Greenway, S.J. Haswell, P.H. Petsul, *Analytica Chimica Acta* **387** (1999) 1-10.

[26] G.E. Collins, Q. Lu, *Sensors and Actuators B: Chemical* **76** (2001) 244-249.

[27] Q. Lu, G.E. Collins, *The Analyst* **126** (2001) 429-432.

[28] S.-J. Chen, M.-J. Chen, H.-T. Chang, *Journal of Chromatography A* **1017** (2003) 215-224.

[29] B.J. White, H.J. Harmon, *Biosensors and Bioelectronics* **20** (2005) 1977-1983.

[30] M. Sequeira, M. Bowden, E. Minogue, D. Diamond, *Talanta* **56** (2002) 355-363.

[31] M. Bowden, D. Diamond, *Sensors and Actuators B: Chemical* **90** (2003) 170-174.

[32] F.A.A. Matias, M.M.D.C. Vila, M. Tubino, *Sensors and Actuators B: Chemical* **88** (2003) 60-66.

[33] N. Sombatsompop, N.-S. Intawong, N.-T. Intawong, *Sensors and Actuators A: Physical* **102** (2002) 76-82.

[34] S. Schrodle, R. Buchner, W. Kunz, *Fluid Phase Equilibria* **216** (2004) 175-182.

[35] K.S. Johnson, C.L. Beehler, C.M. Sakamoto-Arnold, *Analytica Chimica Acta* **179** (1986) 245-257.

[36] G.J. Schmidt, R.P. W. Scott, *The Analyst* **109** (1984) 997-1002.

[37] J.R. Clinch, P.J. Worsfold, H. Casey, *Analytica Chimica Acta* **200** (1987) 523-531.

[38] P.C. Hauser, S.S. Tan, T.J. Cardwell, R.W. Cattrall, I.C. Hamilton, *The Analyst* **113** (1988) 1551-1555.

[39] P.C. Hauser, D.W.L. Chiang, *Talanta* **40** (1993) 1193-1200.

[40] A. Rainelli, R. Stratz, K. Schweizer, P.C. Hauser, *Talanta* **61** (2003) 659-665.

[41] M. Trojanowicz, J. Szpunar-Lobinska, *Analytica Chimica Acta* **230** (1990) 125-130.

[42] P.R. Freeman, I.D. McKelvie, B.T. Hart, T.J. Cardwell, *Analytica Chimica Acta* **234** (1990) 409-416.

[43] J.A. Chediak, Z. Luo, J. Seo, N. Cheung, L.P. Lee, T.D. Sands, *Sensors and Actuators A: Physical* **111** (2004) 1-7.

[44] A. Yamada, M. Sakuraba, J. Murota, *Materials Science in Semiconductor Processing* **8** (2005) 435-438.

[45] J.M. Park, O.J. Shon, H.-g. Hong, J.S. Kim, Y. Kim, H.B. Lim, *Microchemical Journal* **80** (2005) 139-144.

[46] K. Sonne, P.K. Dasgupta, *Analytical Chemistry* **63** (1991) 427-432.

[47] S. Dong, P.K. Dasgupta, *Talanta* **38** (1991) 133-137.

[48] P.K. Dasgupta, H.S. Bellamy, H. Liu, J.L. Lopez, E.L. Loree, K. Morris, K. Petersen, K.A. Mir, *Talanta* **40** (1993) 53-74.

[49] H. Liu, P.K. Dasgupta, H.J. Zheng, *Talanta* **40** (1993) 1331-1338.

[50] P.J. Worsfold, J.R. Clinch, H. Casey, *Analytica Chimica Acta* **197** (1987) 43-50.

[51] H. Liu, P.K. Dasgupta, *Analytica Chimica Acta* **289** (1994) 347-353.

[52] J. Huang, H. Liu, A. Tan, J. Xu, X. Zhao, *Talanta* **39** (1992) 589-592.

[53] N. Gros, *Talanta* **62** (2004) 143-150.

[54] N. Gros, *Talanta* **65** (2005) 907-912.

[55] P.C. Hauser, T.W.T. Rupasinghe, N.E. Cates, *Talanta* **42** (1995) 605-612.

[56] A. Fonseca, J. Raimundo, Ivo M., *Analytica Chimica Acta* **522** (2004) 223-229.

[57] A. Suzuki, J. Kondoh, Y. Matsui, S. Shiokawa, K. Suzuki, *Sensors and Actuators B: Chemical* **106** (2005) 383-387.

[58] K.T. Lau, S. Baldwin, R.L. Shepherd, P.H. Dietz, W.S. Yerzunis, D. Diamond, *Talanta* **63** (2004) 167-173.

[59] K.-T. Lau, S. Baldwin, M. O'Toole, R. Shepherd, W.J. Yerazunis, S. Izuo, S. Ueyama, D. Diamond, *Analytica Chimica Acta* **557** (2006) 111-116.

[60] M. O' Toole, K.T. Lau, D. Diamond, *Talanta* **66** (2005) 1340-1344.

[61] K.-T. Lau, W.S. Yerazunis, R.L. Shepherd, D. Diamond, *Sensors and Actuators B: Chemical* **114** (2006) 819-825.

[62] D. Betteridge, *Analytical Chemistry* **50** (1978) 832A-846A.

[63] Q. Lu, G.E. Collins, M. Smith, J. Wang, *Analytica Chimica Acta* **469** (2002) 253-260.

[64] M. King, B. Paull, P.R. Haddad, M. Macka, *The Analyst* **127** (2002) 1564-1567.

[65] P. Kuban, R. Guchardi, P.C. Hauser, *Trends in Analytical Chemistry* **24** (2005) 192-198.

[66] A. Pacquit, K.T. Lau, H. McLaughlin, J. Frisby, B. Quilty, D. Diamond, *Talanta* **69** (2006) 515-520.

[67] M. Trojanowicz, P.J. Worsfold, J.R. Clinch, *Trends in Analytical Chemistry* **7** (1988).

[68] http://www.kpsec.freeuk.com/components/led.htm

[69] F.M. Mims III, *Scientific American* **263** (1990) 106-109.

[70] F.M. Mims III, *Applied Optics* **31** (1992) 6965-6967.

[71] B.R. Eggins, *Chemical sensors and biosensors*, New York : John Wiley, 2002.

[72] http://en.wikipedia.org/wiki/Microcontroller

[73] www.ccsinfo.com/picc

[74] O. Geschke, H. Klank, P. Tellemann, *Microsystem Engineering of Lab-on-a-chip Devices*, WILEY-VCH, 2004.

[75] http://www.sigmaaldrich.com/catalog/search/ProductDetail/FLUKA/82561

[76] E. Dempsey, D. Diamond, M.R. Smyth, G. Urban, G. Jobst, I. Moser, E.M.J. Verpoorte, A. Manz, H. Michael Widmer, K. Rabenstein, R. Freaney, *Analytica Chimica Acta* **346** (1997) 341-349.

[77] D.R. Lide, *CRC Handbook of Chemistry and Physics*, CRC Press, Boca Raton, FL, 2003-2004.

[78] J.L. Haberer, J.A. Brandes, *Marine Chemistry* **82** (2003) 185-196.

[79] A.G. Vlessidis, M.E. Kotti, N.P. Evmiridis, *Journal of Analytical Chemistry* **59** (2004) 77-85.

[80] G. Hanrahan, M. Gledhill, P.J. Fletcher, P.J. Worsfold, *Analytica Chimica Acta* **440** (2001) 55-62.

[81] K. Higuchi, H. Tamanouchi, S. Motomizu, *Analytical Sciences* **14** (1998) 941-946.

[82] J.B. Mullin, J.P. Riley, *Analytica Chimica Acta* **12** (1955) 162-176.

[83] P.J. Worsfold, L.J. Gimbert, U. Mankasingh, O.N. Omaka, G. Hanrahan, P.C.F.C. Gardolinski, P.M. Haygarth, B.L. Turner, M.J. Keith-Roach, I.D. McKelvie, *Talanta: Analysis of Phosphorus in Environmental and Agricultural Samples* **66** (2005) 273-293.

[84] B. Paull, L. Barron, P. Nesterenko, *Chromatographic Analysis of the Environment*, CRC Press/Taylor & Francis Group Boca Raton, FL., 2005, p. 263-286.

[85] D. Peachey, J.L. Roberts, J. Scot-Baker, *Journal of Geochemical Exploration* **2** (1973) 115-120.

[86] E. Bakker, D. Diamond, A. Lewenstam, E. Pretsch, *Analytica Chimica Acta* **393** (1999) 11-18.

[87] K.L. Linge, C.E. Oldham, *Analytica Chimica Acta* **450** (2001) 247-252.

[88] H.H. Hess, J.E. Derr, *Analytical Biochemistry* **63** (1975) 607-613.

[89] P.P. Van Veldhoven, G.P. Mannaerts, *Analytical Biochemistry* **161** (1987) 45-48.

[90] P. Ekman, O. Jager, *Analytical Biochemistry* **214** (1993) 138-141.

[91] S. Motomizu, T. Wakimoto, K. Tôei, *The Analyst* **108** (1983) 361-167.

[92] J.P. Susanto, M. Oshima, S. Motomizu, H. Mikasa, Y. Hori, *The Analyst* **120** (1995) 187-191.

[93] I.D. McKelvie, D.M.W. Peat, P.J. Worsfold, *Analytical Proceedings* **32** (1995) 437-445.

[94] E. D'Angelo, J. Crutchfield, M. Vandiviere, *Journal of Environmental Quality* **30** (2001) 2206-2209.

[95] S. Motomizu, Z.-H. Li, *Talanta: Analysis of Phosphorus in Environmental and Agricultural Samples* **66** (2005) 332-340.

[96] M. O' Toole, K.-T. Lau, B. Shazmann, R. Shepherd, P.N. Nesterenko, B. Paull, D. Diamond, *The Analyst* **131** (2006) 938 - 943.

[97] L. Barron, P.N. Nesterenko, D. Diamond, M. O'Toole, K.-T. Lau, B. Paull, *Analytica Chimica Acta* **577** (2006) 32-37.

[98] T. Attin, K. Becker, C. Hannig, W. Buchalla, A. Wiegand, *Clinical Oral Investigations* **9** (2005) 203-207.

[99] Q. Kang, N.C. Golubovic, N.G. Pinto, H.T. Henderson, *Chemical Engineering Science* **56** (2001) 3409-3420.

[100] K.K. Unger, D. Kumar, M. Grun, G. Buchel, S. Ludtke, T. Adam, K. Schumacher, S. Renker, *Journal of Chromatography A* **892** (2000) 47-55.

[101] J. Liu, K.J. Volk, M.J. Mata, E.H. Kerns, M.S. Lee, *Journal of Pharmaceutical and Biomedical Analysis* **15** (1997) 1729-1739.

[102] C. Czerwenka, M. Lammerhofer, W. Lindner, *Journal of Pharmaceutical and Biomedical Analysis* **30** (2003) 1789-1800.

[103] P. Wang, Z. Chen, H.-C. Chang, *Sensors and Actuators B: Chemical* **113** (2006) 500-509.

[104] F. Kuhn, M. Oehme, M. Schleimer, *Journal of Chromatography A* **1018** (2003) 203-212.

[105] Y. Shintani, K. Hirako, M. Motokawa, T. Iwano, X. Zhou, Y. Takano, M. Furuno, H. Minakuchi, M. Ueda, *Journal of Chromatography A* **1073** (2005) 17-23.

[106] D. Connolly, D. Victory, B. Paull, *Journal of Separation Science* **27** (2004) 912-920.

[107] E. Sugrue, P. Nesterenko, B. Paull, *Analytica Chimica Acta* **553** (2005) 27-35.

[108] E. Sugrue, P. Nesterenko, B. Paull, *Journal of Separation Science* **27** (2004) 921-930.

[109] A. Atanassova, R. Lam, D.B. Zamble, *Analytical Biochemistry* **335** (2004) 103-111.

[110] P.R. Haddad, P.E. Jackson, *Ion Chromatography - Principles and Applications*, Elsevier, 1990.

[111] J.S. Fritz, D.T. Gjerde, *Ion Chromatography*, Wiley-VCH, 2000.

[112] H. Small, *Ion Chromatography*, Plenum Press, New York and London, 1989.

[113] D.J. Hooley, R.E. Dessy, *Analytical Chemistry* **55** (1983) 313-320.

[114] E.A.G. Zagatto, M.A.Z. Arruda, A.O. Jacintho, I.L. Mattos, *Analytica Chimica Acta* **234** (1990) 153-160.

[115] I.-Y. Eom, P.K. Dasgupta, *Talanta* **69** (2006) 906-913.

[116] P. Jones, *The Analyst* **125** (2000) 803-806.

[117] P. Nesterenko, P. Jones, *Journal of Chromatography A* **770** (1997) 129-135.

[118] S. Jambunathan, P.K. Dasgupta, D.K. Wolcott, G.D. Marshall, D.C. Olson, *Talanta* **50** (1999) 481-490.

[119] M.I. Analysis, in, Metrohm Ion Analysis, 2001.

[120] F.J. Green, *The Sigma-Aldrich Handbook of Stains, Dyes and Indicators*, Aldrich Chemical Company, Inc., 1990.

List of Figures

List of Tables

Publication

Available online at www.sciencedirect.com
SCIENCE DIRECT®
Talanta 66 (2005) 1340–1344
Talanta
www.elsevier.com/locate/talanta

Photometric detection in flow analysis systems using integrated PEDDs

Martina O' Toole, King Tong Lau, Dermot Diamond *

Adaptive Information Clusters, National Centre for Sensor Research, School of Chemical Sciences, Dublin City University, Dublin 9, Ireland

Received 14 September 2004; received in revised form 20 January 2005; accepted 28 January 2005
Available online 26 February 2005

Abstract

A novel inexpensive optical-sensing technique has been developed for colorimetric flow analysis. This sensing system employs two LEDs whereby one is used as the light source and the other as a light detector. The LED used as light detector is reverse biased with a 5-V supply so that the photocurrent generated by the incident light discharges the capacitance. Direct digital output is provided by a simple timer circuit that measures the time taken for this discharge process from 5 V (logic 1) to 1.7 V (logic 0).

This sensing concept has been applied in flow analysis by constructing an optical flow cell with a pair of LEDs. Calibration of the integrated optical flow cell using a dye resulted in a linear response that obeys the Beer–Lambert law. The flow rate, dynamic range, sensitivity and limits of detection were investigated. The system was also used for pH determination in the range of pH 2.5–6.8 using bromocresol green (BCG). The pK_a of BCG was successfully determined by this technique.

Keywords: LEDs; Optical sensing; pH sensing; Transmission measurements; Colorimetric analysis

1. Introduction

At present optical sensing is one of the most active areas of research in analytical chemistry. This is largely due to the availability of inexpensive, low power-consumption components such as LEDs, photodiodes and data acquisition technologies. Desirable qualities like these are vital requirements in the development of (micro) total analysis systems, particularly, with respect to field deployable micro-instruments [1].

Light-emitting diodes (LEDs) are the most energy-efficient means of producing light emission, and are ideal for miniature analytical devices [2]. LEDs are increasingly popular for the fabrication of optical sensors as they offer advantages of being inexpensive, small in size, available over a broad spectral range from ultraviolet to near-infrared (ca. 380–900 nm), have a long lifetime, robust and easy to fabricate into various configurations. When used as light detectors for chemical sensing by measuring the intensity-dependent discharge of capacitance, they have been found to be highly sensitive and could detect sub-micro-molar of dye [3].

Optical sensor configurations generally combine LED light source with photodiodes, which measure the light intensity after passage through the sample [2,4–8]. The use of LEDs in photometric detectors has been reported as early as 1978 when Betteridge et al. [9] used a gallium phosphide LED and a silicon phototransistor for the detection of metal ions. Since then LEDs have improved, for example, in increased range and intensity, and a variety of LED-based optical sensors has been developed [10–12]. Hauser et al. [13] employed seven light-emitting diodes ranging from blue to infrared as a light source with photodiodes as detection. The light from each LED was guided into a single measuring cell using a fibre-optic coupler. Using this configuration, it was possible to determine copper using the cuprizone method and ammonia using the indophenol method with 90% of the sensitivity of a spectrometer. LEDs have also been used in fluorescence intensity-based sensors [14] and phase fluorimetry [15].

* Corresponding author. Tel.: +353 1 7005404; fax: +353 1 7008002.
E-mail address: dermot.diamond@dcu.ie (D. Diamond).

0039-9140/$ – see front matter © 2005 Elsevier B.V. All rights reserved.
doi:10.1016/j.talanta.2005.01.054

A novel configuration for optical sensing is the use of an LED as a light detector. In this approach, two LEDs are employed, whereby one is used as a light source and the second as the light detector. Mims and Forrest [16,17] first investigated using a LED as a crude light detector to measure photocurrent generated by direct sunlight. Previously, we demonstrated the use of a paired emitter detector diode (PEDD) device for colour and pH measurements in static solution [3]. A PEDD consists of two LEDs arranged in various configurations in which one LED is used to provide illumination and the other is used as a light detector for the transmitted or reflected light.

In this paper we propose a novel, simple optical-sensing device for flow analysis using a pair of LEDs. An optical flow cell was constructed using two LEDs which allowed sample to flow inside the cojoined LEDs along the light path. The use of this integrated colorimetric flow analyser to measure colour and pH is reported.

2. Experimental

2.1. Chemicals and reagents

The pH indicator dye used was bromocresol green (BCG) (from Sigma Aldrich, Dublin, Ireland). All samples were made up in a pH 7 buffer stock solution made from buffer tablets (Lennox, Dublin, Ireland) and ultrapure water according to the instructed method. All the reagents used were of analytical grade. Stock solution of 25 mM BCG was prepared by dissolving 0.70 g dye in 250 ml of pH 7 buffer solution from which dilutions were prepared.

A series of dye solutions each containing 40 μM BCG at various pHs (2.5–6.8) was also prepared.

2.2. Fabrication of PEDD optical flow cell

The optical device was fabricated using two identical (5 mm) LEDs (λ_{max} at 621 nm) (Knightbright, France), with emission shown in Fig. 2. The original length of each LED was 10 mm. The PEDD sensor was prepared by first cutting 0.25 mm from the tips of each LED to give a flat top, rather than the usual curved surface. The total length of the PEDD was now 15 mm. The surface of the LEDs was then sanded down using general purpose, fine-grade paper (Homebase, Dublin) to make them smooth and flat before bonding. Using a drill bit of size 1.3 mm, a channel was machined into each LED to a depth of 1.8 mm, resulting in a pathlength of 3.6 mm as shown in Fig. 1. An inlet and outlet were also machined using the same method. Prior to bonding, the two LEDs were accurately aligned to ensure the line of fusion was perfectly round. The LEDs were then fused together using UV curable epoxy glue (Edmund Scientific: Orland 81 extra fast curing, USA), and placed under UV light (380 nm) for 30 min. Green peek tubing (i.d. 0.75 mm) was placed at either end of the channel and sealed into place using araldite

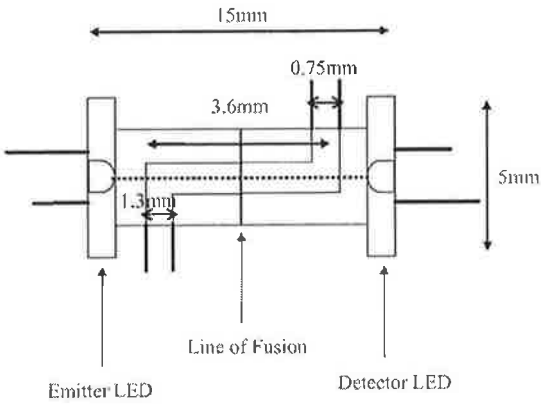

Fig. 1. A schematic of the integrated PEDD flow analysis device used for colorimetric detection.

epoxy glue (Homebase, Dublin). The PEDD cell was left to dry at room temperature for a further 30 min. The optical cell was then painted black to reduce stray light effects.

2.3. Light measurement

A 9-V battery was used to drive the circuitry from which a voltage regulator was used to control the voltage supply to the LEDs. The light detector LED in input mode was charged up to 5 V for 100 μs and then switched to output mode. The photon flux from the emitter LED strikes the detector LED, generating a small photocurrent which gradually discharges the capacitor voltage. The time taken for the discharge process to go from an initial value of 5 V (logic 1) to a preset value of 1.7 V (logic 0) was measured with a simple timer circuit.

2.4. Measurement procedure

Various concentrations of BCG were made up in pH 7 buffer solution and passed through the PEDD flow cell at a flow rate of 0.6 ml/min for ca. 4 min while continuously monitoring the absorbance. All experiments were carried out in triplicate with the exception of BCG calibration, which was repeated 8 times. The data are transported to a PC via RS232 port and captured with the HyperTerminal software, and then saved as a text file for further analysis using Excel™ (Microsoft, Inc., USA).

3. Results and discussion

3.1. Colour measurement using PEDD flow cell

In this study, the measurement is based on the following theoretical model, which has been derived by Lau et al. [18]:

$$\log(t) = \varepsilon Cl + \log(t_0) \quad (1)$$

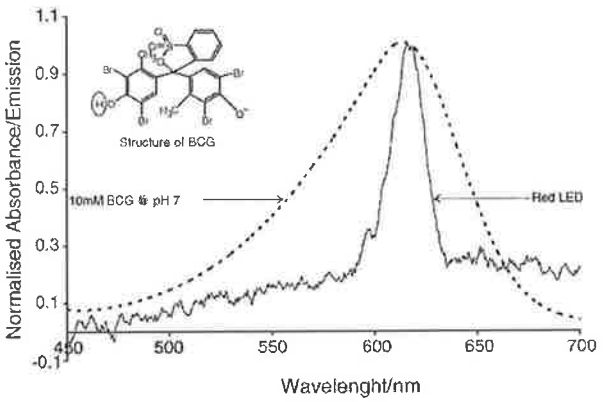

Fig. 2. Emission spectrum (λ_{max} 620 nm) of the LED used in the integrated PEDD flow analysis device and the absorption spectrum (λ_{max} 616 nm) of 10 mM BCG at pH 7 ($\varepsilon = 1.2 \times 10^4$ l mol^{-1} cm^{-1}). The inset is the structure of the deprotonated BCG dye used. Emission and absorbance normalised to range 0–1 by dividing values by λ_{max}.

where l is the optical pathlength through the solution (cm), ε the molar extinction coefficient (mol l^{-1} cm^{-1}) at a particular wavelength, C the concentration of the absorbing species (mol l^{-1}), t_0 a constant that represents discharge time in the absence of the coloured species in solution (μs).

Initial studies carried out involved the calibration of a change in colour intensity or concentration of a pH indicator dye, Bromocresol green in a pH 7 buffer. BCG was selected due to its large molar extinction coefficient of 1.2×10^4. The light intensity transmitted in the flow cell was measured with an LED (λ_{max} 621 nm), which efficiently overlaps the absorbance spectrum of BCG (λ_{max} 620 nm) as shown in Fig. 2. The emission spectrum of the LED was obtained by using ocean optic spectrometer (OOIBase 32^{TM}, Ocean Optics, Inc., Dunedin, USA). Various concentrations of BCG were made up in pH 7 buffer solution and passed through the PEDD flow cell for ca. 4 min per sample, at a flow rate of 0.6 ml/min. The log of the discharge times (log t, μs) was plotted against dye concentration (C) in accordance with the model (Eq. (1)) and the result is presented in Fig. 3. Inset (a) in Fig. 3 shows a large detection range from ca. 0 to 20.5 mM BCG from which a linear range of approximately 0.9–250 μM BCG (R^2 value 0.998) was observed as shown in the main feature plot. It can be seen from that the relative standard deviation of the measurements ($n = 8$, shown as error bars) are very low (ca. 0.4%) and LOD of 0.9 μM.

As a comparison study, the absorbance of the same BCG concentrations was acquired using the μQuant^{TM} platewell reader (Bio-Tek Instruments, Inc., USA). As shown in Fig. 4, the absorbance at λ_{max} plotted against the dye concentration (C) resulted in a linear detection range of 0.5–250 μM (R^2 value 0.999), with an R.S.D. ($n = 3$) of 4% and an LOD of 0.9 μM. It can be seen that the performance of the simple LED-based device matched that of a conventional bench top instrument.

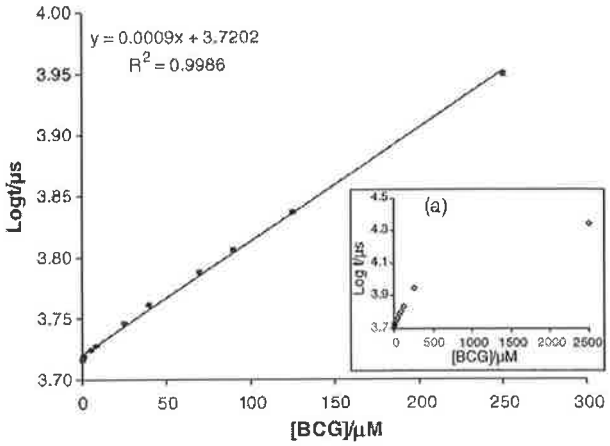

Fig. 3. Linear calibration plot of log of the discharge times log(t) vs. BCG dye concentration. The error bars represent the standard deviations for $n = 8$. The inset (a) shows the full range of responses obtained from the calibration.

3.2. Detector responses to varying light source intensity

A study has been carried out to investigate the effect of varying illumination intensity on the sensitivity of the detector. The emitter intensity was controlled by using a variable resistor connected directly to the emitter LED as the amount of electrical current passing to the emitter LED is directly proportional to its emission intensity. Therefore an increase in the resistance results in a decrease in the light intensity of the emitter LED, which in turn results in an increase in the time taken to discharge the detector LED.

A pH 7 buffer solution was passed through the flow cell for ca. 4 min, followed by 8 μM BCG at pH 7 at a flow rate of 0.6 ml/min. This sample was selected as it gave a significant change in response (discharge time of ca. 100 μs) compared to the pH 7 background. Various light intensities were examined and the results obtained are shown in Fig. 5. The data shows that increasing resistance to reduce light intensity results in a linear increase in responses. The largest R.S.D. ($n = 3$) shown in Fig. 5 appears to be big at ca. 12%. This was

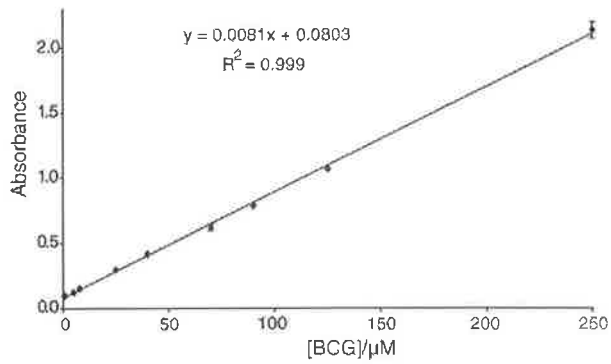

Fig. 4. Calibration plot of absorbance at λ_{max} vs. BCG dye concentration obtained using a platewell reader. The error bars represent the standard deviations for $n = 3$.

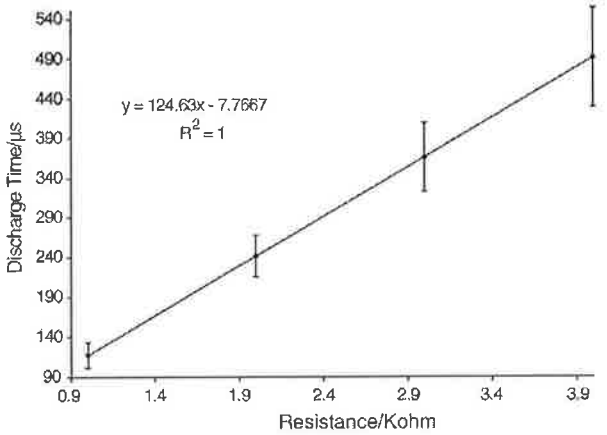

Fig. 5. A plot to illustrate the effect of varying light intensity on the discharge time detected for 8 μM BCG by changing the resistance of the variable resistor connecting to the LED. The error bars represent the standard deviations for $n = 3$.

due to the difficulties associated with using a manual variable resistor to reproduce the exact resistance values after each experiment, which contributed to the big error margin. With fixed resistors the data obtained were much better as shown in Fig. 6, which shows a comparison of the reproducibility of the system with: (1) no additional resistance and (2) at 2 kΩ. Note that the baselines of the two traces were very similar and smooth (R.S.D. 0.03%). The average response to 8 μM BCG obtained from (1) was 104.5 ± 1.9 μs ($n = 3$) whereas the average response from (2) was 416.2 ± 11.6 μs ($n = 3$). Increasing the resistance by 2 kΩ therefore improved the sensitivity by approximately a factor of 4.

3.3. Using PEDD to monitor colour changes

The PEDD flow cell has also been used to monitor the pH-dependent colour change of BCG. A dye concentration of 40 μM was chosen to demonstrate this application as it has good colour density. The plot obtained shown in Fig. 7 is

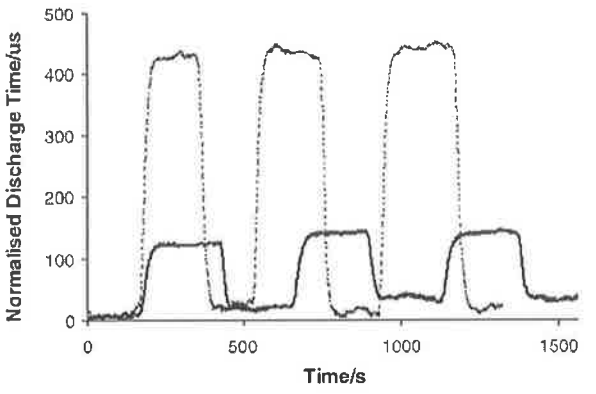

Fig. 6. Real-time traces obtained for 8 μM BCG solution buffered at pH 7 using two resistances (0.006 kΩ, solid line and 2 kΩ, dashed line). The flow rate used was 0.6 ml/min.

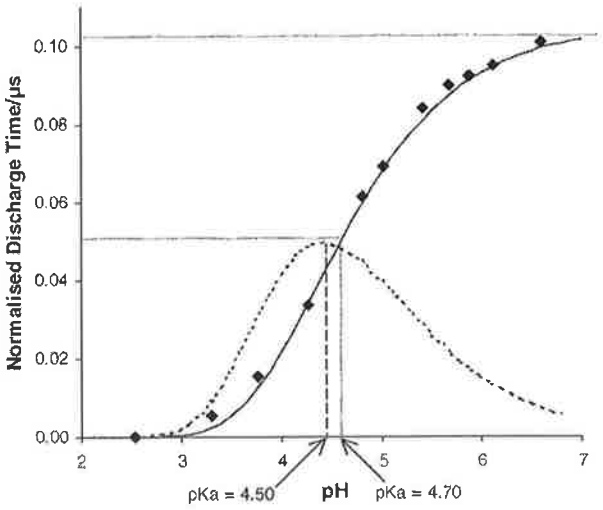

Fig. 7. A plot to illustrate the change in pH of 40 μM BCG solution with the discharge time of the PEDD flow detector (♦). The first derivative (dashed line) of the best-fit line (solid line) for the data gave an estimated pK_a value of 4.50.

sigmoidal in shape with a linear range between pH 3.8 and 5.3. Using Microsoft™ Excel solver and method developed by Diamond and Hanratty, a best-fit line was found for the experimental data [19]. The pK_a was determined to be 4.50 by taking the first derivative of the fitted line, which is slightly lower than the reported pK_a value of 4.74 for BCG at room temperature [20]. This was probably due to the limitation of the data range, which resulted in a non-symmetrical Gaussian plot. An alternative method for pK_a evaluation was used: At pH 2–3, the acid form of the dye was present at about 100%. This corresponds to a discharge time of 0.00 μs. At pH 7, the deprotonated form dominated (close to 100%) and this corresponded to a discharge time of 0.11 μs. At a discharge time of 0.055 μs, there should be equal amounts of these species corresponding to a pK_a of ca. 4.70, which agrees better with the literature data.

3.4. Future developments

The results obtained using the integrated PEDD flow analysis cell has demonstrated that this simple low-cost device can be used as a very sensitive optical detector for colorimetric flow optical sensor for colorimetric flow analysis. The high sensitivity, already evident in this study, may be further improved by increasing the pathlength through modification of the channel geometry. The PEDD flow cell may be used in various colour-based chemical analyses, e.g. detection of phosphates [21] or nitrites [22]. To enable chemical analyses using multiple reagents, a multichannel flow cell is required to perform reagent mixing. With different configurations, the PEDD flow cell can also be used for fluorescence detection. This sensing approach therefore has potential for very broad analytical applications, given that it has the advantages of very low cost, low power consumption

and offers high sensitivity with excellent signal-to-noise characteristics.

4. Conclusions

We have demonstrated that the integrated PEDD flow analysis system is useful for colorimetric analysis. This device while small, compact and inexpensive, is nevertheless highly sensitive and is clearly capable of providing limits of detection in the nanomolar concentration range. The power consumption required is extremely low and the sensor can be operated from a 9-V battery. The PEDD flow cell is therefore very suitable for scale-up and field deployment in autonomous monitoring instruments.

Acknowledgements

The authors wish to thank Science Foundation Ireland SFI for grant support under the Adaptive Information Cluster Award (SFI 03/IN3/1361). We also acknowledge valuable help and support provided by Dr. William S. Yerazunis, Mitsubishi Electric Research Laboratories, Broadway, Cambridge, MA, USA.

References

[1] D. Diamond, Anal. Chem. 76 (2004) 279A–286A.
[2] P.K. Dasgupta, E. In-Yong, K.J. Morris, J. Li, Anal. Chim. Acta 500 (2003) 337–364.
[3] K.T. Lau, S. Baldwin, R.L. Shepherd, P.H. Dietz, W.S. Yerzunis, D. Diamond, Talanta 63 (2004) 167–173.
[4] P.C. Hauser, D.W.L. Chiang, Talanta 40 (1993) 1193–1200.
[5] M. Trojanowicz, J. Szpunar-Lobińska, Anal. Chim. Acta 230 (1990) 125–130.
[6] H. Liu, P.K. Dasgupta, Anal. Chim. Acta 289 (1994) 347–353.
[7] G.E. Collins, Q. Liu, Sens. Actuators B 76 (2001) 244–249.
[8] Q. Lu, G.E. Collins, Analyst 126 (2001) 429–432.
[9] D. Betteridge, E.L. Dagless, B. Fields, N.F. Graves, Analyst 103 (1978) 897–908.
[10] M. King, B. Paull, P.R. Haddad, M. Macka, Analyst 127 (2002) 1564–1567.
[11] F.A.A. Matias, M.M.D.C. Vila, M. Tubino, Sens. Actuators B 88 (2003) 60–66.
[12] M. Bowden, D. Diamond, Sens. Actuators B 90 (2003) 170–174.
[13] P.C. Hauser, T.W.T. Rupasinghe, N.E. Cates, Talanta 42 (1995) 605–612.
[14] S.J. Chen, M.J. Chen, H.T. Chang, J. Chromatogr. A 1017 (2003) 215–224.
[15] G. O' Keeffe, B.D. MacCraith, A.K. McEvoy, C.M. McDonagh, J.F. McGilp, Sens. Actuators B 29 (1995) 226–230.
[16] Mims, M. Forrest, Sci. Am. 263 (1990) 106–109.
[17] Mims, M. Forrest, Appl. Opt. 31 (1992) 6965–6967.
[18] K.T. Lau, S. Baldwin, M. O' Toole, R.L. Shepherd, W.S. Yerzunis, S. Izuo, U. Satoshi, D. Diamond, Analyst, submitted for publication.
[19] D. Diamond, V.C.A. Hanratty, Spreadsheet Applications in Chemistry using Microsoft Excel, Wiley, New York, 1997.
[20] D.R. Lide, CRC Handbook of Chemistry and Physics, CRC Press, Boca Raton, FL, 2003–2004, pp. 8–19.
[21] M. Sequeira, M. Bowden, E. Minogue, D. Diamond, Talanta 56 (2002) 355–363.
[22] P.S. Kumar, S.T. Lee, C.P.G. Vallabhan, V.P.N. Nampoori, P. Radhakrishnan, Opt. Commun. 214 (2002) 25–30.

Available online at www.sciencedirect.com
SCIENCE DIRECT
ELSEVIER
Analytica Chimica Acta 557 (2006) 111–116
ANALYTICA CHIMICA ACTA
www.elsevier.com/locate/aca

A low-cost optical sensing device based on paired emitter–detector light emitting diodes

King-Tong Lau [a,*], Susan Baldwin [a], Martina O'Toole [a], Roderick Shepherd [a], William J. Yerazunis [b], Shinichi Izuo [c], Satoshi Ueyama [c], Dermot Diamond [a,*]

[a] *Adaptive Sensors Group, National Centre for Sensor Research, School of Chemical Science, Dublin City University, Dublin 9, Ireland*
[b] *Mitsubishi Electric Research Laboratories, 201 Broadway, Cambridge, MA 02139, USA*
[c] *Advanced R&D Center, Mitsubishi Electric Corporation, 8-1-1 Tsukaguchi-honmachi, Amagasaki, Hyogo 661-8661, Japan*

Received 14 June 2005; received in revised form 19 October 2005; accepted 19 October 2005
Available online 28 November 2005

Abstract

A low-power, high sensitivity, very low-cost light emitting diode (LED)-based device for intensity-based light measurements is described. In this approach, a reverse-biased LED functioning as a photodiode is coupled with a second LED configured in conventional emission mode. A simple timer circuit measures how long (in microsecond) it takes for the photocurrent generated on the detector LED to discharge its capacitance from logic 1 (+5 V) to logic 0 (+1.7 V). The entire instrument provides an inherently digital output of light intensity measurements for a few cents. This light intensity dependent discharge process has been applied to measuring concentrations of coloured solutions and a mathematical model developed based on the Beer–Lambert Law.

Keywords: Light emitting diode; Photodiode; Colorimetry; Optical sensor; Sensor networks

1. Introduction

The vast majority of analytical measurements are currently made under specialist laboratory conditions using bench-top instruments that are designed to deliver high precision and accuracy for multiple components in samples that often have extremely complex matrices. This is particularly so in important application sectors such as clinical assays, genomic/proteomic research, the pharma industry and environmental monitoring. However, it is becoming clear that developments in and availability of wireless communications (e.g. GSM, 3G, 802.11, Bluetooth, ZigBee, RFID, etc.) and portable computing provide an infrastructure for the functional deployment of wireless sensor networks. While research in this area is overwhelmingly dominated by demonstrator projects employing physical transducers, it is logical to predict that chemical sensors and biosensors will be introduced when inexpensive, reliable devices are available [1–5].

For example, sensor networks targeting important analytes may be deployed to cover a strategically important area, from where the autonomously collected data may be harvested by remote servers that seek out specific events such as threshold crossing, and trawl for patterns in larger scale information sets that may herald the initiation of an environmental pollution event, or the release of hazardous agent [6].

However, the widespread deployment of chemical sensors and biosensors can only be successfully achieved if devices with appropriate operating characteristics are available at very low cost. For example, sensor networks involving many devices will require that each sensor-node (i.e. sensor + signal acquisition electronics + wireless communication) costs a few cents or less and can operate reliably for up to years at a time while simultaneously consuming very low (virtually no) power. This concept poses significant challenges for chemical sensor/biosensor research, as no such devices are currently available, and sensor network research is therefore dominated by physical measurements such as light density and temperature. This situation has

* Corresponding authors.
E-mail addresses: kim.lau@dcu.ie (K.-T. Lau), dermot.diamond@dcu.ie (D. Diamond).

0003-2670/$ – see front matter © 2005 Published by Elsevier B.V.
doi:10.1016/j.aca.2005.10.046

prompted us to explore various strategies for making long-term field measurements using stable reagents in a lab-on-a-chip instrument configuration [7], and simultaneously developing very low-cost device platforms for making analytical measurements [8].

Light emitting diodes (LEDs) are robust, low cost, low power, very efficient in terms of energy conversion, small size and they cover an increasingly broad spectral range from UV to near infrared. These properties are ideal for the development of optical devices and consequently LEDs have been widely used in consumer electronic devices, and in more specialist applications such the illumination source for fibre optical sensors [9–16] and reflectometers [17]. The concept of using LEDs as light detectors has already been explored by Mims and Dietz et al. These workers used a simple circuit that contained an operational amplifier to measure the photocurrent obtained by a reverse-biased LED, and have used this LED sensor for detecting sunlight intensity [18,19].

As LED-photodiodes are considerably less sensitive than commercial photodiodes (we typically find the photocurrent to be around 10–100 times smaller), direct measurement of the photocurrent is difficult without amplification, and requires an expensive picoammeter. However, our previous work [8] has shown that very accurate and precise measurement of the photocurrent is possible using a simple threshold detector and timer circuit. Basically, the sensing LED is reverse-biased to +5 V (logic 1) and on switching to measurement mode, this charge is sustained by the inherent capacitance of the diode (typically picoFarads). The time taken for the photocurrent from the LED sensor to discharge this voltage to logic 0 (+1.7 V) is measured, and is obviously related to the incident light intensity. This extremely low-cost approach provides inherently digital measurement of light intensity without amplification, while simultaneously providing excellent signal-to-noise characteristics, due to the signal integration over the measurement. In this configuration, the sensitivity of the LED-photodiode is improved and becomes more attractive than a conventional (and more expensive) photodiode, which discharges the capacitor much more quickly, making time-based discrimination more difficult and expensive.

2. Theoretical model

A mathematical model has been developed to relate this sensing strategy to conventional analytical measurements based on the Beer–Lambert Law. Fig. 1 is the LED equivalent circuit. The light-sensing LED is reverse-biased to 5 V and is discharged by the photocurrent i_{light} generated by the incoming light.

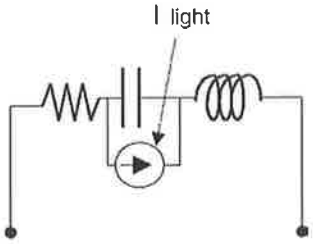

Fig. 1. A schematic of LED equivalent circuit.

Another discharging process also occurs naturally in parallel in which the circuit discharges itself in complete darkness via a small (dark) current i_{dis}, which is normally insignificant compared to i_{light}. Typically, under strong illumination, we have found the discharge time to be in the region of microseconds, whereas in complete darkness, it discharges in ca. 300 ms.

In general, the total discharge time t for the LED equivalent circuit can be described as

$$t = \frac{Q}{i_{dis} + i_{light}} \tag{1}$$

where Q is accumulated charge (a constant).

When $i_{light} \gg i_{dis}$

$$t = \frac{Q}{i_{light}} \tag{2}$$

i.e. the time taken to discharge the capacitor is inversely proportional to the intensity of the incident light, as the quantity of electric charge (Q) is a constant.

When light passes through a coloured sample solution, the emitted light intensity (I) is reduced relative to the incident light intensity (I_o) due to absorbance of the light energy by the analyte at certain wavelengths. The sample absorbance (A) is related to these intensities and the sample concentration by the Beer–Lambert Law,

$$A = \log\left(\frac{I_o}{I}\right) = \varepsilon C l \tag{3}$$

where l is the optical path length through the solution, ε the molar extinction coefficient (mol/l/cm) at a particular wavelength and C is the concentration of the absorbing species. Substituting (2) into (3) we get,

$$A = \log\left(\frac{I_o}{I}\right) = \log\left(\frac{t}{t_o}\right) = \varepsilon C l \tag{4}$$

where t_o is the time to discharge to a preset voltage in the absence of the coloured species in solution (a constant); therefore, we can say,

$$\log(t) = \varepsilon C l + \log(t_o) \tag{5}$$

Eq. (5) predicts that if the Beer–Lambert Law holds, and the dark current from the capacitor is negligible compared to the photo-discharge current, then the concentration of the absorbing analyte is proportional to the log of the discharge time, with the intercept being $\log(t_o)$.

3. Experimental

3.1. Chemicals and materials

Light emitting diodes and photodiodes used in this study were commercially available products from various manufacturers (Kingbright, LED-Tech, Agilent, Nitia-Kagak, Toshiba and Siemens).

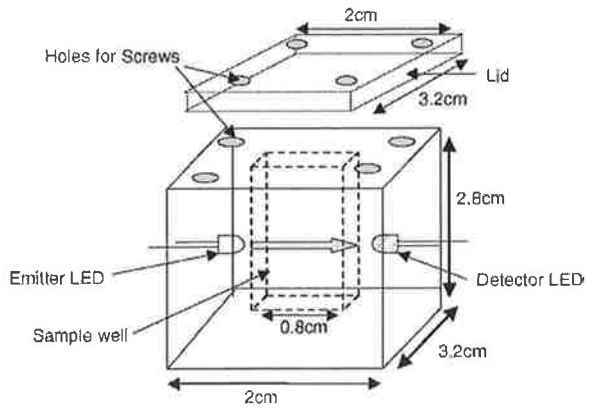

Fig. 2. A schematic of the detector cell used for chemical sensing.

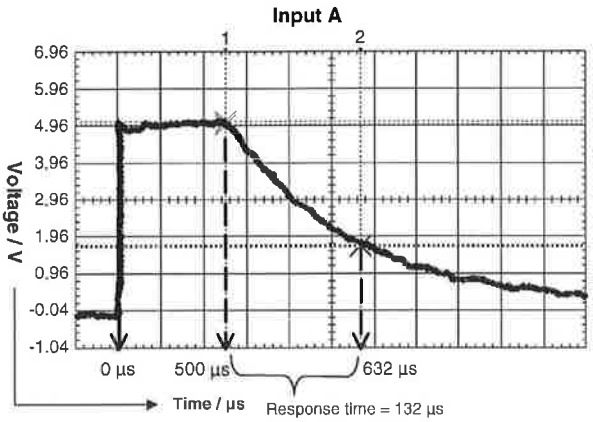

Fig. 3. Typical discharge curve for an LED charged up to 5 V and then discharged to a threshold of 1.7 V under artificial lighting (fluorescent tube).

Bromocresol green, 1,10-phenanthroline and ferrous ammonium sulphate hexahydrate were purchased from Sigma–Aldrich, Dublin, Ireland. All reagents used were of analytical grade.

3.2. Optical cell construction

A simple measuring system was constructed in house (Fig. 2) by firstly milling a cavity (1.3 cm length × 0.4 cm width × 2 cm height) in two separate identical pieces of black nylon (width 2 cm, height 2.8 cm and length 3.2 cm). The two sections were then joined together using black silicon glue to form a sample well (1.3 cm length × 0.4 cm width × 1.5 cm height), which could hold 1 mL of solution. Two small compartment holes ($d = 5$ mm) were fabricated on opposite sides of the cell and the LEDs were secured in facing each other in perfect alignment. PMMA transparent slides (width 1.5 cm and height 2.5 cm) were fixed in front of the LEDs to seal and act as windows for the LEDs using Araldite glue (RS Components, Ireland). The cell was then covered by a black nylon lid (width 2 cm × length 3.2 cm) to exclude ambient light.

4. Results and discussion

4.1. Discharge of LED

The capacitance of light emitting diodes is typically in the region of picoFarads. Hence, the discharge time for such devices will be small ranging from microseconds under bright light to milliseconds in low light conditions. Fig. 3 is a typical discharge profile for an LED with λ_{max} of emission at 610 nm obtained from a Fluke ScopMeter® (Fluke Corporation, WA, USA). The LED was charged up and held at 5 V for 500 µs before being discharged under fluorescent lighting. In this case, the discharge time is ca. 132 µs.

The timer circuit we have developed to measure this discharge time offers 16 bit resolution and a sampling rate of ca. 7 data points/s. Generally, we use a sampling time of 10 s and store the average value obtained.

4.2. Validation of LED light sensor

Experiments were also carried out to verify the response characteristics of the LED light sensors. Fig. 4 (inset) shows the linear relationship between increasing load (current limiting) resistance on an LED emitter ($\lambda_{max} = 620$ nm) and the resulting light intensity observed by a light dependent resistor (LDR). This demonstrates that the LDR response (R) is increased linearly with the current limiting resistance. The response of the LDR to varying light intensity is well established such that light intensity (i_{light}) is inversely proportional to the observed resistance (R). Therefore, it can be deduced that increasing the load resistance reduces LED output intensity and that the output light intensity from an LED is inversely proportional to the current limiting resistance, i.e. $i_{light} \propto 1/R$. This experiment was repeated by substituting the LDR with an LED light sensor ($\lambda_{max} = 620$ nm). The results (Fig. 4) show that the discharge

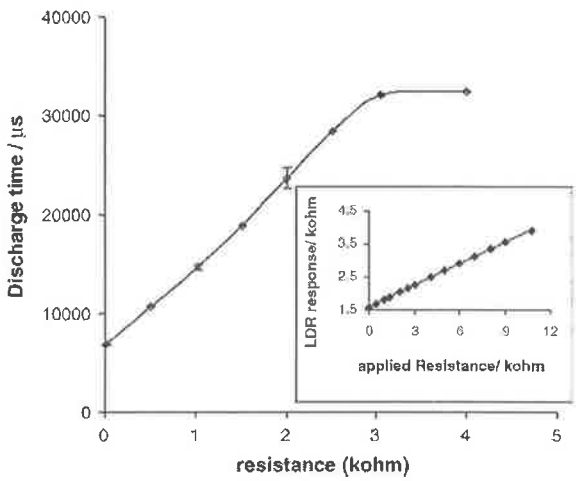

Fig. 4. Decay time of detector LED vs. the current limiting resistance used to control intensity of the emitter. The emitter–detector LEDs were 1 cm apart. Inset: a linear plot obtained by increasing current limiting resistance applied to an LED emitter circuitry which results in a change in light intensity measured with a light dependent resistor.

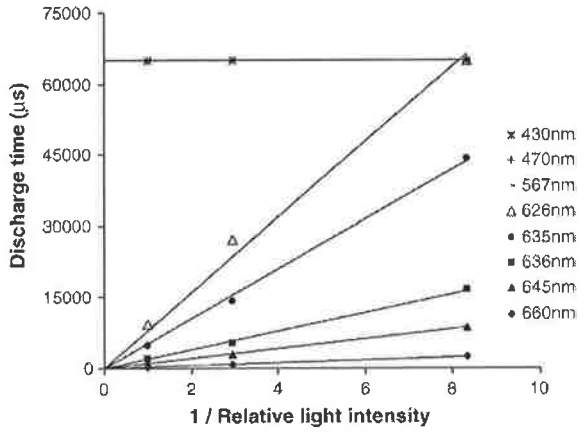

Fig. 5. Detection characteristics of LEDs with varying λ_{max} configured as light sensors. The source used was an LED with emission λ_{max} at 660 nm.

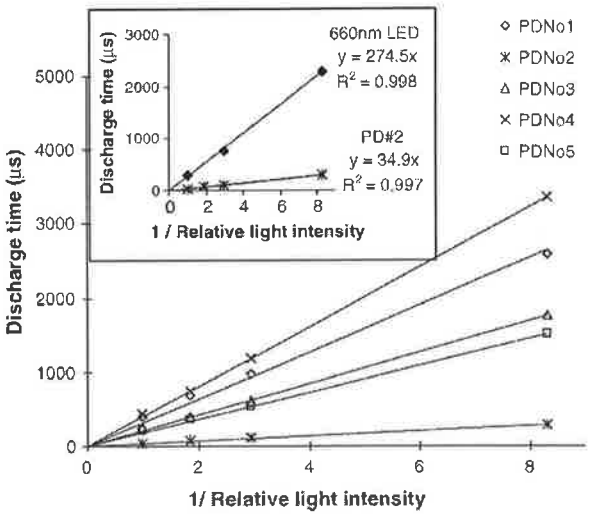

Fig. 6. Detection characteristics of various commercial PD light sensors using decay time light measuring regime. The source used was an LED with emission λ_{max} at 660 nm. Inset: the plots from a PD and an LED when the 660 nm LED light source band gap matches the detectors. The LED detector shows better sensitivity than the PD.

time t increases linearly with current limiting resistance, which may be expressed as the reciprocal of light intensity, and is therefore in agreement with Eq. (2) (i.e. $t \propto 1/i_{light}$) up to a limiting value where the incident light intensity is too low to be distinguished.

4.3. Comparison of various LEDs as light detectors

Using a constant emitter LED (emission $\lambda_{max} = 660$ nm) as an energy source, and series of neutral density filters to vary light output intensity (relative intensities of 1, 2.8 and 8.3), the effect of LED λ_{max} on the sensitivity of LED light sensors was investigated. The results (Fig. 5) show that the LEDs have a linear response to the inverse of incident light intensity, as predicted by Eq. (2). Discharge rate is fastest for the 660 nm LED sensor, and the discharge time increases with decreasing λ_{max}. The 567, 470 and 430 nm LEDs did not produce a photocurrent large enough to be detected by the timer circuit. In LEDs, the photon energy distribution is centred on the λ_{max}, with a relatively small spread, defined by the corresponding distribution of energy levels (band gap) in the semiconductor. In light-sensing mode, the same energy level distributions are involved, and generation of charge carriers can only happen if the incoming photons have enough energy to generate electron transitions across these energy levels. In the case of the 567, 470 and 430 nm LEDs, the band gap is too great for the incoming photons centred on 660 nm to cause transitions. As the λ_{max} of the LED sensor increases towards 660 nm, the band gap becomes correspondingly smaller, the population of photons capable of causing transitions increases, resulting in smaller discharge times from the measurement circuit.

4.4. Comparison to photodiodes

Photodiodes (PDs) are known to be much better light detector than LEDs because they are configured to optimise light detection rather than to emit light. Therefore, a PD would be much more sensitive than an LED when measuring the photocurrent output directly upon light irradiation. However, LED light detector based on measuring charge decay time improves the sensitivity significantly by noise reduction inherent to this technique and by using data averaging. The response characteristics of PDs to varying light intensity were compared to those of LEDs. It has to be stressed that it is *the sensitivity to a change in light intensity* that is important to an intensity-based optical detector. On the other hand, the detector has to offer sufficient sensitivity to low light intensity to detect high concentration of light absorbing species.

Five commercially available photodiodes were used in the circuitry replacing LEDs for light measurement. Fig. 6 shows that similar linear plots to those shown in Fig. 5 were generated by PDs, which suggests that LEDs and PDs are interchangeable in this mode of light measurement. However, it can be seen by comparing Figs. 5 and 6 that photodiodes are (approximately 10 times) more efficient in producing photocurrent and therefore, discharged at a much faster rate than their LED counterparts. However, the lower photocurrent producing efficiency by LEDs turns out to be an advantage in this particular mode of operation. It can be clearly seen that the slopes of response to light intensity by LED detectors are approximately an order of magnitude higher than those obtained by PDs (the range of slopes observed for PDs are ca. $0.3–3 \times 10^2$ μs/unit, whereas for LEDs the observed values are ca. $0.3–5 \times 10^3$ μs/unit). The inset in Fig. 6 compares the responses from an LED detector and a PD in situation when the light source band gap overlaps with that of the detectors. In this case, the slope obtained for LED detector was 274.5 μs/unit, which was eight times higher than that obtained with a PD (34.9 μs/unit). These data have shown that this technique has reversed the order of sensitivity observed by the conventional method that measures directly photocurrent and that LED detectors operated in this proposed technique are superior to PDs.

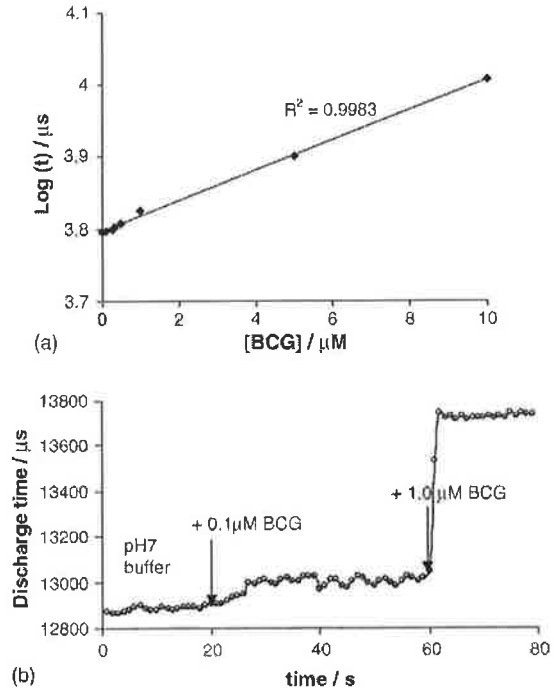

Fig. 7. (a) A plot of LED sensor discharge time (log t) vs. BCG dye concentration ($n=3$ and R.S.D. < 0.1%). (b) The real time response of the system to additions of BCG at low concentrations.

4.5. Colour measurement with paired LED sensor system

Using the optical cell described in Fig. 2, the effectiveness of a paired LED emitter–sensor for photometric measurements was investigated. Various concentrations of bromocresol green solutions made up in pH 7 buffer were placed into the optical cell and the transmitted light intensity measured by the LED detector (emitter λ_{max} = detector λ_{max} = 610 nm) which overlaps strongly with the absorbance spectrum of the dye. The log of the discharge times (log t) obtained were plotted against dye concentration (c) (Eq. (5)), and a straight line with R^2 value of 0.998 was obtained (Fig. 7a). The lowest dye concentration detected was 0.1 μM as shown in Fig. 7b. This real time response trace showed that the discharge time (response obtained) for the baseline was 12,884 ± 10.9 μs for $n=20$ data points, whereas the response obtained for 0.1 μM BCG was, for $n=20$, 13,004.8 ± 17.5 μs, which just exceeded the threshold value of 12,985 μs calculated from [baseline + 3 standard deviation]. These results demonstrate that, even without significant optimisation, the system can be used for analytical measurements with excellent precision and sensitivity (to sub-micromolar levels), and that the mathematical model described by Eq. (5) is obeyed. Furthermore, the sensor response is very rapid, reaching equilibrium in around 4 s to an addition of 1 μM BCG (Fig. 7b).

We also used the same LED combination to determine Iron II in water using 1,10-phenathroline as the complexing agent to form a red coloured complex (λ_{max} = 610 nm). Once again, a very precise linear relationship between the log of the discharge time (t) and concentration of the absorbing species is obtained (Fig. 8), with a linear range up to around 300 μM and a detection limit of ca. 5 μM.

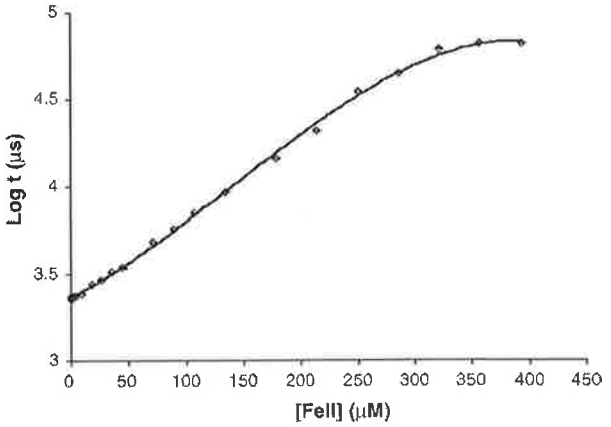

Fig. 8. Calibration plot for 1,10-phenanthroline–Iron II complex detection using paired LED sensor system ($n=3$).

5. Conclusion

These results demonstrate that this very low-cost emitter–detector LED arrangement and timer circuit can be used to make very sensitive analytical measurements. Excellent signal-to-noise characteristics are obtained because of the signal integration during measurements. The circuit provides a digital output, and the sensitivity can be tuned using a variable load resistor on the emitter LED to vary incident light intensity. The entire system can be integrated into a small, inexpensive, low-power package for analytical applications. The diodes can be arranged to make transmission measurements (as in this paper) or for reflectance measurements. This latter arrangement is very useful for monitoring changes in the colour of chromo-responsive dyes immobilised on surfaces (e.g. diagnostic tests and smart packaging) or to monitor colour in flow or microfluidic systems. In addition, one or both diodes can be coated with coloured reagents to provide an inherent chemical sensing function, and an array of devices with differing λ_{max} used cooperatively to generate complementary information for simultaneous multicomponent assays.

Furthermore, LEDs can be used to send/receive data over distances of up to 1 m [19], and the LEDs themselves can indicate status visually over relatively long distances using digital cameras as monitors. Hence, the platform also has the potential to store and transmit data on demand to an external device. Coupled with a longer range (but low-cost and low-power) wireless communication capability, this device, in its various configurations, has the capability of becoming a fundamental building block (or chemical sensing node) for wireless sensor networks.

Acknowledgement

The authors wish to thank Science Foundation Ireland SFI for grant support under the Adaptive Information Cluster Award (SFI 03/IN3/1361).

References

[1] M. Kochhal, L. Schwiebert, S. Gupta, J. Sci. Eng. Comput. 20 (2004) 449–475.
[2] V. Mehta, M. El Zarki, Wireless Networks 10 (2004) 401–412.
[3] R.A.F. Mini, A.A.F. Loureiro, B. Nath, Comput. Commun. 27 (2004) 935–945.
[4] X.P. Yang, K.G. Ong, W.R. Dreschel, K.F. Zeng, C.S. Mungle, C.A. Grimes, Sensors 2 (2002) 455–472.
[5] C.A. Grimes, K.G. Ong, O.K. Varghese, X.P. Yang, G. Mor, M. Paulose, E.C. Dickey, C.M. Ruan, M.V. Pishko, J.W. Kendig, A.J. Mason, Sensors 3 (2003) 69–82.
[6] D. Diamond, Anal. Chem. 75 (15) (2004) 278A–286A.
[7] A. Bowden, D. Diamond, Sens. Actuators B 90 (2003) 170–174.
[8] K.T. Lau, S. Baldwin, R.L. Shepherd, P.H. Dietz, W.S. Yerazunis, D. Diamond, Talanta 63 (2004) 167–173.
[9] B. Mizaikoff, Water Sci. Technol. 47 (2003) 35–42.
[10] I.U. Primak, L.I. Sotskaya, Opt. Quantum Electron. 35 (2003) 275–287.
[11] I. Okura, J. Porphyrins Phthalocyanines 6 (2002) 268–270.
[12] T.A. Canada, L.R. Allain, D.B. Beach, Z.L. Xue, Anal. Chem. 74 (2002) 2535–2540.
[13] L.M. Lechuga, Quim. Anal. 19 (Suppl. 1) (2000) 61–67.
[14] A.K. Ghosh, N.S. Bedi, P. Paul, Opt. Eng. 39 (2000) 1405–1412.
[15] D. Freiner, R.E. Kunz, D. Citterio, U.E. Spichiger, M.T. Gale, Sens. Actuators B 29 (1995) 277–285.
[16] F.A.A. Matias, M.M.D.C. Vila, M. Tubino, Sens. Actuators B 88 (2003) 60.
[17] F.M. Mims, Appl. Opt. 31 (33) (1992) 6965–6967.
[18] F.M. Mims, Sci. Am. 263 (2) (1990) 106–109.
[19] P. Dietz, W. Yerazunis, D. Leigh, International Conference on Ubiquitous Computing, Ubicomp, October 2003 (full text can be accessed at http://www.merl.com/publications/TR2003-035/).

Novel integrated paired emitter-detector diode (PEDD) as a miniaturized photometric detector in HPLC

Martina O'Toole, King-Tong Lau, Benjamin Shazmann, Roderick Shepherd, Pavel N. Nesterenko, Brett Paull and Dermot Diamond*

Received 24th February 2006, Accepted 17th May 2006
First published as an Advance Article on the web 20th June 2006
DOI: 10.1039/b602846b

A novel low power, low cost, highly sensitive, miniaturized light emitting diode (LED) based flow detector has been used as optical detector for the detection of sample components in high performance liquid chromatography (HPLC). This colorimetric detector employs two LEDs, one operating in normal mode as a light source and the other is reverse biased to work as a light detector. Instead of measuring the photocurrent directly, a simple timer circuit is used to measure the time taken for the photocurrent generated by the emitter LED (λ_{max} 500 nm) to discharge the detector LED (λ_{max} 621 nm) from 5 V (logic 1) to 1.7 V (logic 0) to give digital output directly without using an A/D converter. Employing a post-column reagent method, a Nucleosil 100-7 column (functionalised with iminodiacetic acid (IDA) groups) was used to separate a mixture of transition metal complexes, manganese(II) and cobalt(II) in 4-(2-pyridylazo)-resorcinol (PAR). All optical measurements were taken by using both the in-built HPLC variable wavelength detector and the proposed paired-emitter-detector-diode (PEDD) optical detector configured in-line for data comparison. The concentration range investigated using the PEDD was found to give a linear response to the Mn(II) and Co(II) PAR complexes. The effects of flow rate and emitter LED light source intensity were investigated. Under optimised conditions the PEDD detector offered a linear range of 0.9–100 μM and LOD of 0.09 μM for Mn–PAR complex. A linear range of 0.2–100 μM and LOD of 0.09 μM for Co–PAR complex was achieved.

1. Introduction

Sensor research is driven by the need to generate a selective response to a particular analyte.[1] Separation prior to detection essentially eliminates the need for highly selective detection for many applications.[2] HPLC as a separation technique offers excellent selectivity through well established combinations of stationary phase and mobile phase and this is often the method of choice for routine lab-based assays.[3] During the last decade there has been a general trend towards the miniaturization of separation techniques. There are significant advantages that include increased chromatographic resolution, reduced sample volume and reduced solvent consumption.[4,5] These characteristics are also essential criteria for making chromatography instrumentation field-deployable. Coupled with wireless communication, miniaturized field deployable LC systems will have an important role in the future realisation of widely distributed environmental monitoring networks.[6]

However, there are considerable challenges associated with the miniaturization of all components including pumps, columns and detectors into fully integrated systems. Significant advances have been made in recent years in the development of innovative fluid handling based on electro-osmotic[7] and micro-pumps[5,8,9] and of short columns.[10] Comparatively fewer advances have been made in optical detection and UV-vis variable wavelength detectors are still the most commonly used detectors in HPLC. They are expensive (>$3500), relatively large (32 × 12 cm), have high power consumption, and are therefore not suitable for field deployment.

Basic components in a chromatographic separation system include the sample introduction port, the separation column, connecting tubing, fluid control systems (pump, valves), and detector. For miniaturized systems, components should ideally be integrated, small, have low reagent consumption, low power and low cost. The work presented here focuses on developing a miniaturized optical detector for HPLC. LEDs provide a convenient source of light illumination in almost the entire visible spectral range[11] and have long been used as light sources[12,13] as they offer the advantages of being inexpensive, small in size (available as surface mount), robust, covering a broad spectral range from UV to near-IR and exhibiting long lifetimes. In sensor research LEDs to date have been primarily used as light sources in optical sensors. Hauser[14–17] has long advocated the advantages of using LEDs and was the first to report the use of a blue LED as a spectrophotometric source coupled with a photodiode as a detector. Photodiodes are one of the most commonly used detectors in optical sensors.[15,18–21] Schmidt *et al.* produced a flow cell detector based on an LED-photodiode configuration for post-column detection of transition metals. This device successfully detected cations such as copper, manganese and cobalt.[21]

In most micro-analytical systems the light source and the photodetector are normally separate units integrated with the

National Centre for Sensor Research, School of Chemical Sciences, Dublin City University, Dublin 9, Ireland.
E-mail: dermot.diamond@dcu.ie; Fax: +353-1-7008002; Tel: +353-1-7005404

microfluidic manifold.[22] We have previously demonstrated the use of the integrated PEDD device for colour and pH measurements in static solution[23,24] and subsequently fabricated a single unit containing light source, fluid channel and detector for colorimetric flow analysis detection.[25] The PEDD was successfully employed for pH monitoring by using bromocresol green and subsequently the determination of its pK_a.[25] The PEDD integrated flow cell detector is highly sensitive, low power and extremely low cost (<$1).

In this paper we present for the first time the use of an integrated PEDD flow cell as a simple, small, highly sensitive, low cost photometric detector for HPLC. Using a post-column colorimetric detection method commonly used for transition metal ions,[26,27] Mn(II) and Co(II) 4-(2-pyridylazo)-resorcinol (PAR) complexes are separated on a miniature Nucleosil 100-7 iminodiacetic acid (IDA) functionalized column.[28] The coloured metal complexes formed by reacting the transition metal ions with a post-column reagent (PCR) mixture containing PAR and ammonia were detected inline by the HPLC variable wavelength detector and the PEDD device. Spectrophotometric detection of metal complexes with PAR is a rapid, sensitive and convenient technique used for quantitative metal analyses.[29]

2. Experimental

2.1. Equipment

A series 1050 Hewlett Packard HPLC system (Agilent Technologies, Dublin) was used to deliver the eluent at a flow rate of 0.7 mL min^{-1}. Samples were injected using an automated injector with a sample loop of 100 μL. A Nucleosil 100-7 column covalently functionalised with IDA groups of 4 × 14 mm in size was used for the ion separation. A Gilson (Miniplus 3) peristaltic pump, (Anachem, UK) at a flow rate setting of 0.38 mL min^{-1} was used for the introduction of the post-column reagent (PCR), which was mixed at room temperature with the eluent using 0.5 m of PEEK reaction coil (0.25 mm id, VICI® AG International, Switzerland). A single channel PEDD flow cell (Emitter λ_{max} 500 nm, Detector λ_{max} 621 nm, Fig. 1) was used inline with the Hewlett Packard (series 1050) UV-vis variable wavelength detector (Agilent Technologies, Dublin) for the detection of the metal complexes.

2.2. Chemicals and reagents

The PCR reagent used for the detection of the transition metal ions consisted of a mixture of 0.4 mM 4-(2-pyridylazo)-resorcinol monosodium salt hydrate (PAR) (Sigma Aldrich, Dublin, Ireland) and 0.5 M ammonia (35%, BDH, Poole, England), which was adjusted to pH 10.5. Manganese chloride tetrahydrate and cobalt(II) nitrate hexahydrate (Sigma Aldrich, Dublin, Ireland) standards were prepared daily from 1 mM stock solutions. The mobile phase, stock solutions and standard solutions were prepared using water from a Millipore Milli-Q water purification system. All samples were filtered through a 0.45 μm filter and degassed by sonication. The mobile phase used was 3 mM nitric acid (70%, East Anglia Chemicals, Suffolk, England).

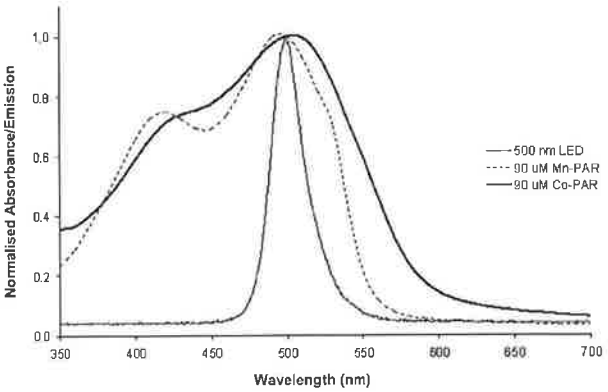

Fig. 1 Emission spectrum (λ_{max} 500 nm) of the emitter LED (solid line) used in the integrated PEDD flow analysis device and the absorption spectrum (λ_{max} 500 nm) of 90 μM Mn–PAR (dashed line) and (λ_{max} 510 nm) 90 μM Co–PAR (bold line).

2.3. Fabrication and operation of integrated PEDD flow cell detector

The integrated detector cell was fabricated as previously described[25] using two 5 mm LEDs (Kingbright, Ireland) as shown in Fig. 2. The detector used was a red LED with a λ_{max} at 621 nm which can detect any wavelength below this point. A green LED with a λ_{max} at 500 nm was used as the emitter.

A 9 V battery was used as the power source to drive the circuitry from which a voltage regulator was used to control the voltage supply to the LEDs. The light detector LED in input mode was charged up to 5 V for 100 μs and then switched to output mode. Then the photon emitted from the green LED hit the red detector LED to generate a small photocurrent to discharge the detector LED. The time taken for the discharge process to go from an initial value of 5 V (logic 1) to a preset value of 1.7 V (logic 0) was measured with a simple timer circuit.[23,25]

2.4. Measurement procedure

Various concentrations of Mn(II) and Co(II) were made up in Milli-Q water and 100 μl aliquots of sample were injected onto the Nucleosil 100-7 column at a flow rate of 0.7 mL min^{-1}.

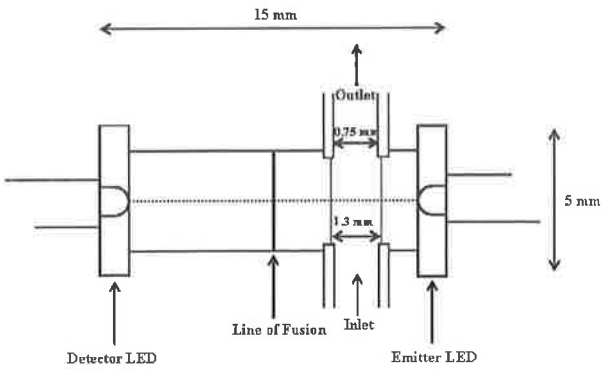

Fig. 2 A schematic of the integrated PEDD flow analysis device used for colorimetric detection.

The analytes were first detected using the UV-vis detector at a wavelength of 500 nm followed directly by the PEDD flow cell. All experiments were carried out in triplicate (n = 3). The chromatograms obtained from the UV-vis variable wavelength detector were analysed using Agilent Chemstation for LC and LC/MS systems software. The data acquired from the PEDD was transported to a PC *via* RS232 port and captured with HyperTerminal software (Microsoft Inc., USA), saved as a text file and then analysed using Excel™ (Microsoft Inc., USA).

3. Results and discussion

3.1. Optimisation of HPLC and PEDD flow cell conditions

Fig. 1 shows that the absorption spectra of manganese(II) and cobalt(II) PAR complexes overlap with the emission spectrum of the PEDD device. The emission spectrum of the green emitter LED was obtained by using an ocean optic spectrometer (OOIBase 32™, Ocean Optics. Inc., Dunedin, USA). The absorbance spectra of manganese(II) and cobalt(II) PAR complexes were acquired using the μQuant™ platewell reader (Bio-Tek Instruments, Inc., USA). The overlap between the absorbing species and the light source provide high sensitivity for the detection of Mn–PAR and Co–PAR.

The data obtained by the PEDD is based on the theoretical model derived by Lau *et al.*[23,24]

$$\log(t) = \varepsilon Cl + \log(t_0) \quad (1)$$

where l is the optical pathlength through the solution (cm), ε the molar extinction coefficient (mol l^{-1} cm^{-1}) at a particular wavelength, C the concentration of the absorbing species (mol l^{-1}), t_0 a constant that represents discharge time in the absence of the coloured species in solution (μs), t is the discharge time of the detector (μs).

Optimisation of HPLC and PEDD parameters such as flow rate and light intensity were carried out. A concentration of 2 μM Mn(II) solution was selected to carry out the study as it provided reproducible responses and good peak size and shape. Optimal separation conditions were determined to be: eluent flow rate of 0.7 mL min^{-1} and peristaltic pump rate setting of 0.38 mL min^{-1}. Previous studies have shown that on decreasing the light intensity of the emitter LED, the change in discharge time (*i.e.* the resolution) can be improved by up to a factor of 4.[25] A (0–10 kΩ) variable resistor was used to determine the optimum light intensity of the green emitter LED to achieve optimum resolution *i.e.* by varying the electrical current applied to the emitter LED. The detector response increases linearly with an increase in electrical resistance at the LED emitter. However, the increase in response was accompanied by an increase in noise and a decrease in baseline stability as shown in Fig. 3. A resistance of 1.5 kΩ was found to provide the optimum light source intensity giving high sensitivity, while maintaining a smooth baseline without drift. These effects are clearly demonstrated in Fig. 3.

For example, at a resistance of 0.005 kΩ, the difference in discharge time (Δt) *i.e.* peak height was 18.33 ± 0.58 μs with an R.S.D. (n = 3) of 3.15%. At an additional applied resistance of 1.5 kΩ the peak height obtained was 142.67 ± 1.15 μs with 0.81% R.S.D. (n = 3). At a resistance of 4 kΩ the peak height achieved was 457.33 ± 13.20 μs with 2.89% R.S.D. (n = 3). Increasing the resistance to 1.5 kΩ improved the change in discharge time by a factor of 8. Further increase in resistance increased the peak height even more, but caused more baseline drift and higher R.S.D. values as shown in Fig. 3.

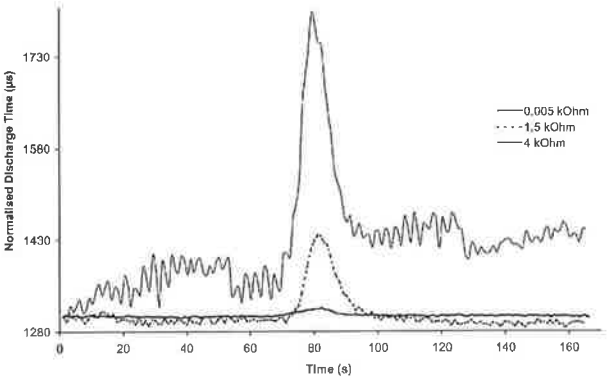

Fig. 3 Real time traces obtained for 2 μM Mn–PAR sample using 3 resistances (0.005 kΩ, bold line, 1.5 kΩ, dashed line and 4 kΩ, solid line). The PCR flow setting used was 0.38 mL min^{-1}.

The optimal PCR delivery rate was determined experimentally. The optimal flow rate was 0.38 mL min^{-1}.

3.2. Separation and detection of manganese(II) and cobalt(II) PAR complexes

To investigate whether the PEDD flow cell caused additional peak broadening a 5 μM mixture of manganese(II) and cobalt(II) was prepared and injected (n = 3). The chromatogram obtained from the UV-vis variable wavelength detector shown in Fig. 4(A) shows two well-resolved peaks (Table 1) with retention times of 1.3 and 2.1 min for manganese(II) and cobalt(II) PAR complexes respectively. The average peak areas calculated for Mn–PAR and Co–PAR had relative standard deviations of 0.29% and 2.71% respectively.

The green light intensity transmitted in the PEDD flow cell efficiently overlaps the absorbance spectrum of PAR complexes with manganese(II) and cobalt(II) as shown in Fig. 1. The PAR complex detection data (discharge time t in μs) was plotted against retention time (min) and presented in Fig. 4(B). As shown in Fig. 4(B) the plot obtained from the PEDD shows identical retention times to that acquired from the UV-vis variable wavelength detector. The mean peak heights (discharge time t in μs) calculated for Mn(II) and Co(II) both had a relative standard deviation of 0.04%. The peak efficiencies calculated for both the UV-vis variable wavelength detector and the PEDD flow device are presented in Table 1. The results obtained show similar peak efficiencies and indicate that the PEDD flow device does not cause additional peak broadening of the sample peaks.

3.3. Calibration using the PEDD flow cell and the UV-vis spectrophotometer

Mixtures containing various concentrations of manganese(II) and cobalt(II) were passed through the HPLC system using the

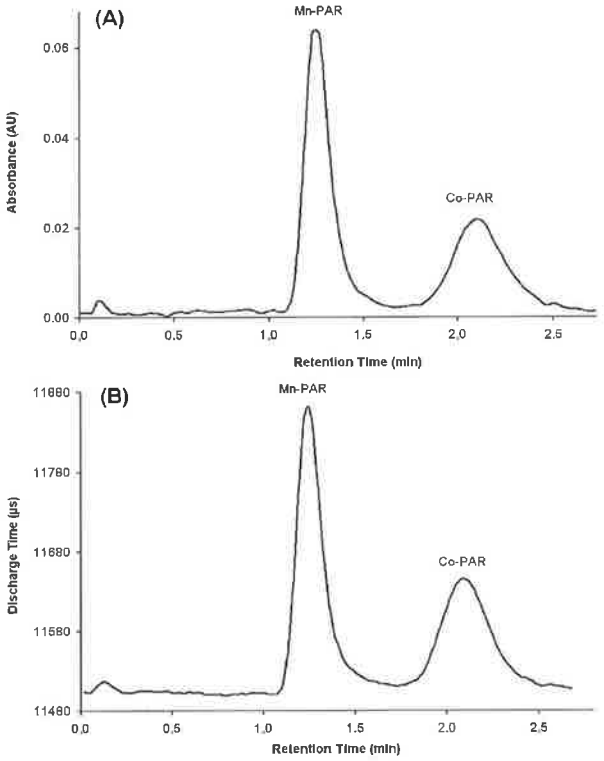

Fig. 4 A comparison of the chromatograms obtained for the detection of 5 μM Mn(II) and Co(II) PAR complexes using the variable wavelength detector (A) and the PEDD flow device (B).

optimal conditions (carrier flow rate of 0.7 mL min^{-1}, PCR flow setting of 0.38 mL min^{-1} and a 1.5 kΩ current limiting resistor on the emitter LED). Each injection was carried out in triplicate (n = 3). Results were acquired simultaneously using a UV-vis variable wavelength detector in-line with the PEDD flow cell.

Table 1 Retention data for transition metal PCR complexes on a Nucleosil 100-7 column (functionalised with IDA), measured by the PEDD detector and the in-built HPLC variable wavelength detector (VWD). The efficiency N was calculated from: $5.54(t_R/W_{½})^2$

	PEDD	VWD
Resolution	2.1	2.0
Mn–PAR efficiency, N	365.7	365.7
Co–PAR efficiency, N	311.6	224.4

Fig. 5 shows results obtained from the PEDD flow cell. The peak heights (log (t/μs)) of each transition metal complex detected were plotted against the input ion concentration (C) in accordance with the model (eqn (1)). A large detection range from 0.09 μM to 500 μM (Fig. 5, inset (A)) with linear ranges of 0.9–100 μM for Mn–PAR (R^2 = 0.997) and 0.2–100 μM for Co–PAR (R^2 = 0.9997) were obtained. An LOD of approximately 0.09 μM was achieved for both Mn–PAR and Co–PAR as shown in Fig. 6. It can be seen from Fig. 5 that the relative standard deviation of the measurements (n = 3, shown as error bars) were very low (<0.08%).

For the data obtained from the UV-vis detector, the peak area was plotted against concentration (C) and the results were presented in Fig. 7 for both manganese and cobalt complexes. A similar detection range from 0.09 μM to 500 μM (Fig. 7, inset (A)) was achieved for Mn–PAR. A detection range of 0.5 μM to 500 μM was obtained for Co–PAR (Fig. 7, inset (A)). The linear ranges obtained were 0.9–100 μM for Mn–PAR (R^2 = 0.9981) and 0.7–100 μM for Co–PAR

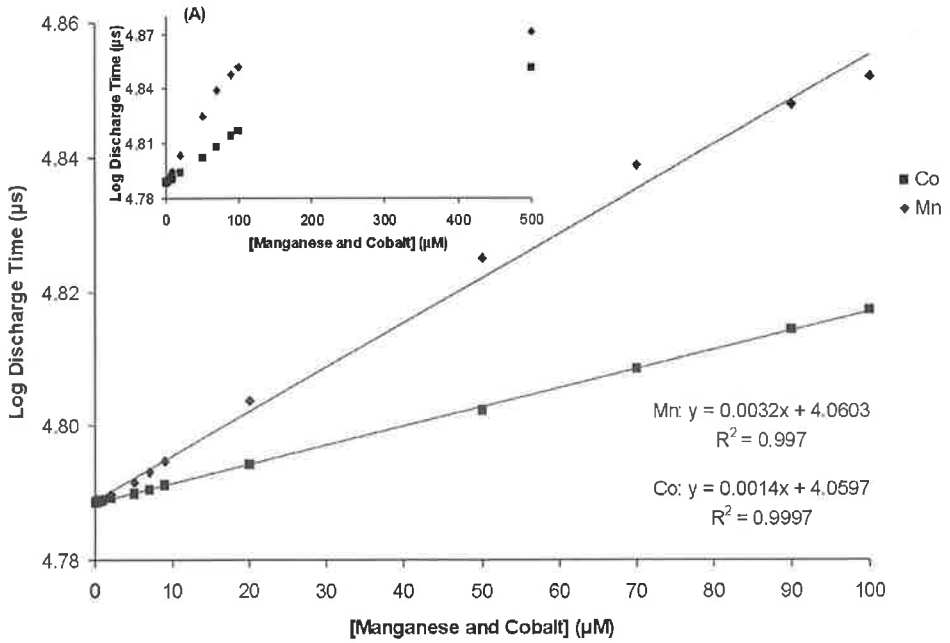

Fig. 5 Log of the discharge times (t) obtained using a PEDD *versus* Mn(II) and Co(II) PAR complex concentration. The error bars represent the standard deviations for n = 3. The inset (A) shows the dynamic range of responses obtained from the calibration.

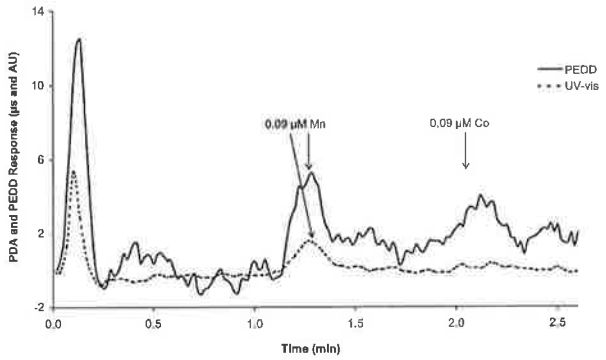

Fig. 6 Real time traces of experimental runs carried out at the LOD concentration of 0.09 µM Mn–PAR and Co–PAR from the PEDD flow device (solid line) and the variable wavelength detector (dashed line).

(R^2 = 0.9997). An LOD of 0.09 µM was obtained for Mn–PAR but a much higher LOD value of 0.7 µM was achieved for Co–PAR (Fig. 6). It can be seen from the inset of Fig. 7 that the relative standard deviations of the measurements (n = 3, shown as error bars) are in the region of 10%.

The simple PEDD flow cell was successful as a post-column detector for the HPLC. The data obtained from this inexpensive, small, power efficient optical detector were comparable to those obtained from the HPLC variable wavelength detector, and sensitivity is significantly higher. For detection of the Mn–PAR complex the PEDD response matched that of a variable wavelength and was six times more sensitive for the detection of the Co–PAR complex. In comparison to the performance of the typical LED-photodiode device employed by Schmidt *et al.* the PEDD achieved similar sensitivity with a path length four times shorter than that of the reported device. This is partly due to the availability of an improved LED light source which more efficiently overlaps with the absorbance of the metal complexes. The improved performance is largely due to the high sensitivity of the PEDD device. A simple PEDD detector cannot replace the existing variable wavelength detector because of the limited bandwidth a single LED can cover, however a more sophisticated PEDD device with multiple LED sources covering a wider range of wavelengths could make this possible. For specific applications where an appropriate operation wavelength can be selected for the analytes a single PEDD flow detector is ideal and preferable to a more complex multi-source detector. This small flow detector when coupled with a miniature low pressure separation column, such as the one used in this work, and a pressure/pumping unit, such as a small gas cylinder, could form a complete miniature HPLC system suitable for rapid small sample analysis. Apart from working as a small bench top analytical device, such a system may also be developed as a field deployable autonomous monitoring device.

4. Conclusions

The results obtained using the integrated PEDD flow analysis cell have demonstrated that this simple, low cost, low power device can be used as a photometric detector in HPLC. Under optimised conditions the PEDD detector offered a linear range of 0.9–100 µM and LOD of 0.09 µM for Mn–PAR complex. A linear range of 0.2–100 µM and LOD of 0.09 µM for Co–PAR complex was achieved. The PEDD flow cell can detect lower concentration levels of Co–PAR than that of an expensive, commercially available bench top instrument. This colorimetric detector represents a significant contribution to the future realisation of field deployable analytical devices based on flow analysis, as it combines high sensitivity with low cost, low power consumption and ease of use.

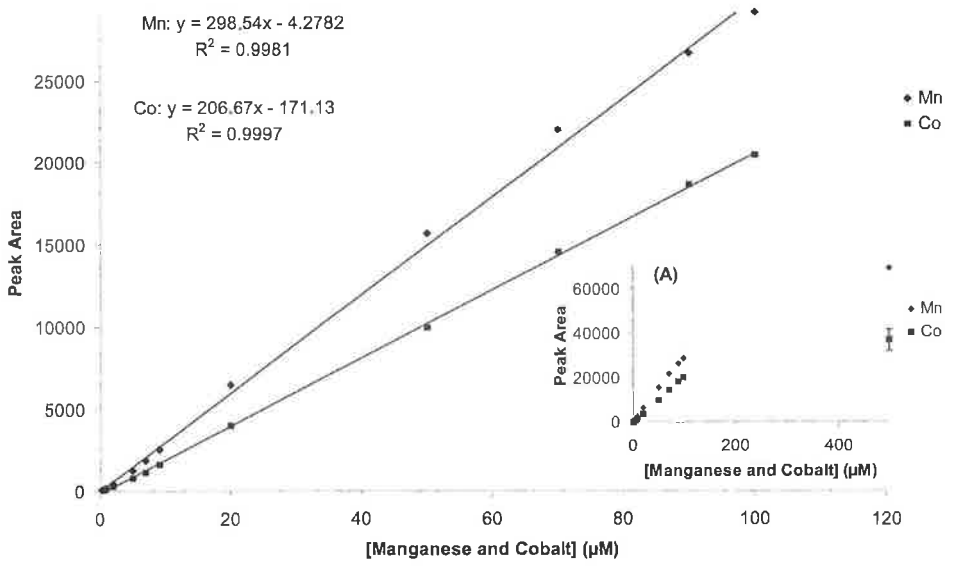

Fig. 7 Absorbance (mAU) *versus* Mn(II) and Co(II) PAR complex concentration for the variable wavelength detector. The error bars represent the standard deviations for n = 3. The inset (A) shows the dynamic range of responses obtained from the calibration.

Acknowledgements

The Authors wish to thank Science Foundation Ireland SFI for grant support under the Adaptive Information Cluster Award (SFI 03/IN3/1361).

References

1 D. Diamond, *Anal. Chem.*, 2004, **76**, 279A–286A.
2 Q. Kang, N.C. Golubovic, N.G. Pinto and H.T. Henderson, *Chem. Eng. Sci.*, 2001, **56**, 3409–3420.
3 K. K. Unger, D. Kumar, M. Grun, G. Buchel, S. Ludtke, T. Adam, K. Schumacher and S. Renker, *J. Chromatogr., A*, 2000, **892**, 47–55.
4 J. Liu, K. J. Volk, M. J. Mata, E. H. Kerns and M. S. Lee, *J. Pharm. Biomed. Anal.*, 1997, **15**, 1729–1739.
5 C. Czerwenka, M. Lammerhofer and W. Lindner, *J. Pharm. Biomed. Anal.*, 2003, **30**, 1789–1800.
6 M. Sequeira, D. Diamond, A. Daridon, J. Lichtenberg, S. Verpoorte and N. F. d. Rooij, *Trends Anal. Chem.*, 2002, **21**, 816–827.
7 P. Wang, Z. Chen and H.-C. Chang, *Sens. Actuators, B*, 2006, **113**, 500–509.
8 F. Kuhn, M. Oehme and M. Schleimer, *J. Chromatogr., A*, 2003, **1018**, 203–212.
9 Y. Shintani, K. Hirako, M. Motokawa, T. Iwano, X. Zhou, Y. Takano, M. Furuno, H. Minakuchi and M. Ueda, *J. Chromatogr., A*, 2005, **1073**, 17–23.
10 D. Connolly, D. Victory and B. Paull, *J. Sep. Sci.*, 2004, **27**, 912–920.
11 A. Zukauskas, M. S. Shur and R. Caska, *Introduction to Solid-State Lighting*, John Wiley & Sons, Inc., New York, 2002.
12 H. Flaschka and R. Barnes, *Microchem. J.*, 1972, **17**, 588–603.
13 H. Flaschka, C. McKeithan and R. Barnes, *Anal. Lett.*, 1973, **6**, 585–594.
14 P. C. Hauser, S. S. Tan, T. J. Cardwell, R. W. Cattrall and I. C. Hamilton, *Analyst*, 1988, **113**, 1551–1555.
15 P. C. Hauser and D. W. L. Chiang, *Talanta*, 1993, **40**, 1193–1200.
16 A. Rainelli, R. Stratz, K. Schweizer and P. C. Hauser, *Talanta*, 2003, **61**, 659–665.
17 P. C. Hauser, T. W. T. Rupasinghe and N. E. Cates, *Talanta*, 1995, **42**, 605–612.
18 P. K. Dasgupta, I.-Y. Eom, K. J. Morris and J. Li, *Anal. Chim. Acta*, 2003, **500**, 337–364.
19 H. Liu and P. K. Dasgupta, *Anal. Chim. Acta*, 1994, **289**, 347–353.
20 P. J. Worsfold, J. Richard Clinch and H. Casey, *Anal. Chim. Acta*, 1987, **197**, 43–50.
21 G. J. Schmidt and R. P. W. Scott, *Analyst*, 1984, **109**, 997–1002.
22 O. Geschke, H. Klank and P. Tellemann, *Microsystem Engineering of Lab-on-a-chip Devices*, WILEY-VCH, Weinheim, 2004.
23 K. T. Lau, S. Baldwin, R. L. Shepherd, P. H. Dietz, W. Yerazunis and D. Diamond, *Talanta*, 2004, **63**, 167–173.
24 K. T. Lau, S. Baldwin, M. O'Toole, R. Shepherd, W. Yerazunis, S. Izuo, S. Ueyama and D. Diamond, *Anal. Chim. Acta*, 2006, **557**, 111–116.
25 M. O'Toole, K. T. Lau and D. Diamond, *Talanta*, 2005, **66**, 1340–1344.
26 E. Sugrue, P. N. Nesterenko and B. Paull, *J. Chromatogr., A*, 2005, **1075**, 167–175.
27 E. Sugrue, P. N. Nesterenko and B. Paull, *Anal. Chim. Acta*, 2005, **553**, 27–35.
28 E. Sugrue, P. N. Nesterenko and B. Paull, *J. Sep. Sci.*, 2004, **27**, 921–930.
29 A. Atanassova, R. Lam and D. B. Zamble, *Anal. Biochem.*, 2004, **335**, 103–111.

Available online at www.sciencedirect.com
ScienceDirect
Analytica Chimica Acta 577 (2006) 32–37
ANALYTICA CHIMICA ACTA
www.elsevier.com/locate/aca

Low pressure ion chromatography with a low cost paired emitter–detector diode based detector for the determination of alkaline earth metals in water samples

Leon Barron, Pavel N. Nesterenko, Dermot Diamond, Martina O'Toole, King Tong Lau, Brett Paull *

National Centre for Sensor Research, School of Chemical Sciences, Dublin City University, Glasnevin, Dublin 9, Ireland

Received 24 April 2006; received in revised form 24 May 2006; accepted 25 May 2006
Available online 18 June 2006

Abstract

The use of a low pressure ion chromatograph based upon short (25 mm × 4.6 mm) surfactant coated monolithic columns and a low cost paired emitter–detector diode (PEDD) based detector, for the determination of alkaline earth metals in aqueous matrices is presented. The system was applied to the separation of magnesium, calcium, strontium and barium in less than 7 min using a 0.15 M KCl mobile phase at pH 3, with post-column reaction detection at 570 nm using *o*-cresolphthalein complexone. A comparison of the performance of the PEDD detector with a standard laboratory absorbance detector is shown, with limits of detection for magnesium and calcium using the low cost PEDD detector equal to 0.16 and 0.23 mg L^{-1}, respectively. Finally, the developed system was used for the determination of calcium and magnesium in a commercial spring water sample.

Keywords: Low pressure ion chromatography; Alkaline earth metals; Post-column reaction; Paired emitter–detector diode detector

1. Introduction

In the field of ion chromatography (IC), there are many important industrial and environmental applications that only require the separation and detection of a small number of ions. In such cases simple low pressure and low cost IC systems can have many useful applications. Recent attempts to develop such low cost, low pressure IC systems have been carried out utilising short modified monolithic columns. For example, Connolly et al. [1] recently used a modified monolithic column in a low pressure IC system based upon the use of peristaltic pumps to replace normal high pressure LC pumps and was able to achieve a separation of five inorganic anions on a short 50 mm × 4.6 mm monolith in 30 min at ~1.5 bar and at 0.2 mL min^{-1}. Victory et al. [2] followed by O'Riordain et al. [3] reduced the above column length to only 10 mm in custom-built low pressure systems and still achieved useful separations of a number of common anions. Most recently, Pelletier and Lucy [4] managed to successfully combine both low pressure and rapid IC separations. Utilising 10 and even 5 mm monolithic columns and careful control of eluent conditions and extra-column band broadening, Pelletier and Lucy [4] have demonstrated the ability to separate five anions in just under 2 min on a 10 mm column at a flow rate of 0.95 mL min^{-1}, delivered with a simple low pressure syringe pump.

Along with reliable low pressure column technology, many other components of a low cost, low pressure IC system require equal attention, not least sensitive low cost detectors. Recent work by Lau et al. [5,6] has described the use of a paired emitter–detector diode (PEDD) device as a flow through detector for photometric analysis, compact and simple in design and comprised of inexpensive components. The PEDD based detector was used within a flow analysis system for determination of bromocresol green (BCG) dye with the final cell design measured approximately 5 mm × 15 mm [7]. Quantitative detection limits for BCG were easily achievable with this design at a demonstrated 5 mg L^{-1} level (8 μM BCG) once an optimised resistance was applied to the emitter LED. Coupled with cir-

* Corresponding author. Tel.: +353 17005060; fax: +353 17005503.
E-mail address: brett.paull@dcu.ie (B. Paull).

0003-2670/$ – see front matter © 2006 Elsevier B.V. All rights reserved.
doi:10.1016/j.aca.2006.05.101

cuitry of approximately 90 mm × 65 mm × 30 mm, this simple detector highlighted that both cost and size could be addressed simultaneously.

The aim of the work presented here was to develop a working portable low cost, low pressure IC system for the determination of alkaline earth metals in aqueous matrices. By utilising simple low pressure pumps together with short monolithic cation exchange columns and a newly designed PEDD based detector incorporating a 574 nm emitter LED, combined with selective post-column reaction detection using *o*-cresolphthalein complexone, the separation and detection of low mg L^{-1} concentrations of alkaline earth metals was investigated. The developed portable low cost, low pressure IC system was fully investigated with respect to ruggedness, sensitivity, linearity and the system applied to mineral water samples.

2. Experimental

2.1. Reagents and procedures

All chemicals were of reagent grade and were ordered from Sigma–Aldrich (Gillingham, UK). For cationic analytes, the chloride salts of each of calcium, magnesium, strontium and barium were used and stock solutions were prepared to a concentration of 1000 mg L^{-1}. Working standards were prepared daily from these stocks. A sample of DunCarrig Still Irish Spring Water was obtained from DunCarrig Spring Ltd. (Roxboro, Ireland), stored at 4 °C and was syringe filtered before use. Ultra pure water used for standards, mobile phases and post-column reagents was obtained from a Millipore Milli-Q water purification system (Millipore, Bedford, MA, USA) with a specific resistance of 18.3 MΩ cm or greater. The optimised mobile phase for elution of cationic species was 0.15 M KCl adjusted to pH 3.0 with glacial acetic acid (Sigma–Aldrich). For coating of the analytical column, dioctylsulfosuccinate (DOSS) was used. The post-column reagent consisted of 0.4 mM *o*-cresolphthalein complexone (*o*-CPC), 0.25 M boric acid adjusted to pH 10.5 with a 50% solution of NaOH. All mobile phases and post-column reagents were degassed and filtered before use using 0.45 μm nylon membrane filters from Gelman Laboratories (Ann Arbor, MI, USA).

2.2. Coating of the analytical column

A solution of DOSS was prepared to a concentration of approximately 10 mM in ultra pure water. After priming of one of the milliGAT pumps with this solution for approximately 5 min, a previously acetonitrile-preconditioned 25 mm × 4.6 mm Phenomenex Onyx monolithic column was coated at 0.5 mL min^{-1} for a 4 h period, switching the column orientation every 15 min to allow for complete coating. The column was then washed with Milli-Q water for a further 4–5 h to remove any excess surfactant.

2.3. Low pressure IC components and supplementary instrumentation

The low pressure IC system used is shown schematically as Fig. 1. All separations were carried out on a Phenomenex Onyx 25 mm × 4.6 mm i.d. monolithic RP-C_{18} analytical column (Torrance, CA, USA) coated with DOSS surfactant. Mobile phase and post-column reagent were delivered via two programmable low pressure milliGAT stepper motor pumps from Global FIA Inc. (Fox Island, WA, USA). Each pump was controlled via a MicroLynx-4 integrated micro stepping motor drive ordered from Intelligent Motion Systems (Marlborough, CT,

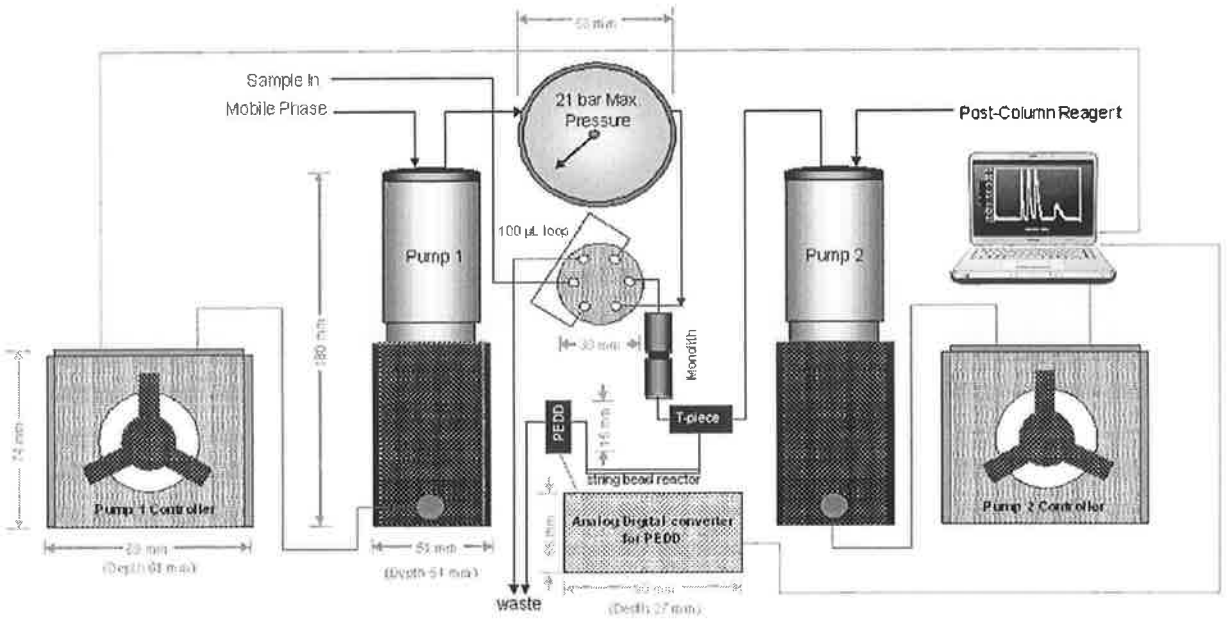

Fig. 1. Low pressure ion chromatograph design and components with dimensions.

USA). Mobile phase from the pump was passed through a pressure gauge from Alltech Associates (Deerfield, IL, USA) before entering an injection valve from Rheodyne LLC (Rohnert Park, CA, USA). Mobile phase and post-column reagent flow rates were each set at 0.5 mL min^{-1}. The injection loop for low pressure separations was 100 μL for increased sensitivity. Addition of post-column reagent was performed via a T-junction connected to a single bead string reactor (Sigma–Aldrich) prior to detection. Tubing prior to the injection valve was of 0.75 mm i.d. PEEK to reduce backpressure and post-injection valve tubing was of 0.10 mm i.d. and was as short as physically possible to maintain chromatographic efficiency. All chromatography was carried out under ambient laboratory temperatures.

Initial detection was achieved using a Waters 486 tuneable absorbance detector (Milford, MA, USA) set to a wavelength of 575 nm. For the final compact low pressure IC system design, a home designed and built paired emitter detector diode (PEDD) was used for detection complete with circuitry and analog-to-digital converter (ADC) similar to that used earlier [7]. Where comparisons of both detectors were performed, the post-column reaction coil was fitted separately to the Waters absorbance detector or the PEDD to fully investigate any band broadening or peak distortions solely due to fabrication of the PEDD. For data acquisition and pump control, a Dell Optiplex GX-320 personal computer was used (Dublin, Ireland) with both Intelligent Motion Systems Terminal pump control software and Pico Log data logging software installed (Pico Technologies Ltd., St. Neots, UK). Simultaneous control of both pumps and data acquisition was performed via a high-speed 4 serial port PCI card (MRi UK Ltd., London, UK) and RS-232 cabling. For digitisation of the output from the Waters absorbance detector, a Pico model ADC-16 analog-to-digital converter was employed. For determination of column coating stability, the freshly coated column was configured into a DX-500 ion chromatograph from Dionex Corporation (Sunnyvale, CA, USA) consisting of a GP50 pump, LC25 chromatography oven and an AD20 UV–vis Absorbance detector configured for the *o*-CPC post-column reaction ($\lambda = 575$ nm). The secondary pump used was a Waters 501 pump. Flow rates were identical to that of the low pressure IC system. Replicate injections were carried out and acquired using PeakNet 6.0 software (Dionex).

2.4. Fabrication and operation of integrated PEDD flow cell detector

The integrated detector cell comprised of two antagonistically oriented 5 mm LEDs from Kingbright (Tapei, Taiwan) with λ_{max} values at 574 and 621 nm corresponding to the emitter and detector, respectively. The design of this cell is shown in Fig. 2. As LEDs are usually manufactured with a curved upper surface, a 0.25 mm section of the tip of each LED was removed and the remaining LED portions sanded with general purpose fine grade sand paper to give smooth, flat bonding surfaces. Using a 1.3 mm drill bit, a hole was drilled through the emitter LED. The two LEDs were then fused together using UV curable epoxy glue (Edmund Scientific: Orland 81 extra fast curing, USA) and placed under UV light (380 nm) for 30 min. The PEDD cell was initially fitted with inlet and outlet green code PEEK tubing and painted with several coats of black paint to reduce stray light effects on analytical signals.

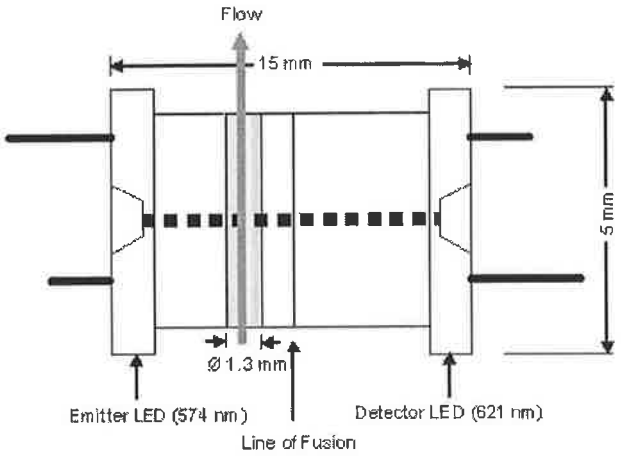

Fig. 2. Schematic of the integrated paired emitter–detector diode device for detection of alkaline earth metals at $\lambda = 574.6$ nm following post column reaction with *o*-CPC.

A 9 V dc mains transformer powered the unit. The light detector LED in input mode was charged up to 5 V for 100 μs and then switched to output mode. The photon emitted from the green LED strikes the red detector LED generating a small photocurrent that discharges the detector LED. The time taken for the discharge process to go from an initial value of 5 V (logic 1) to a preset value of 1.7 V (logic 0) was measured with a simple timer circuit [5,6].

3. Results and discussion

3.1. Practical low pressure column technology—choice of surfactant

The use of DOSS to convert reversed phase monolithic columns into stable cation exchangers has been previously briefly demonstrated by the authors [1]. Here, to fully examine the stability of the DOSS coating, 240 replicate injections of a 10 mg L^{-1} solution of calcium and magnesium were carried out on the DX-500 ion chromatograph using the 0.15 M KCl mobile phase (pH 3.0) and retention times recorded (each run duration = 5.5 min, total run time = 22 h). A similar method was employed in previous work for the assessment of a suitable anion exchange coating [8]. It was found that over this period (approximately 1600 column volumes) no discernable loss in retention was observed for either calcium or magnesium on this DOSS coated monolith with retention time R.S.Ds of 1.20 and 1.25% for magnesium and calcium, respectively (see Fig. 3). Resolution of the two cations over the study lay at 2.79 ± 0.19. Peak asymmetries lay at $1.16 \pm 0.14/1.32 \pm 0.09$ and peak widths at baseline level were of the order of 0.37 ± 0.02 min/0.56 ± 0.08 min for magnesium and calcium, respectively.

It was noticed in initial investigations that operating at higher mobile phase flow rates of ~2–3 mL min^{-1} seemed to induce a

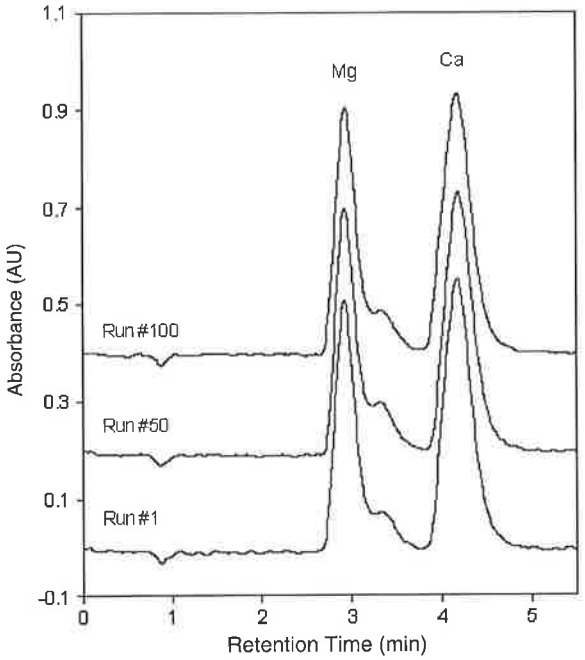

Fig. 3. Overlay of 1st, 50th and 100th runs during stability study of DOSS coated monolith.

continuing rise in column backpressure above a maximum limit for low pressure IC after a few working days (taken as 7 bar, as per MilliGAT pump maximum backpressure specifications). However, it was found that at sub-mL min^{-1} flow rates, using the KCl mobile phase, little or no such effect was observed and the monolith lifetime was considerably extended. Therefore, over the subsequent 1-month method development period, flow rates of 0.5 mL min^{-1} were maintained, with no subsequent noticeable rise in column backpressures. It was found that the 25 mm modified monolith generated backpressures of approximately 2 bar under these conditions. Consequently, overall system backpressure was approximately 5 bar, which included the pressure gauge itself, the injector, column, post-column reaction coil, detector and all PEEK tubing connections and loops. Longer 50 or 100 mm coated monoliths may have improved selectivity but would have increased system backpressure. However, selectivity for the alkaline earth metals on the 25 mm monolith was deemed satisfactory.

3.2. Low pressure IC of alkaline earth metals and detector performance

The well established and highly selective post-column reagent, *o*-cresolphthalein complexone has been shown to be particularly sensitive for calcium and magnesium and to a lesser extent strontium and barium [9,10]. No post-column reaction coil heater was required, limiting system cost and size. Initial investigations used the standard bench-top Waters tuneable absorbance detector. Complete separation of a standard of 3 mg L^{-1} magnesium and calcium, 20 mg L^{-1} strontium and 40 mg L^{-1} barium in Milli-Q water was achieved using the developed system and the Waters UV–vis detector (Fig. 4(a)). This standard was then sequentially diluted 1/10 and 1/100 to give a signal-to-noise ratio of approximately 3:1 and detection limits were calculated in order to compare later with PEDD performance.

To select the appropriate emitter LED for the PEDD detector, a solution of the post-column reagent was taken and spiked with incrementing amounts of both calcium and magnesium (5, 10 and 15 mg L^{-1} of both). The absorption spectra of the resulting mixtures were then obtained, showing $\lambda_{max} = 573 \pm 2$ nm for the metal complex, $n = 3$ scans. Therefore, a green LED (λ_{max} measured at 575 nm; bandwidth = approximately 50 nm) was utilised within the PEDD detector. Fig. 5 represents an overlay of the PEDD emitter LED emission spectrum, the absorption spectra of the post-column reagent only and a 5 mg L^{-1} solution of calcium and magnesium mixed with post-column reagent. It is clear that the emission spectrum λ_{max} of the overlapped satisfactorily with the absorption maxima of the metal complex.

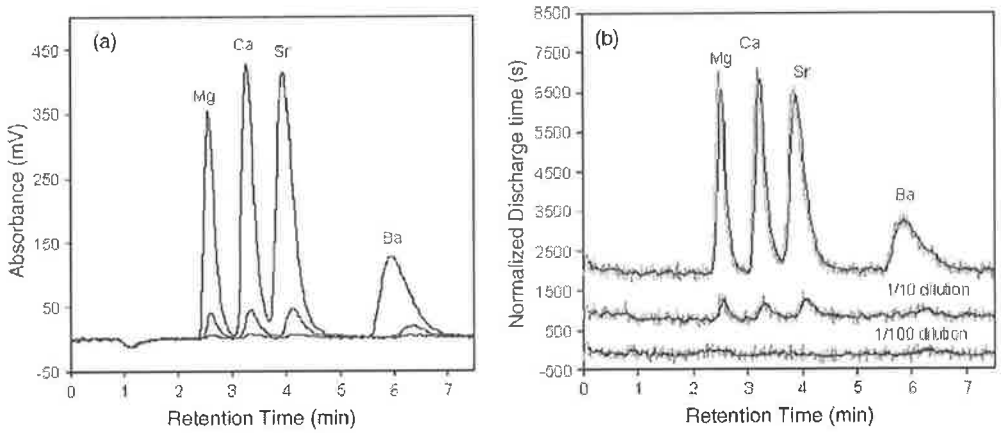

Fig. 4. LPIC of 3 mg L^{-1} magnesium and calcium, 20 mg L^{-1} strontium and 40 mg L^{-1} barium overlaid with 1/10 and 1/100 dilutions using (a) Waters tuneable absorbance detector and (b) using PEDD device as the detection mode. Signals in (b) offset by +1000 μs each for clarity. Grey trace = unsmoothed signal from PEDD. Black trace = 10-point moving average smoothing algorithm to demonstrate any loss in sensitivity or peak shape distortion. System backpressure = ~5 bar (using either detector); column backpressure = ~2 bar.

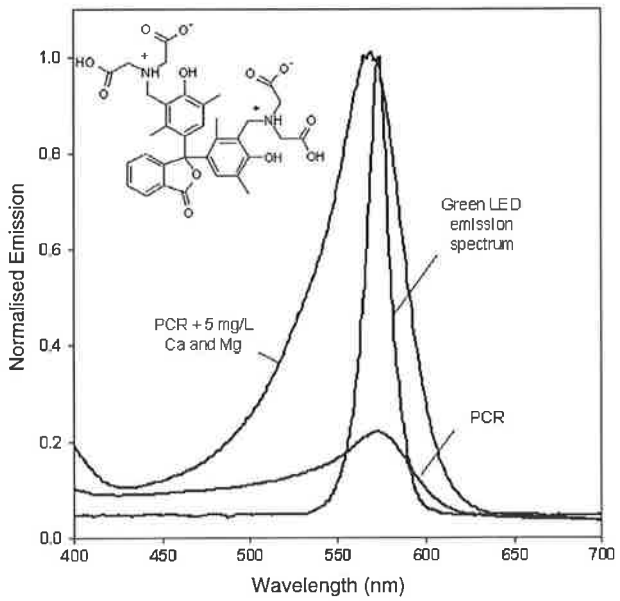

Fig. 5. Overlay of PEDD emitter LED (measured at $\lambda = 574.6$ nm) emission spectrum and absorption spectrum for post-column reagent only followed by a 5 mg L^{-1} solution of magnesium and calcium mixed with post-column reagent. Inset: structure of *o*-cresolphthalein complexone.

In order to directly compare the performance of the PEDD detector to the standard Waters UV–vis absorbance detector, for both peak shape and sensitivity, the same standard solutions injected with the Waters detector above were run once more, this time using the PEDD device. It was found initially that the PEDD suffered from excessive noise and drift to the extent that peaks were barely visible at that level. It was found in previous work [5–7] that application of an optimised resistance to the emitter LED dramatically improved detection limits and was specific to each PEDD device. When a variable resistor was configured in such a way, it was found that maximum sensitivity was achieved with an applied resistance of 1.6 kΩ. Maximising sensitivity for lower concentrations of analytes in this way also caused the upper saturation limit of the detector to decrease. However, this upper limit could be raised by allowing sufficiently more time for the detector LED to discharge at higher analyte concentrations within the timer circuitry settings, albeit resulting in a lower sampling frequency. It was found that by increasing the resistance applied to the emitter from 0 to 1.6 kΩ, that approximately a three-fold improvement in sensitivity was observed in all cases with little or no change in baseline noise intensity.

The data point sampling rate consisted of an average of 16 data points every 0.53 s and noise was of considerably higher frequency in comparison to analyte peak widths. Hence, in an attempt to improve sensitivity of the PEDD device, a moving average smoothing algorithm was applied. Examining the effect of 5- 10- 15 and 20-point moving average algorithms highlighted that sensitivity was in fact reduced at the higher 15- and 20-point averaging levels with a larger distortion in peak shape. An optimised 10-point moving average smoothing algorithm was chosen and resulted in no significant truncation to peak heights compared to the unsmoothed trace, whilst improving signal to noise by a factor of ~2. The application of a 10-point smoothing algorithm is represented in Fig. 4(b) (for the same standard solutions shown in Fig. 4(a)), together with the unsmoothed traces shown underlying in grey. Detection limits for this investigation are represented in Table 1 for both unsmoothed UV and PEDD signals, as well as the 10-point moving average smoothed signal for comparison. Direct comparison of the two detector responses shows the simple PEDD design reduced extra column band broadening, with peak efficiencies improving on average by a factor of 1.4 and resolution of the four metal ions consequently being enhanced.

Clearly, detection limits for the PEDD device were not as sensitive as the standard absorbance instrumentation and differed in sensitivity by an order of magnitude. Future work is required to improve circuitry and cell design to reduce noise levels.

3.3. Analytical performance data

To complete a full analytical performance investigation, further quantities of linearity, range and inter-day repeatability were examined. For linearity, a series of standards were prepared from 1 to 50 mg L^{-1} calcium and magnesium and 10–100 mg L^{-1} strontium and barium ($n = 15$, replicates = 3). It was found that correlation coefficients with respect to peak height of $R^2 > 0.994$ were achieved over a concentration range of 1–10 mg L^{-1}

Table 1
Analytical performance data for low pressure IC for the determination of alkaline earth metals

Analyte	Linearity			Range[a] (mg L^{-1})	PEDD LOD[b] (mg L^{-1})	Waters 486 LOD (μg L^{-1})	N Waters 486/PEDD[c] (plates.m^{-1})	R_s Waters 486/PEDD[c]	Intraday retention time repeatability (R.S.D. %)[d]	Interday retention time repeatability (R.S.D. %)[e]
	R^2	Slope (μs L mg^{-1})	Intercept (μs)							
Magnesium	0.9950	1795	−396	1–10 ($n = 10$)	0.16/0.38	24	29,180/45,190	3.0/3.8	0.2	1.6
Calcium	0.9940	1816	−329	1–15 ($n = 10$)	0.23/0.39	19	35,695/52,235	2.1/2.5	0.8	0.4
Strontium	0.9876	203	1471	10–80 ($n = 8$)	1.36/2.50	206	30,725/41,820	3.9/4.6	0.7	0.5
Barium	0.9885	33	210	20–80 ($n = 7$)	14.1/23.4	469	17,285/23,528	–	0.3	0.1

[a] Based on $n = 15$ standards from 1 to 50 mg L^{-1} magnesium and calcium and 10–100 mg L^{-1} strontium and barium. Values in parenthesis represent the number of standards from $n = 15$ data points that contributed to both the range and the correlation coefficient (R^2) quoted.

[b] Left = 10-point moving average smoothing applied/right, unsmoothed.

[c] Based on a separation of 3 mg L^{-1} of Mg/Ca; 20 mg L^{-1} Sr and 40 mg L^{-1} Ba, where $N = 5.54(t_r/W)^2$ or $R_s = 2(t_{r2}\text{-}t_{r1})/(W_1 + W_2)$.

[d] Based on $n = 6$ replicate injections of a standard of 10 mg L^{-1} magnesium and calcium and 50 mg L^{-1} strontium and barium.

[e] Compared to average intraday retention time repeatability for $n = 2$ replicates for $n + 1$ day.

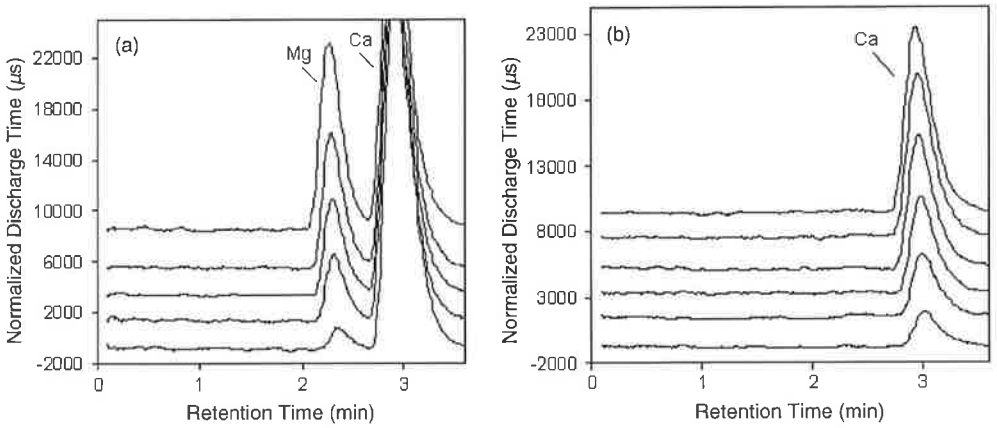

Fig. 6. Chromatograms from standard addition calibration of: (a) a 1/10 dilution of a commercial spring water sample spiked with 4, 6, 8, 10 and 12 mg L^{-1} magnesium and (b) a 1/100 dilution of same sample spiked with 2, 4, 6, 8 and 10 mg L^{-1} calcium. Concentrations = 223 ± 6.9 mg L^{-1} calcium and 14 ± 0.4 mg L^{-1} magnesium. Chromatograms smoothed with a 10-point moving average algorithm and offset by 2000 μs for clarity.

magnesium ($n = 10$) and 1–15 mg L^{-1} calcium ($n = 10$) and $R^2 > 0.988$ for strontium ($n = 8$, range = 10–80 mg L^{-1}) and barium ($n = 7$, range = 20–80 mg L^{-1}) in ultra pure water. Above the ranges quoted for each alkaline earth metal, the mole-mole ratio of the post-column reagent was exceeded or the detector reached saturation point.

The system was then examined for inter-day retention time repeatability. Since >400 injections were performed on this column over a period of approximately 4 weeks, retention times for alkaline earths did show some loss in retention while still remaining resolved. A standard of 10 mg L^{-1} calcium and magnesium and 50 mg L^{-1} strontium and barium was injected and retention times for $n = 6$ replicates on the first day varied by less than 0.8%. Duplicate runs of the same standard on the following day showed an R.S.D. of 1.6% for magnesium (an increase in retention of 0.03 min), but all other analytes showed R.S.D. % < 0.6% compared to the previous day's mean retention time. Linearity, range, limits of detection and repeatability data are summarised in Table 1.

3.4. Application to the determination of alkaline earths in commercial spring water

The developed low pressure IC system was applied to the determination of alkaline earth metals in a commercial mineral water sample. The ionic composition listed on the sample bottle highlighted that the spring water contained no strontium or barium present at mg L^{-1} levels in the sample, but that calcium and magnesium were typically present at 129 and 10 mg L^{-1}, respectively. The sample was filtered and diluted 1/10 and 1/100. Along with a filtered direct injection of sample, a 100 μL volume of each dilution was injected onto the low pressure IC under optimised conditions. The direct injection of sample showed no detectable strontium or barium as defined by the manufacturer. Calcium and magnesium were present in quantifiable amounts and following standard addition calibration ($n = 6$, replicates = 3) it was found that 223 ± 7 mg L^{-1} calcium and 14.2 ± 0.4 mg L^{-1} magnesium were present in the sample. Correlation coefficients for the spiked standard addition curves were both excellent at $R^2 = 0.9912$ and $R^2 = 0.9950$ for magnesium and calcium, respectively. Fig. 6 shows the chromatograms for diluted spring water samples overlaid with spiked samples.

4. Conclusions

A new low cost, portable, low pressure ion chromatograph has been successfully developed here for the determination of alkaline earth metals in aqueous matrices using post-column reaction with *o*-CPC. Although sensitivity is still an issue, future work shows promise with improved detector circuitry. Linearity for all analytes was of $R^2 > 0.98$ and repeatability studies show acceptable stability of the column coating over a 22 h continuous running period. Furthermore the low pressure IC was shown to be suited for quantitative measurements of alkaline earth metals in spring water.

Acknowledgements

The authors wish to thank Enterprise Ireland and Science Foundation Ireland (SFI 03/IN3/1631) for provision of the necessary funding to carry out this project.

References

[1] D. Connolly, D. Victory, B. Paull, J. Sep. Sci. 27 (2004) 912.
[2] D. Victory, P. Nesterenko, B. Paull, Analyst 129 (2004) 700.
[3] Colman O'Riordain, Pavel Nesterenko, Brett Paull, Chem. Commun. (2005) 215–217.
[4] S. Pelletier, C.A. Lucy, J. Chromatogr. A 1118 (2006) 12–18.
[5] K.T. Lau, S. Baldwin, R.L. Shepherd, P.H. Dietz, W.S. Yerzunis, D. Diamond, Talanta 63 (2004) 167.
[6] K.-T. Lau, S. Baldwin, M. O'Toole, R. Shepherd, W.J. Yerazunis, S. Izuo, S. Ueyama, D. Diamond, Anal. Chim. Acta 557 (2006) 111.
[7] M. O' Toole, K.T. Lau, D. Diamond, Talanta 66 (2005) 1340.
[8] C. O'Riordain, L. Barron, E. Nesterenko, P.N. Nesterenko, B. Paull, J. Chromatogr. A 1109 (2006) 111.
[9] J. Stern, W.H.P. Lewis, Clin. Chim. Acta 2 (1957) 576.
[10] B. Paull, M. Macka, P.R. Haddad, J. Chromatogr. A 789 (1997) 329.

Available online at www.sciencedirect.com
ScienceDirect
Analytica Chimica Acta 597 (2007) 290–294
ANALYTICA CHIMICA ACTA
www.elsevier.com/locate/aca

Determination of phosphate using a highly sensitive paired emitter–detector diode photometric flow detector

Martina O'Toole, King Tong Lau, Roderick Shepherd, Conor Slater, Dermot Diamond *

Adaptive Sensors Group, National Centre for Sensor Research, School of Chemical Sciences, Dublin City University, Dublin 9, Ireland

Received 28 May 2007; received in revised form 20 June 2007; accepted 22 June 2007
Available online 27 June 2007

Abstract

The use of a novel inexpensive photometric device, a paired emitter–detector diode (PEDD) has been applied to the colorimetric determination of phosphate using the malachite green spectrophotometric method. The novel miniaturized flow detector applied within this manifold is a highly sensitive, low cost, miniaturized light emitting diode (LED) based detector. The optical flow cell was constructed from two LEDs, whereby one is the light source and the second is the light detector, with the LED light source forward biased and the LED detector reversed biased. The photocurrent generated by the LED light source discharges the junction capacitance of the detector diode from 5 V (logic 1) to 1.7 V (logic 0) and the time taken for this process to occur is measured using a simple timer circuit.

The malachite green (MG) method employed for phosphate determination is based on the formation of a green molybdophosphoric acid complex, the intensity of which is directly related to phosphate concentration. Optimum analytical parameters such as reaction kinetics, reagent to sample concentration ratio and emitter wavelength intensity were investigated for the spectrophotometric method. Linear calibration plots that obeyed the Beer–Lambert law were obtained for phosphate in the range of 0.02–2 μM. The dynamic range, sensitivity and limits of detection are reported.

Keywords: Light emitting diode detector; Malachite green; Phosphate; Colorimetric flow analysis

1. Introduction

Phosphorus, specifically orthophosphate, is an essential nutrient used by plants and animals for growth and energy transport [1]. However elevated concentrations in aquatic ecosystems cause the phenomenon of eutrophication, which can result in algal bloom formation [2]. The rapid growth of aquatic vegetation in turn causes the death and decay of vegetation and aquatic life due to the decrease in dissolved oxygen levels. The resulting eutrophication of natural waters is a subject of utmost concern, and has been recognized by the European Union through legislation that stipulates 0.1 mg L^{-1} PO_4 as an indicator level for possible problematic algal growth in rivers [3].

Spectrophotometric procedures for monitoring orthophosphate include the molybdenum blue method [1,3–7], the yellow vanadomolybdate complex method [8–11] and the malachite green method [12–17]. The malachite green method has been shown to enhance sensitivity by approximately four times when compared to the aforementioned methods [12,18]. A significant advantage of the malachite green method is its lack of sensitivity to experimental conditions such as changes in temperature reagent addition sequence or reaction time [12,19]. Additional advantages include higher sensitivity compared to the molybdenum blue method and the longer optimum detection wavelength than the yellow method [20]. The malachite green method is based on the reaction at low pH between ammonium molybdate, polyvinyl alcohol (PVA) and malachite green (MG) as in the following equations [20]:

$$\underset{\text{(yellow)}}{H_3PMo_{12}O_{40}} + \underset{\text{(yellow, }\lambda_{max}\text{ 446 nm)}}{HMG^{2+}} \rightarrow \underset{\text{(green, }\lambda_{max}\text{ 640 nm)}}{(MG^{+})(H_2PMo_{12}O_{40}^{-})} + 2H^{+} \quad (1)$$

$$(MG^{+})(H_2PMo_{12}O_{40}^{-}) + HMG^{2+} \rightarrow (MG^{+})_2(HPMo_{12}O_{40}{}^{2-}) + 2H^{+} \quad (2)$$

$$(MG^{+})_2(HPMo_{12}O_{40}^{-}) + HMG^{2+} \rightarrow (MG^{+})_3(PMo_{12}O_{40}{}^{3-}) + 2H^{+} \quad (3)$$

* Corresponding author. Tel.: +353 1 7005404; fax: +353 1 7008002.
E-mail address: dermot.diamond@dcu.ie (D. Diamond).

0003-2670/$ – see front matter © 2007 Elsevier B.V. All rights reserved.
doi:10.1016/j.aca.2007.06.048

In the presence of large excess of MG, the reactions (1–3) can occur, and the 3:1 ion associate formed in Eq. (3) can easily precipitate in the acidic aqueous solution. To prevent the formation of the ion association reactions shown in Eqs. (2) and (3), and to stabilize the ion associate in the aqueous solution PVA is added to the solution [14,20].

The optical detection employed in this research to determine phosphates via the malachite green method is a novel, highly sensitive, low cost paired emitter–detector diode (PEDD) photometric detector. The PEDD flow cell consists of two LEDs, whereby one is the light source and the second is the light detector. The LED light source is forward biased while the LED detector is reversed biased. The photon flux from the emitter LED strikes the detector LED, generating a small photocurrent (of the order of nanoampere) that discharges the capacitor voltage over time. The photocurrent produced is not measured directly as this would require an expensive nanoamperometer. Instead, the parameter monitored is the decay time (μs) taken for the discharge process to go from an initial value of 5 V (logic 1) to a preset value of 1.7 V (logic 0) using a simple timer circuit, and a comparator which determines whether the remaining charge is above or below the set point (+1.7 V). The use of LEDs offer advantages such as low cost, compact form, availability across a broad spectral range from UV to near-IR, robust and long lifetimes [21–23]. In most microanalytical systems the light source and the photodetector are normally separate units integrated with the microfluidic manifold [24], however in this case the PEDD is a single unit containing light source, fluid channel and detector for flow analysis [25–27].

In this paper we present the detection of phosphates using this novel detector and a comparative study carried out using both a photodetector comprising of an LED as a light source and a photodiode as the detector and a commercially available platewell reader. Optimum conditions such as time allowed for colour formation, reagent to sample ratio and emitter wavelength and intensity were investigated for the spectrophotometric method. The dynamic range, sensitivity, limits of detection and linear range were determined. Under optimised conditions the low cost PEDD detector (~$1) displayed higher sensitivity and improved precision compared to the commonly employed LED-photodiode detector and a commercially available platewell reader. As such it could provide a route to autonomous, very low cost, low power consuming, highly sensitive, field deployable analytical measurements, which would form the basis of widely deployed chemosensor networks [28].

2. Experimental

2.1. Chemicals and reagents

All solutions were prepared from analytical grade chemicals. Deionised water obtained from a Millipore Milli-Q water purification system was used for all analysis. A stock malachite green reagent was prepared by slowly adding 100 mL concentrated sulphuric acid (H_2SO_4, 98%, Fisher Scientific UK Ltd.) to approximately 400 mL of deionised water. The solution was allowed to cool to room temperature before adding 27 g of ammonium molybdate ($(NH_4)_6Mo_7O_{24}{\cdot}7H_2O$, Fluka, Dublin, Ireland). Malachite green oxalate ($C_{25}H_{22}N_2O_4$) (Baltimore Biological Laboratory, Baltimore, MD.) (0.135 g) was then added to the solution and stirred until dissolved. The solution was then made up to 1 L, vacuum filtered (0.45 μm Nylaflo®, VWR International, Meath, Ireland) and stored at 4 °C. A stock solution of 0.1% (w/v) polyvinyl alcohol (PVA) (Sigma–Aldrich, Dublin, Ireland) was prepared by dissolving 5 g in 500 mL. To assist the dissolution process, the solution was heated to near boiling point while being stirred continuously. Both stock solutions were stored in the dark at 4 °C. The colour reagent was prepared daily by mixing equal amounts of each stock reagent. Standard solutions of phosphorus (P) were prepared daily from a stock solution of 1 mM potassium phosphate dibasic (K_2HPO_4, Sigma–Aldrich, Dublin, Ireland). The stock solution was prepared by dissolving 0.0175 g K_2HPO_4 in 100 mL deionised water. A new stock solution was prepared weekly.

2.2. Measurement procedure

The colorimetric reagent (1 mL) was added to the samples (6 mL) and the solution was left to stand for 30 min for colorimetric development. The absorbance of the solution was measured comparatively using the μQuant™ platewell reader (Bio-Tek Instruments, Inc., USA), the LED-photodiode (λ_{max} 636 nm) photodetector and the PEDD flow cell (λ_{max} 636 nm). The colorimetric reagent was prepared daily by mixing equal amounts of the malachite green and PVA reagents.

2.3. Fabrication of PEDD optical flow cell and the LED-photodiode detector

The integrated PEDD cell was fabricated as previously described [25] using two 5 mm LEDs (Kingbright, Ireland) as shown in Fig. 1.

The detector used was a red LED (λ_{max} at 660 nm) which can detect any wavelength below this point. A red LED (λ_{max} at 636 nm) was used as the emitter LED.

The LED-photodiode detector was fabricated similarly to that of the PEDD illustrated in Fig. 1. A red LED (λ_{max} at 636 nm) was used as the emitter LED with a path length of 1.3 mm. The

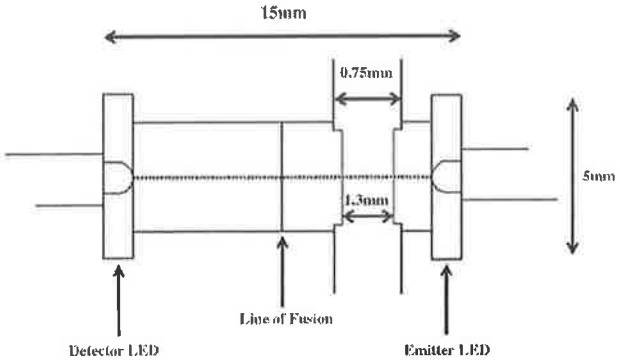

Fig. 1. A schematic of the integrated PEDD flow analysis device used for colorimetric detection.

LED detector was replaced with a Si photodiode, IPL10020BW (Thales Optronics, UK) detector and bonded in the same way as the PEDD.

2.4. Light measurement

A 9 V battery was used as the power source and this was regulated to a stable 5 V using a voltage regulator. The control circuitry used to drive and monitor the PEDD flow detector was operated from the regulated 5 V supply. The light detector LED in output mode was reverse biased at 5 V for 100 μs and then switched to input mode. Photons emitted from the red emitter LED strike the red detector LED to generate a small photocurrent, which in turn discharges the detector LED. The time taken for the discharge process to go from an initial value of 5 V (logic 1) to a preset value of 1.7 V (logic 0) was measured with a simple timer circuit.

The circuitry used to drive the LED photodiode detector is outlined in Fig. S1.

Fig. S1 shows a light emitting diode (D1) illuminating a photodiode (D2) connected to a current to voltage converter. The voltage between V_{out} and GND is then measured by an analogue digital converter on a microcontroller. The current through the LED is adjusted by a potentiometer (R1) thus controlling the illumination. The output current of a photodiode in reverse bias is linearly proportional to the light intensity. To condition the signal for the 10 bit ADC on a PIC16F876 microcontroller a current to voltage converter is employed. A circuit consisting of a FET input operational amplifier (IC1) and a resistor (R2) in feed back was constructed.

In the circuit the output voltage is determined by Eq. (4):

$$V_{out} = -I_p \times R2, \tag{4}$$

where output voltage is V_{out}, I_p is the current through the photodiode and R2 is a 40 MΩ resistor. A capacitor (C1) is not a requirement but was added to reduce noise. Although a circuit with enhanced performance can be constructed, the cost incurred for slight increases in sensitivity by using more precise components and/or higher resolution ADCs would not be justified on a low cost sensor. The reported absorbance (A) measurement was calculated according to Eq. (5):

$$A = -\log\left(\frac{\text{Sample intensity}}{\text{Blank intensity}}\right) \tag{5}$$

where sample intensity is the intensity of the light passing through the cell with sample solution and blank intensity is the intensity of the light passing through the cell with reference solution.

3. Results and discussion

3.1. Absorption spectrum

The measurement is based on the following theoretical model (Eq. (6)), which has been derived by Lau et al. [29].

$$\text{Log}\,(t) = \varepsilon C l + \log\,(t_0) \tag{6}$$

where l is the optical path length through the solution (cm), ε the molar extinction coefficient, C the concentration of the absorbing species (mol L^{-1}), t_0 a constant that represents discharge time in the absence of the coloured species in solution (μs) and t is the discharge time in the presence of the coloured species in solution (μs).

The optimum wavelength to monitor the malachite green–molybdphosphate complex has been variously reported in the literature, typically citing the λ_{max} in the range ca. 600–650 nm [12,13,30]. We therefore determined the λ_{max} under our experimental conditions by obtaining the absorbance spectrum of 0.9 μM PO_4 using the μQuant™ platewell reader (Bio-Tek Instruments, Inc., USA). The λ_{max} of the sample was found to be 640 nm. We therefore selected an emitter LED with a λ_{max} of 636 nm. The light intensity transmitted from the emitter LED (λ_{max} 636 nm) was measured with a detector LED that had a slightly smaller bandgap (λ_{max} 660 nm). The absorbance of the malachite green-molybdphosphate species (λ_{max} 640 nm) as shown in Fig. 2 efficiently overlaps with the emission spectrum of the emitter red LED and will therefore allow high sensitivity. The emission spectrum of the emitter LED was obtained by using Ocean Optics spectrometer (OOIBase 32™, Ocean Optics, Inc., Dunedin, USA).

3.2. Optimisation of standard procedure

The optimum reagent to sample ratio was determined by preparing a range of samples at a concentration of 2 μM PO_4 with varying volumes of reagent (0.1–2 mL) added. The normalized maximum absorbance (R/R_{max}) of each sample was recorded after 40 min and plotted against the volume of reagent added to 6 mL of sample, see Fig. S2.

As shown in Fig. S2 the reagent volume that provides the highest R/R_{max} i.e. the most intense colour was the 6:1 (v/v) sample to reagent ratio (i.e. 6 mL of sample to 1 mL reagent). This was the sample to reagent ratio adopted throughout all remaining experiments.

Previous studies have shown the need to optimise the emitter LED light intensity [25,26], as the change in discharge

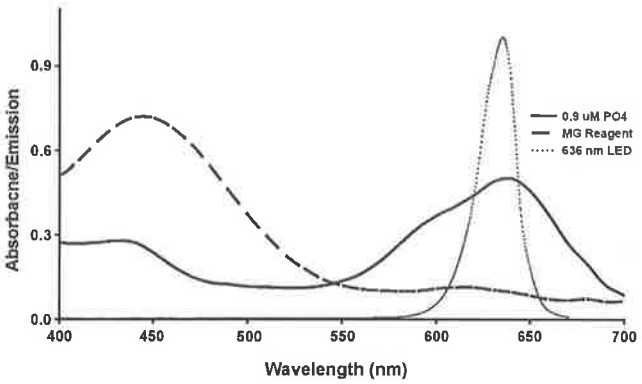

Fig. 2. Emission spectrum (λ_{max} 636 nm) of the emitter LED (dashed line) used in the integrated PEDD flow analysis device, the absorption spectrum (λ_{max} 640 nm) of 0.9 μM PO_4 and MG reagent (solid line) and (λ_{max} 450 nm) MG reagent (bold dashed line).

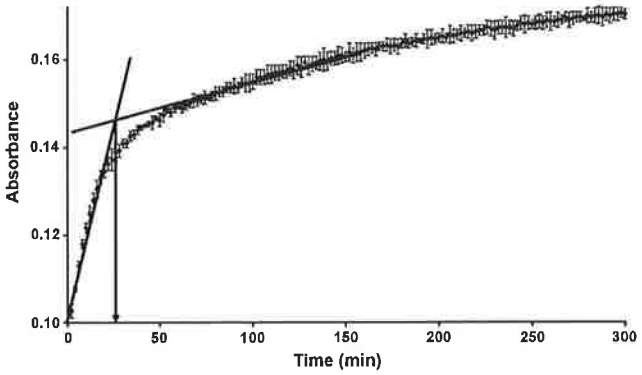

Fig. 3. Kinetic study of the colour formation between 0.5 μM PO_4 and MG reagent ($n = 3$).

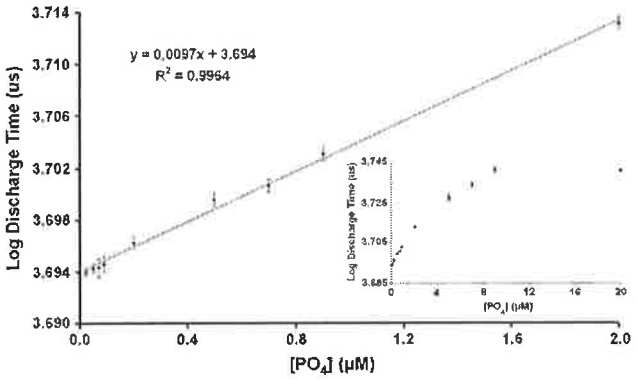

Fig. 4. Log of the discharge times (t) obtained using a PEDD vs. malachite green–molybdphosphate complex concentration. The error bars represent the standard deviations for $n = 3$. The inset shows the dynamic range of responses obtained from the calibration.

time (i.e. the resolution) can be improved by up to a factor of 8. As LEDs vary with regard to their light intensity it was necessary to determine the optimum resistance required for a 636 nm LED. The optimization of the light intensity was carried out as previously described using a (0–10 kΩ) variable resistor [26]. A resistance of 1.58 kΩ was found to provide the optimum light source intensity resulting in high sensitivity, while maintaining a smooth baseline without drift. A 12-pt moving average has been applied to the data shown in Fig. S3. The effects of decreasing the light intensity on the response are clearly demonstrated in Fig. S3. For example, at a resistance of 0.004 kΩ, the difference in discharge time (Δt) i.e. peak height was 4.78 ± 0.19 μs with an R.S.D. ($n = 3$) of 3.90%. At an additional applied resistance of 1.58 kΩ the peak height obtained was 32.59 ± 0.44 μs with 1.35% R.S.D. ($n = 3$). The standard deviation ($n = 3$) of the baseline was 6.95 μs. At a resistance of 6.02 kΩ the peak height achieved was 144.87 ± 0.78 μs with 0.54% R.S.D. ($n = 3$). Increasing the resistance to 6.02 kΩ further improved the change in discharge time but the standard deviation ($n = 3$) of the baseline deteriorated to 29.37 μs.

Further increases in resistance increased the peak height even more, but caused more baseline drift and higher R.S.D. values as shown in Fig. S3. Applying a moving average to the data set can compensate for the increase in baseline noise. An additional disadvantage however of over-increasing the emitter resistance is that the resulting decrease in emitted light intensity can lead to a reduction in the dynamic range.

3.3. Kinetics study

Linge and Oldham [12] reported a stand time for sample and reagent colour development of approximately 30 min. The development of the malachite green–molybdphosphate colour intensity with 0.5 μM PO_4 was monitored using the μQuant™ platewell reader by taking an absorbance measurement every 2 min.

As shown in Fig. 3 the colour formation increased rapidly until approximately 27 min after which the rate of increase decreased to a much slower stage. This was in agreement with the time allowed for colour developed outlined by Linge and Oldham [12].

3.4. Phosphate measurement using PEDD flow cell, LED photodiode flow cell and the μQuant™ platewell reader

Working calibration solutions between 0.002 and 20 μM were prepared from the stock standard. The malachite green method has a limited range of up to 20 μM before precipitation of MG occurs. Various concentrations of phosphate were prepared in deionised water and passed through the PEDD flow cell for ca. 4 min per sample, at a flow rate of 0.6 mL min^{-1}. The log of the discharge times (log t, μs) was plotted against malachite green–molybdphosphate complex concentration (C) in accordance with the model (Eq. (6)) and the result is presented in Fig. 4. The inset plot Fig. 4 shows a large dynamic range from ca. 0 to 20 μM malachite green–molybdphosphate complex from which a linear range of approximately 0.02–2 μM malachite green–molybdphosphate (R^2 value 0.9964) was observed as shown in main feature plot. The relative standard deviation of the measurements ($n = 3$, shown as error bars) is very low (ca. 0.05%) and a LOD of ca. 2 nM of the malachite green–molybdphosphate complex as shown in Fig. 5.

An LOD of 2 nM was achieved using the PEDD (λ_{max} 636 nm). The response (change in discharge time, μs) obtained was 8.49 ± 0.82 μs with an R.S.D. of 9% ($n = 3$).

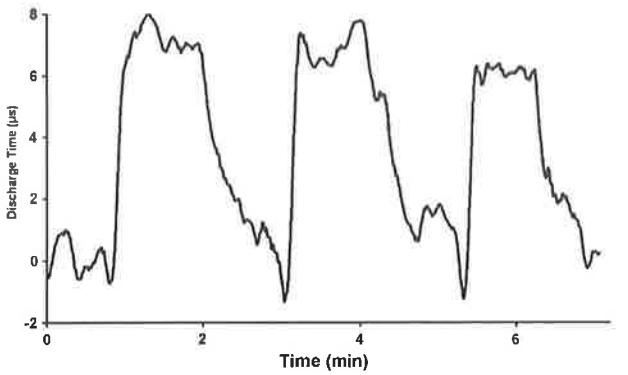

Fig. 5. Determination of the LOD of the malachite green–molybdphosphate complex concentration (2 nM).

As a comparison study, the absorbance of the same malachite green–molybdphosphate complex concentrations were acquired employing both the commonly used LED-photodiode detector and a μQuant™ platewell reader.

As shown in Fig. S4 the mean normalized maximum absorbance (R/R_{max}) was plotted against malachite green–molybdphosphate complex concentration (C) resulting in a dynamic range of 0.2–20 μM. A linear range of (R^2 value 0.9947) of 0.2–2 μM was achieved, with an R.S.D. ($n=3$) of 8.7%. A significantly higher LOD of 0.2 μM was determined using the μQuant™ platewell reader.

A low cost LED-photodiode detector was investigated to compare its performance with that of the PEDD. As shown in Fig. S5 the mean change in absorbance, i.e. peak height was plotted against malachite green–molybdphosphate complex concentration (C) resulting in a dynamic range of 0.9–10 μM. A linear range of (R^2 value 0.9816) of 2–10 μM was achieved, with an R.S.D. ($n=3$) of 6.4%. A significantly higher LOD of 2 μM was determined using this comparative LED-photodiode detector.

4. Conclusions

We have demonstrated that the novel, low cost, miniaturized PEDD flow analysis system is highly sensitive for the detection of phosphate. Under optimised conditions the PEDD detector offered a linear range of 0.02–2 μM and an LOD of 2 nM. For comparative purposes a simple, low cost LED-photodiode detector and a μQuant™ platewell reader were investigated. The LED-photodiode detector achieved an LOD in the micromolar range (2 μM). Enhanced performance of the LED-photodiode can be achieved by using more precise components and/or higher resolution ADCs, however, the cost incurred for slight increases in sensitivity would not be justified on a low cost sensor. The PEDD device exhibited sensitivity in the nanomolar concentration range, which was approximately 100 times lower than that of the commercially available bench top platewell reader. The PEDD offers advantages of extremely low power consumption, no requirement for an A/D converter or operational amplifier and the sensor can be operated from a 9 V battery. This low cost detector could therefore be used in an autonomous instrument for remote monitoring of phosphate levels in situ.

Acknowledgements

The authors wish to thank Science Foundation Ireland SFI for grant support under the Adaptive Information Cluster Award (SFI 03/IN3/1361), and to acknowledge the assistance of Mitsubishi Electric Research Laboratory, Cambridge, MA, in the development of the PEDD detector concept.

Appendix A. Supplementary data

Supplementary data associated with this article can be found, in the online version, at doi:10.1016/j.aca.2007.06.048.

References

[1] J.L. Haberer, J.A. Brandes, Marine Chem. 82 (2003) 185–196.
[2] A.G. Vlessidis, M.E. Kotti, N.P. Evmiridis, J. Anal. Chem. 59 (2004) 77–85.
[3] G. Hanrahan, M. Gledhill, P.J. Fletcher, P.J. Worsfold, Anal. Chim. Acta 440 (2001) 55–62.
[4] K. Higuchi, H. Tamanouchi, S. Motomizu, Anal. Sci. 14 (1998) 941–946.
[5] J.B. Mullin, J.P. Riley, Anal. Chim. Acta 12 (1955) 162–176.
[6] P.J. Worsfold, L.J. Gimbert, U. Mankasingh, O.N. Omaka, G. Hanrahan, P.C.F.C. Gardolinski, P.M. Haygarth, B.L. Turner, M.J. Keith-Roach, I.D. McKelvie, Analysis of phosphorus in environmental and agricultural samples, Talanta 66 (2005) 273–293.
[7] B. Paull, L. Barron, P. Nesterenko, Chromatographic Analysis of the Environment: Revised and Expanded, third ed., CRC Press/Taylor & Francis Group, Boca Raton, FL, 2005, p. 263–286.
[8] M. Sequeira, M. Bowden, E. Minogue, D. Diamond, Talanta 56 (2002) 355–363.
[9] M. Bowden, D. Diamond, Sens. Actuators B: Chem. 90 (2003) 170–174.
[10] D. Peachey, J.L. Roberts, J. Scot-Baker, J. Geochem. Explor. 2 (1973) 115–120.
[11] E. Bakker, D. Diamond, A. Lewenstam, E. Pretsch, Anal. Chim. Acta 393 (1999) 11–18.
[12] K.L. Linge, C.E. Oldham, Anal. Chim. Acta 450 (2001) 247–252.
[13] H.H. Hess, J.E. Derr, Anal. Biochem. 63 (1975) 607–613.
[14] P.P. Van Veldhoven, G.P. Mannaerts, Anal. Biochem. 161 (1987) 45–48.
[15] P. Ekman, O. Jager, Anal. Biochem. 214 (1993) 138–141.
[16] S. Motomizu, T. Wakimoto, K. Tôei, Analyst 108 (1983) 361–367.
[17] J.P. Susanto, M. Oshima, S. Motomizu, H. Mikasa, Y. Hori, Analyst 120 (1995) 187–191.
[18] I.D. McKelvie, D.M.W. Peat, P.J. Worsfold, Anal. Proc. 32 (1995) 437–445.
[19] E. D'Angelo, J. Crutchfield, M. Vandiviere, J. Environ. Qual. 30 (2001) 2206–2209.
[20] S. Motomizu, Z.-H. Li, Analysis of phosphorus in environmental and agricultural samples, Talanta 66 (2005) 332–340.
[21] P.K. Dasgupta, I.-Y. Eom, K.J. Morris, J. Li, Anal. Chim. Acta 500 (2003) 337–364.
[22] A. Zukauskas, M.S. Shur, R. Gaska, Introduction to Solid-State Lighting, John Wiley & Sons, Inc., 2002.
[23] Y. Taniyasu, M. Kasu, T. Makimoto, Nature 441 (2006) 325–328.
[24] O. Geschke, H. Klank, P. Tellemann, Microsystem Engineering of Lab-on-a-chip Devices, WILEY-VCH, 2004.
[25] M. O' Toole, K.T. Lau, D. Diamond, Talanta 66 (2005) 1340–1344.
[26] M. O' Toole, K.-T. Lau, B. Shazmann, R. Shepherd, P.N. Nesterenko, B. Paull, D. Diamond, Analyst 131 (2006) 938–943.
[27] L. Barron, P.N. Nesterenko, D. Diamond, M. O'Toole, K.T. Lau, B. Paull, Anal. Chim. Acta 577 (2006) 32–37.
[28] D. Diamond, Anal. Chem. 76 (2004) 279A–286A.
[29] K.-T. Lau, S. Baldwin, M. O'Toole, R. Shepherd, W.J. Yerazunis, S. Izuo, S. Ueyama, D. Diamond, Anal. Chim. Acta 557 (2006) 111–116.
[30] T. Attin, K. Becker, C. Hannig, W. Buchalla, A. Wiegand, Clin. Oral Invest. 9 (2005) 203–207.